TECHNISCHE UNIVERSITÄT MÜNCHEN

Professur für Molekulare Katalyse

# Heteroleptic Fe(II)-Hexa-NHC complex with 130 ps MLCT lifetime & Mechanism study of photocatalyzed synthesis of medium sized ring compounds

**Han Li**

Vollständiger Abdruck der von der Fakultät für Chemie der Technischen Universität München zur Erlangung des akademischen Grades eines

**Doktors der Naturwissenschaften**

genehmigten Dissertation

| | |
|---|---|
| Vorsitzender: | Prof. Dr. Tom Nilges |
| Prüfer der Dissertation: | 1. Prof. Dr. Fritz. E. Kühn |
| | 2. Prof. Dr. Hao Guo |

Die Dissertation wurde am 25.01.2021 bei der Technischen Universität München eingereicht und durch die Fakultät für Chemie am 31.03.2021 angenommen

# Acknowledgements

*First of all, I would like to express my great gratitude to my supervisor Prof. Dr. Fritz E. Kühn.*

*Thank you very much for giving me this opportunity and providing me with an excellent working environment. I have learned a lot and I have grown a lot here.*

*I am very grateful for your understanding and patience!*

*This is not a thank you out of polite, but a sincere gratitude from the bottom of my heart: Thank you very much!*

*Great Acknowledgements go to Prof. Hao Guo. Thank you very much for your great help. I am very grateful for your giving me the greatest sense of security when I am confused about the future. Words are bare to express my gratitude. Thank you so much for your selfless encouragement and support for so long!*

*I would like to thank Dr. Robert M. Reich for your efforts to make our group operate normally and orderly. It is because of your huge contribution that to support everyone in the group to concentrate on their work. Same acknowledgements go to Ms Ulla Hifinger, thank you for your work to make our group family well connected.*

*I would like to thank* Jonas *Schlagintweit, Macro Bernd, Eva-Maria Esslinger and Christian Jandl. Thank you very much for your help and company. Also, thank you for teaching me the German words. In the coming days, I will miss you very much. Thank you! I also highly appriciate Dr. Markus Drees for his meaningful work. Thank you for helping me a lot.*

*Thank Felix, Paulina and Bruno for the warm memories. I miss you guys!*

*Thanks to everyone in our group and everyone around!*

*Special acknowledgement goes to my friend as well as colleague Dr. Dawen Xu. Thank you for your great help during my PHD period! Thank you for always being there! Same acknowledgement goes to Pan Huang. Thank you!*

*Thank my girlfriend Yang Shen for her company over the past two years.*

*To my beloved, my parents and aunt, I am very grateful for your selfless support for me. Thanks You may not know what work I am doing, but you have always been there.I love you!*

*Finally, I would like to thank myself for not giving up.*

*The period you feel the most difficult, might be the time you grow fastest.*

*Thanks for all the frustrations along the way.*

# Abstract

For many years, chemists have been committed to exploring new alternative energy sources, and solar energy is one of the most attractive. Among many related fields, visible light photoredox catalysis has developed rapidly in the past 20 years. In the past ten years, much attention has been focused on exploring the possibility of Fe-Complex as new visible light photoredox catalyst species. However, Fe complexes suffer from extremely fast MLCT state deactivation due to its low-lying MC state. Many strategies and methods have been developed to stabilize the MLCT state of Fe complex. Among these strategies, the introduction of strong σ-donating ligands N-Heterocyclic Carbene has been proven to be a success, which has greatly increased the excited state lifetime of Fe complex.

In this work, two heteroleptic Fe(II) complexes **Fe-1** and **Fe-2** have been designed and synthesized. The electrochemical properties of these two complexes have been studied by cyclic voltammetry measurements. Both **Fe-1** and **Fe-2** exhibit excellent electrochemical properties, both showing two reversible one-electron redox cycles. The details of CV curve have also been deeply studied and verified through a series of comparisons. The steady absorption properties of **Fe-1** and **Fe-2** have been studied through UV-Vis absorption. Through the horizontal comparison between the two complexes and the vertical comparison of their oxidation state absorption spectra, the absorption of **Fe-1** and **Fe-2** have been carefully assigned and verified. The transient absorption spectra (TAS) measurement has been conducted to study the properties of the two complexes' excited states. After carefully assign the 16ps to the vibrational cooling processes of $^5T_2$ state, **Fe-1** only shows lifetime of the MLCT state with less than 1ps. However, **Fe-2** exhibits a MLCT lifetime of up to 130 ps, which is the second highest MLCT lifetime of all known Fe(II) complexes, and the highest among the heteroleptic Fe(II) complexes. This successful result provides new strategies and possibilities for Fe(II) complexes being utilized as solar cells in the future.

Medium and macrocyclic compounds are widely presented in nature and have been widely used in medicine, pesticide, food and other fields. Scientists have explored a variety of methods to construct medium and macrocyclic compounds, such as acid catalysis, base catalysis, and free radical cyclization. However, each method has its limitations, in this end, chemists have been always trying to explore new strategies for constructing different medium and macrocyclic compounds.

It has been discovered in this work a visible light-induced reaction to synthesize many mid-ring compounds with good to excellent yields under mild condition by cascading

[2+2]-photocycloaddition and retro- [2+2]-photocycloaddition. During the work, the substrate scope of the reaction has been further expanded. The mechanism has been studied in detail and in depth. Two key intermediates in the reaction have been discovered and separated, which reversed our perception of the reaction process. A deep understanding of every factor in the reaction has been formed through step-by-step control experiments. A series of compounds have been designed and synthesized to verify the mechanism explored. As a result, a more practical mechanism of the reaction was proposed. It is worth pointing out that this reaction provides a new strategy and method for the synthesis of mid-ring compounds. We also expect that this method can be expanded and widely used in the construction of medium ring compounds.

# Kurzzusammenfassung

Seit vielen Jahren beschäftigen sich Chemiker mit der Erforschung neuer alternativer Energiequellen, wobei Solarenergie eine der attraktivsten darstellt. Unter vielen verwandten Bereichen hat sich die Photoredoxkatalyse mit sichtbarem Licht in den letzten 20 Jahren rasant entwickelt. Im letzten Jahrzehnt lag der Fokus auf der Erforschung von Fe-Komplex als mögliche neue Photoredoxkatalysatoren mit sichtbarem Licht. Fe-Komplexe leiden jedoch aufgrund ihres tief liegenden MC-Zustands unter einer sehr schnellen Deaktivierung des MLCT-Zustands. Viele Strategien und Methoden wurden entwickelt, um den MLCT-Zustand des Fe-Komplexes zu stabilisieren. Unter diesen Strategien hat sich die Einführung N-heterocyclisches Carbene als starke σ-Donorliganden als vielversprechend herausgestellt, was die Lebensdauer des angeregten Zustands des Fe-Komplexes erheblich verlängert.

In dieser Arbeit wurden zwei heteroleptische Fe(II) -Komplexe **Fe-1** und **Fe-2** entworfen und synthetisiert. Die elektrochemischen Eigenschaften dieser beiden Komplexe wurden mittels Cyclovoltammetrie untersucht. Sowohl **Fe-1** als auch **Fe-2** zeigen geeignete elektrochemische Eigenschaften und jeweils zwei reversible Einelektronen-Redoxprozesse. Die Details der CV-Kurve wurden ebenfalls eingehend untersucht und mit einer Reihe ähnlicher Komplexe verglichen. Die Absorptionseigenschaften von **Fe-1** und **Fe-2** wurden durch UV-Vis Spektroskopie untersucht. Durch den horizontalen Vergleich zwischen den beiden Komplexen und den vertikalen Vergleich ihrer Absorptionsspektren für den Oxidationszustand wurde die Absorption von **Fe-1** und **Fe-2** sorgfältig zugeordnet und verifiziert. Die transienten Absorptionsspektren (TAS) wurden gemessen, um die Eigenschaften der angeregten Zustände der beiden Komplexe zu untersuchen. Nach sorgfältiger Zuordnung der 16 ps zu den Schwingungskühlungsprozessen im 5T2-Zustand zeigt **Fe-1** nur die Lebensdauer des MLCT-Zustands von weniger als 1 ps. **Fe-2** weist jedoch eine MLCT-Lebensdauer von bis zu 130 ps auf. Dies ist die zweithöchste MLCT-Lebensdauer aller bekannten Fe(II) Komplexe und die höchste unter den heteroleptischen Fe(II) Verbindungen. Dieses erfolgreiche Ergebnis bietet neue Strategien und Möglichkeiten für die zukünftige Verwendung von Fe(II) Komplexen als Solarzellen an.

Mittlere und makrocyclische Verbindungen sind in der Natur weit verbreitet und wurden in der Medizin, in Pestiziden, in Lebensmitteln und auf anderen Gebieten weit verbreitet eingesetzt. Wissenschaftler haben eine Vielzahl von Methoden untersucht, um mittlere und makrocyclische Verbindungen herzustellen, u.a. Säurekatalyse, Basenkatalyse und Radikalcyclisierung. Jede Methode hat jedoch ihre Grenzen. Zu diesem Zweck haben

Chemiker immer versucht, neue Synthesestrategien für verschiedene mittlere und makrocyclische Verbindungen zu erforschen.

In dieser Arbeit wurde eine durch sichtbares Licht induzierte Reaktion zur Synthese vieler Mittelringverbindungen mit hohen bis sehr hohen Ausbeuten unter milden Bedingungen durch Kaskadierung der [2 + 2] -Photocycloaddition und Retro- [2 + 2] -Photocycloaddition entwickelt. Während der Arbeit wurde der Substratumfang der Reaktion erweitert. Der Mechanismus wurde eingehend untersucht. Zwei Schlüsselintermediate in der Reaktion wurden isoliert, was unsere bisherige Annahme des Reaktionsmechanismus veränderte. Durch schrittweise Kontrollexperimente wurde ein tiefes Verständnis für jeden Faktor in der Reaktion gewonnen. Eine Reihe von Verbindungen wurde entworfen und synthetisiert, um den untersuchten Mechanismus zu verifizieren. Als Ergebnis wurde ein praktischerer Reaktionsmechanismus vorgeschlagen. Diese Reaktion stellt eine neue Strategie und Methode für die Synthese von Mittelringverbindungen dar. Wir erwarten auch, dass diese Methode erweitert und bei der Konstruktion von Mittelringverbindungen weit verbreitet werden kan

# Table of Content

# Background

## 1. Common utilized Visible Light Photoredox Catalysts (VLPCs).

### 1.1 The origin and development of photochemistry

The sun light has been the source of all energy on the earth since the existence of life on earth. The physical and chemical reactions involving light constitute one of the cornerstones of the operation of the world. As the oldest and most popular photochemical reaction in nature, photosynthesis is one of the most important means of light utilization on earth (**Scheme 1**). The most important fossil fuels in contemporary society, coal and oil, are the utilization, transformation and collection of solar energy through photosynthesis by the earth for countless years. Therefore, earth’s accumulation of solar energy have been relied on for hundreds of millions of years to support the energy needed for the production and progress of our society [1].

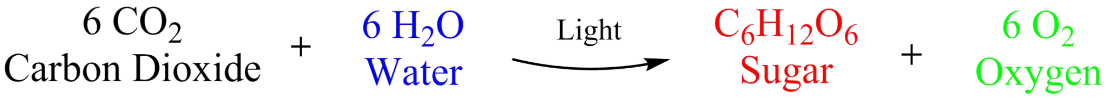

$$6\ CO_2 + 6\ H_2O \xrightarrow{Light} C_6H_{12}O_6 + 6\ O_2$$

**Scheme 1**: photosynthesis on earth.

However, with the continuous development of society and industry, these limited feedstocks will inevitably not support our endless requests. In reality, our utilization of solar energy is only a small part of the energy radiated by the sun on earth. Therefore, exploring new methods to efficiently utilize solar energy is one of the hot spots that we must face in future scientific development.

The existence of photochemistry provides direction and action for this goal, with photocatalysis being one of the most important methods in the field. The evolution and development of the concept of photocatalysis also illustrates the progress of scientists' understanding towards the photochemistry. The turning point for photochemistry to become a relatively independent science is that scientists have realized that it is different from traditional thermochemistry. In fact, until the beginning of the 20th century, most scientists' understanding of “light” in photochemistry remained more focused on the physical properties of light, that is, light can radiate to generate heat, thereby promoting the chemical reactions.

This cognition is essentially thermochemistry, except for the way to provide heat for the reaction has been changed from heating to light. As the first scientist who noticed the distinctive role of light in reactions, Giacomo Ciamician conducted an in-depth study of the photo reactions[2]. His research shows that in some chemical reactions, while maintaining the same reaction process as thermochemistry, light can be used to accelerate the reaction. He called these chemical reactions "photochemical reactions", and derived the concept of photocatalysis[3]. His research also aroused the attention of other scientists to photochemistry. In the definition of photocatalysis from 1914, Bodenstein mentioned the electronic excited state in photocatalysis. As he referred, the substrate of a photochemical reaction will enter a special reactive excited state after absorbing light energy, which is different from the traditional thermochemical reaction intermediate state. This theory was later confirmed and widely known.

Traditional thermochemistry promotes the reaction by increasing the internal energy of the reactant and increasing the activity and collision of the reactant molecules. While this process promotes the target response, it also promotes some side reactions. Therefore, the reducing of side reactions has always been one of the topics of thermochemistry. In contrast, photochemical reactions, especially visible light catalysis, often have good targeting properties, and can transfer energy through the catalyst to the photoactive sites with relative accuracy. This type of reactions can even be carried out at ultra-low temperatures, which largely compensates for the inevitable side reactions in traditional thermochemistry due to heating.

Although the concept of photocatalysis was proposed very early, it was not until the 1870s that photocatalysis was truly widely accepted and applied, and photocatalysis was derived from this as an independent scientific subject[4]. One of the driving forces for the development of photocatalysis is the crisis of fossil fuels. Due to the rapid development of industry, people are increasingly aware that limited fossil fuels cannot meet the needs of human society for continuous progress. Therefore, human beings have to seek new alternative energy sources to solve this crisis. And one of the most important research directions is the improvement of sunlight utilization.

The initial research direction of photocatalysis is how to store solar energy or use solar energy to produce fuel as well as the splitting of water to produce hydrogen[5]. In addition, the application of photocatalysis to solve the pollution problem caused by industrial development is also in the focus of research[6]. For example, photocatalysis is used to purify chemicals in sewage or chemical components in the air. With the development of modern chemical sciences, people are increasingly studying the mechanism of photochemical reactions[7]. The rise of modern organic chemistry synthesis disciplines has also triggered widespread attention on the role of photocatalysis in the field of chemical synthesis[8]. Especially in the past two decades, the progress made in the field of visible light catalysis has made it one of the most concerned research directions in the field of chemistry.

## 1.2 Common utilized VLPCs

### 1.2.1 The mechanism and application of the catalyst $Ru(bpy)_3^{2+}$

Exploring new alternative clean energy has always been one of the research hotspots of modern scientific development. Solar energy is undoubtedly one of the biggest research areas, and photocatalysis is one of many fields that utilize solar energy. Earlier studies from 2004 to 2007 have been therefore been focusing majorly on photocatalysis with metal oxides, generation of solar hydrogen through photoinduced water splitting and progress in photovoltaic and dye-sensitized solar cells (DSSCs)[9].

Photovoltaic devices and dye-sensitized solar cells implicate titanium dioxide ($TiO_2$) to generate electrical power due to low cost and stability of this metal oxide[10]. First concepts of DSSCs already established back in the 1990s. The major topics of current studies have been focused on the enhancement of efficacy of DSSCs by the increasing efficiency of energy conversion. Therefore, the development and usage of different stable and durable dyes is indispensable. The common mechanism of dye sensitized solar cells or photochemical solar cells is the photoexcitation of the sensitizer followed by injection of an electron into the conduction band of the metal-oxide, conveniently $TiO_2$, semiconductor film. Subsequently the dye is regenerated by a redox system[11].

In the following research, scientists gradually turned their attention to optical catalysts centered on transition metal complexes[12]. The reason why transition metal complexes have received widespread attention is due to their unique properties in structure, photochemistry, and photophysical field. Amongst those, Ruthenium complexes are one of the most widely studied metal inorganic compounds as photocatalysts. It has been widely used as luminophores in photochemistry and electrochemistry. It is also used as a photosensitizer for photoelectric energy conversion between multiple components, especially in the field of photochemical conversion of solar energy.

As the most prominent representative, the polypyridine complex of ruthenium, $Ru(bpy)_3^{2+}$ (bpy = 2,2-bipyridine) (**Scheme 2**), has good solubility in a variety of solvents, thermodynamic stability and kinetic inertness[13]. In addition, it also exhibits good optical absorption properties. It can enter the excited state after absorbing photon energy, and shows a broad and strong absorption peak in the visible light region around 450 nm. More importantly, its optically active triplet metal-to-ligand charge transfer state($^3$MLCT) excited state has a lifetime of up to 800 ns, which allows it to have enough time in the reaction to transfer energy from its excited state to the reactants. $Ru(bpy)_3^{2+}$ also shows good electrochemical properties under room temperature. It undergoes extremely superior single electron cyclic process whether it is a metal-centered oxidation process or a ligand-centered reduction process. This means that $Ru(bpy)_3^{2+}$ is able to act as both an oxidant and a reducing agent in a potential reaction.

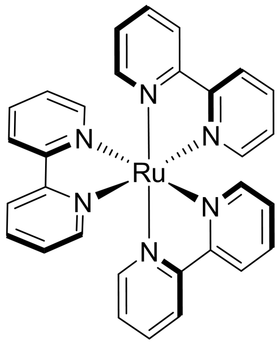

$Ru(bpy)_3^{2+}$

**Scheme 2**: Structure of most classic ruthenium VLPC

Next, $Ru(bpy)_3^{2+}$ will be taken as an example to illustrate how visible light photo redox catalysts undergoes the photocatalysis process in a typical photochemical reaction (**Scheme 3**)[14]:

One of $Ru(bpy)_3^{2+}$'s electron from the metal-centered $t_{2g}$ orbitals will be excited to the ligand-centered $\pi^*$ orbital soon after absorpting a proton from the visible region. This metal-to-ligand charge transfer transition undergoes rapid intersystem crossing (ISC) to give triplet MLCT state. This transition specie is more active, which can be both more oxidizing and reducing compared with its ground state. As a result, $Ru(bpy)_3^{2+*}$ is able to act as either oxidant or reductant.

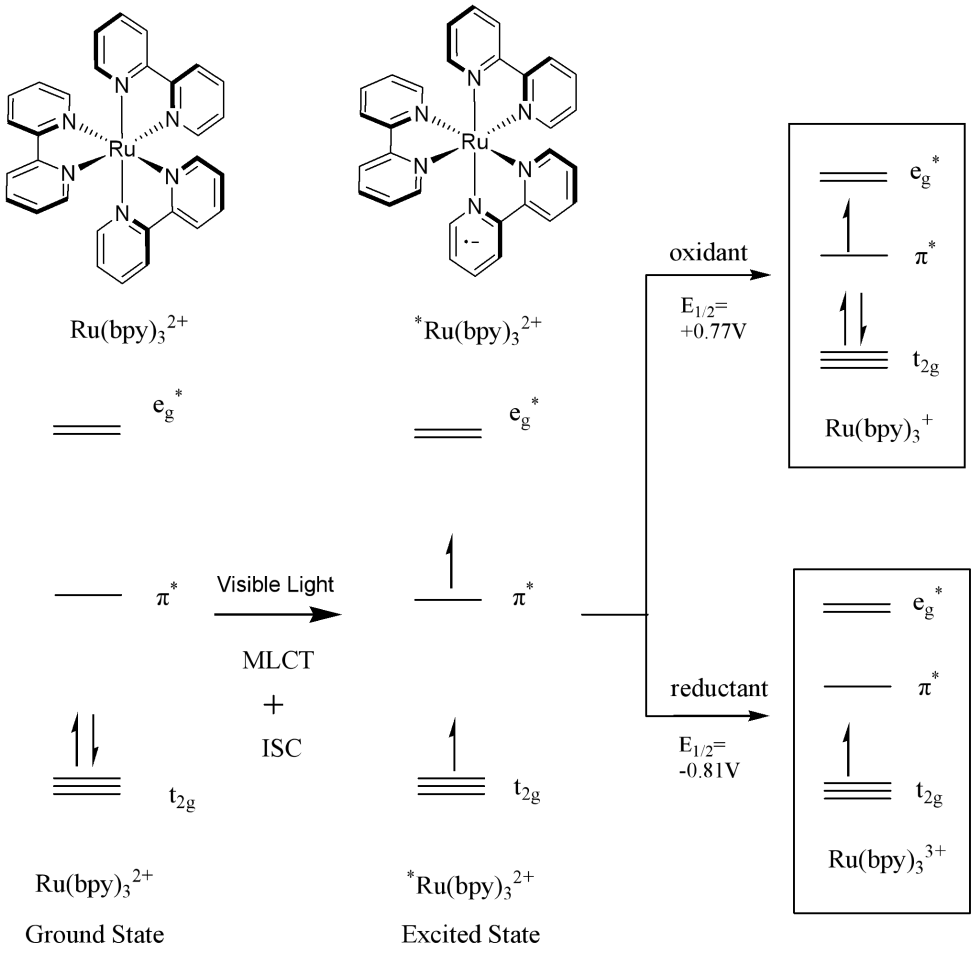

**Scheme 3**: Photocatalysis process of $Ru(bpy)_3^{2+}$ in a typical photochemical reaction

When $^*Ru(bpy)_3^{2+}$ acts as a reductant, it will reduce the electron acceptor (A) through single electron transfer (SET). Through this SET process, the reductant radical anion $A^-$ and oxidized product $Ru(bpy)_3^{3+}$ are thus formed. The species returns to the ground state after accepting an electron from the electron donor D. Similarly, $^*Ru(bpy)_3^{2+}$ can also function as a oxidant in a reductive quenching cycle. During the process, $^*Ru(bpy)_3^{2+}$ is reducted to $Ru(bpy)_3^{+}$after accepting an electron from D. The Ru(I) intermediate is oxidized to the Ru(II) ground state subsequently after donating an electron to electron acceptor A (**Scheme 4**).

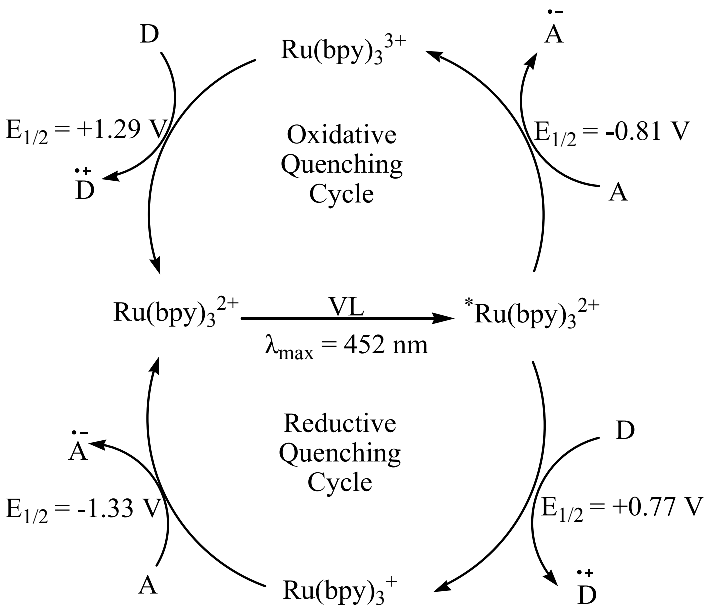

**Scheme 4**: Oxidative and reductive process of ruthenium complexes

Photoredox catalysts like $Ru(bpy)_3^{2+}$ are usually stable. Although these complexes are usually poor reductants or oxidants at their ground state, they can be easily excited to be very potent single-electron-transfer species under irradiation of sunlight, thus making it remarkably easier to participate in the catalytic processes.

$Ru(bpy)_3^{2+}$ has been used as a photo redox catalyst in the field of organic synthesis for a long time. Early in 1981, Sakurai and coworkers have demonstrated a photocatalytic reduction of electron-deficient olefins *via* neutral α-acyl radicals, with $Ru(bpy)_3^{2+}$ as photo oxidative catalyst and 1-benzyl-1,4 dihydronicotinamide (BANH) as the terminal reductan[15]. In this reaction, $Ru(bpy)_3^{2+}$ obtains an electron from BANH through an oxidation cycle after excitation, and then further reduces the olefins (**Scheme 5**). Similar transformations for the reduction of activated alkyl halides *via* the fragmentation of neutral alkyl radicals and halide anions have also been reported.

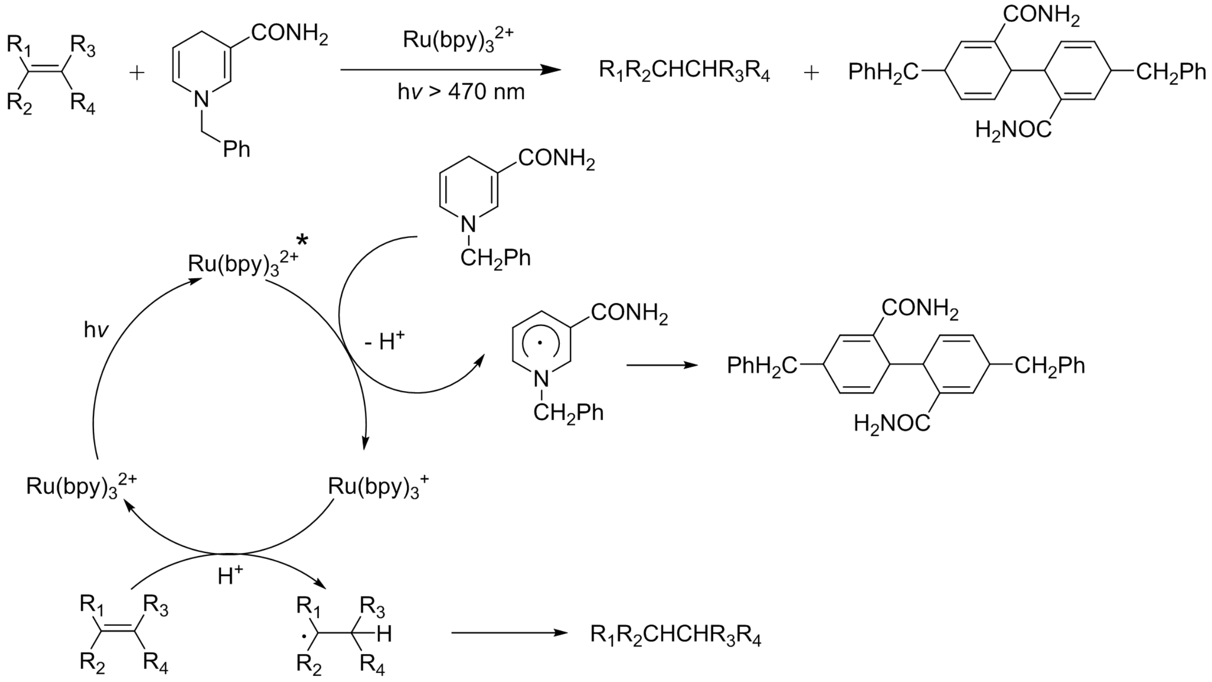

**Scheme 5:** photocatalytic reduction of electron-deficient olefins via neutral α-acyl radicals

The reductive catalytic cycle of $Ru(bpy)_3^{2+}$ as an optical catalyst was reported as early as 1984 for the oxidation of terminal alcohols (**Scheme 6**)[16].

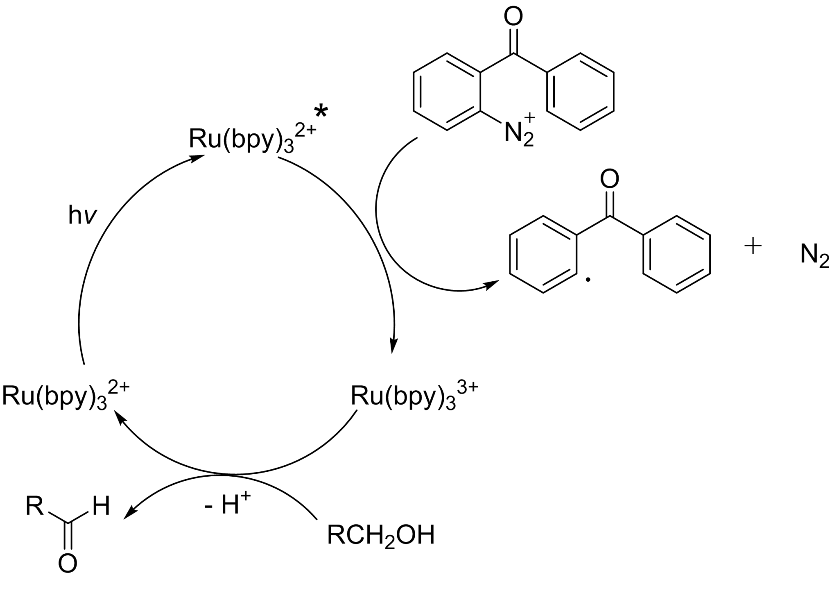

**Scheme 6:** $Ru(bpy)_3^{2+}$ function process in the oxidation of terminal alcohols

In 2008, MacMillan further reported on the α-alkylation reaction of aldehydes with good enantioselectivity using $Ru(bpy)_3^{2+}$ and organic chiral amines as catalysts[17]. This work completely opened the prelude to the research of visible light redox catalytic reaction. In the following decades until now, the research on this type of visible light catalytic reaction has undoubtedly become one of the biggest hot spots in the field of chemical organic catalysis.

Despite more than ten years of research in this field, the most commonly used visible light photoredox catalysts are still complexes centered on transition metals such as Ru and Ir. At present, most researches are still focused on how to deeply tap the potential of known catalysts. That is, how to use the known catalysts to explore and catalyze various reactions. Some modifications to current catalysts can also change their photophysical and electrochemical properties accordingly to meet the needs of different catalytic reactions. Therefore, the most popular catalysts are still a series of polypyridines coordinated Ru complexes and benzene-pyridine coordinated Ir complexes.

## 1.2.2 Common utilized Ru centered VLPCs

Ru-based polypyridine complexes have very excellent photochemical and photophysical properties. Their application as VLPCs in the field of organic synthesis can be described as phenomenal. The common Ru type visible light catalysts will be listed as below.

$Ru(bpy)_3^{2+}$ is undoubtedly the most studied and most popular VLPC. A detailed description of it has been discussed above.

$Ru(bpm)_3^{2+}$ was first synthesized and reported in 1977[18]. Ludi and coworkers studied and demonstrated its excited state lifetime under different conditions and temperatures. In solution, the lifetime of MLCT state of $Ru(bpm)_3^{2+}$ varies smoothly from 96 ns at 1.5 °C to 64 ns at 30 °C, whereas for a solid sample, it increases greatly from 110 ns at 278 K to 7250 ns at 7.6 K. Most of the following up researches on $Ru(bpm)_3^{2+}$ are mainly focused on the photochemical and photophysical properties. Until 2013, Yoon's group firstly utilized $Ru(bpm)_3^{2+}$ as a photoredox catalyst, achieving the intermolecular [2 + 2] cycloadditions of styrenes and olefins (**Scheme 7**)[19].

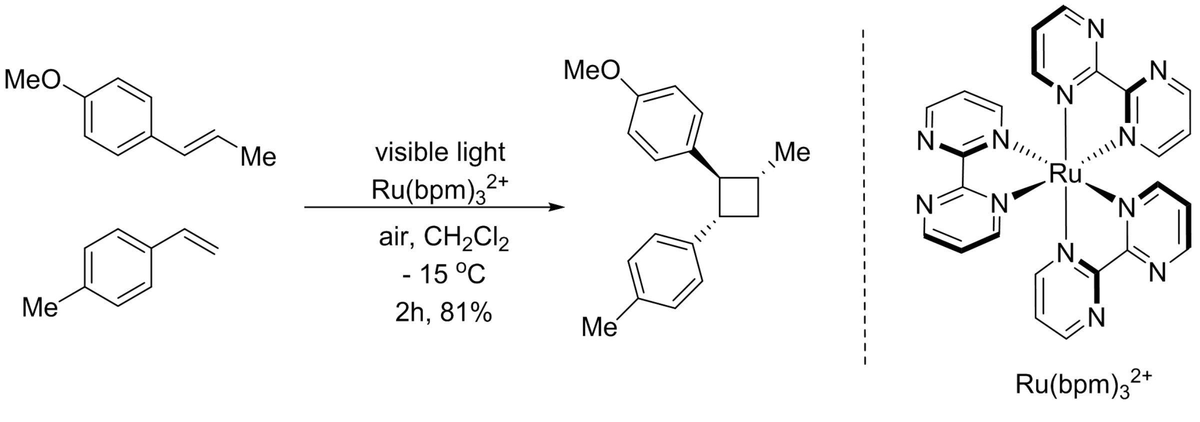

**Scheme 7**: $Ru(bpm)_3^{2+}$ catalyzed intermolecular crossed [2 + 2] cycloaddition

$Ru(phen)_3^{2+}$ may be one of the earliest studied photocatalysts as early as the 1940s. Reports in the early years focused on the synthesis and optical absorption of $Ru(phen)_3^{2+}$. In the subsequent continuous research, the optical excited state of $Ru(phen)_3^{2+}$ was gradually studied and reported. Until recent years, $Ru(phen)_3^{2+}$ has been widely used as a classic photo catalyst in organic synthesis[20]. One of the most classic application comes from the work published by MacMillan's research group in *Nature* in 2011[21]. In this work, they successfully accomplished direct trifluoromethylation of arene C−H bonds under photoredox conditions using $Ru(phen)_3^{2+}$ as visiblelight photoredox catalyst (**Scheme 8**).

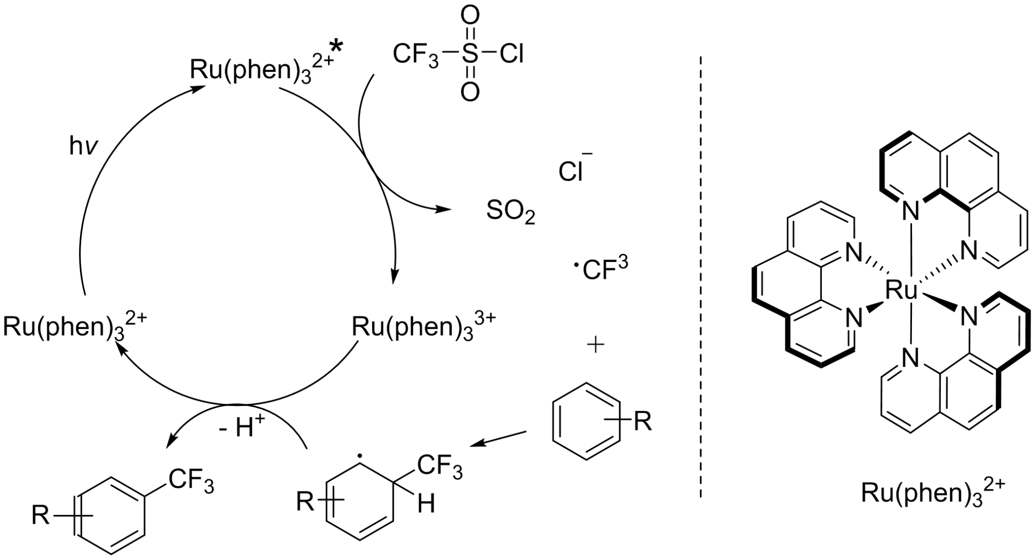

**Scheme 8**: $Ru(phen)_3^{2+}$ catalyzed trifluoromethylation of arenes

Early in 1980, Crutchley and Lever have conducted relatively in-depth theoretical research on $Ru(bpz)_3^{2+}$ as a potential optical catalyst[22]. The spectrum of $Ru(bpz)_3^{2+}$ shows bands at 241 nm and 296 nm belonging to n-π* and π-π* intra ligand transitions, respectively. The band at 443 nm is attributed as π-π* charge-transfer (CT) transition. The emission of $Ru(bpz)_3^{2+}$ locates at 603 nm and has a lifetime of 1.04 μs in argon deaerated aqueous solution. $Ru(bpz)_3^{2+}$ also shows similar CV properties with $Ru(bpy)_3^{2+}$, undergoing three reversible one-electron reductions, giving successively $Ru(bpz)_3^{2+}$ ($E_{1/2} = -0.86$ V), $Ru(bpz)_3^{1+}$ ($E_{1/2} = -1.02$ V), and $Ru(bpz)_3^{0}$ ($E_{1/2} = -1.26$ V). The early actual application of $Ru(bpz)_3^{2+}$ as a photo catalyst is mostly focused on the reduction of carbon dioxide. Until recent years, it has been widely used in organic synthesis as a classic VLPC. In 2011, Zheng and coworkers reported the reduction of hydrazides and hydrazines under VLPCs, utilizing $Ru(bpz)_3^{2+}$ as photo redox catalyst[23]. Yoon group also reported accomplishment of radical cation-mediated [4+2] cycloadditions of electronically-mismatched dienes and dienophiles with the same catalyst (**Scheme 9**)[24].

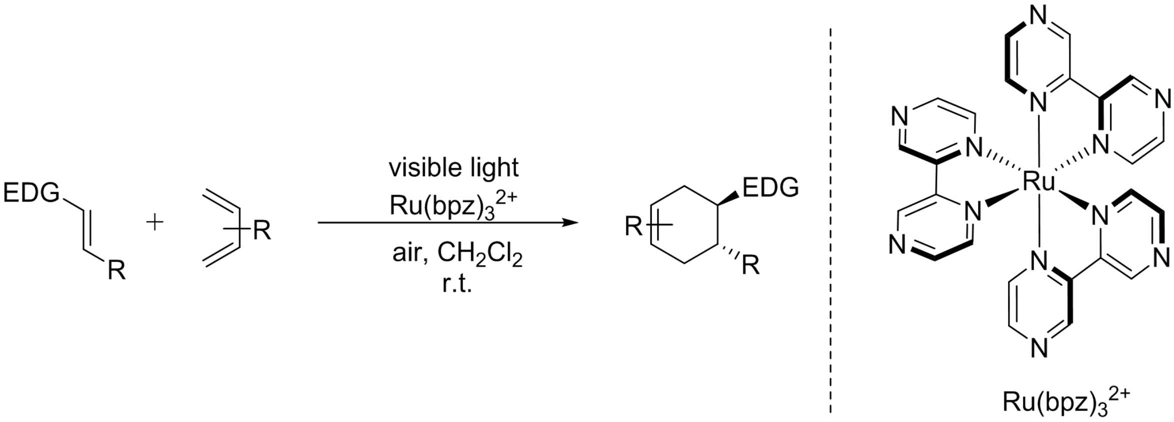

**Scheme 9**: Ru(bpz)$_3^{2+}$ catalyzed [4+2] cycloadditions of olefins

Other common utilized Ru-based catalysts are mostly modified on the basis of the catalysts described above to meet the photochemical and electrochemical needs of scientific researchers for electrode potentials[25]. For example, Ru(dtbbpy)$_3^{2+}$ and Ru(dmbyp)$_3^{2+}$ are based on Ru(bpy)$_3^{2+}$ with tert-butyl and methyl groups added to the polypyridine ligand, respectively. By adding such electron donating groups, the electron density of the metal center can be effectively increased, thereby enhancing the reducing ability of the catalysts (**Scheme 10**). Ru(dtbbpy)$_3^{2+}$ is used in the photoredox catalyzed formation of C-P bond[26], direct synthesis of polysubstituted furans[27] and other reactions[28]. While Ru(dmbyp)$_3^{2+}$ is utilized in the photocatalytic reduction of carbon dioxide and [4 + 2] cycloaddition reactions[29].

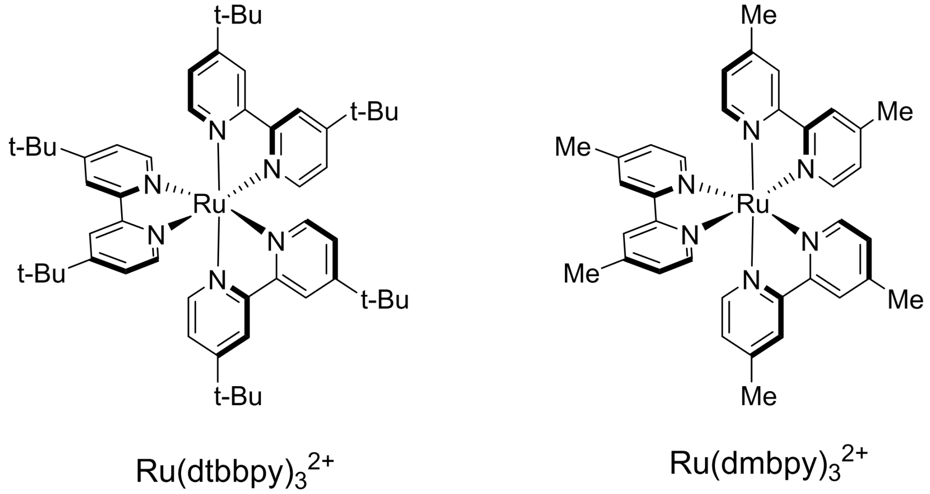

**Scheme 10**: Other common utilized Ru-centered catalysts

## 1.2.3 Common utilized Ir centered VLPCs

As the diagonal metal of Ru, $d^7$ metal Ir complexes also have very good photochemical and photophysical properties. Ir-based catalysts are the only ones that are comparable to Ru-centered photo catalysts reported to date. Most of the common utilized Ir catalysts are complexes of phenylpyridine ligands. Basically, all Ru catalysts are homogeneous, while Ir catalysts have more variations. Detailed information about how to influence the photochemical and photophysical properties of Ir catalysts through modification of ligands will be discussed as below.

Ir-centered visible light photoredox catalysts can be divided into two categories according to the types of ligands coordination, Homoleptic Iridium Photocatalysts and Heteroleptic Iridium Photocatalysts.

### 1.2.3.1 Homoleptic Iridium Photocatalysts

The most classic Homoleptic Iridium Photocatalysts is *fac*-$Ir(ppy)_3$ (**Scheme 11**). The role of *fac*-$Ir(ppy)_3$ in Ir catalysts is equivalent to that of $Ru(bpy)_3^{2+}$. The research on the photochemical and photophysical properties of *fac*-$Ir(ppy)_3$ can be traced back to early 1980s[30]. The study on the excited state of *fac*-$Ir(ppy)_3$ has never stopped[31].

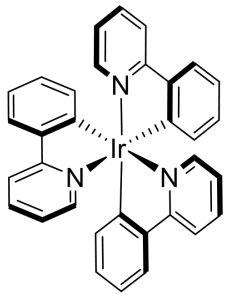

*fac*-$Ir(ppy)_3$

| Item | *fac*-$Ir(ppy)_3$ |
|---|---|
| $E_{1/2}$ ($Ir^+$/ Ir *) (v) | -1.73 |
| $E_{1/2}$ ( Ir */ $Ir^-$) (v) | 0.31 |
| $E_{1/2}$ ( $Ir^+$/ Ir ) (v) | 0.77 |
| $E_{1/2}$ ( Ir */ $Ir^-$) (v) | -2.19 |
| Excited-state Lifetime (ns) | 1900 |
| Excitation λmax (nm) | 375 |
| Emission λmax (nm) | 494 |

**Scheme 11**: photophysical and photochemical properties of *fac*-$Ir(ppy)_3$

As one of the most common Iridium photocatalysts, *fac*-$Ir(ppy)_3$ is widely used in the field of organic synthesis[32], such as formation of C-P bond[33], direct arylation of arenes and heteroarenes (**Scheme 12**)[34], and synthesis of nitrones[35].

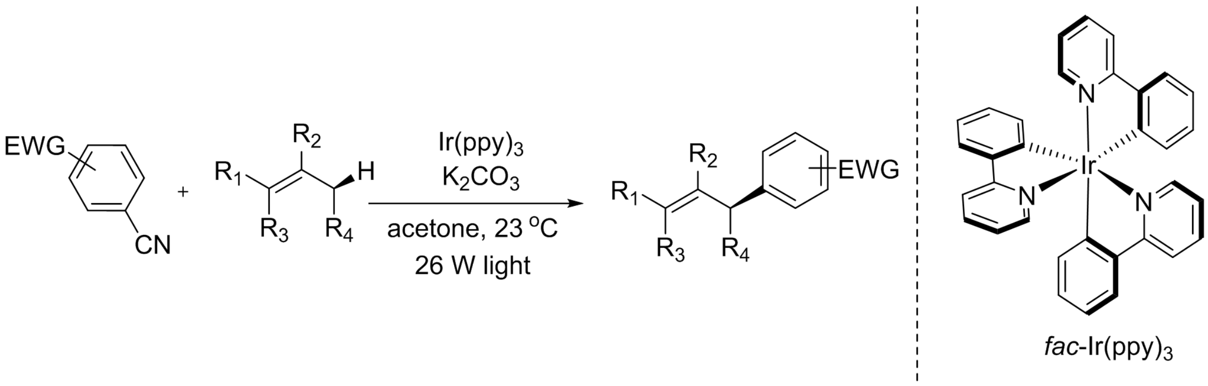

**Scheme 12**: *fac*-Ir(ppy)$_3$ catalyzed arylation of arenes

Other homoleptic Iridium photocatalysts are mostly modified on the basis of fac-Ir(ppy)$_3$. By modifying the ligand, the properties of the catalysts can be effectively affected (**Scheme 13**). For example, adding electron-withdrawing substituents such as F and trifluoromethyl to benzene can increase the π-accepting ability of the ligands, thereby correspondingly reducing the energy of the π anti-bonding orbital[36]. Such modification can further stabilize the MLCT state, and increase its oxidative ability at the same time[37].

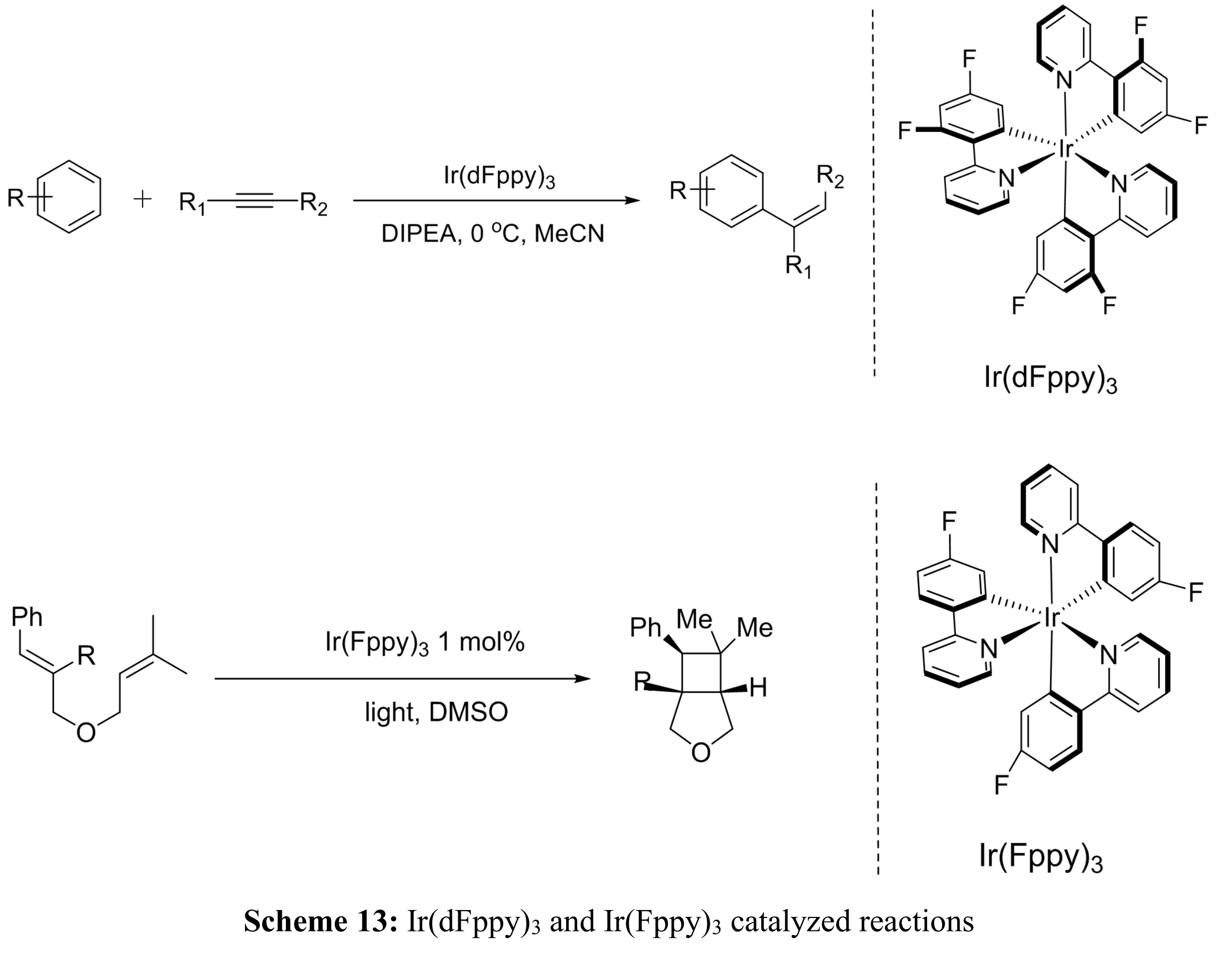

**Scheme 13:** Ir(dFppy)$_3$ and Ir(Fppy)$_3$ catalyzed reactions

### 1.2.3.2 Heteroleptic Iridium Photocatalysts

Homoleptic Iridium photocatalysts are generally neutral, while heteroleptic Iridium photocatalysts are mostly cation complexes of Ir. The currently known heteroleptic Iridium photocatalysts normally replace one of the phenylpyridine ligands with a bipyridine ligand. In this case, the LUMO of the complex is located on the bipyridine ligand, while the HOMO lies on the metal center and phenyl ring of the phenylpyridine. Since HOMO and LUMO are almost orthogonal, the reduction and oxidation abilities of the complex can be individually controlled by modifying the ligand without affecting each other. In this way, the complex can be selectively modified the according to the different requirements of the reactions. The most commonly used heteroleptic Iridium photocatalyst is $Ir(ppy)_2(bpy)^+$, which replaces one of $Ir(ppy)_3$'s phenylpyridine ligand with bipyridine ligand (**Scheme 14**)[38]. And most of the other heteroleptic Ir catalysts are also modified on the basis of $Ir(ppy)_2(bpy)^+$.

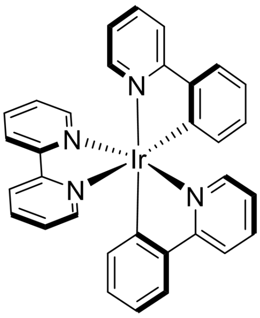

$Ir(ppy)_2(bpy)^+$

| Item | $Ir(ppy)_2(bpy)^+$ |
|---|---|
| $E_{1/2}$ ($Ir^{2+/+*}$) / V | -1.17 |
| $E_{1/2}$ ( $Ir^{+*/0}$ ) /V | +1.01 |
| $E_{1/2}$ ( $Ir^{+/0}$) / V | +1.24 |
| $E_{1/2}$ ($Ir^{2+/+}$) / V | -1.40 |
| Excited-state Lifetime (ns) | 337 |
| Excitation λmax (nm) | 336 |
| Emission λmax (nm) | 550 |

**Scheme 14:** photophysical and photochemical properties of $Ir(ppy)_2(bpy)^+$

$Ir(ppy)_2(bpy)^+$ not only has excellent photochemical and photophysical properties, but also has excellent redox electrochemical properties, so it has a very wide range of applications in organic synthesis, such as formation of C-P bond[35], synthesis of nitrones[33], amongst others (**Scheme 15**).

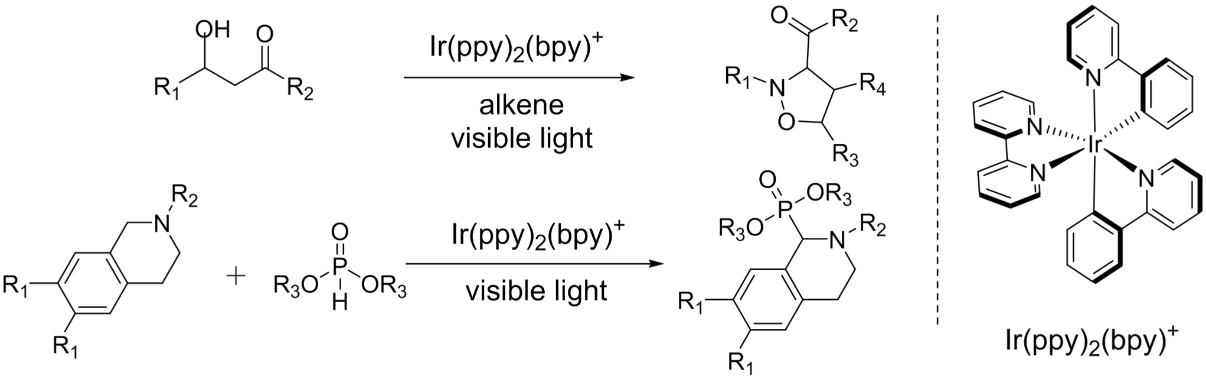

Scheme 15: Ir(ppy)$_2$(bpy)$^+$ catalyzed photoreactions

Adding electron-withdrawing substituents, such as trifluoromethyl or fluorine, to the phenylpyridine ligands can effectively increase the π electron accepting capacity of the ligand, and thus reducing the metal electron density and enhancing the oxidation ability. In 2015, the Knowles research group continuously reported the alkene amidation reaction achieved through SET process with Ir(dFCF$_3$ppy)$_2$(bpy)$^+$ as photocatalyst (**Scheme 16**)[39].

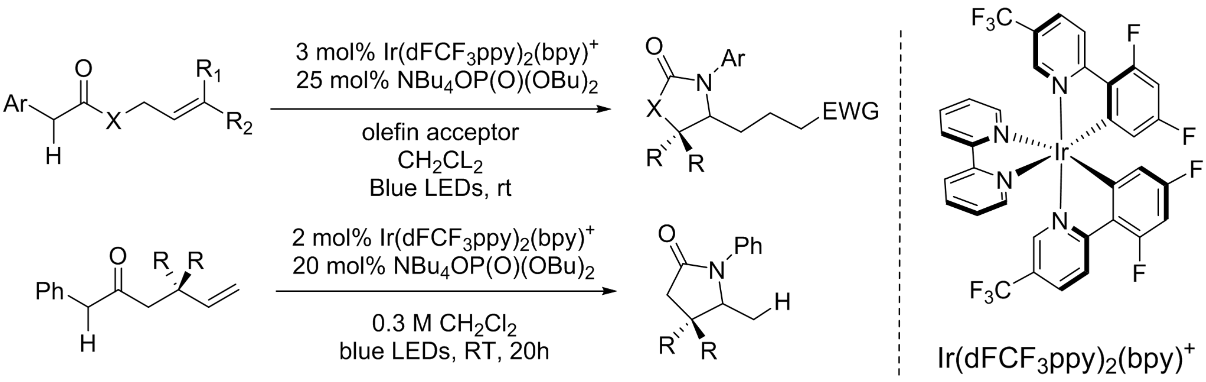

Scheme 16: Ir(dFCF$_3$ppy)$_2$(bpy)$^+$ catalyzed alkene amidation reaction

Add electron-donating groups, such as *tert*-butyl substituents, to the bipyridine ligand of Ir(ppy)$_2$(bpy)$^+$ and then Ir(ppy)$_2$(dtbbpy)$^+$ can be obtained (**Scheme 17**). This di-*tert*-butyl-substituted analogue enables a variety of transformations due to its fine-tuned oxidizing and reducing power. The Macmillan research group used Ir(ppy)$_2$(dtbbpy)$^+$ as a photocatalyst to continuously achieve a series of reactions, such as α-trifluoromethylation of aldehydes[40], α-heteroarylation of amine[41], selective radical-radical cross-couplings[42].

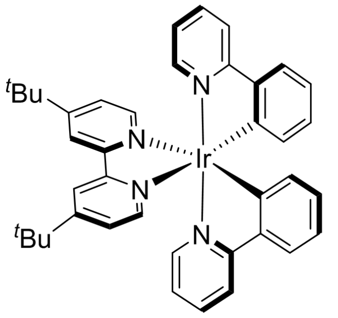

$Ir(ppy)_2(dtbbpy)^+$

| Item | $Ir(ppy)_2(bpy)^+$ |
|---|---|
| $E_{1/2}$ ($Ir^{2+/+*}$) / V | -0.96 |
| $E_{1/2}$ ( $Ir^{+*/0}$ ) /V | +0.66 |
| $E_{1/2}$ ( $Ir^{+/0}$) / V | +1.21 |
| $E_{1/2}$ ($Ir^{2+/+}$) / V | -1.51 |
| Excited-state Lifetime (ns) | 557 |
| Emission λmax (nm) | 550 |

**Scheme 17:** Photochemical and photophysical properties of $Ir(ppy)_2(dtbbpy)^+$

Compared with $Ir(ppy)_2(bpy)^+$, its di-*tert*-butyl-substituted analogue $Ir(ppy)_2(dtbbpy)^+$ has superior photochemical and photophysical properties. Since the HOMO and LUMO of heteroleptic Iridium photocatalysts are orthogonal, the ligands can be modified specifically. The LUMO of heteroleptic Ir complex is located on the bipyridine ligand. Therefore, adding the electron-donating group di-*tert*-butyl substituent on the bipyridine increases the electron density on the bipyridine, thereby increasing the LUMO orbital energy and the excited state of MLCT. This change will not significantly affect the lifetime of the MLCT state of $Ir(ppy)_2(dtbbpy)^+$, but the increase in the energy of the excited state can enable it to have a greater catalytic driving force.

Therefore, most of the other heteroleptic Iridium photocatalysts are modified from the benzopyridine ligand of $Ir(ppy)_2(dtbbpy)^+$ (**Scheme 18**). For example, when adding electron-donating substituents to the benzopyridine ligand, such as methyl and *tert*-butyl, it will effectively increase the electron density on the benzopyridine ligand, thereby increasing the electron density of the metal center Ir. This change increases the reducibility of the catalyst, so that it can better and more widely catalyze reductive reactions.

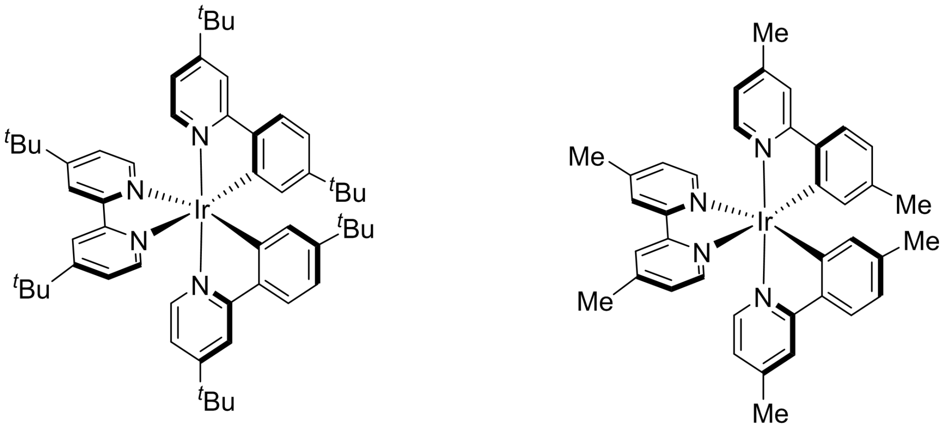

$Ir(dtbppy)_2(dtbbpy)^+$ $Ir(dmppy)_2(dtbbpy)^+$

**Scheme 18:** Structure of $Ir(ppy)_2(dtbbpy)^+$ and $Ir(ppy)_2(dtbbpy)^+$

This change can be directly reflected through the reaction. For example, in the direct *β*-alkylation of aldehydes reaction, a *β*-enaminyl radical needs to be catalyzed by photocatalyst first, and then the *β*-enaminyl radical is added to a Michael acceptor[43]. When $Ir(ppy)_3$ is applied as the catalyst, the yield is only 7%. However, when $Ir(ppy)_2(bpy)^+$ is used as the catalyst under same condition, the yield increases to 80%. Further, when $Ir(dmppy)_2(dtbbpy)^+$ is utilized as photocatalyst, the yield of the reaction will be further improved to 87% (**Scheme 19**). This result shows that the modification of the catalyst can effectively affect its efficiency.

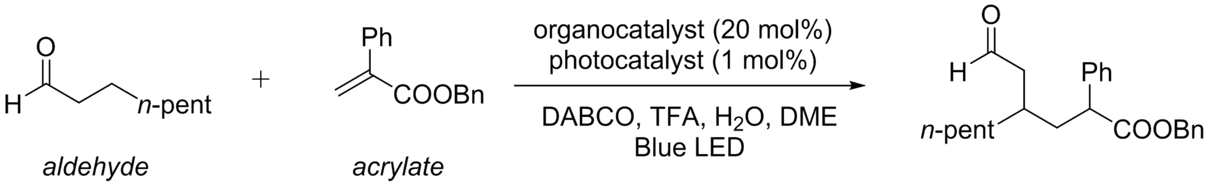

| $Ir(ppy)_3$ | $Ru(bpy)_{32}^{+}$ | $Ir(ppy)_2(dtbbpy)^+$ | $Ir(dmppy)_2(dtbbpy)^+$ | $Ir(dtbppy)_2(dtbbpy)^+$ |
|---|---|---|---|---|
| 7% yield | 50% yield | 80% yield | 84% yield | 56% yield |

**Scheme 19:** Ir catalysts effection in direct *β*-alkylation of aldehydes reaction

When electron-withdrawing substituents are added to the benzopyridine ligand of $Ir(ppy)_2(dtbbpy)^+$, the properties of the catalyst can also be changed in response to the existence of electron-withdrawing groups, which will reduce the electron density on the benzopyridine (**Scheme 20**). Through this change, the electron density around the metal center Ir will be decreased, and the oxidative ability of the catalyst is correspondingly strengthened. These relatively strong oxidizing catalysts can oxidize some functional groups with relatively high oxidation potential, such as carboxylic acid groups, amine, and trifluoroborates[44].

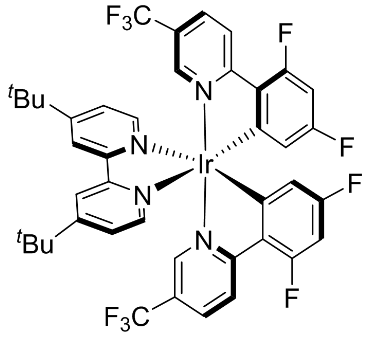

Ir(dFCF$_3$ppy)$_2$(dbtbpy)$^+$

| Item | Ir(ppy)$_2$(bpy)$^+$ |
|---|---|
| $E_{1/2}$ ($Ir^{2+/+*}$) / V | -0.89 |
| $E_{1/2}$ ( $Ir^{+*/0}$ ) /V | +1.21 |
| $E_{1/2}$ ( $Ir^{+/0}$) / V | +1.69 |
| $E_{1/2}$ ($Ir^{2+/+}$) / V | -1.37 |
| Excited-state Lifetime (ns) | 2300 |
| Excitation λmax (nm) | 380 |
| Emission λmax (nm) | 470 |

**Scheme 20:** photochemical and photophysical properties of Ir(dFCF$_3$ppy)$_2$(dtbbpy)$^+$

However, Ir(ppy)$_2$(dtbbpy)$^+$ will cause its benzopyridine ligand to have certain electrophilic properties due to the strong electron withdrawing group on the ligand. As a result, in the reaction systems with carbon radical intermediates, the strong nucleophilic carbon radical may be added to the catalyst ligand. Such side reactions will not only cause the catalyst to lose activity, but also greatly reduce the yield and efficiency of the reaction. Therefore, in this case, it is necessary to further modify the ligands of the catalysts, such as removing the strong electron withdrawing group on the benzopyridine ligand, or adding electron donating groups. By this means, the oxidation performance of the catalyst can be fine-tuned to meet the needs of reaction systems (**Scheme 21**). Ir(dFHppy)$_2$(dbtbpy)$^+$, Ir(dFMeppy)$_2$(dbtbpy)$^+$, and Ir(FMeppy)$_2$(dbtbpy)$^+$ are synthesized under such ligands modification control[45], and their oxidability decreases in turn[46].

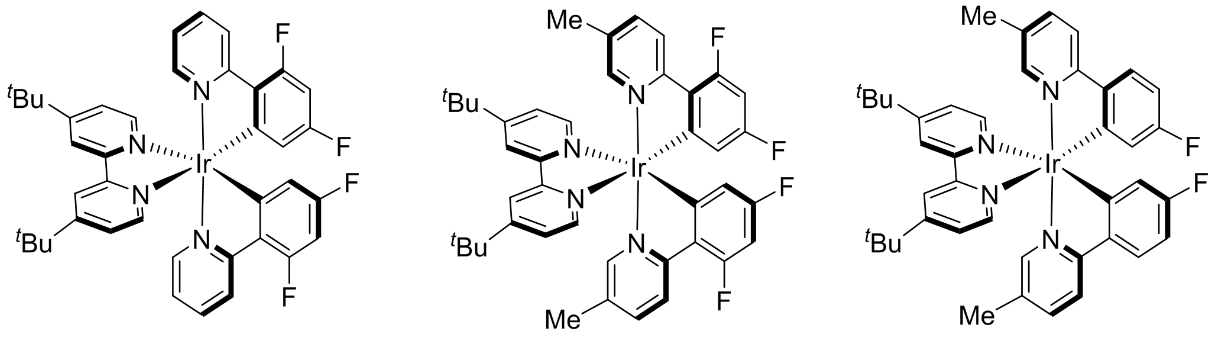

$Ir(dFHppy)_2(dbtbpy)^+$ $Ir(dFMeppy)_2(dbtbpy)^+$ $Ir(FMeppy)_2(dbtbpy)^+$

**Scheme 21:** Structure of $Ir(dFHppy)_2(dbtbpy)^+$, $Ir(dFMeppy)_2(dbtbpy)^+$, and $Ir(FMeppy)_2(dbtbpy)^+$

Such modification can affect the efficiency of the catalytic reaction by adjusting the redox properties of the catalyst. For example, in the photocatalytic decarboxylation of carboxylic acid and vinyl halide, when the strong oxidizing $Ir(ppy)_2(dtbbpy)^+$ is applied as catalyst, the highest yield is only 61%. A large amount of alkylation catalysts were detected in the reaction product, which indicated that the *in-situ* produced carbon radicals were directly added to the catalyst ligands with electrophilic properties. When $Ir(dFMeppy)_2(dbtbpy)^+$ was utilized, the yield of the reaction was increased to 92% (**Scheme 22**), showing that the modification of the catalyst ligand can effectively affect the reaction performance of the catalyst[47].

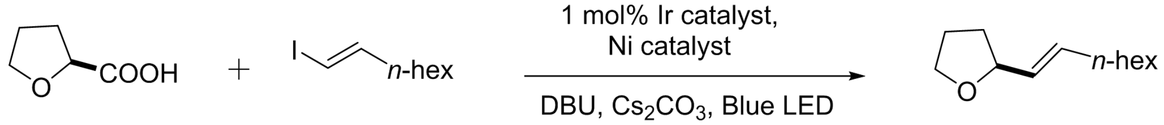

| Ir photocatalyst | Yield |
|---|---|
| $Ir(ppy)_2(dtbbpy)^+$ | 61 % |
| $Ir(dFMeppy)_2(dbtbpy)^+$ | 92 % |

**Scheme 22:** Catalysts influence in photocatalytic decarboxylation of carboxylic acid

The other extreme modification of Ir catalyst is introducing strong electron-withdrawing groups on both benzopyridine ligands and bipyridine ligands (**Scheme 23**). The result of this modification is to greatly reduce the electron density of the metal center, thereby greatly enhancing its oxidation ability, such as $Ir(dFCF_3ppy)^2(5,5\text{-}bpy)^+$[48]. Such a catalyst can be applied to some strong oxidation systems, and can also be adapted to the reaction systems which is sensitive to reducing agents to avoid side reactions[49].

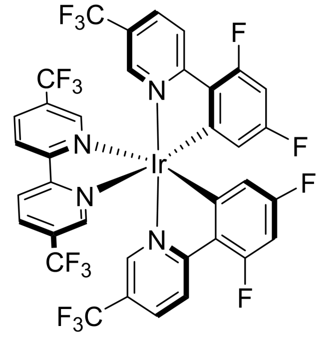

Ir(dFCF$_3$ppy)$_2$(5,5bpy)$^+$

**Scheme 23:** Structure of Ir(dFCF$_3$ppy)$^2$(5,5-bpy)$^+$

## 1.2 On the path to utilize Fe Complexes as VLPCs

### 1.2.1 Advantages and limitations of Fe complex as a potential VLPCs

The common utilized Ir and Ru visible light photoredox catalysts (VLPC) have been discussed in the previous section. However, scientists have never stopped their search for new optical catalysts. Because both Ir or Ru catalysts have relatively large limitations in practical applications. These limitations are mainly reflected in 1. Both Ir and Ru are precious metals, and their low output and high price make them impossible to be applied on a large scale in actual industrial production. 2. Ir and Ru are both toxic as heavy metals. In the post-processing process, careful and scientific measures must be taken to prevent them from spreading into the natural environment and causing pollution.

In recent years, the interest of replacing the rare metal VLPCs (Ir, Ru) by more earth abundant alternatives has been growing significantly. Compared with 4d and 5d metals, 3d metals are cheaper and easier to obtain. So, there is no doubt that these metals have also been relatively extensively studied, such as Zr, Mo, Ce, W, Cu[50] or U and so on. However, among all 3d metals, Fe is, to some extent, the perfect alternative[51].

1. Fe is the fourth most common element in the Earth's crust. If calculated by mass, Fe is the most abundant element on the earth (32.1%). It is by far the most common-used and important metal in society.

2. Fe is one of the most environmentally friendly metals among the metals currently known. It is the most important element among the dozens of trace elements necessary for the human body. At the same time, it is the most important metal element of the most important photochemical reaction on earth - photosynthesis,

3. Fe and Ru are in the same group, so there is a certain similarity in chemical properties. Fe complexes have exhibited good optical properties, such as absorption and emission properties in the visible light region, and good electrochemical properties. In addition, Fe complexes also perform well in catalytic reactions such as photolysis of water[52]. Also, $d^6$ metal, Fe complexes are expected to exhibit optical properties similar to Ru.

Fe-nitrogen coordination complexes were also the first to be studied as potential optical catalysts. In 2000, McCusker's research group reported an Iron(II) polypyridyl complex with femtosecond MLCT excited-state[53]. In this report, tris(2-pyridylmethyliminoethyl)amine was applied as a ligand for the Fe(II) complex **FeC-1** (**Scheme 24**), reaching $^1$MLCT excited state upon irradiation at 400 nm. However, the lifetime of this excited state is extremely short, and only a time of less than 100 fs was reported. The result shows that the iron complex can have good absorption and emission in the visible light region, and can effectively enter the excited state. However, the femtosecond level of its lifetime is far from comparable to the hundreds of nanoseconds lifetime of Ru complexes. This result did not dispel scientists' enthusiasm for the study of iron complexes, because it also demonstrated the possibility of Fe-based compounds as potential optical catalysts.

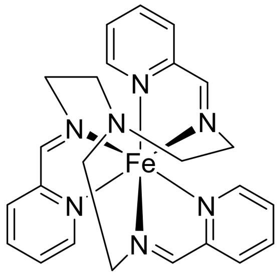

**FeC-1**

**Scheme 24**: **FeC-1** with 100 fs lifetime MLCT state

The most classic Ru-centered photocatalyst is undoubtedly the bipyridine complex of Ru. In 2007, Chergui's group conducted research on the photodynamic properties of Fe bipyridine complexes (**Scheme 25**)[54]. Regrettably, this most classic ligand in Ru-centered optical catalysts does not have the same effect in Fe. In the study, iron(II)-tris(bipyridine) is excited into the $^1$MLCT upon excitation at 400 nm. This state shows an emission band at around 600 nm and ultrafast lifetime of around 20 fs under transient absorption spectrum (TAS) studies. A weak emission around 660 nm was also observed, and attributed to the $^3$MLCT, which is transferred through intersystem crossing (ISC) soon after the $^1$MLCT state.

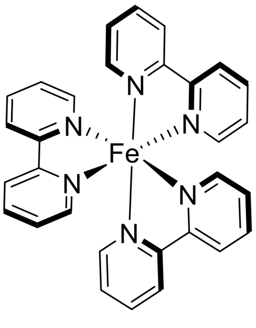

**FeC-2**

**Scheme 25:** **FeC-2** with 120 fs lifetime MLCT state

In fact, the TAS studies show two different stages of stagnation of excited states, among which the extremely fast excited state that absorbs below 400 nm is $^3$MLCT, and the other longer lived excited state absorption decay was attributed as the lowest excited high-spin quintet state $^5T_2$ lifetime, which is photo-inactive in photo catalysis. The whole process can be summarized as that Fe(II)-tris(bipyridine) enters the excited state of $^1$MLCT after absorbing light, and changes to $^3$MLCT *via* intersystem charge transfer within the ultrafast time. After being retained for less than 150 fs, it further rapidly passivation into the metal centered state (MC) (**Scheme 26**).

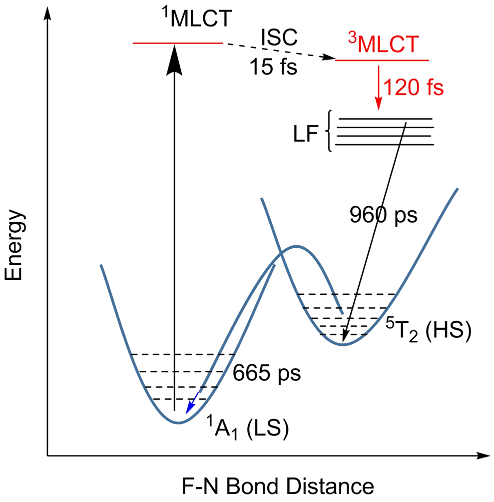

**Scheme 26:** Deactivation process of excited state for **FeC-2**

Therefore, the Fe(II)-tris(bipyridine) complex does not exhibit excellent photophysical properties similar to Ru(II)-tris(bipyridine). There are two reasons for this situation: one is that the energy of $^3$MLCT is too high, and the other is that the energy of the Metal-centered state is too low. This energy difference, which is the opposite of $Ru(bpy)_3^{2+}$, makes $Fe(bpy)_3^{2+}$ unable to exist in the $^3$MLCT excited state for a long time, but transfers to the MC state within ultrafast time, and then returns to the ground state.

In fact, all other Fe-centered complexes have such a problem, which is also the biggest reason why iron has not been a substitute for Ru so far. The core of this reason is the nature of Fe as a 3d$^6$ metal. As d$^6$ metal, iron complexes are six-coordinated and have a regular octahedral structure like ruthenium[55]. In the normal octahedral ligand field, the d orbitals of the metal will split into the $t_{2g}$ and $e_g$ levels. In general, the complex is not a perfectly symmetrical regular octahedral structure since the metal ligands are usually bidentate or tridentate. This will have a certain impact on the splitting of the metal d orbital, but the trend of the deviation in the influence of external factors stays unchanged. In order to have a better understanding and a relatively more precise explanation, $d_{xy}$, $d_{xz}$, and $d_{yz}$ of the five degenerate orbitals of d-orbital were defined as $t_{2g}$ and orbitals derived from $d_{x2-y2}$ and $d_{z2}$ were defined as $e_g$ or $e_g$*.

Compared to 3d transition metals, the metal-ligand interactions of 4d and 5d metal complexes are stronger. This results in a stronger ligand field splitting, which leads to $e_g$* orbitals and $t_{2g}$ orbitals to split with each other more effectively. Take $Ru(bpy)_3^{2+}$ as an example, its strong ligand field splitting ability makes its $e_g$* orbitals are so well separated from its $t_{2g}$ orbitals that the energy of the $e_g$* orbitals are even higher than the energy of π* orbitals of the bipyridine ligands. Thus, the lowest unoccupied molecular orbital (LUMO) of $Ru(bpy)_3^{2+}$ locates at the bi-pyridine ligands. While the highest occupied molecular orbital (HOMO) locates at the $t_{2g}$ orbitals of the metal center. Therefore, this HOMO orbital filled with 6 electrons has metal character. For $Ru(bpy)_3^{2+}$, the energy needed to excited state $^3$MLCT is the energy required from the $t_{2g}$ orbitals of the metal to the π* orbital of the ligand, and it is also the lowest energy required from HOMO to LUMO. There is no doubt that the energy of the MLCT excited state is higher than that of the MC state. In most cases, radiationless metal centered (MC) triplet or quintet states ($^3$MC/$^5$MC) are responsible for the deactivation of photo-active $^3$MLCT states. However, in $Ru(bpy)_3^{2+}$, this passivation process needs to overcome the energy barriers between its $^3$MLCT and MC state. This is also the reason why the lifetime of $^3$MLCT state of $Ru(bpy)_3^{2+}$ can be as long as hundreds of nanoseconds, that is, the energy barrier in the passivation process from $^3$MLCT excited state to MC excited state effectively extends the existence of MLCT state.

For $3d^6$ Fe complexes, the ligand field splitting ability is quite low due to the relatively weak interaction between the metal and the ligand. This leads to the iron centered $t_{2g}$ orbitals and $e_g$* orbitals fail to split sufficiently. In $Fe(bpy)_3^{2+}$, the energy of the $e_g$* orbital is lower than that of the ligand π* orbital due to insufficient d orbital splitting. Thus, the LUMO locates at the $e_g$* orbital of the metal center. However, due to the d-d transitions between $t_{2g}$ orbitals and $e_g$* orbitals are Laporte-forbidden, the MLCT state is still popular. The final problem is that the energy of MLCT is determined by the transition energy from metal centered $t_{2g}$ orbitals to the π* orbital of the ligand center, while the energy of the radiationless MC state is related to the energy of $t_{2g}$ and $e_g$* orbitals. Obviously, the energy of the MLCT state is much higher than that of the MC state. In this case, the barrierless transition to the lower lying MC states will be conducted in ultra-fast time scale. This is also the problem faced by most Fe-centered complexes (**Scheme 27**).

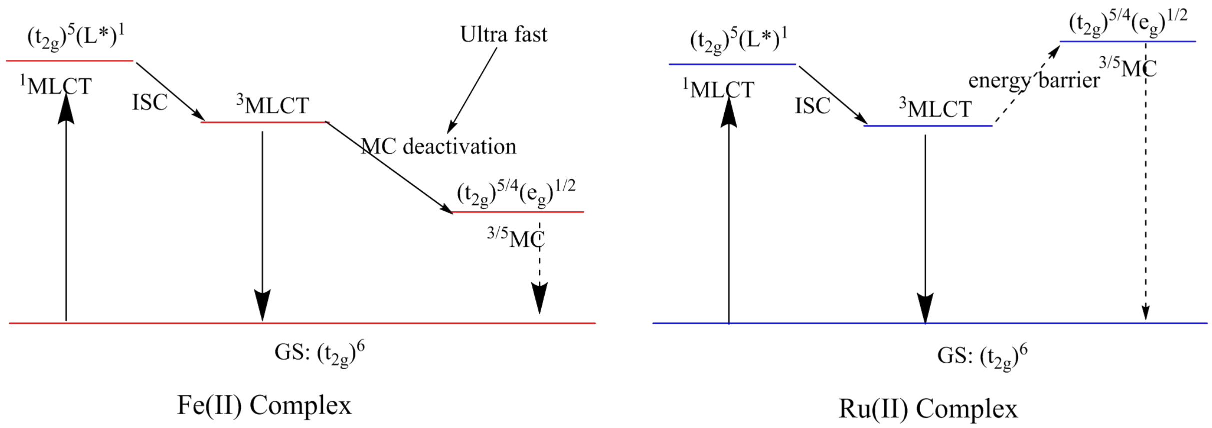

**Scheme 27:** Deactivation processes of Fe(II) complex and Ru(II) complex

## 1.2.2 Strategies to improve the photophysical properties of Fe complex

In summary, for normal iron complexes with very low ligand fields splitting ability, the following deactivation cascade upon irradiation is usually envisaged: excitation from GS into $^1$MLCT, $^3$MLCT, $^3$MC, $^5$MC, GS. Fe complexes generally suffer extremely short-lived MLCT state. If iron complexes are utilized as potential photocatalysts in the future the problem of how to increase the lifetime of photoactive MLCT state of iron complexes must be solved. Based on our knowledge and discussion above, this problem can be divided into two parts:

1. How to decrease the energy of MLCT state of Fe complex

Because the energy of MLCT state of complex is determined by the energy required for the transition from the metal centered $t_{2g}$ orbitals to the ligand centered π* orbital. Therefore, how to reduce the energy of MLCT state can be approximately understood as how to reduce the energy of the ligand π anti-bond orbital, or how to increase the ligand π electron accepting ability. Among the currently known feasible measures, increasing the π-electron conjugate system of the ligand, or adding strong electron-withdrawing substituents on the ligand can be effective.

With the expansion of the π-conjugated system of the ligand, its π electron accepting ability increases as well. Therefore, during the MLCT state, the ligand can more easily accept electrons from the metal center, thereby decreasing the energy of the ligand's π anti-bonding orbital. Similarly, adding a strong electron-withdrawing substituent on the ligand can make the π electron density of the ligand closer to the electron-withdrawing group, thereby increasing the positive charge of the ligand part near the metal center. This action can also greatly reduce the difficulty of transferring electrons from the metal center to the ligand, and thus decreasing the energy of the ligand's π* orbital.

2. How to increase the energy of the MC excited state of the complex

The energy of MC state is more related to the energy of metal centered $e_g$* orbital. Therefore, the core of increasing the energy of the MC excited state is how to increase the energy of the $e_g$* orbital. However, the low $e_g$* orbital energy of Fe complex is due to its weak ligand field splitting ability. Therefore, the core of this strategy can be further attributed to how to enhance the ligand field split of the complex.

For octahedral complexes, one of the feasible ways to increase the ligand field is to use strong $\sigma$ donating ligands. One of such ligands is N-heterocyclic carbenes (NHCs) which features a divalent six-electron carbon atom stabilized by adjacent nitrogen atoms[56]. The extra electron density provided by the NHCs ligands to the metal center can enhance the ligand field, thus destabilize the $e_g$* orbitals. Compared with the influence of $\pi$ electron system on metal center, $\pi$-donation or $\pi$ back-donation, the interaction $\sigma$-donation with the metal center is way more effective (**Scheme 28**).

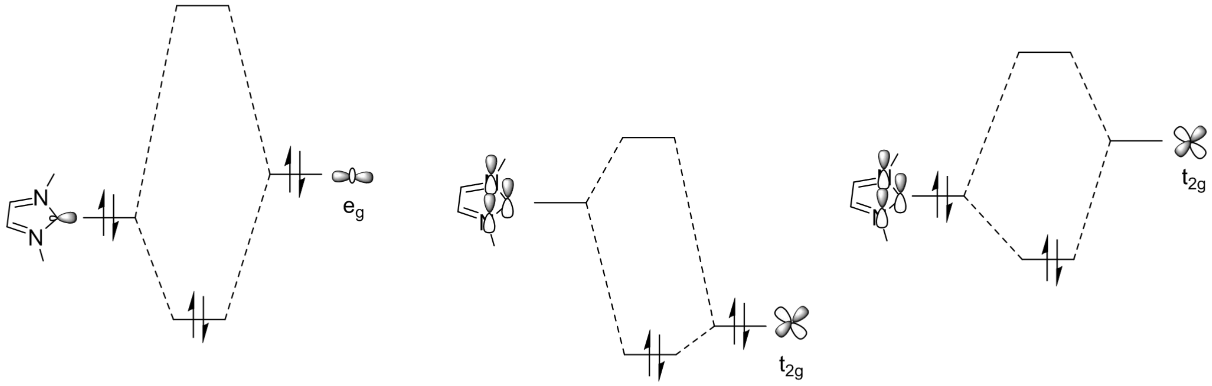

**Scheme 28:** Influence of $\sigma$ donation, $\pi$-acceptor and $\pi$ donation towards metal centered orbitals

Another way to improve the ligand field of the regular octahedral complex is to make the configuration of the regular octahedron more perfect. The more the regular octahedron conforms to the geometric configuration, the stronger its field splitting ability is. However, in reality, it is difficult for us to achieve such a goal, because it is difficult for us to balance the degrees of freedom and conjugation between the ligands. Striving for the realization of perfect configuration will inevitably lose the advance offered by other factors. Thus this strategy can be takek into consideration under appropriate circumstances, instead of designing complexes based on this strategy (**Scheme 29**).

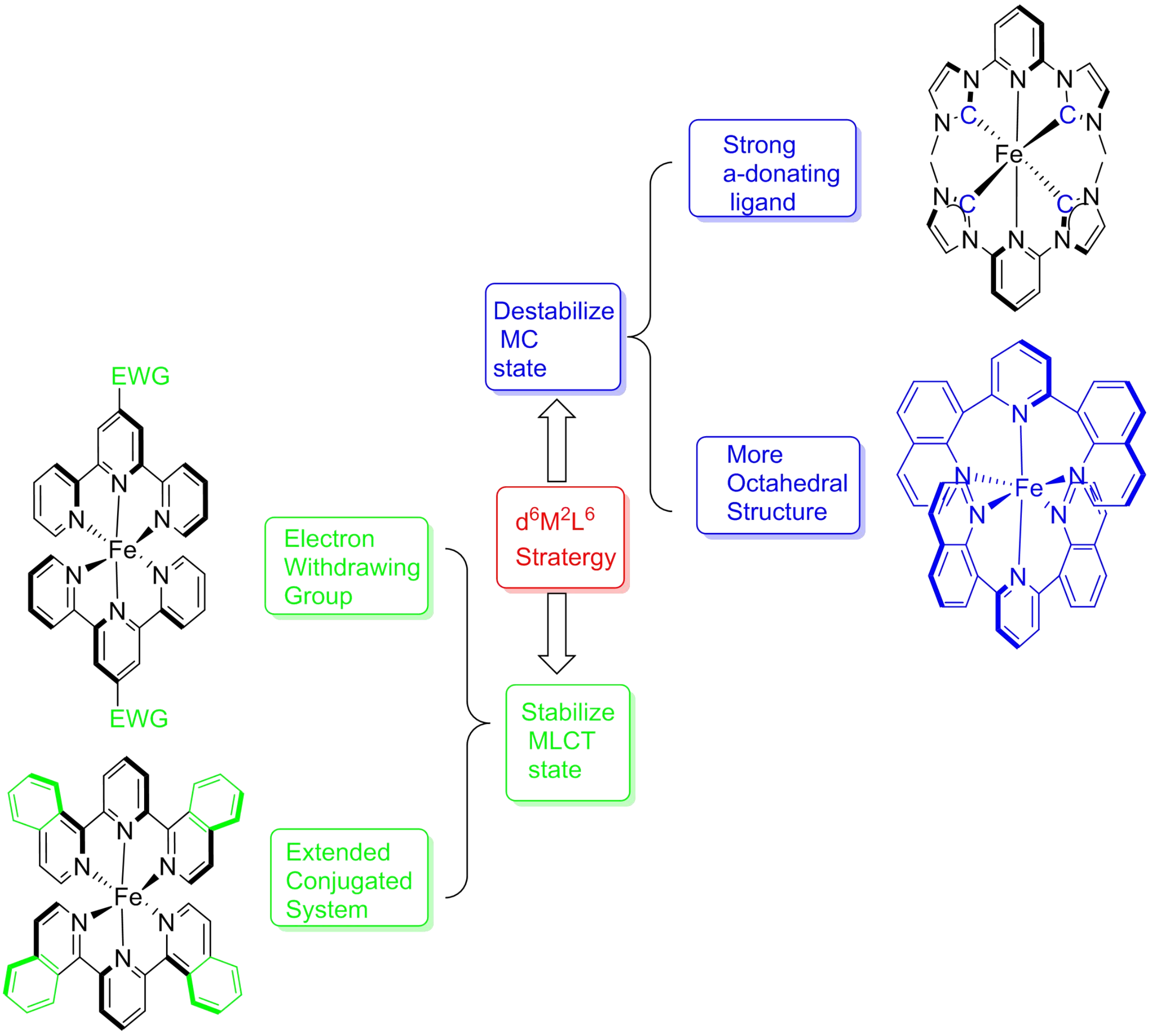

**Scheme 29:** Strategies to improve the photophysical properties of Fe complex

As discussed above, the excited state properties of the complex can be controlled by designing and modifying the complex ligand. However, it is unrealistic to consider all the favorable factors, because some factors themselves conflict with each other to some extent. For example, when adopting strong $\sigma$-donating ligands, NHCs, the $e_g$* orbitals of the complex can be effectively destabilized , and the MC state can thereby be further destabilized. However, the introduction of NHCs ligands will inevitably decrease the π-conjugated system of the ligands, thereby decreasing the π electron accepting ability of the ligands. This reverse effect will increase the energy of the π* orbital of the ligand, which further leads to an increase in the excited state energy of the complex MLCT. However, although these two effects are contradictory, in general, the positive effect of NHCs ligands on the energy change of the MC state is much greater than its negative influence on the $^3$MLCT state energy. Therefore, although it is difficult to take all the beneficial effects into account, the modification which brings the most positive impact can be chosen.

In addition, while studying how to improve the lifetime of $^3$MLCT state, one must also consider the changes of other properties of the complex affected by the decoration of the ligand, such as the electrode potential and optical absorption. For an excellent photo catalyst, these chemical properties are also very important. For instance, when increasing the lifetime of MLCT state through stabilizing $^3$MLCT state, one may encounter low excited state energy resulting in low reaction driving force. Thereby greatly reducing the practical application function of the catalyst. Similarly, when adopting the strategy of introducing strong $\sigma$-donating ligands, thereby increasing the energy of the MC state and extending the lifetime of $^3$MLCT state, it will lead to the destabilization of $t_{2g}$ orbitals due to the high electron density around the metal center. This will finally result in a more negative effect towards the Fe(III/II) oxidation potential , that is, weaken the oxidation ability of complex.

In the past ten years, this field has attracted the attention of many chemists. Although the short lifetime of the excited state of iron complexes has not been perfectly solved, with the efforts of many scientists, especially the introduction of strong $\sigma$-donating ligands NHC ligands, this time-centered number has been firmly moving forward. From the femtosecond-level excited state lifetime of Fe bipyridine complexes to the picosecond-level excited state lifetime of Fe-NHC complexes, to the recent nanosecond-level LMCT excited state lifetime of trivalent Fe-NHC complexes, we are right on the way to utilize iron as solar cells[57].

In fact, almost all the advances in this field in the past ten years are based on the introduction of strong $\sigma$-donating ligands N-heterocyclic carbenes. According to the mechanism of how strong $\sigma$-donating ligands affect the energy of the $e_g$* orbitals, the amount of NHC carbenes in the complex will have a positive correlation with the lifetime of MLCT state. That is, the stronger $\sigma$-donating ligands in the complex, the higher the energy of $e_g$* orbitals will be. The energy of the MC state will increase accordingly, resulting is the corresponding longer lifetime of MLCT state. Therefore, the current development of Fe complexes in this field will be discussed with the classfication of the number of NHCs ligands as follows.

### 1.2.3 Fe-NHC complex with 2 N-heterocyclic carbenes

There are not many homoleptic Fe-NHC Complexes with two N-heterocyclic carbenes coordination sites. On the one hand, although the introduction of strong $\sigma$-donating ligands can strengthen the ligand field splitting ability of Fe complexes, only two N-heterocyclic carbenes cannot effectively increase the energy of $e_g$* orbitals of the complexes. Therefore, the effect on the lifetime of MLCT state is also limited. On the other hand, with two N-heterocyclic carbenes in homoleptic complex, it means that the ligand of this complex can only be two identical tridentate ligands, and there is only one N-heterocyclic carbene in each ligand. This greatly limits the design diversity of this type of complex.

In 2018, the Philippe C. Gros group mentioned an unpublished work in their review. In order to explore the relationship between the number of NHC carbenes and the photophysical properties of the complex, they synthesized a homogeneous Fe-NHC complex **FeC-3** with only 2 NHC ligands[58]. Matthias Bauer's research group also reported the similar complex **FeC-4** in 2018[59]. The difference is the substituent attached to N on the carbene. Although the introduction of strong *σ*-donating ligands will lead to an increase in the energy of the MC state, the influence on the lifetime of MLCT state is not significant. This is because two NHC ligands cannot increase the energy of the MC state to a qualitative change, while it will cause a relative decrease in the conjugated system, reducing the energy of *π** orbital, and correspondingly reducing the energy of the MLCT excited state. Therefore, the positive benefits brought by NHC ligands are partially offset, resulting in the lifetime of the MLCT of 120 fs and 100 fs respectively (**Scheme 30**).

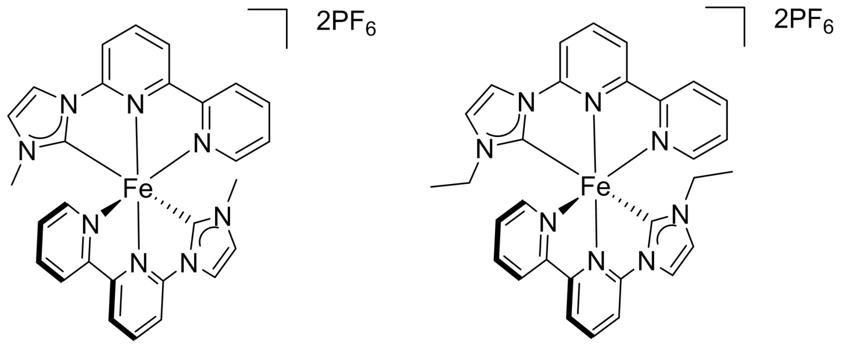

**FeC-3** **FeC-4**

| Fe Complex | **FeC-3** | **FeC-4** |
|---|---|---|
| λ abs max / nm | 560 | 557 |
| Lifetime of MLCT | 120 fs | 100 fs |
| $E_{1/2}$ (FeIII/II) / V vs. NHE | 1.08 | 1.07 |
| $E_{1/2}$ ($L^-$/0) / V vs. NHE | -1.11 | -1.11 |

**Scheme 30**: Structures, and photo properties of **FeC-3** and **FeC-4**

The introduction of two NHCs in homoleptic Fe-NHC Complexes not only fails to bring about a qualitative change to the energy change of MC state, but also causes an increase in the energy state of MLCT. This inevitable positive effect offset effect can be solved in heteroleptic Fe-NHC complexes. Because in heteroleptic Fe-NHC complexes, one can introduce NHC ligand into one ligand to destabilize the MC state. At the same time, one can introduce a large conjugated system into another ligand to stabilize the MLCT state, thus solved the problem.

Matthias Bauer's research team reported the research work of heteroleptic Fe-NHC complex **FeC-5** with two N-heterocyclic carbenes in 2017[60]. He connected 2,6-diisopropylphenyl substituent to the carbene ligands to compensate for the loss of the conjugation system caused by the introduction of NHC ligands. The original intention of this research is to destabilize MC state through bis-NHC ligand, while ensuring the intense absorption of complex through the tripyridine ligand. However, **FeC-5** is not successful from the perspective of improving the lifetime of MLCT states. This is because the π* orbital of **FeC-5** is determined by the tripyridine ligand, therefore, the 2,6-diisopropylphenyl substituent added to the NHC ligands cannot effectively stabilize the π* orbital, it will affects the interaction between the ligand and the metal due to the large steric hindrance. As a result, although **FeC-5** complex introduced strong *σ*-donating ligands, the complex still only has less than 100 fs of MLCT state lifetime (**Scheme 31**).

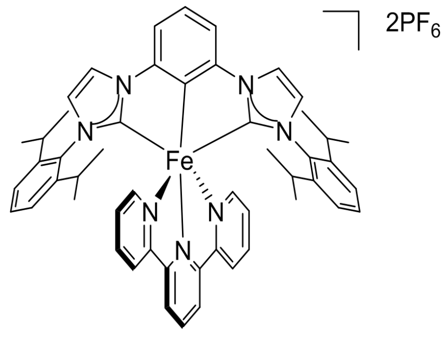

**FeC-5**

| Fe Complex | **FeC-5** |
|---|---|
| λ abs max / nm | 502, 540 |
| Lifetime of MLCT | < 100 fs |
| $E_{1/2}$ (FeIII/II) / V vs. NHE | 1.19 |
| $E_{1/2}$ ($L^-$/0) / V vs. NHE | -1.02 |

**Scheme 31**: Structure, and photo properties of **FeC-5**

The work of the Philippe C. Gros research group in 2018 reported a heteroleptic Fe-NHC complex **FeC-6**[61]. The difference from **FeC-5** is that this work did not make additional conjugation modifications to the bi-NHC ligand. Instead, they connected an additional pyridine to the tri-pyridine ligand to further expand the π-conjugated system (**Scheme 32**).

Since the $e_g^*$ orbital and $\pi^*$ orbital of the complex are orthogonal, which means that the $e_g^*$ orbital and the $\pi^*$ orbital are determined by the bi-NHCs ligand and *tert*-pyridine ligand respectively, and they will not interfere with each other. In this case, the extension of the partial conjugation of the pyridine ligand can effectively reduce the energy of the MLCT state by stabilizing the $\pi^*$ orbitals. Similarly, the introduction of NHCs ligands can effectively destabilize MC states by increasing the energy of $e_g^*$ orbitals. Through such hybrid coordination, more ideas and strategies can be provided for the design of Fe-NHC complexes in the future. Compared with **FeC-5**, the design strategy of **FeC-6** is more reasonable, and it naturally shows better photophysical properties with 2.7 ps lifetime of MLCT.

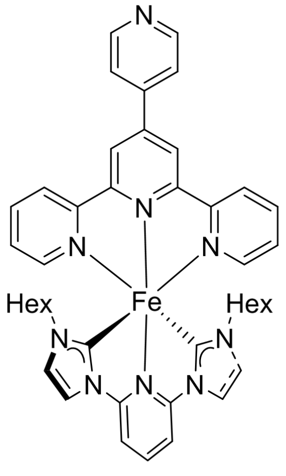

**FeC-6**

| Fe Complex | **FeC-6** |
|---|---|
| λ abs max / nm | 373,522,560 |
| Lifetime of MLCT | 2.7 ps |
| $E_{1/2}$ (FeIII/II) / V vs. NHE | 0.56 |
| $E_{1/2}$ ($L^-$/0) / V vs. NHE | -1.65 |

**Scheme 32**: Structure, and photo properties of **FeC-6**

In 2018, Matthias Bauer's research group modified **FeC-6** to obtain **FeC-7**. The ultimate goal of this work is to connect an additional Co complex to the 2-ylidene]pyridine ligand to form **FeC-8**, in order to study the effect of the additional system on the excited state of the Fe complex[62]. The modification of replacing the *n*-hexyl group in **FeC-6** with 2,6-diisopropylpheny (DIPP) does not have a positive effect on **FeC-7**. Just like **FeC-5**, DIPP will weaken the interaction between the metal and the ligand due to the huge steric hindrance, which will counteract the increase of the $e_g^*$ orbital energy. The TAS results also show that the MLCT lifetime of **FeC-7** is lower than that of **FeC-6**, only 1.1 ps.

For **FeC-8**, although Co complex can enhance the π electron accepting ability of *tert*-pyridine ligand to some extent, this additional Co complex is too far away from the center of Fe complex, so it is not very effective in affecting the overall excited state of **FeC-8**. Therefore, **FeC-8**'s MLCT excited state lifetime will show a limited improvement over **FeC-7**. As inferred, the MLCT lifetime of **FeC-8** has been slightly improved, 1.4 ps (**Scheme 33**). However, such a complicated system will lead to more complicated UV-Vis absorption spectra, cyclic voltammetry and other photophysical properties.

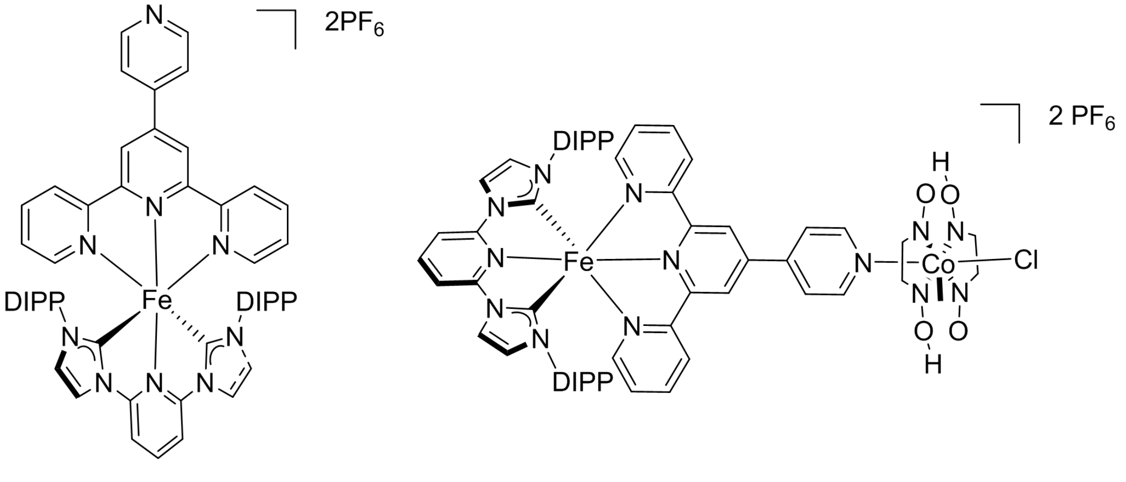

**FeC-7** **FeC-8**

| Fe Complex | **FeC-7** | **FeC-8** |
|---|---|---|
| λ abs max / nm | 515,553,630 | 379,520,558,630 |
| Lifetime of MLCT | 1.1 ps | 1.4 ps |
| $E_{1/2}$ (FeIII/II) / V vs. NHE | 1.23 | 1.26 |
| $E_{1/2}$ ($L^{-}$/0) / V vs. NHE | -1.13$^{a}$ | -0.27$^{a}$ |

*a* : irreverisible

**Scheme 33**: Structures, and photo properties of **FeC-7** and **FeC-8**

## 1.2.4 Fe-NHC complex with 3 N-heterocyclic carbenes

In the study on the relationship between the photophysical properties of Fe-NHC complex and the number of N-heterocyclic carbenes published by Matthias Bauer's research group in 2018, the complex **FeC-9** of 3 NHCs ligand was involved[58]. Based on the complex in **FeC-5**, one of the lateral pyridines in the tri-pyridine ligand was further replaced with NHC. Stronger $\sigma$-donating ligand NHC results in a larger splitting of the metal d orbitals. With the further increase of the energy of $e_g$* orbitals, the MLCT state can be better stabilized. TAS shows an excited state lifetime of 3.6 ps for **FeC-9**, which illustrates the great effect of strong $\sigma$-donating ligand in enhancing the ligand field(**Scheme 34**).

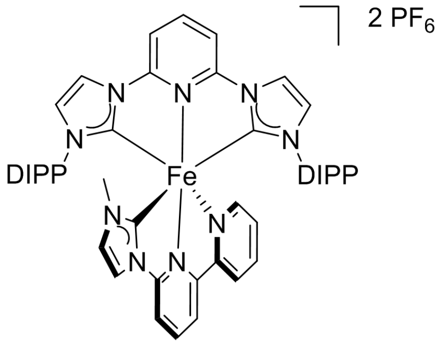

**FeC-9**

| Fe Complex | **FeC-9** |
|---|---|
| λ abs max / nm | 409,466,506,538 |
| Lifetime of MLCT | 3.6 ps |
| $E_{1/2}$ (FeIII/II) / V vs. NHE | 1.09 |
| $E_{1/2}$ ($L^-$/0) / V vs. NHE | -1.30$^a$ |

*a* : irreverisible

**Scheme 34**: Structure, and photo properties of **FeC-9**

In 2018, Antonio Monari's group reported the homoleptic Fe complex with 3 N-heterocyclic carbenes **FeC-10**[63]. This work demonstrated the *fac*- and *mer*- configurations of **FeC-10**. The mechanism of the excited state decay has been studied in detail. This work did not characterize the lifetime of MLCT state. However, from the existing strategy and the structure of **FeC-10**, the three NHC coordination sites will further enhance the ligand field splitting ability. However, the replacement of pyridine with NHCs will further reduce the conjugation system of the ligand. Therefore, compared to the FeC complex mentioned earlier, **FeC-10** has the highest energy MC excited state, but it also has the highest energy MLCT excited state. The lifetime of its MLCT can be predicted around 2 ps (**Scheme 35**).

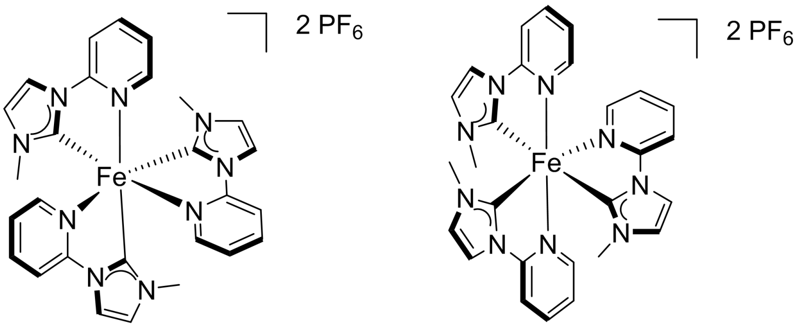

*fac*-**FeC-10**    *mer*-**FeC-10**

| Fe Complex | **FeC-10** |
|---|---|
| λ abs max / nm | 430 |
| Lifetime of MLCT | - |
| $E_{1/2}$ (FeIII/II) / V vs. NHE | 0.89 |
| $E_{1/2}$ ($L^-$/0) / V vs. NHE | -1.73$^a$ |

*a* : irreverisible

**Scheme 35**: Structures, and photo properties of **FeC-10**

Philippe C. Gros research group reported Fe(II) Complexes **FeC-11** with 3 N-heterocyclic carbenes in 2019[64]. This work uses triethylamine to fix the orientation of each ligand, thereby solving the separation difficulties caused by the two different configurations of **FeC-10**, finding a way to easily synthesize *fac*-FeNHC complex **FeC-11**. Similar with **FeC-10**, **FeC-11** has a relatively high-energy $e_g$* orbit, but it also has a relatively high-energy π* energy. As a result, FeC-11 exhibited a MLCT state lifetime of 2-3 ps. This result is in line with our reasoning and expectations(**Scheme 36**).

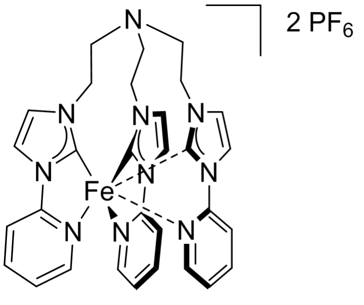

**FeC-11**

| Fe Complex | **FeC-11** |
|---|---|
| λ abs max / nm | 438 |
| Lifetime of MLCT | 2-3 ps |
| $E_{1/2}$ (FeIII/II) / V vs. NHE | 0.85 |
| $E_{1/2}$ ($L^-$/0) / V vs. NHE | -1.70[a] |

*a* : irreverisible

**Scheme 36**: Structure, and photo properties of **FeC-11**

## 1.2.5 Fe-NHC complex with 4 N-heterocyclic carbenes

Kenneth Waörnmark's research group first reported the introduction of N-heterocyclic carbene ligands as strong *σ*-donating ligands to stabilize the MLCT state of Fe(II) complexes in 2013. This work used 2,6-bis(imidazol-2-ylidene)pyridine as the ligand to synthesize the Fe-NHC complex **FeC-12** of hexacoordinate-4 NHCs-2 pyridine[65]. The four NHC coordination sites can more powerfully enhance the ligands field splitting effect of the complex on the metal d orbital. The energy of $e_g$* orbitals of **FeC-12** has been further improved, and destabilize the MC state to the point close to the energy of the MLCT state. Although the complex has no additional conjugation compensation, the positive effects brought by the four NHCs ligands are far greater than the negative effects, and finally **FeC-12** exhibits the MLCT lifetime of 9 ps.

This result is a huge breakthrough, and it has also greatly encouraged other scientists to conduct in-depth research in this field. In fact, a considerable part of the subsequent series of Fe-NHC complexes are all substituted and modified on the basis of **FeC-12**. In the same research work, they also reported **FeC-13**. **FeC-13** replaces the methyl substituent on the **FeC-12** carbene ligand nitrogen with *tert*-butyl substituent. However, this substituent will hinder the interaction between the ligand and the metal center due to its large steric hindrance.

The results of the TAS test also show lifetime of **FeC-13** MLCT state is significantly lower than that of **FeC-12**, only 0.3 ps (**Scheme 37**). The negative effect brought by the *tert*-butyl substituent of **FeC-13** also exceeded our expectations, indicating that the steric hindrance caused by the substituents should also be carefully considered when designing or modifying new Fe complexes.

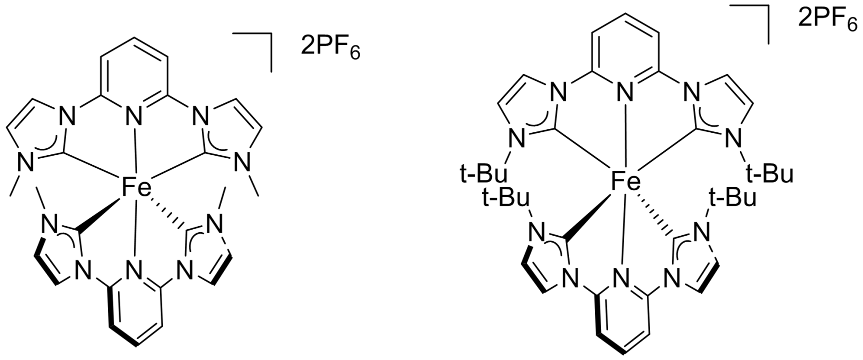

**FeC-12** **FeC-13**

| Fe Complex | **FeC-12** | **FeC-13** |
|---|---|---|
| λ abs max / nm | 457 | 478 |
| Lifetime of MLCT | 9 ps | 0.3 ps |
| $E_{1/2}$ (FeIII/II) / V vs. NHE | 0.94 | 1.03 |
| $E_{1/2}$ ($L^-$/0) / V vs. NHE | -1.76 | -1.72 |

**Scheme 37:** Structures, and photo properties of **FeC-12** and **FeC-13**

The **FeC-14** reported by Matthias Bauer's group in 2017[60] and **FeC-15** reported by Philippe C. Gros's group in 2014[61] both belong to the derivatives of **FeC-12**. They replaced the methyl substituents on the NHCs with isopropyl and hexyl respectively on the basis of **FeC-12**. Since isopropyl is two-dimensional, its steric hindrance is much smaller than that of three-dimensional *tert*-butyl. **FeC-14** also exhibited lifetime between **Fec-12** and **FeC-13**, 8.1 ps, which is in consistent with our inference. This result shows that the decrease of steric hindrance can indeed help stabilize the MLCT state. In our expectation, **FeC-15** should have a lower lifetime than **FeC-14**. Surprisingly, **FeC-15** has a lifetime of MLCT states of up to 12 ps (**Scheme 38**). This abnormal result can be explained by the fact that long-chain substituents do not have substantial steric hindrance. Moreover, the long-chain substituents can have possible hyper-conjugation with the conjugated system of the ligands, which plays an active role in the stabilization of MLCT state.

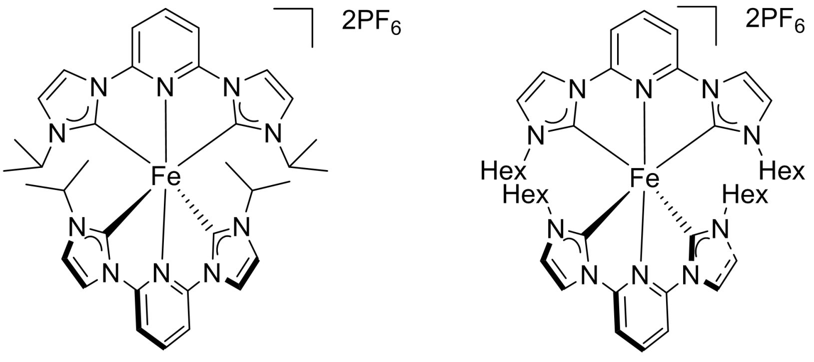

**FeC-14** **FeC-15**

| Fe Complex | **FeC-14** | **FeC-15** |
|---|---|---|
| λ abs max / nm | 458 | 460 |
| Lifetime of MLCT | 8.1 ps | 12 ps |
| $E_{1/2}$ (FeIII/II) / V vs. NHE | 1.06 | 1.04 |
| $E_{1/2}$ ($L^{-}$/0) / V vs. NHE | -1.68$^{a}$ | -1.71$^{a}$ |

*a* : irreverisible

**Scheme 38:** Structures, and photo properties of **FeC-14** and **FeC-15**

Both Philippe C. Gros and Kenneth Wärnmark group[66] reported **FeC-16** in 2015[67], that is, a strong electron-withdrawing substituent carboxylate was added to the 4 position of the pyridine ligand of **FeC-12**. As mentioned earlier, the introduction of strong electron withdrawing group carboxylate can effectively enhance the π electron accepting ability of the ligand, thereby destabilizing the MC state. This is also one of the classic strategies to stabilize the MLCT state by reducing the ligand π* orbital energy. Facts have proved that this strategy is useful. **FeC-16** exhibited an excited-state lifetime of 18 ps in MeCN solution and 37 ps in aluminum oxide (**Scheme 39**). Further research shows that the iron complex **FeC-16** is able to generate photoelectrons and inject into the conduction band of $TiO_2$ with 92% quantum yield.

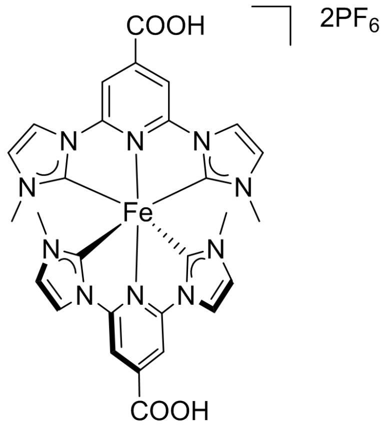

**FeC-16**

| Fe Complex | **FeC-16** |
|---|---|
| λ abs max / nm | 520 |
| Lifetime of MLCT | 18(37)$^a$ ps |
| $E_{1/2}$ (FeIII/II) / V vs. NHE | 1.09 |
| $E_{1/2}$ (L$^-$/0) / V vs. NHE | -1.11$^b$ |

*a* : measured in solid $Al_2O_3$
*b*: irreverisible

**Scheme 39:** Structure, and photo properties of **FeC-16**

The Philippe C. Gros research group continued to report a series of heteroleptic Fe-NHC complexes **FeC-17**, **FeC-18** and **FeC-19** in 2016[68]. **FeC-17** is similar with **FeC-16**, except that the carboxylate group of one of the ligands is removed. Such modification will not bring substantial improvement in photophysical properties, but will provide a new strategy for complex design, and this new design idea is reflected in **FeC-18** and **FeC-19**. Both **FeC-18** and **FeC-19** choose to modify only the ligands substituted by carboxylate, and replace the methyl group with a larger conjugated group to further increase the π electron accepting ability of this distributor, which can effectively stabilize its π* orbital. The theoretical basis of this hybridization concept is to make the LUMO and HOMO of the complexes orthogonal, so that the modification of one orbital will not affect the energy of the other. For **FeC-18** complex, the authors replaced the methyl group with 4-methoxybenzyl, while in **FeC-19**, the researchers chose triphenylamine with greater conjugation to replace the methyl group. The original intention of this modification was expecting the newly added benzene ring substituent could be hyperconjugated with the pyridine group of another ligand, thereby stabilizing its π orbital, but this idea was not achieved as expected. The MLCT state lifetimes of **FeC-18** and **FeC-19** did not show an increase, and decreased to 10 ps and 12 ps, respectively (**Scheme 40**). This also further shows that the steric hindrance effect of the ligand substituent will have a negative impact on the interaction between the metal and the ligand.

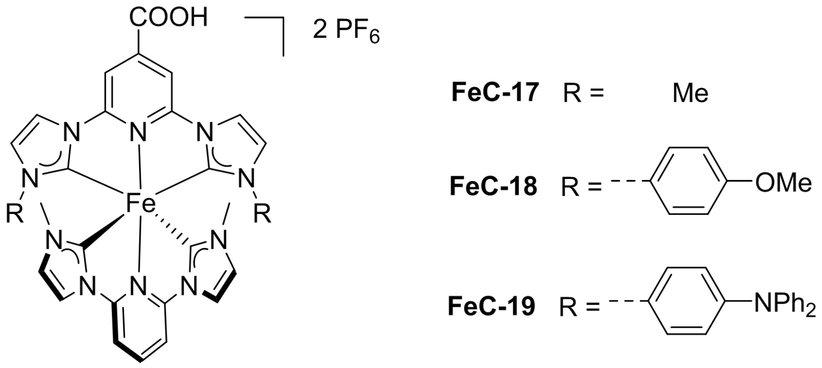

| Fe Complex | **FeC-17** | **FeC-18** | **FeC-19** |
|---|---|---|---|
| λ abs max / nm | 505 | 509 | 509 |
| Lifetime of MLCT | 14 ps | 10 ps | 12 ps |
| $E_{1/2}$ (FeIII/II) / V vs. NHE | 1.06 | 1.05 | 1.06 |
| $E_{1/2}$ ($L^-/0$) / V vs. NHE | -1.11[a] | -1.09[a] | -1.10[a] |

*a* : irreverisible

**Scheme 40:** Structures, and photo properties of **FeC-17**, **FeC-18**, and **FeC-19**

In order to solve the loss of ligand conjugation system caused by the introduction of NHC ligands, in addition to the introduction of strong electron-withdrawing groups to increase the π electron-accepting ability of ligands, such as **FeC-16,** the conjugation systems can be also extended as **FeC-18** and **FeC-19**. However, adding a large conjugated group to the nitrogen atom of the carbene ligand will inevitably introduce a large steric hindrance group, thereby affecting the interaction between the metal center and the ligand. But adding a conjugated system from the back of the ligand will not have this problem. The Philippe C. Gros research group continued to report a homoleptic Fe(II) complex **FeC-20** and **FeC-21** in 2016[69], exhibiting the lifetime of $^3$MLCT state with 16 ps and 26 ps respectively, promoted by benzimidazolylidene-based ligands. **FeC-20** uses benzimidazolylidene as strong $\sigma$-donating ligand instead of imidazolylidene in **FeC-12**. This design not only introduces NHCs ligand, but also increases the conjugate system of the ligand. Compared with **FeC-12**, **FeC-20**'s MLCT excited state lifetime has been increased from 9 ps to 16 ps. Similarly, **FeC-21** has been made the same modification on the basis of **FeC-16**, and its MLCT state lifetime has also increased from 18 ps of **FeC-16** to 26 ps. It can be roughly deemed that in such a system, the extra conjugation system brought by benzimidazolylidene can increase the lifetime of MLCT state by approximately 8 ps (**Scheme 41**).

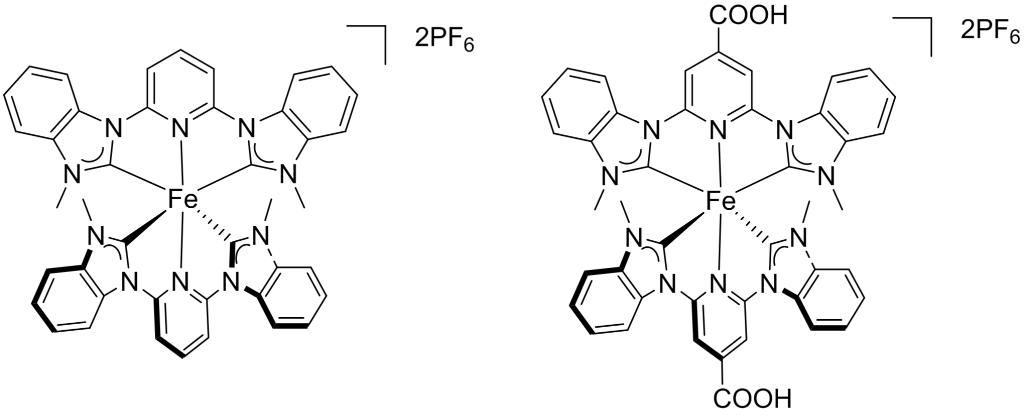

**FeC-20** **FeC-21**

| Fe Complex | **FeC-20** | **FeC-21** |
|---|---|---|
| λ abs max / nm | 440 | 501 |
| Lifetime of MLCT | 16 ps | 26 ps |
| $E_{1/2}$ (FeIII/II) / V vs. NHE | 1.28 | 1.37 |
| $E_{1/2}$ ($L^{-}/0$) / V vs. NHE | -1.56[a] | -0.99[a] |

*a* : irreverisible

**Scheme 41:** Structures, and photo properties of **FeC-20** and **FeC-21**

The **FeC-15** complex shows that the hexyl substituent on the N of the NHCs ligand has a positive effect on helping to stabilize its MLCT state. In view of this, the Philippe C. Gros research group replaced the N methyl group on the **FeC-20** NHC ligand with hexane in 2018. This modification also has a positive effect on the stabilization of MLCT state of **FeC-22**, which is increased from 16 ps to 20 ps (**Scheme 42**). This also proves once again that although the N atom substituent of the carbene ligand will affect the interaction between the complex metal and the ligand due to steric hindrance, when this substituent is a long chain alkane, it will help the stability of the MLCT state of the complex.

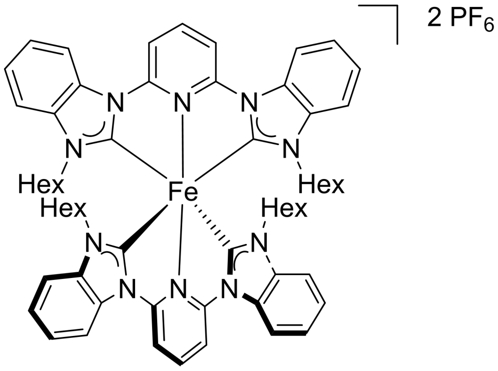

**FeC-22**

**Scheme 42:** Structure of **FeC-22**

Based on the work of **FeC-22**, Prof. Philippe C. Gros's group continued to study the effect of non-pyridine ligands on MLCT state of Fe-NHC complex. In their work in 2019[70], they reported a series of homoleptic Fe(II) complexes with CNC ligands utilizing diazines instead of pyridine center, **FeC-23** - **FeC-26**. Among them, **FeC-23** replaces the pyridine in **FeC-22** with 1,4-diazine. The research carried out a lot of theoretical calculations to prove that the introduction of diazine is beneficial to stabilize the MLCT state. After diazine obtains electrons from the metal center, it breaks the number of electrons in the aromatic compound 4n+2. This result will lengthen the Fe-N bond to a certain extent, which can contribute to the stability of MLCT from the computational perspective. Finally, **FeC-23** exhibited the lifetime of 32 ps for MLCT. In contrast, due to the reduction of the ligand conjugated system of **FeC-24**, the lifetime of MLCT has also been reduced to 22 ps. Compared with 15 ps lifetime of its analog **FeC-15**, the 7 ps extension can also reversely explain the positive effect of diazine on stabilizing the MLCT state. Similarly, **FeC-25** also exhibits a good MLCT lifetime of 23 ps. **FeC-26** uses 1,3-diazine instead of pyridine in the ligand. The results showed that 1,3-diazine did not show the same effect as its analogue 1,4-diazine. **FeC-26** shows only 12 ps lifetime of MLCT under TAS results. However, this result shows improvement compared to the 9 ps of **FeC-12**, which proves that 1,3-diazine has a slight positive effect on stabilizing the MLCT over pyridine (**Scheme 43**).

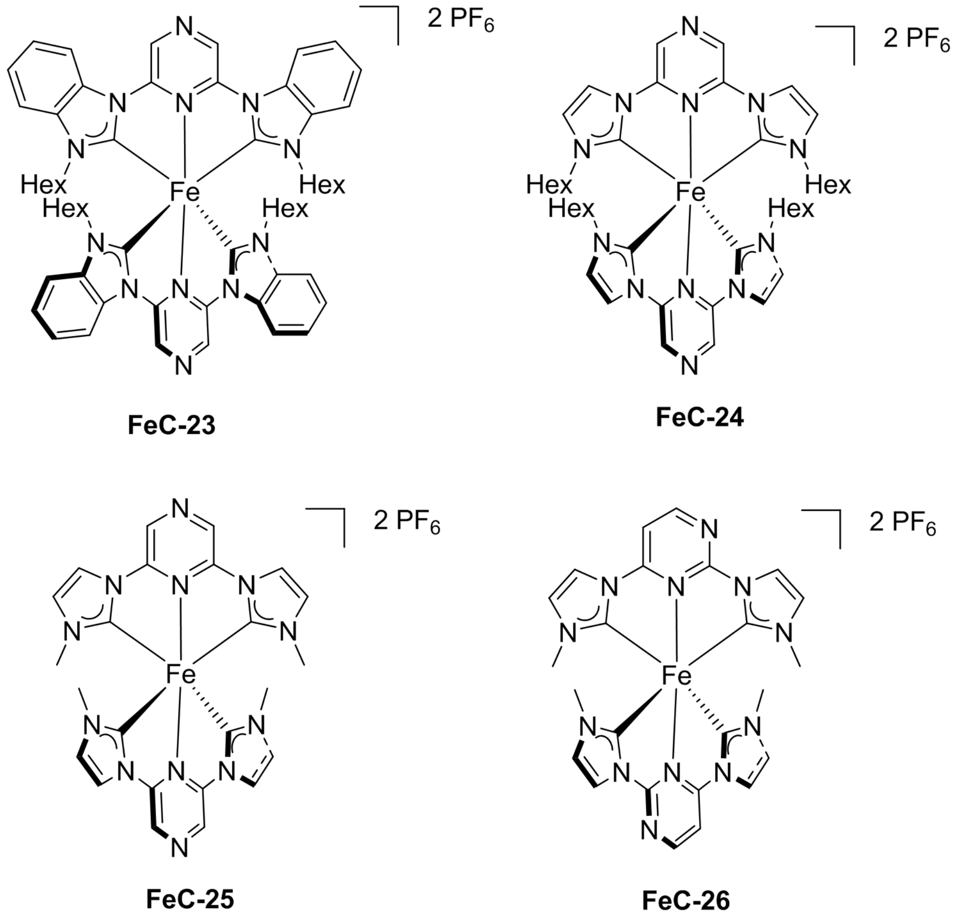

**FeC-23** **FeC-24** **FeC-25** **FeC-26**

| Fe Complex | **FeC-23** | **FeC-24** | **FeC-25** | **Fe-26** |
|---|---|---|---|---|
| λ abs max / nm | 479 | 493 | 487 | 477 |
| Lifetime of MLCT | 32 ps | 22 ps | 23 ps | 12 ps |
| $E_{1/2}$ (FeIII/II) / V vs. NHE | 1.46 | 1.33 | 1.22 | 1,17 |
| $E_{1/2}$ ($L^-$/0) / V vs. NHE | -0.97 | -1.08 | -1.15 | 1.46[a] |

*a* : irreverisible

**Scheme 43:** Structures, and photo properties of **FeC-23**, **FeC-24**, **FeC-25** and **FeC-26**

Kenneth Wärnmark and Villy Sundström reported a heteroleptic Iron(II) complex **FeC-27** with mesoionic bis(1,2,3-triazol-5-ylidene) as ligands in 2015[71]. The more strongly $\sigma$-donating mesoionic ligand can destablize the MC state of the complex more effectively. However, the hybrid bipyridine ligand cannot stabilize the energy of the excited state of MLCT well. Therefore, although the four stronger NHC $\sigma$-donating ligands can better enhance the splitting effect of the ligand field on the metal d orbital, **FeC-27** exhibits a pertinent MLCT excited state lifetime of 13 ps. It is worth pointing out tha**t FeC-27** exhibits an ultra-low (Fe III/II) oxidation electrode potential, only 0.28 V (**Scheme 44**). This is a side effect that the mesoionic bis (1,2,3-triazol-5-ylidene) has stronger $\sigma$-donating ability over normal NHC ligands.

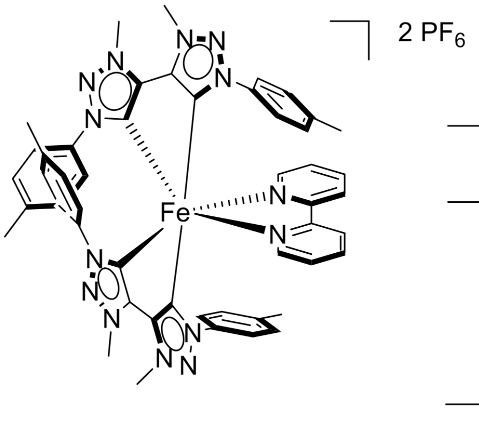

**FeC-27**

| Fe Complex | **FeC-27** |
|---|---|
| λ abs max / nm | 432,609,720 |
| Lifetime of MLCT | 13 ps |
| $E_{1/2}$ (FeIII/II) / V vs. NHE | 0.28 |
| $E_{1/2}$ ($L^{-}$/0) / V vs. NHE | -1.65[a] |

*a* : irreverisible

**Scheme 44:** Structure, and photo properties of **FeC-27**

## 1.2.6 Fe(II)-NHC complex with 6 N-heterocyclic carbenes

Kenneth Wärnmark's research group reported Fe(II) hexa N heterocyclic carbene complex **FeC-28** with 3,3′-dimethyl-1,1′-bis(p-tolyl)-4,4′-bis(1,2,3-triazol-5-ylidene) (btz) as ligands in 2018[72]. **FeC-28** has 6 N-heterocyclic carbenes 1,2,3-triazol ligands with stronger $\sigma$-donating ability than traditional imidazole. Six stronger $\sigma$-donating ligands endow the complex with super strong ligand field splitting ability, so that the d orbital of Fe is greatly differentiated. As a result, the energy of the MC state of **FeC-28** has been greatly improved. In addition, the 4-methylphenyl attached to 1,2,3-triazol also extends the $\pi$-conjugated system of the ligand very well, thus stabilizing the $\pi^*$ orbital, which further stabilize the MLCT state of the complex. In summary, the MC excited state of **FeC-28** is sufficiently passivated, and at the same time the MLCT excited state is fully stabilized. Finally, **FeC-28** exhibited an ultra-high MLCT excited state lifetime of 528 ps, which is also the longest MLCT state lifetime of known Fe complexes by now (**Scheme 45**).

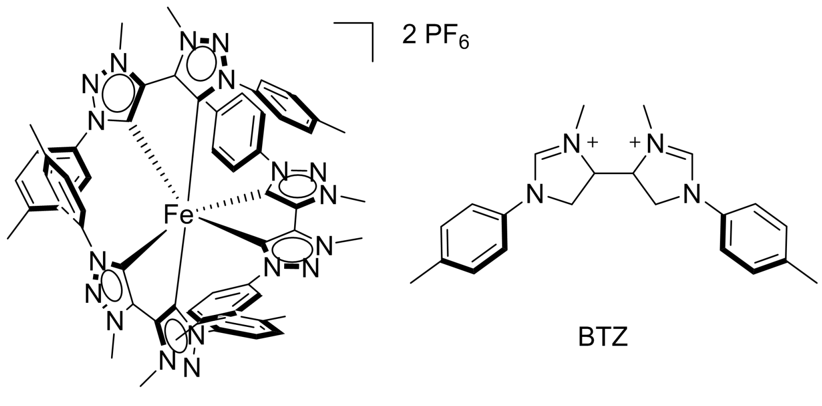

**FeC-28**

BTZ

| Fe Complex | **FeC-28** |
|---|---|
| λ abs max / nm | 440,510,690,825 |
| Lifetime of MLCT | 528 ps |
| $E_{1/2}$ (FeIII/II) / V vs. NHE | 0.05 |
| $E_{1/2}$ ($L^-/0$) / V vs. NHE | -1.75 |

**Scheme 45:** Structure, and photo properties of **FeC-28**

## 1.2.7 Fe(III)-NHC complex with 6 N-heterocyclic carbenes

For a long time, many studies have focused on the study of metal-to-ligand charge transfer state of Fe(II) complex. In 2017, Kenneth Wärnmark first reported the study of ligand-to-metal charge transfer state on Fe(III)-NHC complex **FeC-29**[57]. In fact, **FeC-29** is mono-oxidized **FeC-28**. The MLCT state of the Fe(II) complex is the excitation from the HOMO $t_{2g}$ of the complex to the π* orbital of the ligand, while the Fe(III) complex is the excitation from the π orbital of the ligand to the metal-centered $t_{2g}$ orbital. Although their excitation processes are different, their deactivation processes from the optically active excited state (MLCT or LMCT) to the non-optically active excited state are similar. Whether it is Fe(II) or Fe(III) complexes, the deactivation to the metal-centered state with relatively low energy is the reason for the ultra-fast lifetime of their optically active excited states (**Scheme 46**).

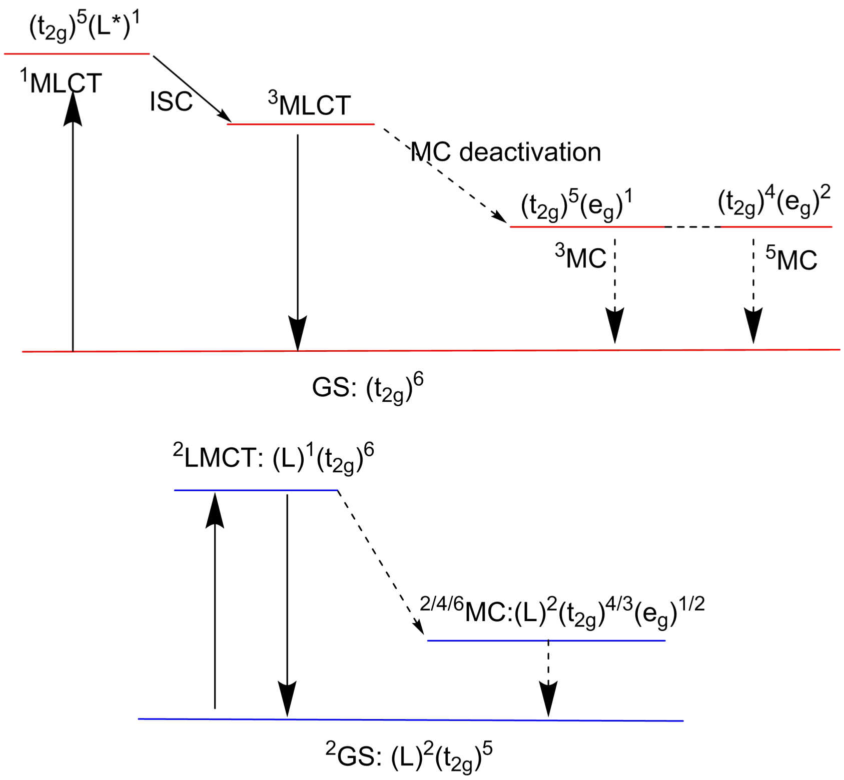

**Scheme 46:** Deactivation processes of Fe(II) and Fe(III) complex upon excitation

Therefore, the strategy of using strong $\sigma$-donating ligands or designing a perfect octahedral spatial geometry to enhance the ligand field of the complex to strengthen the splitting of the metal d orbital is still applicable to the Fe(III) complex. As for the strategy applicable to Fe(II) complexes to reduce the excited state energy of MLCT, increasing ligand conjugation and the use of strong electron-withdrawing substituents are no longer fully applicable here. In order to reduce the energy of the LMCT state of the Fe(III) complex, the π-electron conjugate system of the ligand and the energy of the π orbital still need to be increased, thereby reducing the difficulty of the electron transition from ligand centered π orbital to the metal $t_{2g}$ orbitals. In addition, in contrast to the Fe(II) complexes that use strong electron withdrawing groups to enhance the ligand's π electron accepting ability, donating electron groups are required to enhance the ligand π electron donation ability, thereby reducing energy of LMCT excited state. **FeC-29** shows a lifetime of LMCT state with 100 ps (**Scheme 47**). This result shows that the LMCT excitation of Fe(III) complexes has a very good prospect on the road of utilizing Fe complexes as photo catalysts.

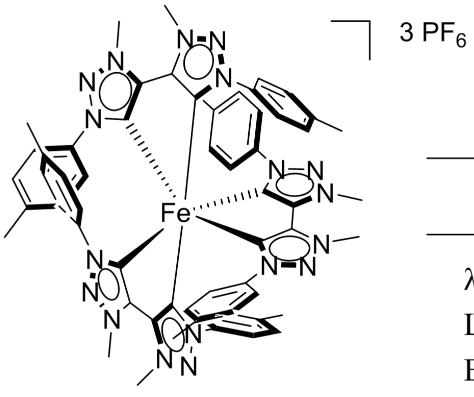

**FeC-29**

| Fe Complex | **FeC-29** |
|---|---|
| λ abs max / nm | 400,528,558 |
| Lifetime of MLCT | 100 ps |
| $E_{1/2}$ (FeIII/II) / V vs.($Fc^{+}$/0) | -0.58 |

**Scheme 47:** Structure, and photo properties of **FeC-29**

Having discovered the feasibility of the LMCT state[73], Kenneth Wärnmark continued to conduct in-depth research in this direction. In 2019, they reported almost perfect octahedral coordination of Fe(III) complex **FeC-30** by two mono-anionic facial tris-carbene ligands henyl[tris(3-methylimidazol-1-ylidene)] borate[74]. In the research, **FeC-30** exhibits strong, visible, room temperature photoluminescence with the LMCT lifetime as long as 2 ns (**Scheme 48**). In addition to using the classic 6 NHC ligands, the author believes that the nearly perfect octahedral geometry configuration of **Fe-30** makes its ligand field splitting ability to be maximized. Moreover, as a good electron donor, boron can effectively strengthen the electron donation ability of the ligand, thereby stabilize the LMCT state. This study also showed that **Fe-30** has excellent electrical properties, and is reversible by one electron in the reduction cycles. This gives it great potential for its photochemical applications in the future.

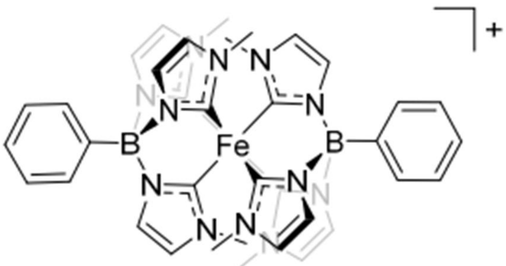

**FeC-30**

| Fe Complex | **FeC-30** |
|---|---|
| λ abs max / nm | 502 |
| Lifetime of MLCT | 1.96 ns |
| $E_{1/2}$ (FeIV/III) / V vs. $Fc^{+/0}$ | - 1.9 |
| $E_{1/2}$ (FeII/III) / V vs. $Fc^{+/0}$ | 1.0 |

**Scheme 48:** Structure, and photo properties of **FeC-30**

# 1.3 Synthesis and application of medium and macrocyclic compounds

## 1.3.1 Research and development of medium and macrocyclic compounds

medium sized ring (seven-membered ring to eleven-membered ring) and macrocyclic (12-membered ring and above) compounds are widely found in land plants, marine organisms, pathogenic fungi and bacteria. The research on such compounds has a long history. In the early days of the development of chemistry, many chemists successfully extracted and separated a series of medium and macrocyclic compounds from nature.The initial interest of chemists in such compounds came from the study of various marine algal toxins.

In 1984, Francis J. Schmitz and co-workers isolated a potent cytotoxic macrolide, which was designated tedanolide from the widely distributed sponge in the Caribbean. This sponge extracts containing a 12-membered macrocycle showed cytotoxicity and *in vivo* tumor Inhibition[75]. In 1985, Richard E. Moore's research group extracted four aplysiatoxin-related compounds from marine blue-green algae belonging to Oscillatoriaceae through gel filtration and reverse-phase chromatography and crystallization[76]. The structures of these compounds were determined by spectral studies and chemical degradation (**Scheme 49**).

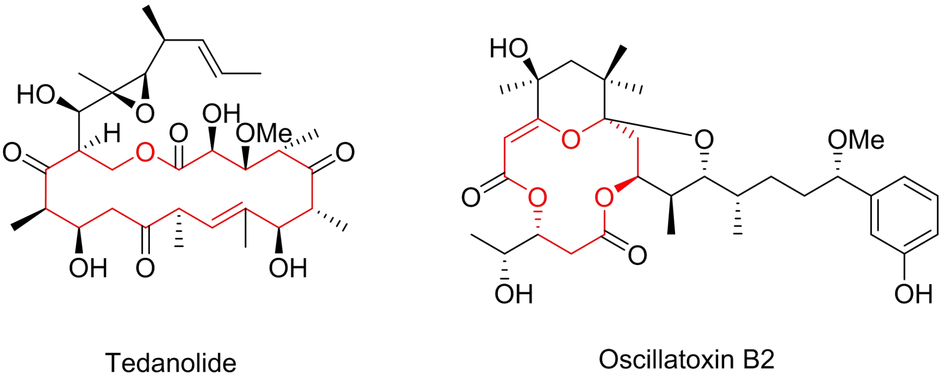

**Scheme 49**: Structures of Tedanolide and Oscillatoxin B2

Yuzuru Shimizu's research group also reported a new polycyclic ethers toxin extracted and separated from red tide dinoflagellate in 1985 (**Scheme 50**)[77].

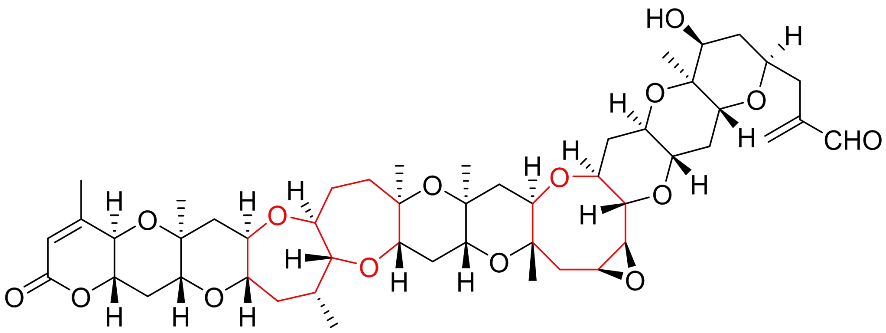

(27S,28R)-27,28-Epoxy-27,28-dihydrobrevetoxin-B

**Scheme 50**: Structure of Dihyhrobrevetoxin-B

Jun'ichi Tanaka and Tatsuo Higa also reported a new diterpene, hydroxydictyodial in 1984[78]. They found that when feeding the fish, the fish would avoid the presence of Dictyota spinulosa. This antifeedant constituents aroused their interest in dictyota spinulosa, and separated and extracted the components to obtain this hydroxydictyodial toxin. In 1984, Matsumoto Takeshi's research group reported the structures of the unique C15 non terpenoids[79]. The structure and configuration of the new C-15 bromoallene isolated from the red alga Laurencia okamurai Yamada, were confirmed by X-ray crystallographic analysis (**Scheme 51**).

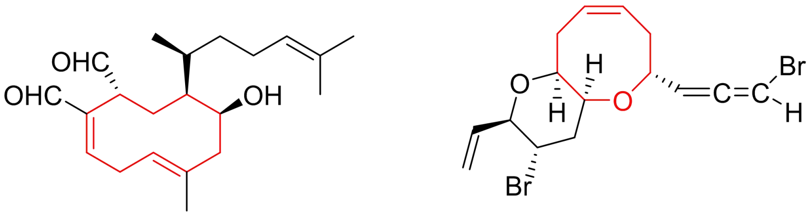

Hydroxydictyodial

Microcladallenes B

**Scheme 51**: Structures of Hydroxydictyodial and Microcladallenes B

With the continuous development of chemical technology and scientific methods, today's scientists are more and more efficient in the separation, extraction and research of macrocyclic compounds in nature. There are more and more reports on medium and macrocyclic compounds in nature[80] (**Scheme 52**).

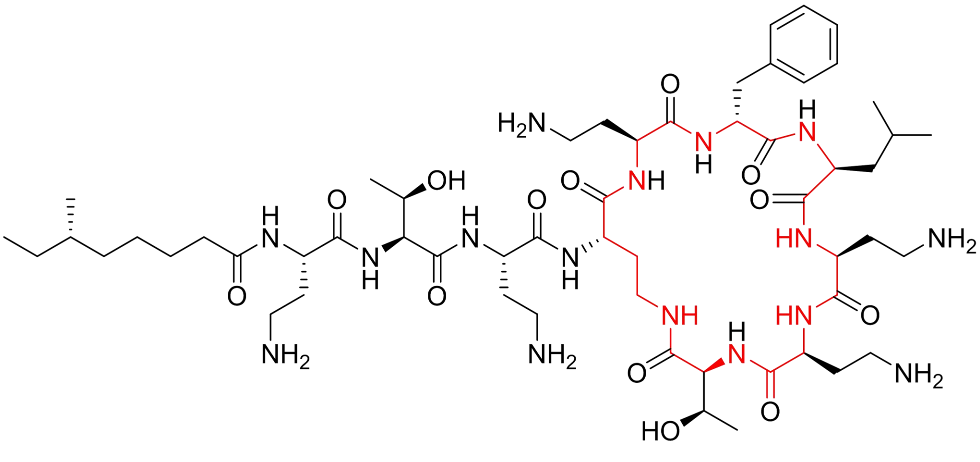

Polymyxin B1

**Scheme 52**: Structures of Ploymyxin B1

Over the years, the extraction, separation, and research of mid-ring and macrocyclic compounds have enabled scientists to have a better understanding of their properties. As a result, these compounds are widely used in human society due to their unique properties, such as in the fields of anticancer drugs, antibiotics, pesticides and other biomedicine.

Paclitaxel is a natural macrocyclic anticancer drug. It has been widely used clinically in the treatment cancer. In 1991, Pierre Portier's group studied the ability of various synthetic analogues of paclitaxel to inhibit the breakdown of microtubules[81]. In this work, their performance on 40 synthetic taxane-type compounds. These compounds can act as potential inhibitors of disassembly of mammalian tubulin (**Scheme 53**).

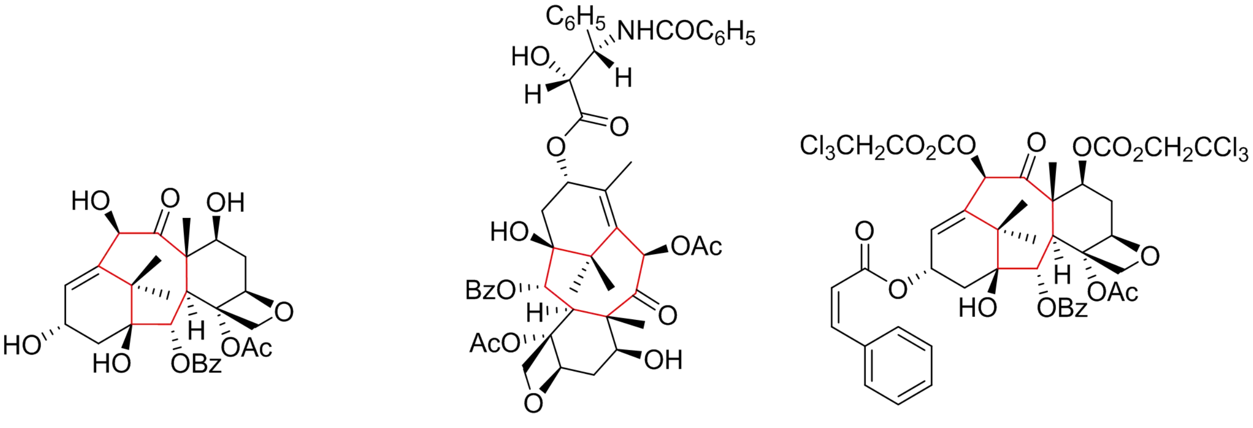

10-Deacetylbaccatin III

Taxol

Cinnamate Ester

**Scheme 53**: Structures of 10-Deacetylbaccatin, Taxol and Cinnamate Ester *β*-lactam antibiotics are a wide variety of antibiotics, including penicillin and its derivatives, cephalosporins, monoamide rings, carbapenem and penicillin enzyme inhibitors. It is the most widely used type of existing antibiotics. The research and synthesis of midcyclic lactam compounds has always attracted the attention of many scientists. For example, Xin-Yuan Liu's research group reported a new synthesis method of Medium-Sized Lactams in 2018[82]. This provides a new feasibility for its future application in the field of medicinal chemistry (**Scheme 53**).

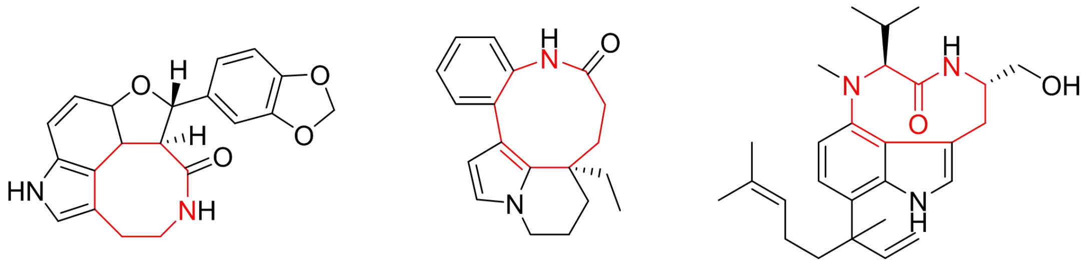

Decursivine Rhazinilam Lyngbyatoxin

**Scheme 53**: Structures of different midcyclic lactam compounds

The Guido Verniest research group reported the regio- and diastereoselectivity research of nine-membered lactams with *Z* double bond towards the formation of blocks for medicinal chemistry in 2019[83]. Keiji Mori's research team also reported the highly diastereoselective synthesis of medium-sized carbocycle-fused piperidines in the same year (**Scheme 54**).

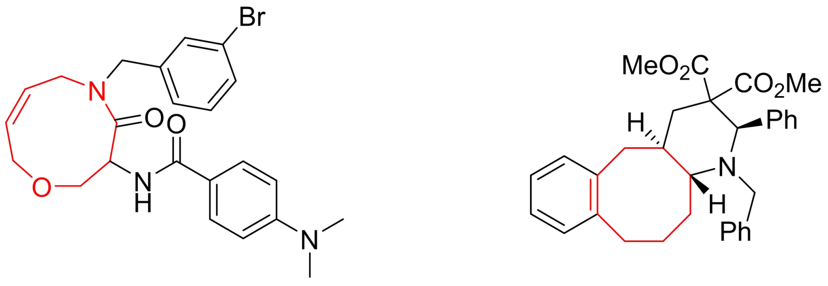

3-Aminohexahydrooxazinone Piperidine Derivative

**Scheme 54**: Structures of high diastereoselective medium-sized ring compounds

## 1.3.2 Common construction strategies for mid-ring compounds

With the continuous deepening of research in this field and development of chemical technology and methods, scientists' research on medium and macrocyclic compounds is no longer limited to extraction and separation from nature. In addition, scientists began to artificially synthesize a variety of different mid-ring and macrocyclic compounds in accordance with the social requirements. Nowadays, exploring methods to efficiently construct such cyclic skeletons has been one of the research hotspots in this field. In addition, these methods are used to efficiently synthesize some required natural products or molecules with physiological activities, so as to further promote the development of modern synthesis, medicine and pesticide industries.

Current construction strategies and methods of medium and macrocyclic compounds will be briefly summarized. The construction strategies of mid-ring compounds mainly include the following categories:

### 1.3.2.1 Acid catalysis (Lewis acid/Bronsted acid)

Professor Yu Zhixiang reported the reaction of six-membered nitrogen heterocycles catalyzed by gold Lewis acid to synthesize eight-membered nitrogen heterocycles[84]. He synthesized a series of eight-membered compounds through the expansion and spirocyclization of 2-propynyl-*β*-tetrahydrocarbyl under gold catalysis, which provided a new method for the synthesis of azoindole derivatives (**Scheme 54**).

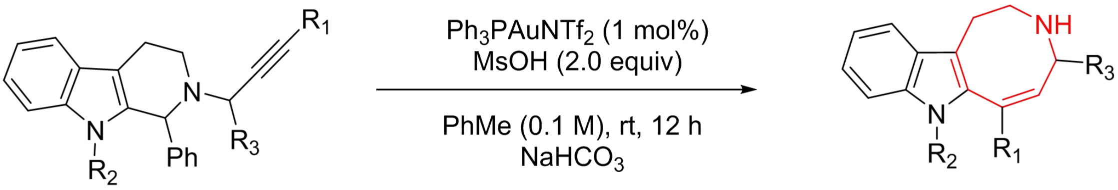

**Scheme 54**: gold Lewis acid synthesized synthesis of azoindole derivatives

Professor Zhu Shifa also used gold catalysis to achieve the synthesis of medium sized ring compounds through  the migration and rearrangement of acyl oxygen. In this study, they demonstrated the gold(I)-catalyzed reaction of enyne-ethers to rapidly construct oxa-bridged medium sized ring compounds *via* a tandem 1,2-acyloxy migration/intramolecular oxonium formation/1,2-rearrangement process[85] (**Scheme 55**). However, this synthesis method has certain limitations on the substrate, requiring a strong electron withdrawing group on the oxazole ring of the reaction substrate.

**Scheme 55**: gold (I)-catalyzed synthesis of oxa-bridged medium sized ring compounds

Professor Ye Longwu used Bronsted acid/Lewis acid synergistic catalyzed hydrogen alkoxylation-rearrangement method to synthesize eight- and nine-membered ring compounds[86]. In the report, they used TfOH as acid catalysts to achieve stereoselective synthesis of medium sized (8, 9) lactams enabled by metal-free hydroalkoxylation and stereospecific [1,3]-rearrangement (**Scheme 56**).

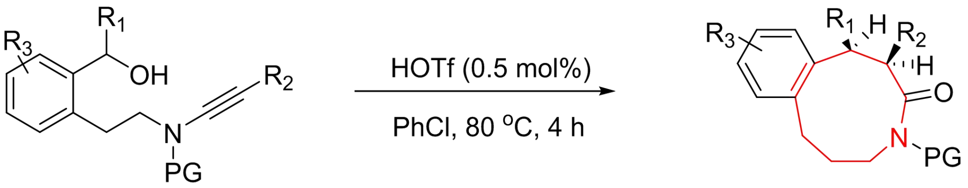

**Scheme 56**: Lewis acid catalyzed synthesis of 8- and 9- memberd lactams

This method is a relatively mature strategy for constructing mid-ring compounds. However, it has relatively high requirements for the reaction substrate, which requires the functional group containing a lone pair of electrons to interact with the acid.

### 1.3.2.2 Base catalysis (Lewis base/Bronsted base)

Professor Li Yanzhong reported a straightforward and efficient way to synthesize seven-membered-ring benzolactams or chromone derivatives[87]. They used base as catalyst to selectively catalyze the cleavage of the carbon-carbon bond of indolinone and further add to alkynes to form a series of seven-membered ring compounds (**Scheme 57**).

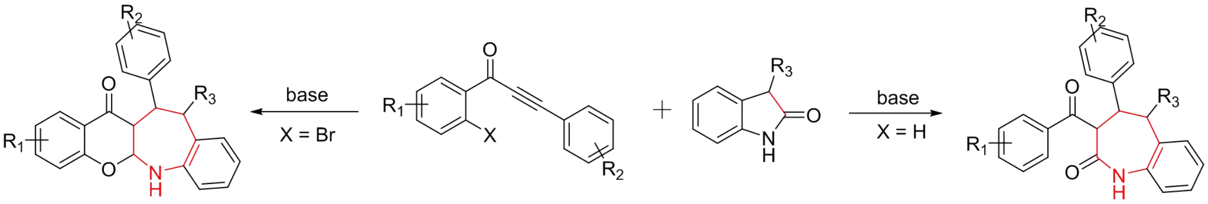

**Scheme 57**: Base catalyzed selective synthesis of seven-membered ring compounds

Professor Unsworth used nitrogen anions to attack the carbonyl group and expand the ring, and obtained up to eleven-membered ring lactam [88](**Scheme 58**). This method has been widely used in the synthesis of dozens of medium sized ring compounds in various chemical fields. The application of compounds in biomedicine and other fields provides more possibilities.

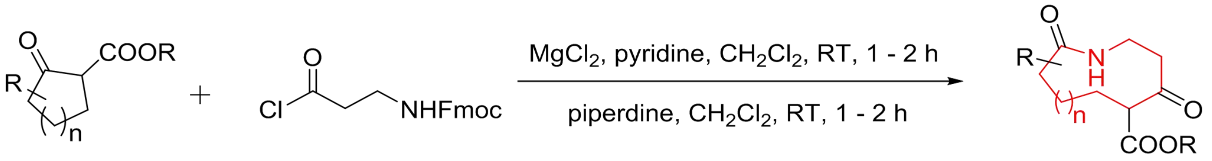

**Scheme 58**: nitrogen anions catalyzed synthesis of medium sized ring lactams.

For this method of synthesizing medium sized ring compounds using Lewis bases or Bronsted bases as catalysts, the ring expansion reaction is generally achieved through the nucleophilic reaction of anion intermediates. Therefore, this method has certain requirements on the substrate, that is, acid hydrogen is required in the substrate so that it can react with alkali to generate anion intermediates.

### 1.3.2.3 Free radicals involved Cyclization

Researcher Li Ang reported the syntheses of daphenylline, daphnipaxianine A, and himalenine D, three Daphniphyllum alkaloids from the calyciphyllineA subfamily[89] (**Scheme 59**). The original atom-transfer radical cyclization and the Lu [3+2] cycloaddition strategy was applied in the total synthesis of Daphenylline, through which a series of seven-membered ring intermediates were synthesized.

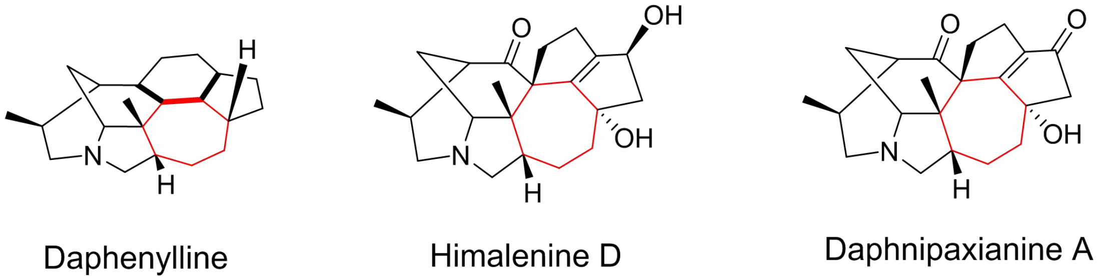

**Scheme 59**: Synthesis of medium sized ring compounds through atom-transfer radical cyclization

Professor Chida, Professor Ruan Zhixiong and Professor Liu Xinyuan used samarium iodide[90], electrocatalysis[91], and photocatalysis[82] to initiate free radicals respectively, thereby constructing different medium sized ring compounds (**Scheme 60**).

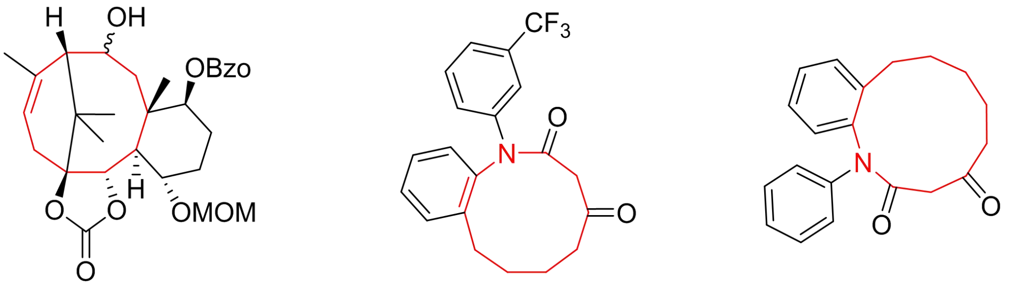

**Scheme 60**: Structures of medium sized ring compounds through different methods.

The key point of such methods is how to design and generate free radical intermediates. Since there are many methods that can produce free radical intermediates under relatively mild conditions, the reaction conditions of this type of reaction are often relatively mild. Despite this, due to the high activity of free radicals, this type of reaction often has certain requirements on the reactivity and concentration of the substrate.

### 1.3.2.4 Cyclic olefin metathesis (RCM)

Professor Ku Xuegong used the RCM reaction in the total synthesis of the natural product Pepluanol B to construct an eight-membered ring intermediate[92]; Ansari used the RCM reaction to construct a nine-membered ring compound[93] (**Scheme 61**).

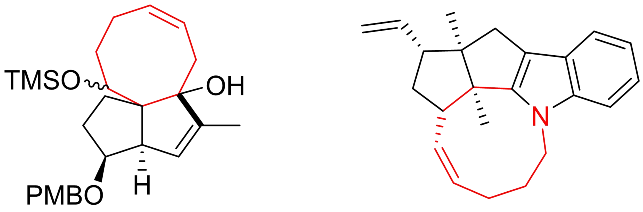

**Scheme 61**: Structures of 8-membered ring intermediates synthesized through RCM

This type of reaction tends to be relatively mild. However, as far as the reported reactions are concerned, the presence of terminal olefins in the substrate is often required to successfully generate midcyclic compounds.

### 1.3.2.5 Cycloaddition and ring expansion

Prof. Hongbin Zhai used the [3+2]-cycloaddition strategy to synthesize the seven-membered ring intermediate of the natural product Diterpenoid (+)-Harringtonolide [94](**Scheme 62**).

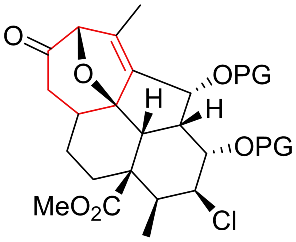

**Scheme 62**: Structures of 7-membered ring intermediate synthesized through cycloaddition

Professor Hongchao Guo also used [3+2]-cycloaddition and subsequent Cope rearrangement to construct a series of chiral nine- and ten-membered ring products[95] (**Scheme 63**). Under this method, VECs with different substituents can be successfully produced in a palladium-catalyzed asymmetric tandem reaction with coumarate or pyrone under mild conditions, producing corresponding medium sized heterocyclic compound with high yield and extremely high enantioselectivity.

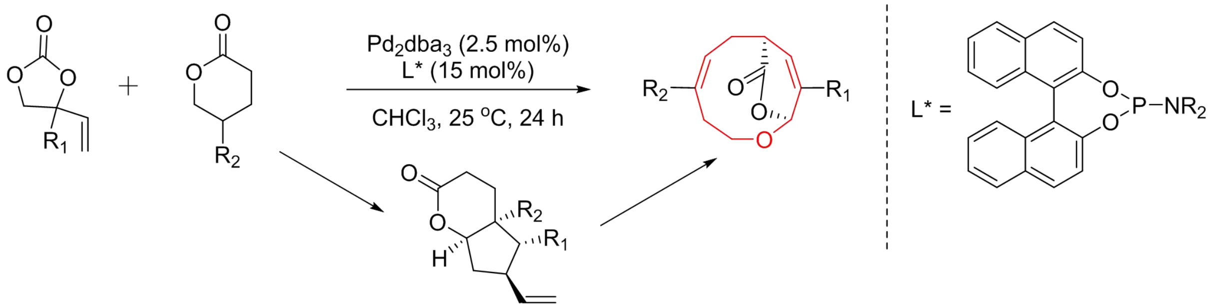

**Scheme 63**: Synthesis of chiral nine- and ten-membered ring compounds through [3+2]-cycloaddition

Professor Deng Weiping reported palladium-catalyzed asymmetric [4+3] cyclization of trimethylenemethane, and constructed a chiral seven-membered ring compound[96]. This strategy successfully provides an alternative way to synthesize chiral azepines by a transition-metal-catalyzed asymmetric [4+ 3] cyclization (**Scheme 64**).

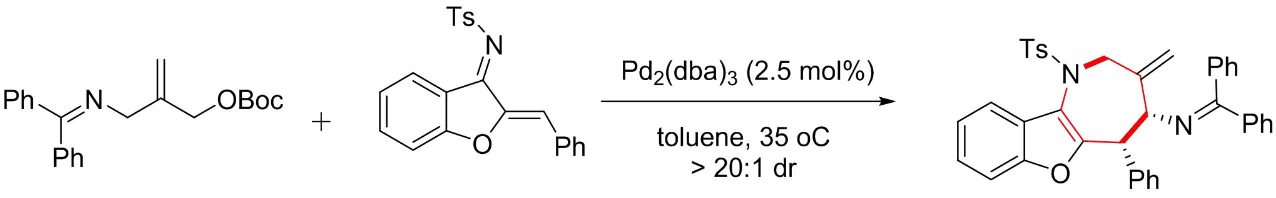

Scheme 64: Palladium-catalyzed asymmetric [4+3] cyclization

Moreover, Lu and coworkers reported highly enantioselective phosphine-catalyzed formal [4+4] annulation, affording azotines bearing either benzofuran or indole moiety with excellent yields and enantioselectivity[97]. This is also the first efficient asymmetric synthesis of optically eight-membered rings through phosphine catalysis (**Scheme 64**).

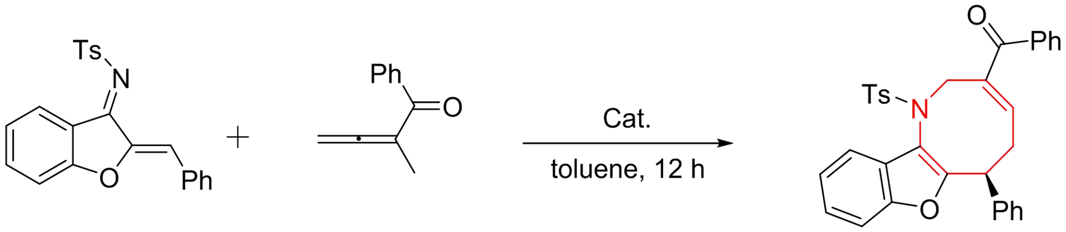

**Scheme 64**: Highly enantioselective phosphine-catalyzed formal [4+4] annulation

Hu Xiangping's group reported a palladium-catalyzed [n+2]-cycloaddition reaction, which can be used to synthesize nine-, ten-, and eleven-membered ring compounds with phenoxy linkages [98](**Scheme 65**).

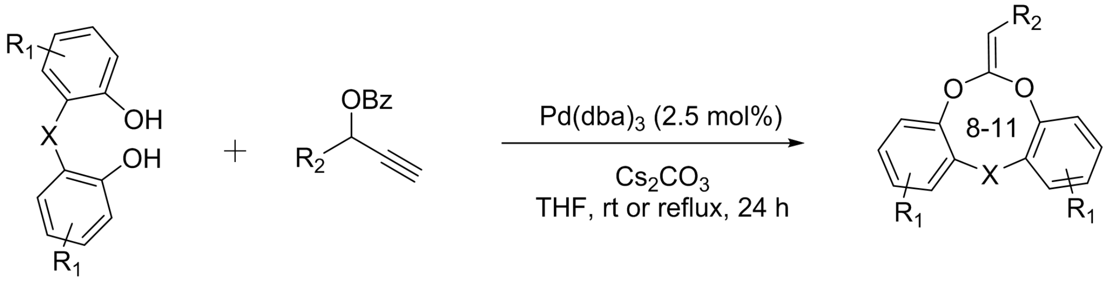

**Scheme 65**: Palladium-catalyzed [n+2]-cycloaddition reaction

The cycloaddition strategy is relatively ingenious and has high atomic economy. However, it often has specific requirements for the structure of the reactant which means special design of the substrate is required. Therefore, this strategy has relatively low universality for the synthesis and application of mid-ring compounds.

### 1.3.2.6 Other strategies

In addition to the relatively common strategies for the construction of the medium sized ring skeleton mentioned above, there are also some other methods. For example, the iridium-catalyzed allyl dearylation/reverse Mannich reaction/hydrolysis tandem reaction reported by researcher You Shuli[99]. Professor Qin Yong used oxidation-cyclization in the total synthesis of natural product Vincamine[100] (**Scheme 66**). The strategy can also be effectively used in medium sized ring compounds synthesis.

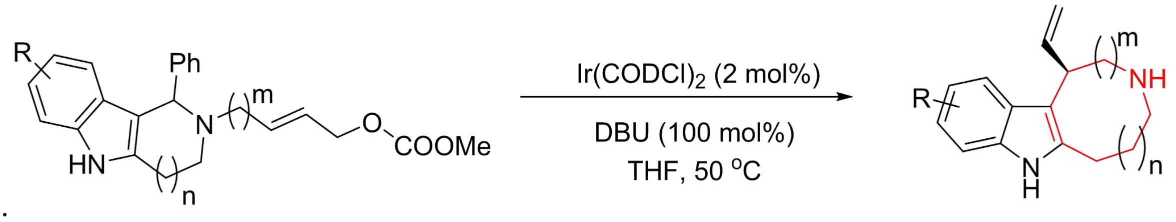

**Scheme 66**: oxidation-cyclization to synthesis medium sized ring compounds

## 1.3.3 Construction strategy of macrocyclic compounds

The construction strategy of the macrocyclic compound is similar to that of the medium sized ring because it is essentially the same type of reaction. However, due to the increase of the ring system, the competition of the intermolecular reactions during the construction process will increase significantly, and more complex oligomers and even polymers are easily generated. Professor Ye Longwu reported an efficient Yttrium-catalyzed Claisen rearrangement reaction[101]. He used Lewis acid-catalyzed intramolecular hydrogen alkoxylation to synthesize multiple twelve to nineteen-membered ring macrocyclic compounds at ultra-low concentrations (**Scheme 67**). This is a typical acid-catalyzed strategy to build a macrocycle, but the concentration requirements are very strict.

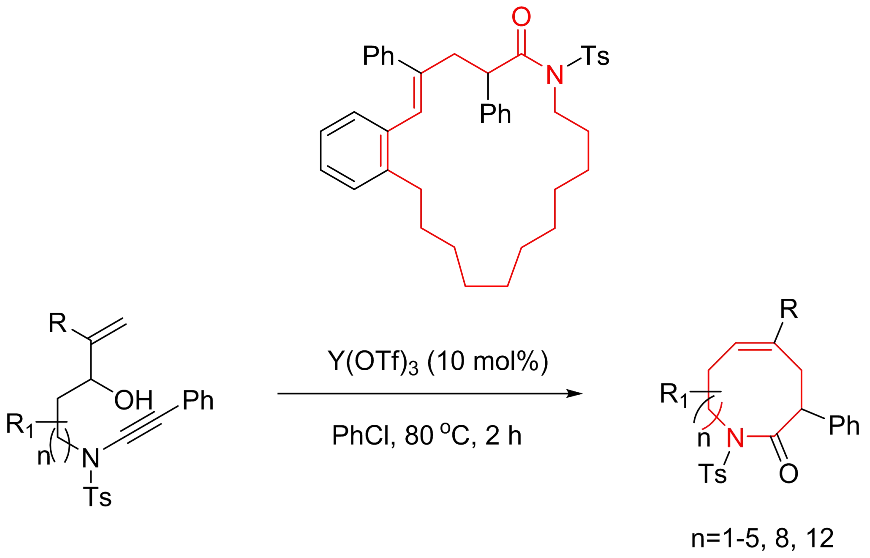

**Scheme 67**: Lewis acid-catalyzed synthesis of macrocyclic compounds

Using the strategy of base catalysis, Hong Ran's group reported the syntheses of lankacidinol and lankacyclinol which feature the biomimetic Mannich macrocyclization[102]. In this study, they used the intramolecular Mannich reaction to synthesize the seventeen-membered ring intermediate of Lankacidin (**Scheme 68**).

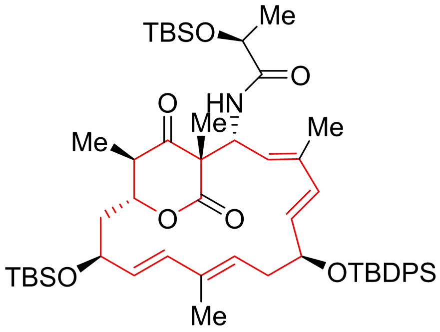

**Scheme 68**: Structure of seventeen-membered ring synthesized through base catalysis

The strategy of using free radical intermediates to construct macrocyclic skeletons is very challenging due to the high activity of free radicals and the short life span. Because the synthesis process of macrocycles often requires a relatively dilute concentration, this also adds difficulty to the application of this strategy. Therefore, such reports are relatively rare. Similarly, due to the competition of intermolecular reactions, there are few reports on the construction of macrocycles by RCM and some metal-catalyzed reactions with more kinetic advantages have been developed. Professor Li Bijie reported a catalytic macrolactonization through oxidative cyclization of alkynyl alcohol with the synergistic function of Lewis-acid and transition-metal catalysis[103]. Using Rhodium and Ytterbium catalyzed macrocyclization reaction, the reaction can be carried out at a higher concentration, generating macrocyclic compounds with more than eighteen member rings (**Scheme 69**). This provides a strategically distinct method to macrolactones.

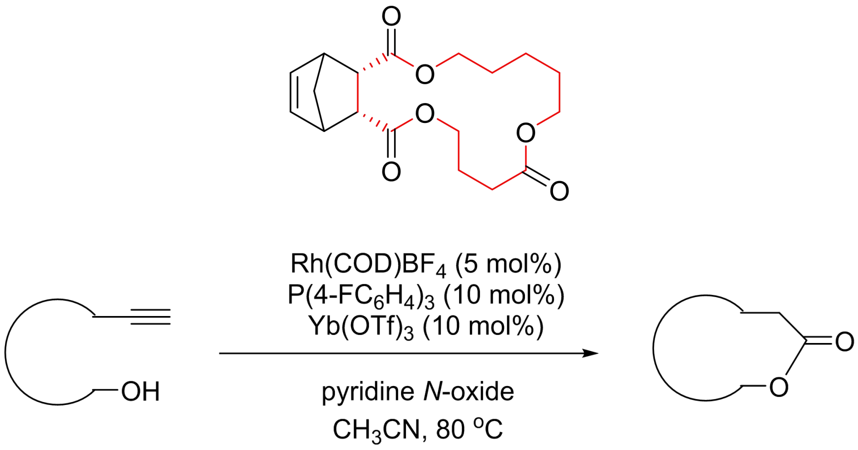

**Scheme 69**: Catalytic macrolactonization through oxidative cyclization of alkynyl alcohol

Professor Huan Wang developed a new strategy for the macrocyclization of biaryl-bridged peptides through Pd-catalyzed C($sp^2$)−H arylatio[104]. They used this method to synthesize a series of macrocyclic compounds of polyaromatic hydrocarbons up to 26-membered ring, with various biologically active molecules (**Scheme 70**).

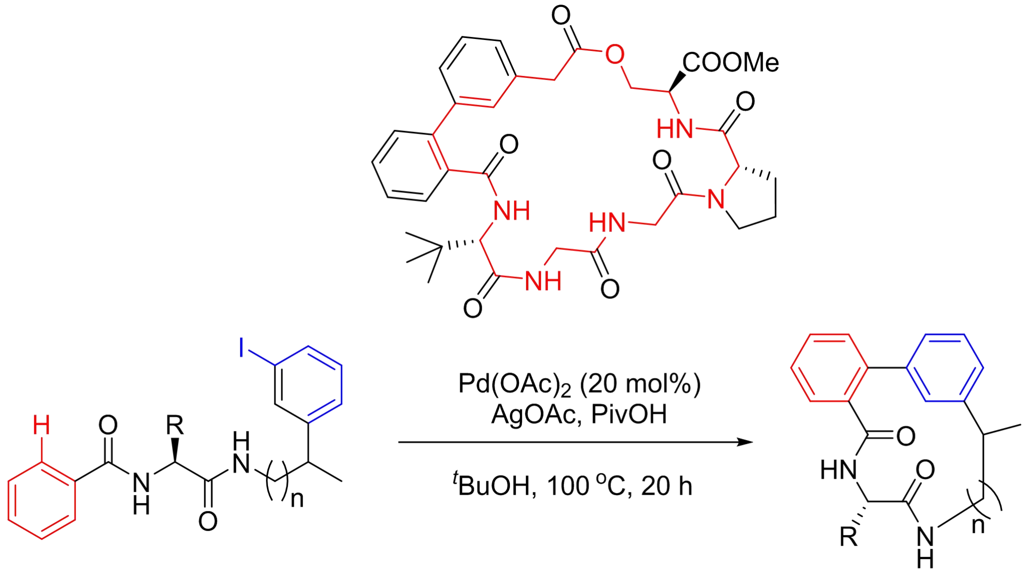

**Scheme 70**: Pd-catalyzed macrocyclization of biaryl-bridged peptides

Cycloaddition reactions have relatively few applications in the construction of macrocycles. The ring expansion strategy is a relatively clever way of thinking. Professor Jian Wang developed a highly enantio-selective intramolecular annulation reaction of 1,3-diols utilizing triazolium N-heterocyclic carbene (NHC) as precatalyst, and synthesized cyclic ketone derivatives with up to 12-membered macrocycles [105] (**Scheme 71**).

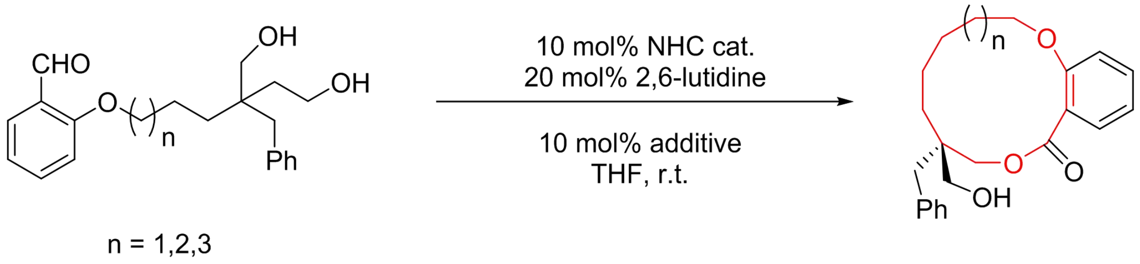

**Scheme 71**: Synthesis of macrocyclic ketone derivatives through intramolecular annulation

Unsworth's research group successfully synthesized dicarbonyl ring compounds with a maximum of twenty-four-membered ring using the ring expansion strategy[106]. The successive ring-expansion protocol enables the insertion of both natural and nonnatural amino acid fragments into lactams (**Scheme 72**). Through this method, without the need of high dilution concentration, the amino acid is iteratively inserted into the macrocyclic compound according to the needs, providing an effective way for the future synthesis of important medicinally cyclic peptide mimetics

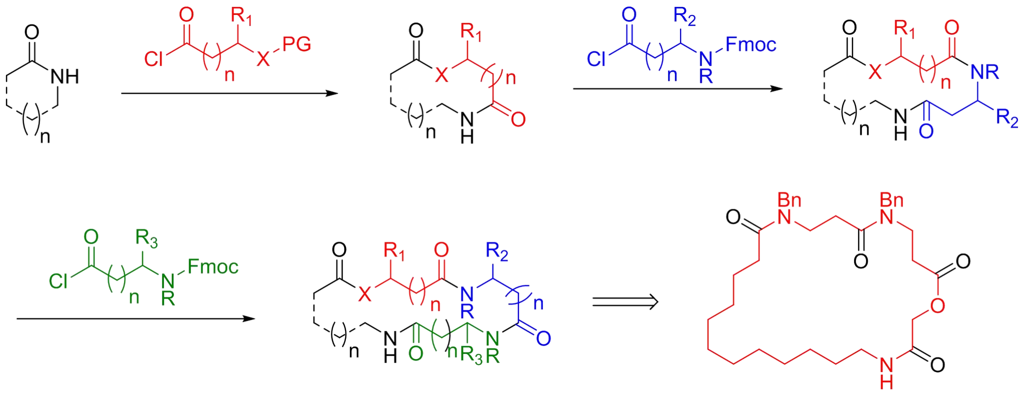

**Scheme 72**: Synthesis of macrocyclic dicarbonyl compounds using ring expansion strategy

As mentioned above, with the advancement of the chemical field and the improvement of scientific methods, chemists have developed many methods for the synthesis of mid-ring and macrocyclic compounds. However, these methods still have some problems. For example:

A. One strategy can usually only synthesize ring skeletons of a single size. A few methods can synthesize but are limited to two or three ring skeletons. There is no universal method that can synthesize a series of medium and large ring skeletons;

B. Many methods require the use of transition metals. However, the synthesis of many cyclic compounds is ultimately dedicated to applications in biomedicine and other pathways, so the problem of transition metal residues in the application of this type of compound will be greatly restricted;

C. In the synthesis of macrocyclic compounds, there is an obvious intermolecular competitive dimerization reaction. Although extremely dilute concentrations can achieve the synthesis of macrocyclics to a certain extent, the reaction rate is very slow and requires a large amount of solvents. Fundamentally avoid the occurrence of intermolecular side reactions.

The existence of these problems shows that it is necessary and challenging to develop new methods and approaches to achieve high-efficiency synthesis of mid-ring and macro-ring skeletons. Based on the accumulation of photochemical research work, develop a new, efficient, green and universal method to efficiently construct various types of medium and large ring frameworks.

### 1.3.4 [2+2] photocycloaddition reaction

In recent years, with the rapid development of photochemistry, various types of visible light catalysis have been widely used in the field of organic synthesis. At the same time, photosynthesis, as one of the most basic organic synthesis reactions in nature, can obtain the energy of sunlight to enable green plants to synthesize various natural products. Among these natural products, there are many mid-ring and macrocyclic compounds with various important physiological activities. For a long time, chemists hope to mimic the magical synthetic methods of nature in the laboratory. Therefore, many chemists have noticed the development of visible light catalysis in the field of organic synthesis and began to try to synthesize various cyclic compounds using photocyclization reactions in the laboratory. Among them, the most classic type of reaction is the [2+2]-halocyclization reaction. Chemists have used this type of reaction to successfully synthesize a variety of cyclic compounds covering small ring, medium sized ring, and macrocyclic skeletons.

Yoon's research group reported a photocatalytic [2+2] cycloaddition reaction, synthesizing 4-4-4-6-6 five-ring fused compounds[107] (**Scheme 73**). This compound has a three-dimensional structure, and its partial structure is similar to that of a rectangular parallelepiped. This work is more to show a method of synthesizing ring structures, also a synthetic art.

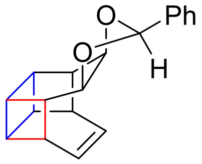

**Scheme 73**: Structure of 4-4-4-6-6 five-ring fused compound

Wang Zhigang's research group reported the rapid construction of [5-6-7] tri-cyclic-ring skeleton of calyciphylline alkaloid daphnilongeranin B[108]. A four-fused polycyclic ring was formed through a photocatalytic [2+2] cycloaddition reaction. Under the function of base, the [5-6-7] tri-cyclic-ring medium sized ring compound was further synthesized (**Scheme 74**).

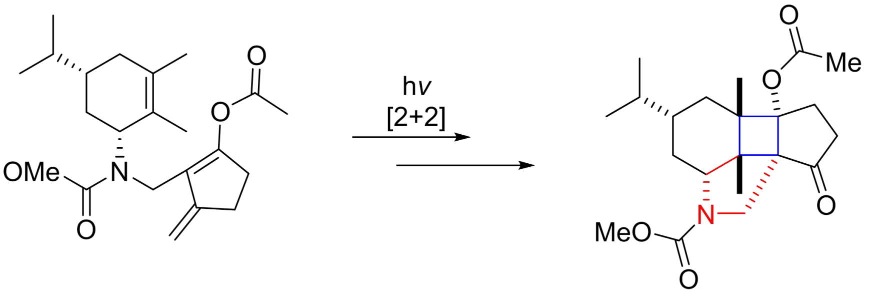

**Scheme 74**: Synthesis of fused ring compounds through photocatalytic [2+2] cycloaddition

In 2004, Thorsten Bach's research group reported the synthesis of 4-(2-Aminoethyl)quinolones with a four fused six-membered ring through a photocatalytic [2+2] cycloaddition reaction[109]. This reaction has a high stereoselectivity and very good yield for both intramolecular and intermolecular reactions (**Scheme 75**).

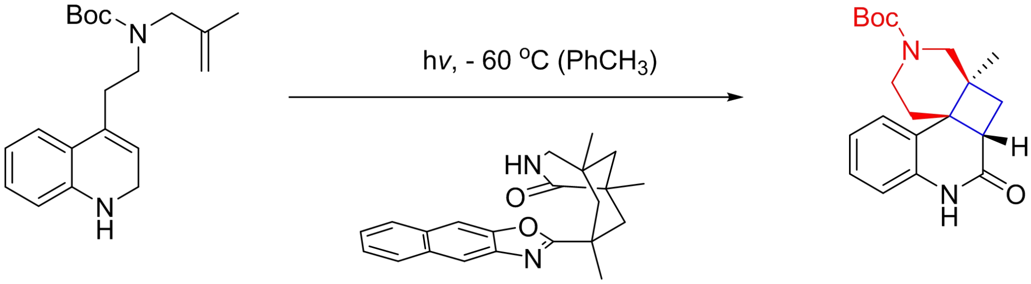

**Scheme 75**: Synthesis of 4-(2-Aminoethyl)quinolones through photocatalytic [2+2] cycloaddition

After that, Professor Thorsten Bach reported an enantioselective intramolecular [2+2] photocycloaddition reaction with Lewis acid catalyst in 2013[110] (**Scheme 76**). One of the products synthesized was applied as a key intermediate in the synthesis of (+)-thermopsine.

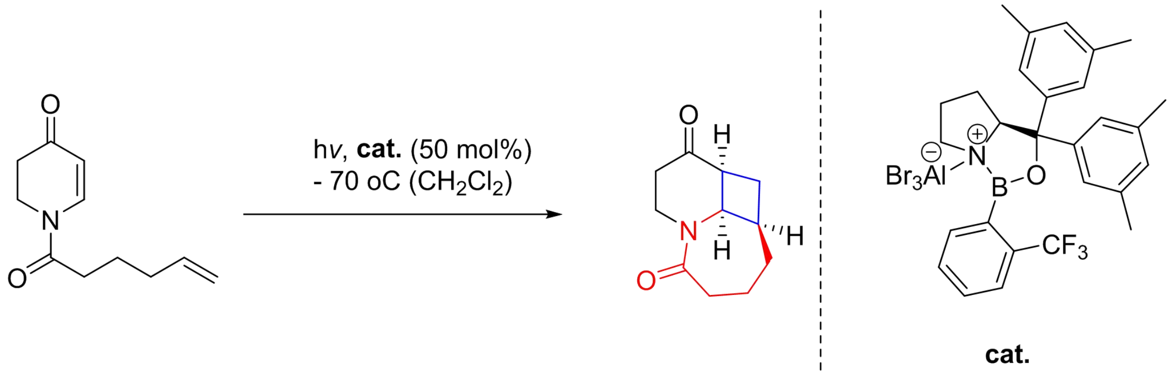

**Scheme 76**: Enantioselective Intramolecular [2+2] photocycloaddition

There is a lot of work to construct cyclic compounds through photocatalytic [2+2] cycloaddition reactions[111] (**Scheme 77**). Although this kind of reaction has received a lot of attention and research, it still has a very big limitation. Starting from the [2+2]-photocyclization reaction, it can only synthesize a four-fused X ring skeleton, but cannot obtain a monocyclic skeleton. However, the four-membered ring is slightly unstable because of its relatively strong spatial distortion tension, therefore it is not a structural system that can be widely used. Especially in natural products, the tetra-X-membered ring skeleton is not a widely existing structure, but more of a variety of cyclic skeletons that exist individually. In the work of total synthesis, what is needed is a method that can efficiently construct independent medium and large rings.

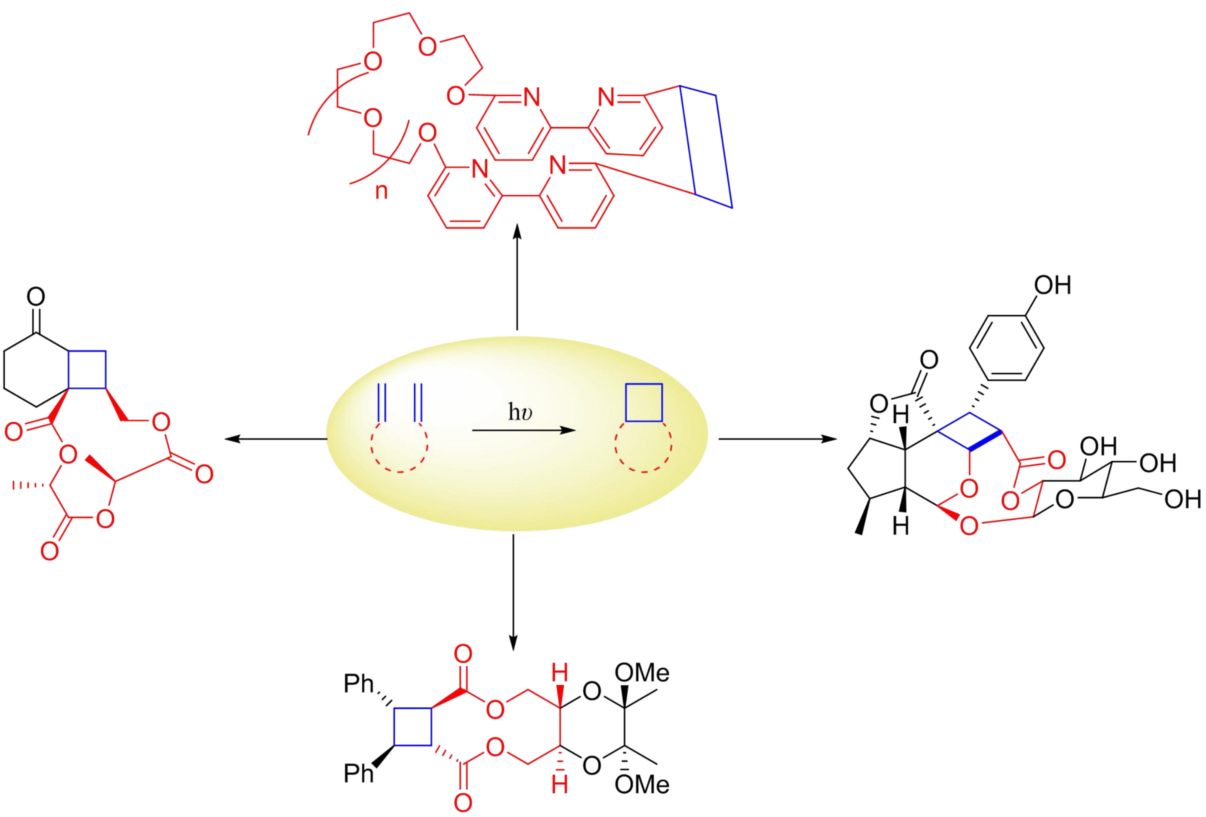

**Scheme 77**: Structures of medium and macrocyclic ring compounds through [2+2]-photocyclization

Life in nature should be based on various basic chemical reactions to gradually synthesize a variety of complex medium and macrocyclic natural products. Perhaps, the [2+2]-photocyclization reaction that chemists are currently familiar with is the basis for the further synthesis of more complex natural products of the ring system. Thus, we look forward to developing methods for constructing medium and macrocyclic frameworks starting from basic reactions such as [2+2]-photocyclization reactions in the future.

# References：

[1] D. Ravelli, D. Dondi, M. Fagnoni, A. Albini, *Chem. Soc. Rev.*, **2009**, *38*, 1999.

[2] G. Ciamician, *Science*, **1912**, *36*, 385-394.

[3] A. Albini, M. Fagnoni, *ChemSusChem*, **2008**, *1*, 63-66.

[4] N. Serpone, A. V. Emeline, *Int. J. Photoenergy*, **2002**, *4*, 91-131.

[5] A. Fujishima, K. Honda, *Nature*, **1972**, *238*, 37-38.

[6] S. Pacala, *Science*, **2004**, *305*, 968-972.

[7] P. Ceroni, A. Credi, M. Venturi, V. Balzani, *Photochem. Photobiol. Sci.*, **2010**, *9*, 1561.

[8] M. Fagnoni, D. Dondi, D. Ravelli, A. Albini, *Chem. Rev.*, **2007**, *107*, 2725-2756.

[9] F. Puntoriero, A. Sartorel, M. Orlandi, G. La Ganga, S. Serroni, M. Bonchio, F. Scandola, S. Campagna, *Coord. Chem. Rev.*, **2011**, *255*, 2594-2601.

[10] J. van de Lagemaat, K. D. Benkstein, A. J. Frank, *J. Phys. Chem. B*, **2001**, *105*, 12433-12436.

[11] M. S. Dresselhaus, I. L. Thomas, *Nature*, **2001**, *414*, 332-337.

[12] V. Balzani, G. Bergamini, S. Campagna, F. Puntoriero, **2007**, *280*, 1-36.

[13] S. Campagna, F. Puntoriero, F. Nastasi, G. Bergamini, V. Balzani, **2007**, *280*, 117-214.

[14] C. K. Prier, D. A. Rankic, D. W. C. MacMillan, *Chem. Rev.*, **2013**, *113*, 5322-5363.

[15] C. Pac, M. Ihama, M. Yasuda, Y. Miyauchi, H. Sakurai, *J. Am. Chem. Soc.*, **1981**, *103*, 6495-6497.

[16] H. Cano-Yelo, A. Deronzier, *Tetrahedron Lett.*, **1984**, *25*, 5517-5520.

[17] D. A. Nicewicz, D. W. C. MacMillan, *Science*, **2008**, *322*, 77-80.

[18] M. L. Hunziker, A. , *J. Am. Chem. Soc.*, **1977**, 7370-7371.

[19] M. A. Ischay, M. S. Ament, T. P. Yoon, *Chem. Sci.*, **2012**, *3*, 2807.

[20] X. G. Mei juanYuan, Nan Li, Qing Li, Sibo Wang, Chun-Sen,Liu, Huan Pang, *ChemSusChem*, **2016**, *9*, 667 –675.

[21] D. A. Nagib, D. W. C. MacMillan, *Nature*, **2011**, *480*, 224-228.

[22] R. J. Crutchley, A. B. P. Lever, *J. Am. Chem. Soc.*, **1980**, *102*, 7128-7129.

[23] N. Zheng, M. Zhu, *Synthesis*, **2011**, *2011*, 2223-2236.

[24] S. Lin, M. A. Ischay, C. G. Fry, T. P. Yoon, *J. Am. Chem. Soc.*, **2011**, *133*, 19350-19353.

[25] E. P. Farney, T. P. Yoon, *Angew. Chem. Int. Ed.*, **2014**, *53*, 793-797.

[26] M. Rueping, S. Zhu, R. M. Koenigs, *Chem. Commun.*, **2011**, *47*, 8679.

[27] M. Rueping, C. Vila, A. Szadkowska, R. M. Koenigs, J. Fronert, *ACS Catalysis*, **2012**, *2*, 2810-2815.

[28] L. Feng, H. Yan, C. Yang, D. Chen, W. Xia, *J. Org. Chem.*, **2016**, *81*, 7008-7022.

[29] S. Meister, R. O. Reithmeier, A. Ogrodnik, B. Rieger, *ChemCatChem*, **2015**, *7*, 3562-3569.

[30] P. J. S. K.A. King, R.J. Watts, *J. Am. Chem. Soc.*, **1985**, *107*, 1432-1432.

[31] S. Lamansky, P. Djurovich, D. Murphy, F. Abdel-Razzaq, R. Kwong, I. Tsyba, M. Bortz, B. Mui, R. Bau, M. E. Thompson, *Inorg. Chem.*, **2001**, *40*, 1704-1711.

[32] J. D. Cuthbertson, D. W. C. MacMillan, *Nature*, **2015**, *519*, 74-77.

[33] M. Rueping, S. Zhu, R. M. Koenigs, *Chem. Commun.*, **2011**, *47*, 12709.

[34] M. Tobisu, T. Furukawa, N. Chatani, *Chem. Lett.*, **2013**, *42*, 1203-1205.

[35] H. Hou, S. Zhu, F. Pan, M. Rueping, *Org. Lett.*, **2014**, *16*, 2872-2875.

[36] C. J. F. a. J. D. W. A. Singh, *Chem. Sci.*, **2016**, *7*, 6796.

[37] A. Arora, J. D. Weaver, *Org. Lett.*, **2016**, *18*, 3996-3999.

[38] M. Nonoyama, *J. Organomet. Chem.*, **1974**, *82*, 271-276.

[39] (a) G. J. Choi, R. R. Knowles, *J. Am. Chem. Soc.*, **2015**, *137*, 9226-9229; (b) D. C. Miller, G. J. Choi, H. S. Orbe, R. R. Knowles, *J. Am. Chem. Soc.*, **2015**, *137*, 13492-13495.

[40] D. A. Nagib, M. E. Scott, D. W. C. MacMillan, *J. Am. Chem. Soc.*, **2009**, *131*, 10875-10877.

[41] C. K. Prier, D. W. C. MacMillan, *Chem. Sci.*, **2014**, *5*, 4173-4178.

[42] J. L. Jeffrey, F. R. Petronijević, D. W. C. MacMillan, *J. Am. Chem. Soc.*, **2015**, *137*, 8404-8407.

[43] E. R. Welin, A. A. Warkentin, J. C. Conrad, D. W. C. MacMillan, *Angew. Chem. Int. Ed.*, **2015**, *54*, 9668-9672.

[44] (a) R. W. Bernd Mühldorf *Chem. Commun.*, **2015**, *51*, 8425-8428; (b) J. M. R. N. Joseph W. Tucker , Pinkey S. Shah, Corey R. J. Stephenson, *Chem. Commun.*, **2011**, *47*, 5040-5042.

[45] A. G. Capacci, J. T. Malinowski, N. J. McAlpine, J. Kuhne, D. W. C. MacMillan, *Nat. Chem.*, **2017**, *9*, 1073-1077.

[46] Y. Y. Loh, K. Nagao, A. J. Hoover, D. Hesk, N. R. Rivera, S. L. Colletti, I. W. Davies, D. W. C. MacMillan, *Science*, **2017**, *358*, 1182-1187.

[47] X. Zhang, D. W. C. MacMillan, *J. Am. Chem. Soc.*, **2016**, *138*, 13862-13865.

[48] G. J. Choi, Q. Zhu, D. C. Miller, C. J. Gu, R. R. Knowles, *Nature*, **2016**, *539*, 268-271.

[49] Q. Zhu, D. E. Graff, R. R. Knowles, *J. Am. Chem. Soc.*, **2018**, *140*, 741-747.

[50] A. Barbieri, G. Accorsi, N. Armaroli, *Chem. Commun.*, **2008**, 2185.

[51] J. Chen, W. R. Browne, *Coord. Chem. Rev.*, **2018**, *374*, 15-35.

[52] J. D. Blakemore, R. H. Crabtree, G. W. Brudvig, *Chem. Rev.*, **2015**, *115*, 12974-13005.

[53] J. E. Monat, J. K. McCusker, *J. Am. Chem. Soc.*, **2000**, *122*, 4092-4097.

[54] W. Gawelda, A. Cannizzo, V.-T. Pham, F. van Mourik, C. Bressler, M. Chergui, *J. Am. Chem. Soc.*, **2007**, *129*, 8199-8206.

[55] J. K. McCusker, *Science*, **2019**, *363*, 484-488.

[56] M. N. Hopkinson, C. Richter, M. Schedler, F. Glorius, *Nature*, **2014**, *510*, 485-496.

[57] P. Chábera, Y. Liu, O. Prakash, E. Thyrhaug, A. E. Nahhas, A. Honarfar, S. Essén, L. A. Fredin, T. C. B. Harlang, K. S. Kjær, K. Handrup, F. Ericson, H. Tatsuno, K. Morgan, J. Schnadt, L. Häggström, T. Ericsson, A. Sobkowiak, S. Lidin, P. Huang, S. Styring, J. Uhlig, J. Bendix, R. Lomoth, V. Sundström, P. Persson, K. Wärnmark, *Nature*, **2017**, *543*, 695-699.

[58] T. Duchanois, L. Liu, M. Pastore, A. Monari, C. Cebrián, Y. Trolez, M. Darari, K. Magra, A. Francés-Monerris, E. Domenichini, M. Beley, X. Assfeld, S. Haacke, P. Gros, *Inorganics*, **2018**, *6*, 63.

[59] P. Zimmer, L. Burkhardt, A. Friedrich, J. Steube, A. Neuba, R. Schepper, P. Müller, U. Flörke, M. Huber, S. Lochbrunner, M. Bauer, *Inorg. Chem.*, **2017**, *57*, 360-373.

[60] P. Zimmer, P. Müller, L. Burkhardt, R. Schepper, A. Neuba, J. Steube, F. Dietrich, U. Flörke, S. Mangold, M. Gerhards, M. Bauer, *Eur. J. Inorg. Chem.*, **2017**, *2017*, 1504-1509.

[61] T. Duchanois, T. Etienne, M. Beley, X. Assfeld, E. A. Perpète, A. Monari, P. C. Gros, *Eur. J. Inorg. Chem.*, **2014**, *2014*, 3747-3753.

[62] P. Zimmer, L. Burkhardt, R. Schepper, K. Zheng, D. Gosztola, A. Neuba, U. Flörke, C. Wölper, R. Schoch, W. Gawelda, S. E. Canton, M. Bauer, *Eur. J. Inorg. Chem.*, **2018**, *2018*, 5203-5214.

[63] A. Francés-Monerris, K. Magra, M. Darari, C. Cebrián, M. Beley, E. Domenichini, S. Haacke, M. Pastore, X. Assfeld, P. C. Gros, A. Monari, *Inorg. Chem.*, **2018**, *57*, 10431-10441.

[64] K. Magra, E. Domenichini, A. Francés-Monerris, C. Cebrián, M. Beley, M. Darari, M. Pastore, A. Monari, X. Assfeld, S. Haacke, P. C. Gros, *Inorg. Chem.*, **2019**, *58*, 5069-5081.

[65] Y. Liu, T. Harlang, S. E. Canton, P. Chábera, K. Suárez-Alcántara, A. Fleckhaus, D. A. Vithanage, E. Göransson, A. Corani, R. Lomoth, V. Sundström, K. Wärnmark, *Chem. Commun.*, **2013**, *49*, 6412.

[66] T. C. B. Harlang, Y. Liu, O. Gordivska, L. A. Fredin, C. S. Ponseca, P. Huang, P. Chábera, K. S. Kjaer, H. Mateos, J. Uhlig, R. Lomoth, R. Wallenberg, S. Styring, P. Persson, V. Sundström, K. Wärnmark, *Nat. Chem.*, **2015**, *7*, 883-889.

[67] T. Duchanois, T. Etienne, C. Cebrián, L. Liu, A. Monari, M. Beley, X. Assfeld, S. Haacke, P. C. Gros, *Eur. J. Inorg. Chem.*, **2015**, *2015*, 2469-2477.

[68] M. Pastore, T. Duchanois, L. Liu, A. Monari, X. Assfeld, S. Haacke, P. C. Gros, *Physical chemistry chemical physics : PCCP*, **2016**, *18*, 28069-28081.

[69] L. Liu, T. Duchanois, T. Etienne, A. Monari, M. Beley, X. Assfeld, S. Haacke, P. C. Gros, *Phys. Chem. Chem. Phys.*, **2016**, *18*, 12550-12556.

[70] M. Darari, E. Domenichini, A. Francés-Monerris, C. Cebrián, K. Magra, M. Beley, M. Pastore, A. Monari, X. Assfeld, S. Haacke, P. C. Gros, *Dallton Trans.*, **2019**, *48*, 10915-10926.

[71] Y. Liu, K. S. Kjaer, L. A. Fredin, P. Chábera, T. Harlang, S. E. Canton, S. Lidin, J. Zhang, R. Lomoth, K.-E. Bergquist, P. Persson, K. Wärnmark, V. Sundström, *Chem. Eur. J.*, **2015**, *21*, 3628-3639.

[72] P. Chábera, K. S. Kjaer, O. Prakash, A. Honarfar, Y. Liu, L. A. Fredin, T. C. B. Harlang, S. Lidin, J. Uhlig, V. Sundström, R. Lomoth, P. Persson, K. Wärnmark, *J. Phys. Chem. Lett.*, **2018**, *9*, 459-463.

[73] P. Chábera, L. Lindh, N. W. Rosemann, O. Prakash, J. Uhlig, A. Yartsev, K. Wärnmark, V. Sundström, P. Persson, *Coord. Chem. Rev.*, **2021**, *426*, 213517.

[74] K. S. Kjær, N. Kaul, O. Prakash, P. Chábera, N. W. Rosemann, A. Honarfar, O. Gordivska, L. A. Fredin, K.-E. Bergquist, L. Häggström, T. Ericsson, L. Lindh, A. Yartsev, S. Styring, P. Huang, J. Uhlig, J. Bendix, D. Strand, V. Sundström, P. Persson, R. Lomoth, K. Wärnmark, *Science*, **2019**, *363*, 249-253.

[75] F. J. Schmitz, S. P. Gunasekera, G. Yalamanchili, M. B. Hossain, D. Van der Helm, *J. Am. Chem. Soc.*, **1984**, *106*, 7251-7252.

[76] A. J. B. Michael Entzeroth, Jon S. Mynderse, Richard E. Moore, *J. Org. Chem.*, **1984**, *50*, 1255-1259.

[77] H.-N. Chou, Y. Shimizu, G. Van Duyne, J. Clardy, *Tetrahedron Lett.*, **1985**, *26*, 2865-2868.

[78] J. i. Tanaka, T. Higa, *Chem. Lett.*, **1984**, *13*, 231-232.

[79] M. Suzuki, E. Kurosawa, A. Furusaki, S.-i. Katsuragi, T. Matsumoto, *Chem. Lett.*, **1984**, *13*, 1033-1034.

[80] P. S. Sebastian Gotze, *Nat. Prod. Rep.*, **2020**, *37*, 29-54.

[81] F. Gueritte-Voegelein, D. Guenard, F. Lavelle, M. T. Le Goff, L. Mangatal, P. Potier, *J. Med. Chem.*, **1991**, *34*, 992-998.

[82] N. Wang, Q.-S. Gu, Z.-L. Li, Z. Li, Y.-L. Guo, Z. Guo, X.-Y. Liu, *Angew. Chem. Int. Ed.*, **2018**, *57*, 14225-14229.

[83] B. Schurgers, J. Wouters, A. De Blieck, G. Van Lommen, C. Menet, G. Verniest, *Eur. J. Org. Chem.*, **2019**, *2019*, 36-40.

[84] Y. W. L. Zhang, Z.-J. Yao, S. Wang, Z.-X. Yu, *J. Am. Chem. Soc.*, **2015**, *137*, 13290-13300.

[85] J. Zhang, L. Zhou, Q. Sun, H. Ming, L. Sun, C. Wang, Y. Wu, K. Guan, L. Wang, J. Ming, *Chem. Eur. J.*, **2019**.

[86] Y.-Q. Z. B. Zhou, K. Zhang, M.-Y. Yang, Y.-B. Chen, Y. Li, Q. Peng, S.-F. Zhu, Q.-L. Zhou, L.-W. Ye, *Nat. Commun.*, **2019**, *10*, 1-11.

[87] M. Wang, Y. Yang, B. Song, L. Yin, S. Yan, Y. Li, *Org. Lett.*, **2019**, *22*, 155-159.

[88] L. G. Baud, M. A. Manning, H. L. Arkless, T. C. Stephens, W. P. Unsworth, *Chem. Eur. J.*, **2017**, *23*, 2225-2230.

[89] Y. Chen, W. Zhang, L. Ren, J. Li, A. Li, *Angew. Chem.*, **2018**, *130*, 964-968.

[90] K. Fukaya, Y. Tanaka, A. C. Sato, K. Kodama, H. Yamazaki, T. Ishimoto, Y. Nozaki, Y. M. Iwaki, Y. Yuki, K. Umei, T. Sugai, Y. Yamaguchi, A. Watanabe, T. Oishi, T. Sato, N. Chida, *Org. Lett.*, **2015**, *17*, 2570-2573.

[91] Z. H. Zhongnan Xu, Yueheng Li, Rositha Kuniyil, Chao Zhang, Lutz Ackermann, Zhixiong Ruan, *Green Chem.*, **2020**, *22*, 1099-1104.

[92] J. Zhang, M. Liu, C. Wu, G. Zhao, P. Chen, L. Zhou, X. Xie, R. Fang, H. Li, X. She, *Angew. Chem. Int. Ed.*, **2020**, *59*, 3966-3970.

[93] S. Kotha, R. R. Keesari, S. Ansari, *Synthesis*, **2019**, *51*, 3989-3997.

[94] H.-J. Zhang, L. Hu, Z. Ma, R. Li, Z. Zhang, C. Tao, B. Cheng, Y. Li, H. Wang, H. Zhai, *Angew. Chem. Int. Ed.*, **2016**, *55*, 11638-11641.

[95] X. Gao, M. Xia, C. Yuan, L. Zhou, W. Sun, C. Li, B. Wu, D. Zhu, C. Zhang, B. Zheng, D. Wang, H. Guo, *ACS Catalysis*, **2019**, *9*, 1645-1654.

[96] Y. Z. Liu, Z. Wang, Z. Huang, X. Zheng, W. L. Yang, W. P. Deng, *Angew. Chem. Int. Ed.*, **2019**, *59*, 1238-1242.

[97] H. Ni, X. Tang, W. Zheng, W. Yao, N. Ullah, Y. Lu, *Angew. Chem. Int. Ed.*, **2017**, *56*, 14222-14226.

[98] Z. T. Liu, X. P. Hu, *Adv. Synth. Catal.*, **2018**.

[99] L. Huang, L.-X. Dai, S.-L. You, *J. Am. Chem. Soc.*, **2016**, *138*, 5793-5796.

[100] X.-Y. Liu, Y. Qin, *Acc. Chem. Res.*, **2019**, *52*, 1877-1891.

[101] B. Zhou, L. Li, X.-Q. Zhu, J.-Z. Yan, Y.-L. Guo, L.-W. Ye, *Angew. Chem. Int. Ed.*, **2017**, *56*, 4015-4019.

[102] K. Zheng, D. Shen, R. Hong, *J. Am. Chem. Soc.*, **2017**, *139*, 12939-12942.

[103] W.-W. Zhang, T.-T. Gao, L.-J. Xu, B.-J. Li, *Org. Lett.*, **2018**, *20*, 6534-6538.

[104] Q. Bai, Z. Bai, H. Wang, *Org. Lett.*, **2019**, *21*, 8225-8228.

[105] Z. Wu, J. Wang, *ACS Catalysis*, **2017**, *7*, 7647-7652.

[106] M. L. Thomas C. Stephens, AndrewM.Steer,Yun Lin, MatthewT.Gill, WilliamP.Unsworth, *Chem. Eur.J.*, **2017**, *23*, 13314 –13318.

[107] H. Gan, M. G. Horner, B. J. Hrnjez, T. A. McCormack, J. L. King, Z. Gasyna, G. Chen, R. Gleiter, N.-c. C. Yang, *J. Am. Chem. Soc.*, **2000**, *122*, 12098-12111.

[108] I. Coldham, A. J. M. Burrell, H. l. n. D. S. Guerrand, N. Oram, *Org. Lett.*, **2011**, *13*, 1267-1269.

[109] T. Bach, S. Brandes, P. Selig, *Synlett*, **2004**, *2004*, 2588-2590.

[110] T. B. R. Brimioulle, *Science*, **2013**, *342*, 840-843.

[111] S. Inokuma, M. Kuramami, S. Otsuki, T. Shirakawa, S.-i. Kondo, Y. Nakamura, J. Nishimura, *Tetrahedron*, **2006**, *62*, 10005-10010.

# 2. Design and Synthesis of Heteroleptic Fe(II)-Hexa-N-Heterocyclic Carbene Complex with 130 ps Metal-to-Ligand Charge-Transfer state lifetime

## 2.1 Introduction

The fossil fuel crisis has prompted scientists to explore new types of energy. Among the many new energy sources, sunlight is naturally one of the best choice. At present, the utilization of sunlight by human beings is only a very small part of the energy that the sun radiates to the earth. For decades, scientists have been continuously exploring new ways of using sunlight and improving utilization efficiency[1]. Among the many strategies, photovoltaic devices based on light harvesting[2] and its conversion into electricity have been actively investigated[3].

In the past ten years, the field of visible light photoredox catalysis has made considerable progress. Scientists can realize the construction of a series of chemical bonds under extremely mild conditions under the action of photocatalyst. The currently commonly used visible light catalysts are still polypyridine or phenylpyridine complexes centered on Ru[2] and Ir. Both Ru[4] and Ir photocatalysts have exhibited excellent photochemical and photophysical properties and have already made considerable progress in the fields of organic synthesis. However, they are still limited in actual production due to that they're rare heavy metals. The high price will greatly limit their application in industrial production, and their toxicity will also greatly restrict their application in biomedicine, food and other synthetic fields. In this view, chemists have been working to explore alternatives to Ru and Ir catalysts. Compared to 4d and 5d metals, 3d metals are usually cheaper and easier to obtain. Among those, earth-abundant, low-cost and environmentally friendly iron are particularly attractive. As the most widely used metal on the earth, Fe is a well-deserved green metal, which is widely present in nature and organisms. In addition, Fe has also exhibited good photophysical properties. It is worth pointing out that, as the most important photochemical reaction on earth

- photosynthesis, its action process cannot be separated from the participation of iron. In 2000, McCusker's research group explored the photophysical properties of Fe-N complexes as potential optical catalysts for the first time[5]. Unfortunately, this complex only exhibits an excited state lifetime of 100 fs. Moreover, this extremely fast excited state passivation phenomenon occurs in all Fe-N complexes, including the bipyridine ligand, which has contributed to the most successfully photo catalyst[6]. This is because the 3d metal iron complex does not have the strong ligand field split like 4d metal Ru and 5d metal Ir. As a result, the $e_g$ orbitals related MC state is largely stabilized[7]. Various studies and calculations have shown that low-lying metal-centered (MC) states are responsible for the ultrafast deactivation of the MLCT state in Fe-N complexes[8].

Some conventional strategies can be used to slow down this deactivation process, such as introducing strong σ-donating ligand and constructing a perfect octahedral structure to destabilize the MC state, or extend π conjugate system and introduce strong electron absorption groups to stabilize MLCT state. Facts have proved that these strategies are effective, especially the introduction of strong σ-donating ligand N heterocyclic carbene, which has brought dawn to the solution of this problem[9].

The most successful Fe(II) complex at present comes from the work reported by Kenneth Wärnmark's group in 2018, with 3,3′-dimethyl-1,1′-bis(p-tolyl)-4,4′-bis-(1,2,3-triazol-5-ylidene (btz) as the ligand. The btz ligand provides 6 strong σ-donating NHC ligands, which effectively destabilizes the MC state. Meanwhile, the p-tolyl group effectively stabilizes the MLCT state. As a result, $Fe(btz)_3^{2+}$ shows a MLCT excited state lifetime of 528 ps[10] (**Scheme 1**).

However, for the homoleptic Fe(II) complex, it is difficult to achieve greater improvement if there is no stronger σ-donating ligand such as silylenes. Inspired by the excellent performance of heteroleptic Ir catalysts, our attentions are drawn to the design of heteroleptic Fe(II) complex. The most successful heteroleptic Fe(II) complex by far comes from the report of Kenneth Wärnmark in 2015 with 13 ps excited state lifetime[11] (**Scheme 1**). Refer to heteroleptic Ir catalysts, he replaced one of the btz ligands in $Fe(btz)_3^{2+}$ with a bipyridine ligand. However, this change reduces the number of strong σ-donating ligands, and also greatly reduces the excited state lifetime of the Fe complex.

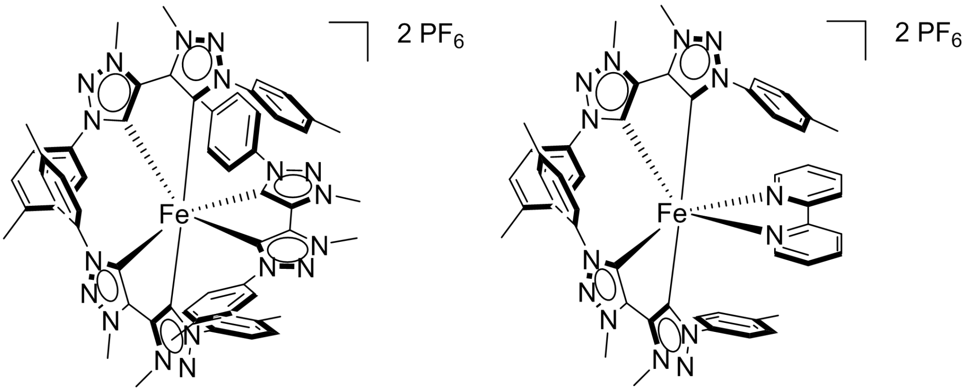

528 ps MLCT lifetime

13 ps MLCT lifetime

**Scheme 1**: Structure of homoleptic Fe(II) complex and heteroleptic Fe(II) complex with longest MLCT state lifetime

In addition, Heteroleptic Fe(II) complex has an unparalleled advantage in the targeted regulation of the photophysical and electrochemical properties. Because its HOMO and LUMO are orthogonal, the modification of one ligand will not interfere with the influence of the other ligand on the properties of the complex. As a great example, heteroleptic Ir catalysts have exhibited extremely good performance in this aspect.

## 2.2 Design idea

On this basis, the design ideas of heteroleptic Fe(II) complex has been intergrated as follows:

1. The strong σ-donating ligand (NHCs)[12], the more effectively the MC state of the complex can be destabilized[13].

2. The larger the ligand conjugation system which determines the LUMO of the complex, the more effectively the MLCT state can be stabilized.

In view of the work of our laboratory, the following Fe(II)-Hexa-N-Heterocyclic Carbene Complexes **FeC-1** and **FeC-2** have been designed and synthesized (**Scheme 2**). Their photophysical, photochemical and electrochemical properties have also been characterized and carefully studied.

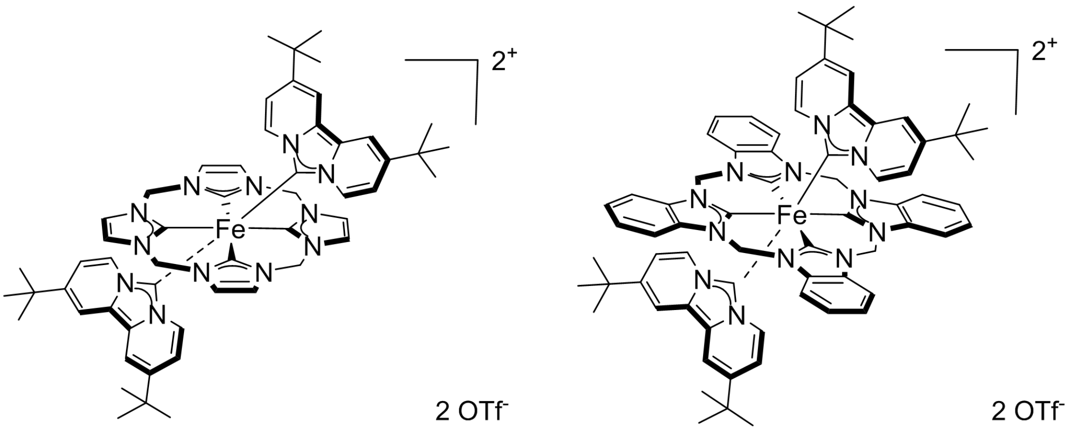

**Fe-1** **Fe-2**

**Scheme 2**: Structures of **FeC-1** and **FeC-2**

As shown in the figure, both **Fe-1** and **Fe-2** are Fe(II) six-carbene complexes. According to a large number of previous experiments and calculations, the number of NHC ligands is positively correlated with the energy of the MC state of the complex. Therefore, in the complexes we designed, the MC energy state can be largely destabilized.

For **Fe-1** and **Fe-2**, the HOMO of the complex is determined by the $t_{2g}$ orbital of the metal center, while the LUMO of the complex is determined by the axial ligands 2,10-di-*tert*-butylimidazo-dipyridin carbene (DBIDP) due to its larger π system.

## 2.3 Synthesis

### 2.3.1 Synthesis of DBIDP

The synthesis of Axial NHC ligands starts with 4,4'-di-*tert*-butyl-2,2'-bipyridine, and finally generate the free carbene DBIDP through three steps (**Scheme 3**). It is worth pointing out that DBIDP is soluble in ether, pentane, acetonitrile and many organic solvents. The solution state of DBIDP will slowly produce dimers, while the solid state is relatively stable under dry Argon.

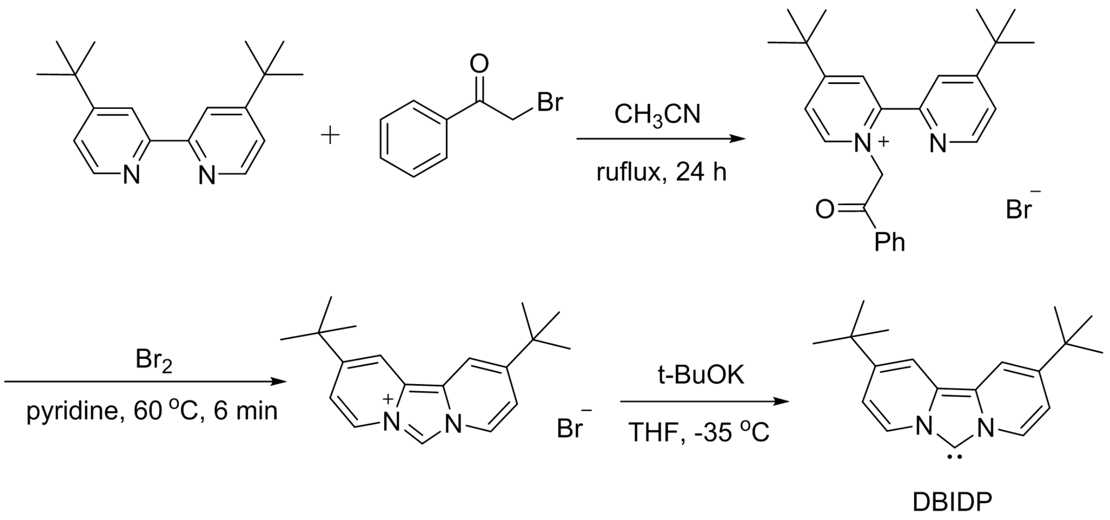

**Scheme 3**: Synthesis of axial NHC ligands DBIDP

## 2.3.2 Synthesis of Fe-1

The synthesis of **Fe-1a** refers to previous work in the lab. Starting from imidazole and paraformaldehyde, **Fe-1a** was obtained after four steps of synthesis, and then further reacted with free carbene DBIDP at room temperature to obtain **Fe-1** with a yield of up to 90%. When **Fe-1a** reacted with DBIDP 1:2, the target product **Fe-1** cannot be obtained. When the equivalent of DBIDP was increased to 4 times high, **Fe-1a** can be completely converted into **Fe-1**. In addition, the single crystal cultured by various methods failed to test successfully due to the unknown special structure of **Fe-1** (**Scheme 4**).

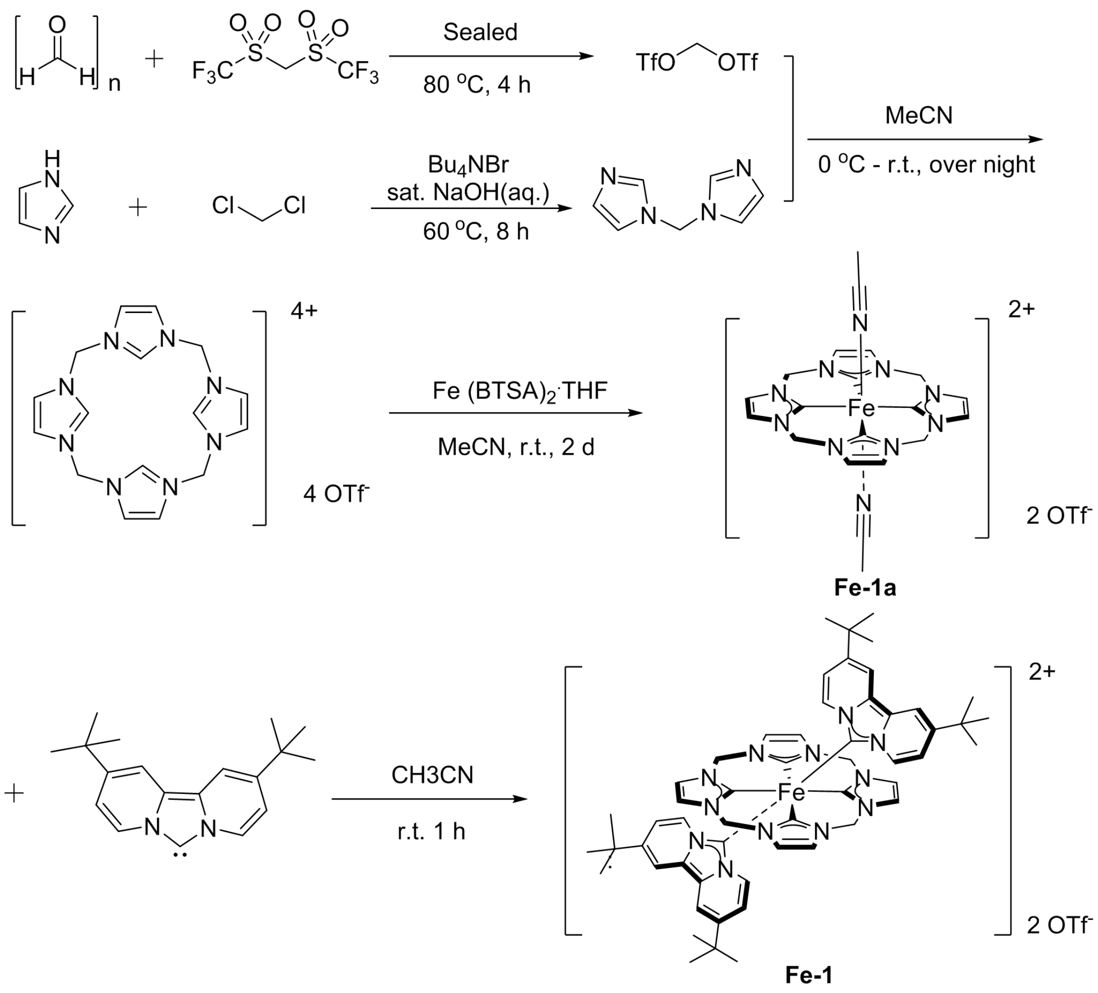

**Scheme 4**: Synthesis of **Fe-1**

## 2.3.3 Synthesis of Fe-2

The synthesis of **Fe-2** and **Fe-1** was similar, the difference was that the starting material was changed from imidazole to benzimidazol. After 5 steps, **Fe-2** can be obtained smoothly. The structure of **Fe-2** was also confirmed by single crystal analysis (**Scheme 5**).

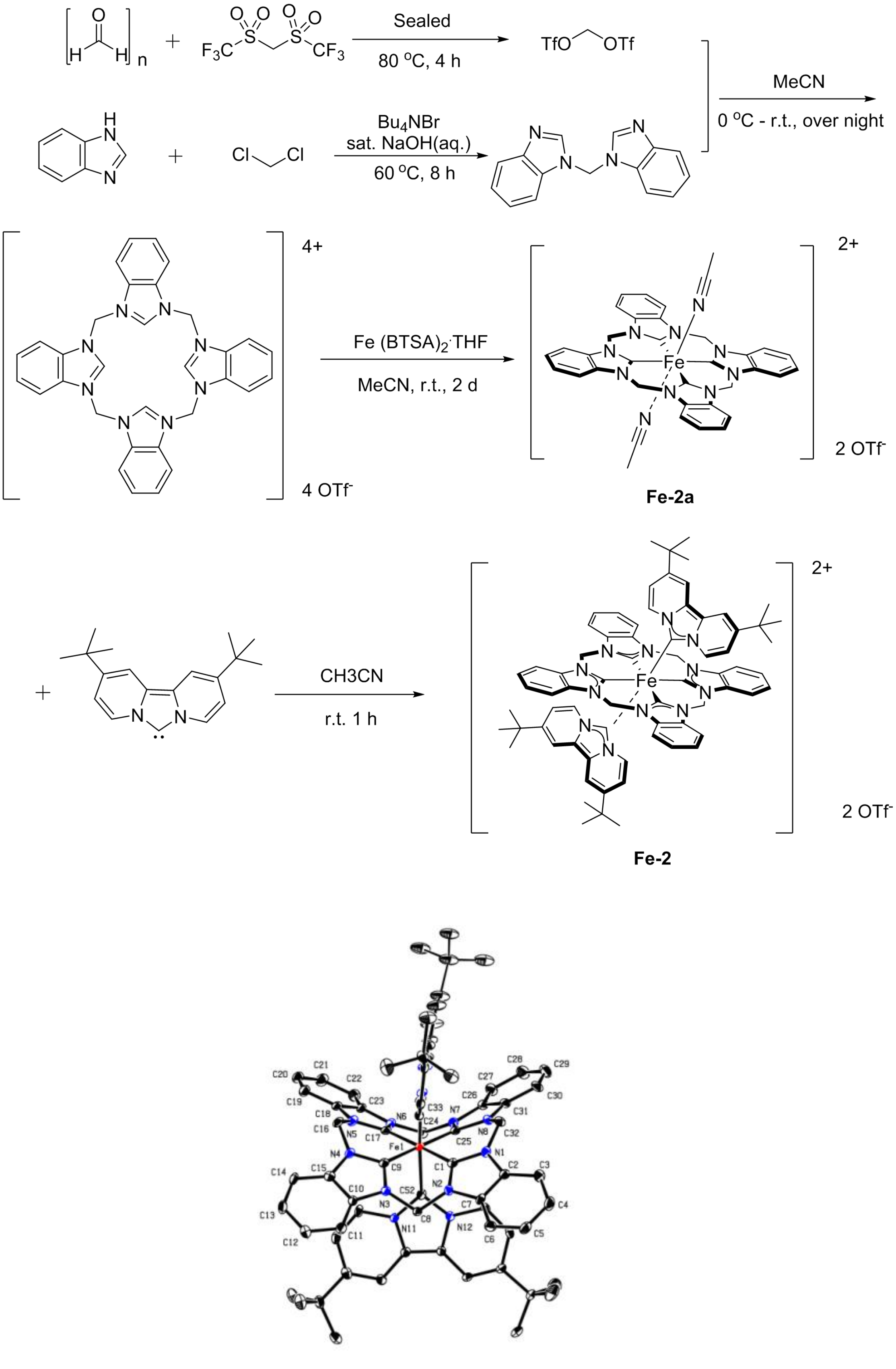

**Scheme 5**: Synthesis of **Fe-2**

## 2.3.4 Oxidation of Fe-1 and Fe-2

In the follow-up research, in order to conduct a more in-depth study on the steady-state absorption of **Fe-1** and **Fe-2**, **Fe-1** and **Fe-2** were chemically oxidized respectively. By studying and comparing the UV-Vis absorption of its oxidation state, the absorption peaks of **Fe-1** and **Fe-2** can be better assigned. In our expectation, **Fe-1a** was firstly oxidized to obtain **Fe(III)-1a**, and then **Fe(III)-1a** was replaced with DBIDP by ligand replacement. However, the reaction process showed unexpected results.

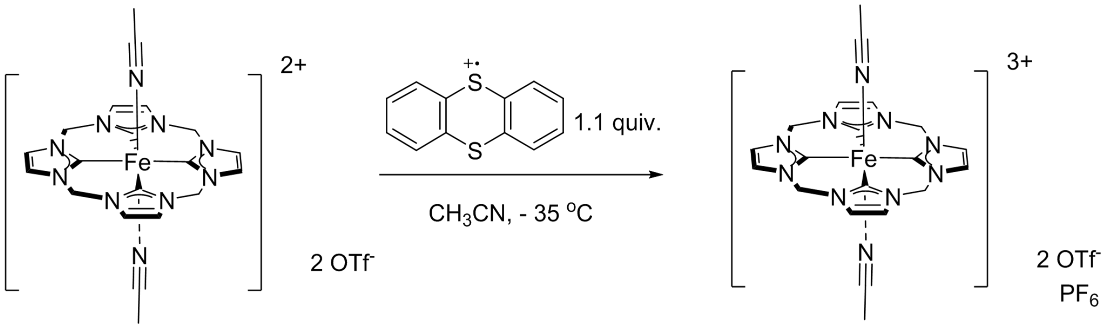

**Fe(III)-1a**

**Scheme 6**: Oxidation of **Fe-1a**

When **Fe(III)-1a** reacted with two equivalents of DBIDP, the final result showed a mess. When the DBIDP was increased to 4 times the equivalent, the reaction obtained **Fe-1** with a very high yield. This result allows us to re-examine the progress of the reaction and conclude that **Fe(III)-1a** will first be reduced to **Fe-1a** under the action of DBIDP, and then **Fe-1a** will continue the ligand replacement to form **Fe-1** with DBIDP (**Scheme 6**).

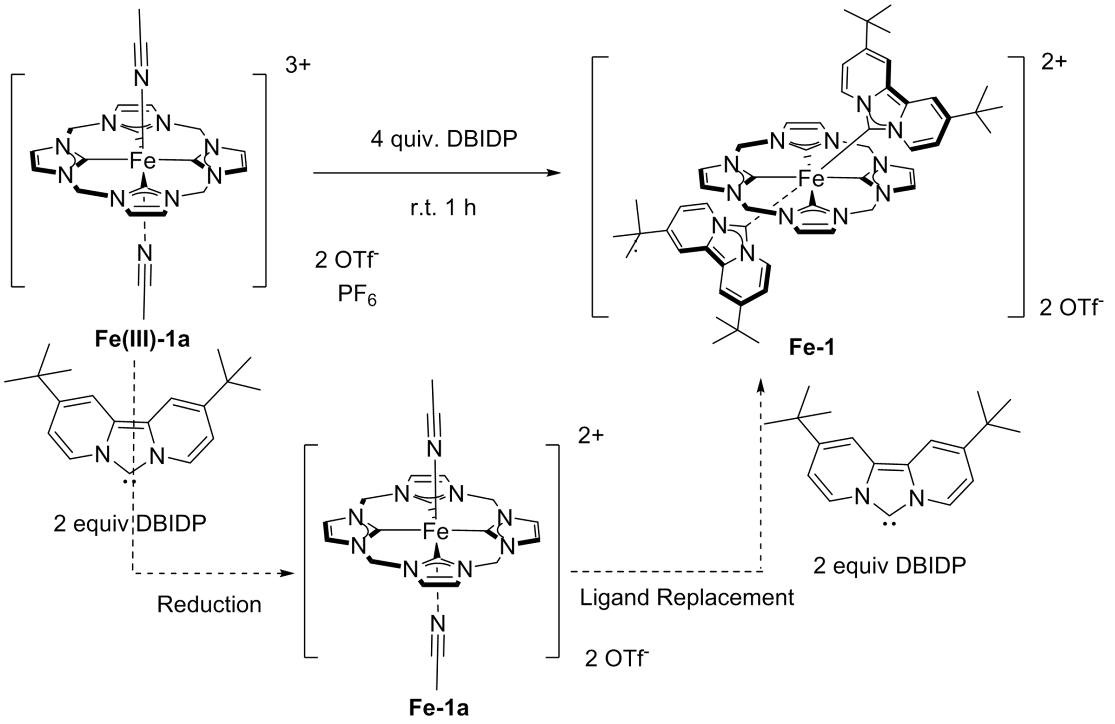

**Scheme 6**: Ligand replacement of **Fe(III)-1a**

Therefore, our strategy had been changed and **Fe-1** was oxidized directly, and finally **Fe(III)-1** was obtained (**Scheme 7**).

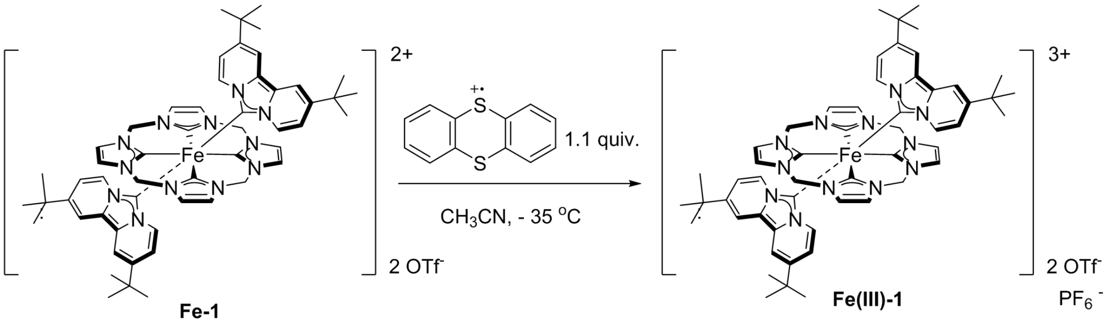

**Scheme 7**: Oxidation of **Fe-1**

This phenomenon also appears in the oxidation of **Fe-2** (**Scheme 8**).

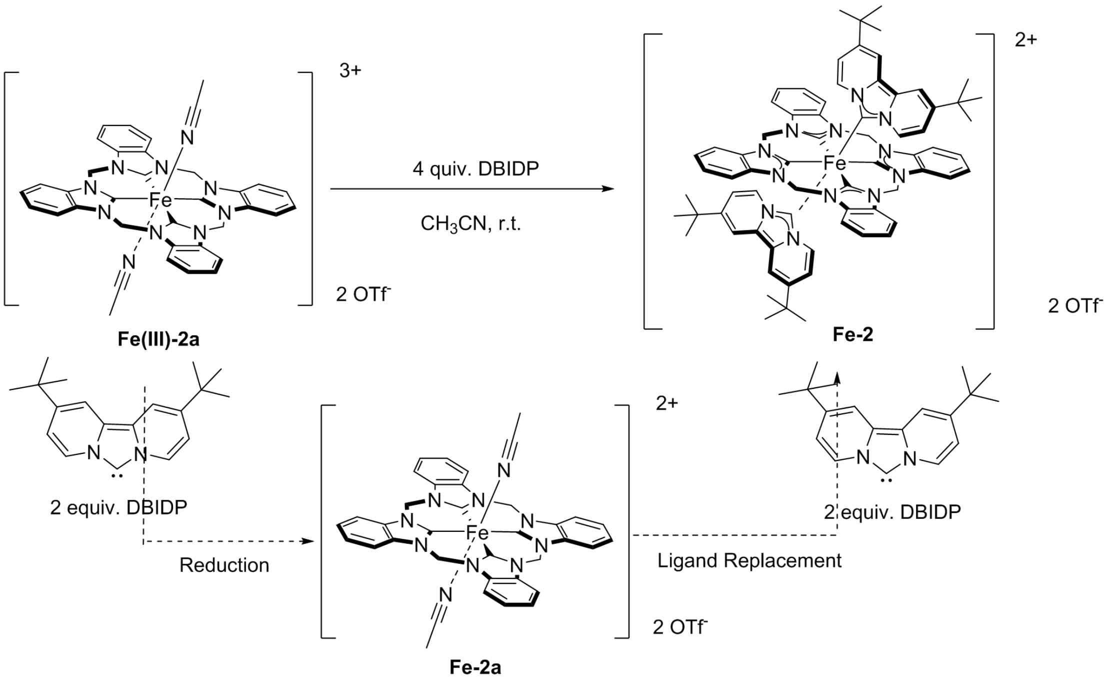

**Scheme 8**: Ligand replacement of **Fe(III)-2a**

## 2.4 Electrochemical Investigations

Cyclic voltammetry (CV) measurement had been conducted to study the electrochemical properties of **Fe-1** and **Fe-2**. The measurement was performed in acetonitrile (anhydrous and oxygen-free) solution with tetrabutylammonium hexafluorophosphate as the supporting electrolyte. Both **Fe-1** and **Fe-2** were able to undergo two fully reversible one-electron redox processes. The first reversible cycle was assigned to the Fe(II)/Fe(III) redox couple, while the second cycle was attributed as axial NHC ligands DBIDP's $L/L^+$ redox couple.

### 2.4.1 Analysis for Fe-1

Firstly, **Fe-1** was taken as the research object (**Scheme 9**). For the reversible redox cycle of complex **Fe-1**, the half-cell potentials $E_{1/2}$ was determined with -0.34 V, The peak separation ΔEp was calculated as 110 mV, which was slightly above the typical value (80 mV) for a one-electron process reversible. It was meaningful to make a comparation between **Fe-1** and **Fe-1a**[14].The half-cell potential of **Fe-1a** was determined with $E_{1/2} = 0.15$ V by previous work.

Compared to the **Fe-1a** bearing tetra-carbene ligands and axial acetonitrile ligands, the even lower value of -0.34 V for **Fe-1** was attributed as the effect of extra two axial carbene ligands. With respect to the strong σ-donating property of NHC ligands, the extreme low half-cell potential of -0.34 V was a direct consequence of the high electron density around the iron center of **Fe-1**, which was induced by six NHC ligands.

In addition, **Fe-1a** performs only one reversible redox cycle of Fe(II)/Fe(III), which demonstrates that the tetra-NHC ligands cannot perform a reversible redox cycle. Thus the second reversible redox cycle following the Fe(II)/Fe(III) cycle in **Fe-1** can only belong to the L/L+ cycle of axial NHC ligands, or the cycle of Fe(III)/Fe(IV) redox couple. However, the single-electron reversible cycle of Fe(III)/Fe(IV) is generally rare, a separate CV test of the axial NHC ligand DBIDP was conducted for comparision. Although DBIDP alone cannot perform a single electron reversible cycle due to the instability of its free carbene state, the oxidation potential is similar to that of the second reversible redox cycle in **Fe-1**, which proves that the second redox cycle belongs to the axial NHC ligand L/L+ redox couple. The half-cell potential $E_{1/2}$ of the ligand DBIDP L/L+ is 0.27 V, and the peak separation ΔEp is 138 mV.

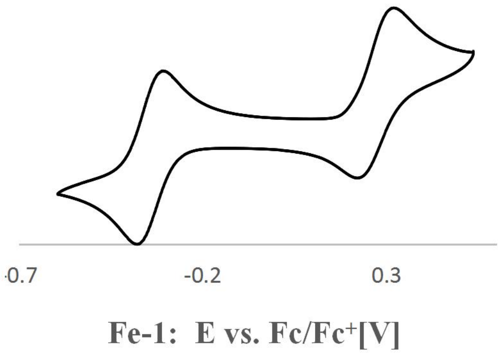

**Scheme 9**: CV curve of **Fe-1** and **Fe-1a** measured in MeCN solution

## 2.4.2 Analysis of Fe-2

Similarly, the first reversible redox cycle in **Fe-2** belongs to the Fe(II)/Fe(III) redox couple, the half-cell potentials $E_{1/2}$ was determined with -0.12 V (**Scheme 10**). This extremely low value also gets benefits from the strong σ-donating property of 6 NHC ligands, which results in the high electron density around the Fe center. This value is lower than 0.44 V of **Fe-2a**, which can be attributed to the additional electron density brought by the replacement of two acetonitrile molecules with axial NHC ligands. Compared with **Fe-1**, the half-cell potentials slightly shift from -0.34 V to -0.12 V, which can be interpreted as the result of replacing tetra-imidazole carbene in **Fe-1** with tetra benzimidazol carbene. The extended π conjugated system will enhance the π electron accepting ability of the ligand, which results in a decrease in the electron density of the metal center and further lead to the positive shift of the half-cell potential. The peak separation ΔEp was calculated as 117 mV, which was similar with that of **Fe-1**

The second reversible redox cycle of **Fe-2** can also be attributed to the axial NHC ligand DBIDP L/L+ redox couple. The half-cell potentials $E_{1/2}$ was determined with 0.34 V, which shows a slightly positive shift of 0.07 V. This can be explained by the fact that the ligand is affected by the decrease in the electron density of the metal center, thereby slightly shifting to the positive direction. The peak separation ΔEp also shows a slight difference of 0.014 V, valuing 152 mV. This small difference perfectly corresponds to the difference of the half-cell potentials,

$\Delta\,[{}^{\mathbf{Fe\text{-}2}}\Delta Ep(L/L^{+}) - {}^{\mathbf{Fe\text{-}1}}\Delta Ep(L/L^{+})]\text{-}=2\,\Delta\,[\,{}^{\mathbf{Fe\text{-}2}}E_{1/2}(L/L^{+}) - {}^{\mathbf{Fe\text{-}1}}E_{1/2}(L/L^{+})]$.

This fully shows that the second reversible redox cycle of **Fe-1** and **Fe-2** belongs to the ligand (L/L+) redox couple. Assumed that it belongs to the metal Fe(III)/Fe(IV) redox couple, then the second cycle of **Fe-1** and **Fe-2** will be independent of each other, and there will be no such close correlation.

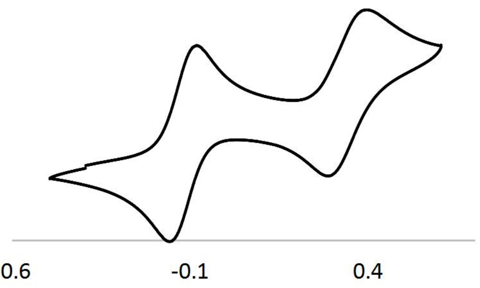

**Fe-2: E vs. Fc+[V]**

**Scheme 10**: CV curve of **Fe-2** measured in the MeCN solution

Overall, the CV measurements show that the strong σ-donor abilities of the NHC ligands, which have significantly affect the electrochemical properties of Fe complex.

6 NHC ligands have greatly increased the electron density of Fe center, which shifts the oxidation potential sharply from 0.15 V (**Fe-1a**) and 0.44 V(**Fe-2a**)[15], to -0.34 V (**Fe-1**) and -0.12 V (**Fe-2**), respectively. In addition, the extended conjugated system of ligands also showed a reduction in the oxidation potential of metal complexes due to its stronger π electron back donation ability. This change of π system shifts the oxidation potential of both reversible cycles from -0.34 V (**Fe-1**) and 0.27 V (**Fe-1**) to -0.12 V(**Fe-2**) and 0.34 V(**Fe-2**), respectively.

## 2.5 Steady-State Absorption Spectrum

Since our goal is to explore the possibility of Fe complexes as photo catalysts, it is necessary to study the optical absorption of **Fe-1** and **Fe-2**. In addition, the further study of the excited state of the complex requires us to have a deep understanding of its steady-state absorption spectrum. Therefore, the measurements of steady-state absorption of **Fe-1** and **Fe-2** has been conducted and studied carefully (**Scheme 11**). The ground state absorption of **Fe-1** and **Fe-2** is shown in Fig,1. Both **Fe-1** and **Fe-2** exhibit two intense absorption bands in the UV region (250 nm and 300 nm), which was attributed to the ligand centered π-π* transition. Meanwhile, there is one another notable peak of **Fe-1**, located around 337 nm, which is corresponding to the MLCT transition of metal-to-tetracarbene-ligand charge transfer state. The location of this peak redshifted upon the ligands switching from the imidazolylidene of **Fe-1** to benzimidazolylidene of **Fe-2,** ascribed to stabilization of the π* energy level of the ligand. This also can be illustrated that the extended π-conjugated system will effectively enhance the ligand's π electron-accepting ability, thereby effectively reducing the difficulty of electron transfer from the metal to the ligand, thereby stabilizing the MLCT state. The bands at higher wavelength above 400 nm can be assigned to the MLCT transition of Fe-to axial-NHC-ligand charge transfer state. This attribution is due to that the wavelength above 400 nm are not affected by the ligands switch from **Fe-1** to **Fe-2**.

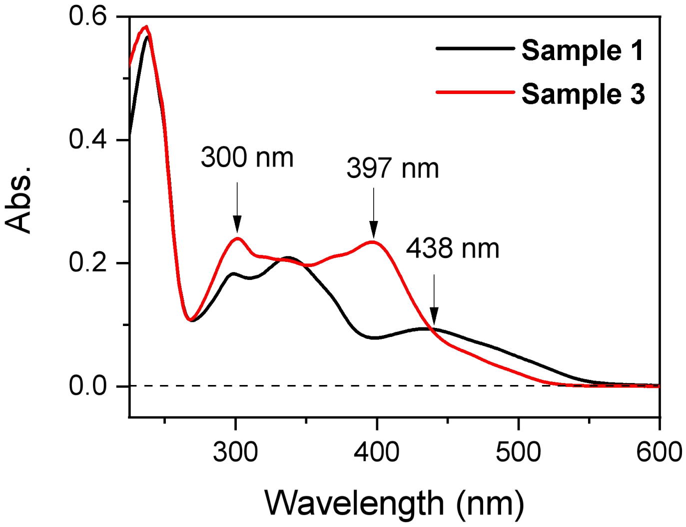

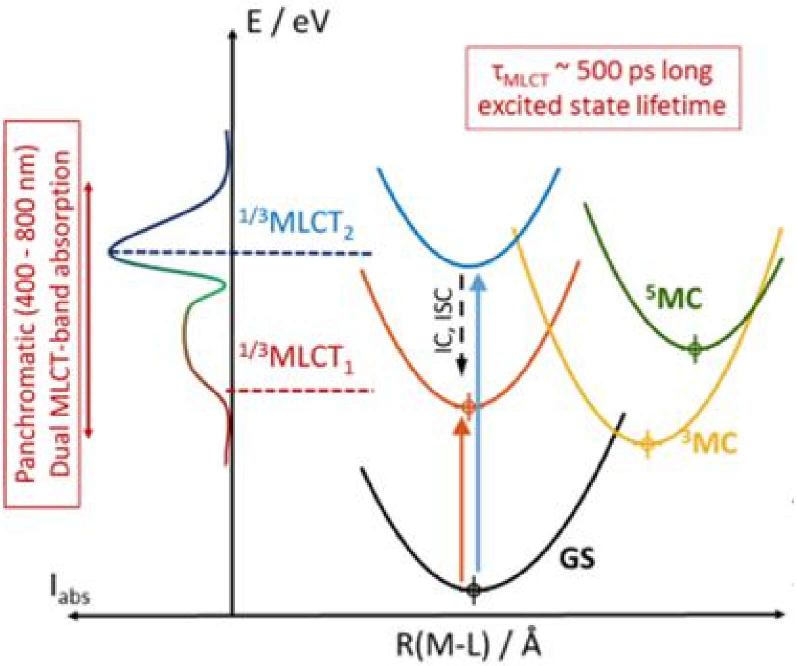

**Scheme 11**: Ground-state absorption spectrum (a) of **Fe-1** and **Fe-2** in acetonitrile. The energetics scheme together with parabolic energy surface

## 2.6 Transient absorption spectroscopy

### 2.6.1 Kinetics analysis of photoexcitation and deactivation

Before going in detail to interpret the excited state dynamics of the complexes, the general photophysics of the metal complexes are first analyzed and the methods to distinguish their features are also discussed. Charge transfer excitation can be interpreted as intramolecular redox reaction.

$$[\mathrm{Fe^{II}(L_1)_2L_2)}]^{2+} \xrightarrow{h\nu} \mathrm{Fe^{III}(L_1^{\bullet-})\,(L_1)\,L_2}]^{2+*} \qquad \textbf{(1)}^{a}$$

$$^{1}[\mathrm{Fe^{III}(L_1^{\bullet-})\,(L_1)\,L_2)}]^{2+*} \xrightarrow{k_{\mathrm{isc}}} {}^{3}[\mathrm{Fe^{III}(L_1^{\bullet-})\,(L_1)\,L_2)}]^{2+*} \qquad \textbf{(2)}$$

$$[\mathrm{Fe^{III}(L_1^{\bullet-})\,(L_1)\,L_2}]^{2+*} \xrightarrow{k_{\mathrm{nr}}} [\mathrm{Fe^{II}(L_1)_2L_2)}]^{2+}\mathrm{+heat} \qquad \textbf{(3)}$$

$$[\mathrm{Fe^{III}(L_1^{\bullet-})\,(L_1)\,L_2}]^{2+*} \xrightarrow{k_{\mathrm{nr}}} {}^{5}\mathrm{T_2+heat} \qquad \textbf{(4)}$$

*a*: L1 = axial NHC carbene ligand (DBIDP); L2 = tetra carbene ligand

Metal to ligand charge transfer (MLCT) excitation would result in ligand field state and oxidized metal state, as illustrated in **equation 1**. The excited state will further transfer to $^3$MLCT within ultrafast time (<100 fs) through intersystem cross following the initial photoexcitation as shown in **equation 2**. It has been verified theoretically by the very small changes in the calculated geometries between ground state to the $^3$MLCT state. The excited electron on $^3$MLCT state can further non-radiatively to the ground state or $^5$MC state (**equation 3 and 4**). The absorptive features of the MLCT state can be approximated by a superposition of the spectra of reduced ligand and oxidized metal. Spectroelectrochemistry has been a validate tool to differentiate the spectroscopic properties of the charge-transfer excited state especially in the ultrafast measurements. On one hand, oxidation would eliminate the $Fe^{II}$ species ($[Fe^{II}(L_1)_2L_2]^{2+} \rightarrow [Fe^{III}(L_1)_2L_2)]^{2+}$), hence the intensity of lowest MLCT transition would be attenuated. On the other hand, the $L_1^-$ radical species ($[Fe^{II}(L_1)_2L_2)]^{2+} \rightarrow [Fe^{III}(L_1^-)\ (L_1)\ L_2]^{2+}$), generally, absorbs in the near-UV as well as in the mid-visible ($\pi^* \rightarrow \pi^*$ in nature). A new absorption is expected to rise assigned as LMCT from the ligand $L_1$ to $Fe^{III}$. These sorts of assignments of the excited state absorption can be critical for data interpretation.

## 2.6.2 Analysis of ultrafast transient absorption spectroscopy

Ultrafast transient absorption (TA) spectroscopy was applied to investigate the impact of the BIm ligand on excited-state dynamics of $Fe^{II}$-NHC complexes. The acquired ultrafast transient absorption data can be sorted as single-wavelength and full spectrum data. The former can be used to derive time constants and the latter to monitor spectral evolution.

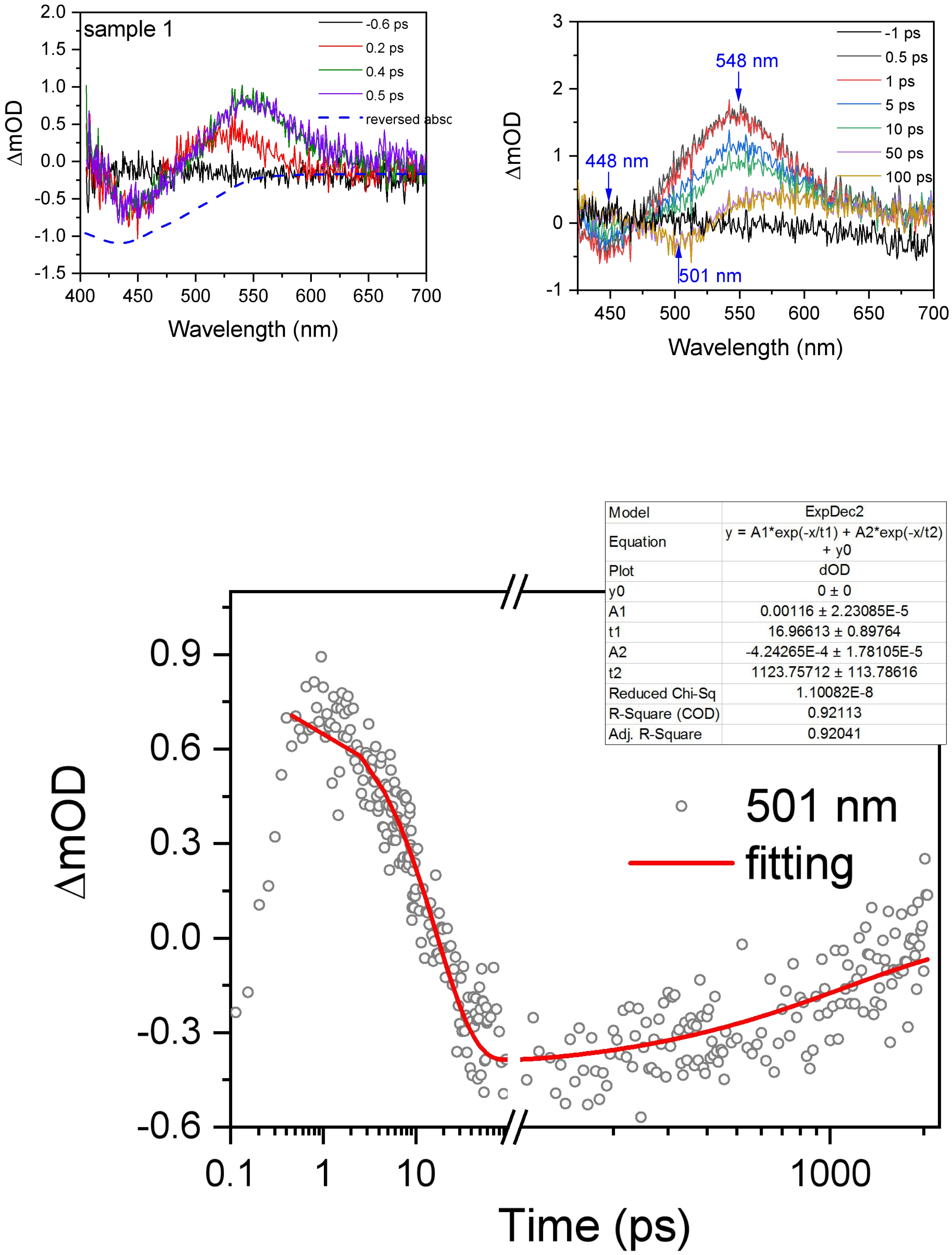

| Model | ExpDec2 |
|---|---|
| Equation | y = A1*exp(-x/t1) + A2*exp(-x/t2) + y0 |
| Plot | dOD |
| y0 | 0 ± 0 |
| A1 | 0.00116 ± 2.23085E-5 |
| t1 | 16.96613 ± 0.89764 |
| A2 | -4.24265E-4 ± 1.78105E-5 |
| t2 | 1123.75712 ± 113.78616 |
| Reduced Chi-Sq | 1.10082E-8 |
| R-Square (COD) | 0.92113 |
| Adj. R-Square | 0.92041 |

**Scheme 12**: Femtosecond transient absorption spectra of **Fe-1** at different time delays from -0.6 ps to 0.5 ps upon excitation at 400 nm. The inverted absorption spectra is also shown as dashed line.

The TA spectra of **Fe-1** and **Fe-2** in MeCN solution recorded at selected time delays following excitation at 400 nm are showed in (**Scheme 12**). The TA spectra displayed a weak ground-state bleach (GSB) from 400 to 475 nm with a strong excited-state absorption feature above 475 nm. The broken line referred to the reversed normalized steady-state absorption scaled at 450 nm that is the maximum of GSB. The ground state bleach was caused by depletion of the ground state due to the photoexcitation by the pump pulse. No sample degradation was observed judging from their UV-vis absorption spectra before and after the TA measurement.

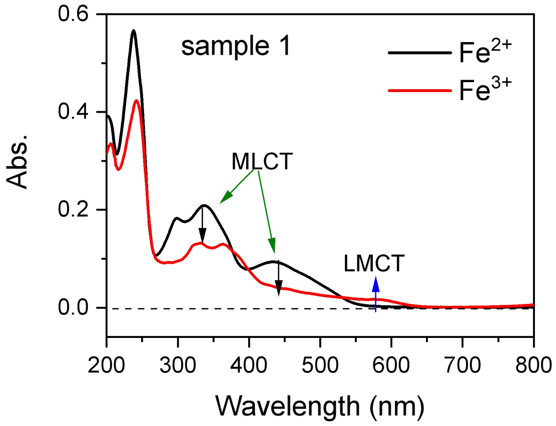

**Scheme 13**: UV-Vis absorption of **Fe(II)-1** and **Fe(III)-1**

Based on the previous discussion on the signature of LMCT and MLCT, absorption spectra of Fe(II) and Fe(III) complex in (**Scheme 13**) can be used to interpret the TA spectra of **Fe-1**. The major difference between Fe(II) and Fe(III) complexes above 400 nm is that the intensity is attenuated in the range 400-550 nm, while enhanced from 550-650 nm. Based on this difference, it can be inferred that the excited state absorption in the 400-550 nm is due to MLCT, while the ESA in 550-650 nm is attributed to LMCT. The excited state absorption is a signature of the MLCT state, as already established from spectroelectrochemical studies of Fe(II)-polypyridine complexes[16]. This feature has also been evidenced in both $Fe^{II}$- and $Ru^{II}$-centered systems[5]. Moreover, there has growing number of evidence that $^1A_1 \rightarrow {}^1MLCT$ excitation of iron complexes will fast intersystem crossing to the manifold of charge transfer within time resolution and finally rest in the high-spin ligand-field state ($^5T_2$) as the lowest energy excited state. The spectroscopic feature of the state $^5T_2$ is a transient bleach. Contrast to the bleach in 448 nm originating from ground state absorption, the bleach centered at 500 nm possessing totally different kinetics can be attributed to high-spin ligand-field state ($^5T_2$). The fitting returns two components of 16 ps and 1123 ps. The first component is probably related to the vibrational cooling processes of $^5T_2$ state, while 1123 ps can be assigned to ground state $^5T_2 \rightarrow ^1A_1$ recovery time.

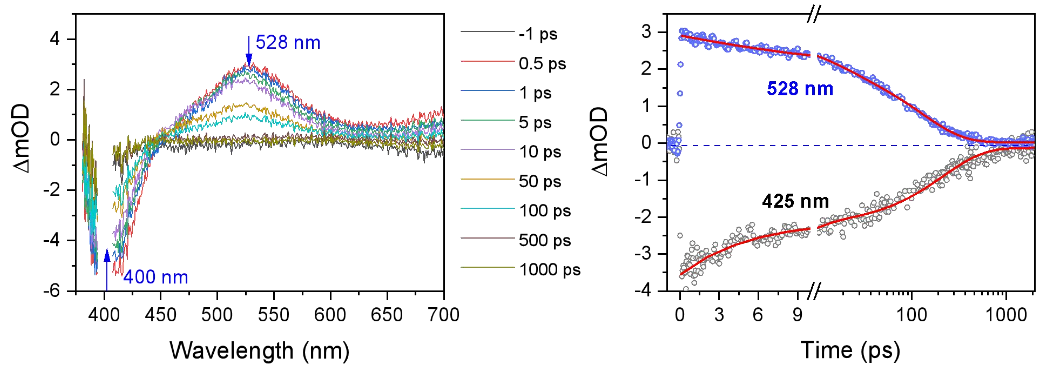

**Scheme 14**: Transient absorption data revealing the long-lived $^3$MLCT states. (a) time resolved spectra in acetonitrile. Data in the 390-410 nm region are removed manually due to the pump laser scattering. (b) Comparation of kinetic traces of ESA at wavelength 528 nm and GSB at wavelength 425 nm.

Generally, there is large energy gap between the $^3$MLCT manifold and the $^5T_2$ state, and the excess energy is dissipated into vibrational energy. The time scale for the vibration cooling[17] is of several picoseconds. The timescale for ground state recovery time is reasonable evidenced by many researches about the non-radiative decay process[18]. For **Fe-2**, the TA spectra was dominated by only one ground state bleach and one pronounced ESA. Unlike **Fe-1**, the ESA keeps its shape and doesn't show any stokes shift with time growing. Two remarkable features highlight how the additional benzene ring modify the excited state relaxation scheme with respect to Fe-6-NHC complexes and induce a significant stabilization of the $^3$MLCT state. First, the kinetics and corresponding fits of the GSB and ESA are plotted in (**Scheme 14**), from which it shows that the 525 nm band decays almost simultaneously with GSB. However, besides the long-time component 130 ps, the kinetics also has another component 15 ps, almost same number as the vibrational cooling processes of $^5T_2$ state in **Fe-1**. It means that the excited electrons in $^3$MLCT states partially relaxed to $^5T_2$ state and largely decays back into ground state $^1A_1$. The conjecture is reasonably made based on the total lost feature of $^5T_2$ state. The weak intensity of $^5T_2$ state probably is totally covered by the strong ESA. The second is the excited state lifetime is much more enhanced, as the lifetime of $^3$MLCT has largely been enhanced, perfectly fitted by exponential decays of 130 ps. The suppression of the $^3$MLCT-$^5T_2$ relaxation is the probably due to the large geometry difference between the electronic states.

### 2.6.3 Summary of TAS research

In summary， **Fe-1** does not exhibit good excited state properties as expected. After carefully assign the 16ps to the vibrational cooling processes of $^5T_2$ state, **Fe-1** only shows lifetime of the MLCT state with less than 1ps. This much lower than expected value cannot be explained properly temporarily.

However, **Fe-2** exhibits an MLCT lifetime of up to 130 ps, which is the second highest of all Fe(II) NHC complexes by now, only lower than the work of Kenneth Wärnmark's group in 2018, in which the complex shows 528 ps of MLCT lifetime.

In addition, in our design thinking, the tetra-benzimadizole was designed to limit the stretching of Fe-C bonds in the excited state, thereby forcibly strengthening the interaction between the metal and the ligand in the excited state. However, this idea has not been realized as expected. On the contrary, the existence of tetra-benzimadizole ligand limits the spatial structure of the complex and stabilizes the MC state. But this result also provides direction and guidance for our future work.

At the same time, 130 ps is also the highest MLCT lifetime among all current heteroleptic Fe(II) complexes. Compared with homoleptic Fe(II) complex, heteroleptic Fe(II) complexes like **Fe-2** can more easily regulate their own photophysical, photochemical and electrochemical properties through micro-modification of ligands. Therefore, **Fe-2** not only exhibits MLCT excited state lifetime up to 130 ps, but also provides a new strategy and new potential in the direction of utilizing Fe as photo catalysts.

## 2.7 Conclusion

Two heteroleptic Fe(II) complex **Fe-1** and **Fe-2** have been designed. In-depth and detailed studies on the electrochemical properties of these two compounds have been conducted. Both **Fe-1** and **Fe-2** exhibit good electrochemical performance, and both can perform two reversible redox cycles, which belong to the metal-centered Fe(II)/Fe(III) redox couple and the ligand-centered $L/L^+$ redox couple, respectively. After comparing with **Fe-1a** and **Fe-2a**, an in-depth analysis of various changes in its redox cycle have been conducted, the influence of strong σ-donating NHC ligands and extended π system on its potential have been carefully discussed.

Both **Fe-1** and **Fe-2** exhibit good optical absorption. By comparing the two with each other, each of their absorption peaks have been assigned. And through its oxidation state absorption spectrum, this attribution has been verified.

In-depth studies on the transient absorption spectra of **Fe-1** and **Fe-2** have been conducted. **Fe-1** does not exhibit good excited state properties as expected. After carefully assign the 16 ps to the vibrational cooling processes of $^5T_2$ state, **Fe-1** only shows lifetime of the MLCT state with less than 1 ps.

However, Fe-2 exhibits an MLCT lifetime of up to 130 ps, which is the second highest MLCT lifetime of all Fe(II) NHC complexes, and the highest among the heteroleptic Fe(II) complexes. This successful result provides new strategies and possibilities for Fe(II) complexes to become the photo catalyst in the future..

## 2.8 Experiment section

### 2.8.1 Gerenal experimental methods

$^1$H (400 MHz) and $^{13}$C (100 MHz) NMR spectra were acquired on a Bruker Avance Ultrashield 400 MHz and a Bruker DPX 400 MHz spectrometer. Anhydrous solvents were obtained from SPS machine. Reactions related Fe and DBIDP were conducted in the glovebox.

### 2.8.2 Synthesis

**Synthesis of 4,4'-di-*tert*-butyl-1-(2-oxo-2-phenylethyl)-[2,2'-bipyridin] bromide 1**

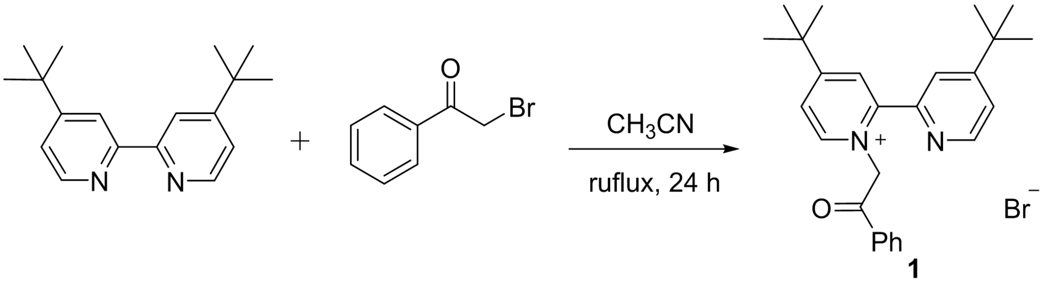

**1**

4,4'-di-*tert*-butyl-2,2'-bipyridine (12.0 g, 14.9 mmol) and 2-brom-acetophenon (9.2g 36 mmol) were added into a 500 ml flask. MeCN (150 ml) was added subsequently. The solution was refluxed at 80 $^{o}$C for 24 h. The solvent was removed *via* rotary evaporator, resulting in orange-red solid. Th solid was separated *via* silica gel column through gradient elution with DCM, EA and MeCN as eluents. The component with fluorescent blue was collected and dried, giving product **1** (16.33g) as orange solid with 73% yield. $^1$H NMR (400 MHz, DMSO-$d_6$) δ 9.09-9.08 (d, $J$ = 6.4 Hz, 1H), 8.46-8.44 (dd, $J$ = 2.4, 2.0 Hz, 1H), 8.38-8.37 (d, $J$ = 2.0 Hz, 1H), 8.34 (s, 1H), 8.24-8.23 (d, $J$ = 5.2 Hz, 1H), 7.99-7.95 (m, 3H), 7.78-7.74 (m, 2H), 7.63-7.58 (m, 3H), 6.30 (s, 2 H), 1.50 (s, 9 H), 1.31 (s, 9 H).

**Synthesis of 2,10-di-*tert*-butylimidazo-dipyridin bromide 2**

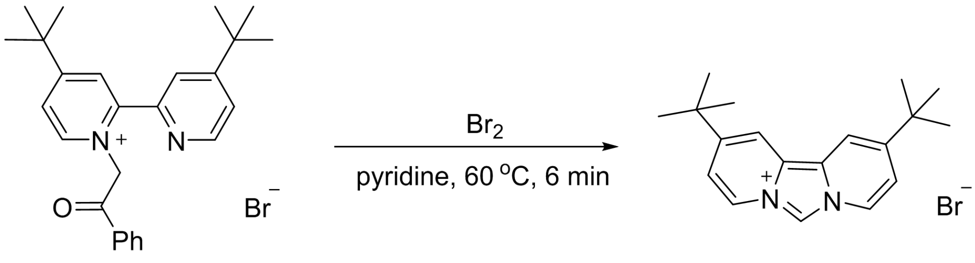

**1** **2**

**1** (4.0 g, 8.6 mmol) was dissolved in anhydrous pyridine (60 ml) in a 250 ml Schlenk flask under Ar. The solution was heated up to 60 °C. Bromine (0.44 ml, 8.6 mmol) was dropped into the solution slowly *via* syringe while stirring vigorously under Ar. The solution was stirred for 8 min under 60 °C and the heater was removed immediately after the time was up. The mixture was cooled to room temperature and the solvent was removed under vacuum. The dark brown residue was dissolved with solvent (MeOH/$H_2O$ = 1:1, 20 ml). The mixture was filtrated through neutral $Al_2O_3$ column with MeOH/$H_2O$ = 1:1 as eluent. The liquid was collected and dried under vacuum, resulting a dark brown residue. The residue was separated through silica gel column with ethyl acetate and methanol as eluents. The green fraction was collected and dried, resulting in a dark green residue. The residue was washed with acetone (3 x 50 ml), giving the product **2** (0.96 g) as yellow solid with 31% yield. $^1$H NMR (400 MHz, DMSO-$d_6$) δ 10.17 (s, 1H), 8.98-8.96 (dd, $J$ = 1.6, 1.2 Hz, 2H), 8.64 (s, 1H), 7.74-7.71 (dd, $J$ = 2.0, 2.0 Hz, 2H), 1.4 (s, 18H).

**Synthesis of 2,10-di-*tert*-butylimidazo[1,5-a:3,4-a']dipyridin-5-ium-6-ide (DBIDP) 3**

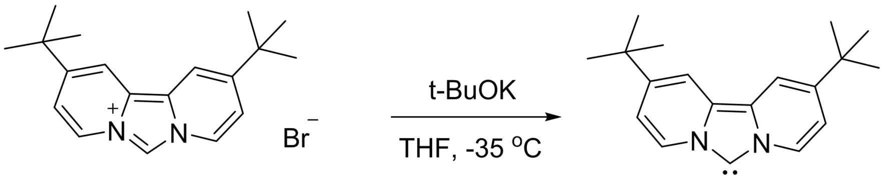

**2** DBIDP **3**

The synthesis of DBIDP **3** was conducted in the golvebox.

2,10-Di-*tert*-butylimidazo-dipyridin bromide **2** (720 mg, 2 mmol) was dissolved in THF (15 ml) into a 100 ml flask and cooled to - 35 °C. Potassium *tert*-butoxide (336 mg, 3 mmol) was dissolved in THF (15 ml) and cooled to - 35 °C. The latter solution was dropped in the solution of **2** and the color was changed from pale gray to yellow. The solution was passed through the celite column with THF as eluent. The yellow fraction was collected and dried, resulting in the crude product. The crude product was washed with pentane and diethyl ether (3 x 20 ml). DBIDP **3** (240 mg) was obtained as yellow solid with 43% yield. $^1$H NMR (400 MHz, $C_6D_6$-*d*$_6$) δ 8.52-8.50 (d, *J* = 7.6 Hz, 2H), 7.42 (s, 1H), 6.32-6.29 (dd, *J* = 2.0, 2.4 Hz, 2H), 1.12 (s, 18H).

**Synthesis of Bis-(trifluoromethanesulfonate) 4**

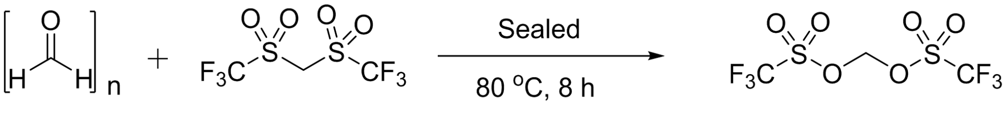

**4**

Paraformaldehyde (3.03 g, 100 mmol) was added to a 100 ml Schlenk Tube, and then trifluoromethanesulfonic anhydride (16.8 ml, 100 mmol) was added *via* syringe. The Schlenk Tube was sealed and the reaction mixture was stirred at 80 ºC for 8 hours. The mixture changed to dark brown clear solution gradually. The solution was dried through vacuum after cooled down to room temperature, resulting in black residue. A small amount of DCM was added and the suspension was filtrated through a silica gel column with DCM as eluent. The first colorless fraction was collected and dried under vacuum, giving **4** (5.30 g) as pale purple oil with 17 % yield. $^1$H NMR (400 MHz, Chloroform-*d*) δ 6.06 (s, 2H)

**Synthesis of di(1H-imidazol-1-yl)methane 5**

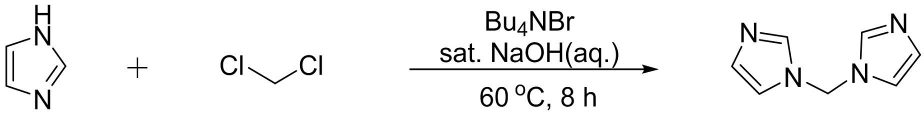

**5**

Imidazole (50.0 g, 734 mmol) and tetra-*n*-butylammonium bromide (7.1 g, 22 mmol) were added in to a 2000 ml round flask. Saturated NaOH solution (500 ml, 9.5 mmol) and dichloromethane (500 mL) were added subsequently. The suspension was refluxed at 60 °C for 8 h. After cooling down, DCM was removed through rotary evaporator and a lot white solid precipitated. The suspension was filtered and the white solid was collected. The solid was washed with hot DCM (5x 100 mL) and the liquid was collected and dried through rotary evaporator giving light yellow crude product. The crude product was purified through recrystallization in water giving the product **5** (46.7 g) as white crystalline with 43 % yield. $^1$H NMR (400 MHz, DMSO-*d6*) δ 7.93 (s, 2H), 7.40 (s, 2H), 6.91 (s, 2H), 6.22 (s, 2H).

**Synthesis of Calix-tetra-imidazolium trifluoromethanesulfonate 6**

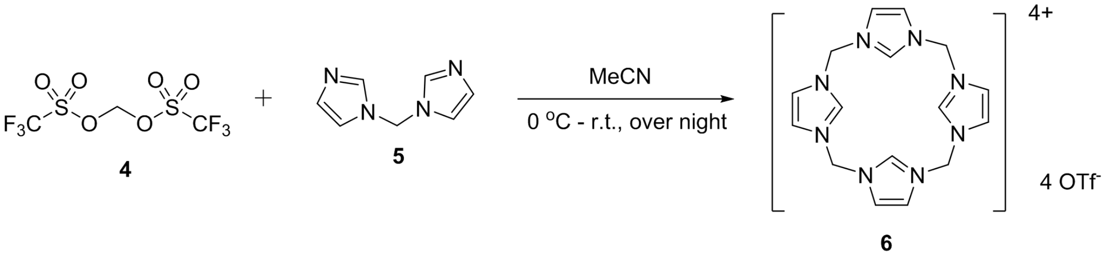

Methylene bisimidazole **5** (1.9 g, 12.8 mmol) and acetonitrile (400 mL) were added into a 1000 ml round flask. The solution was cooled down to 0 °C *via* ice bath. Bis(trifluoromethanesulfonate) **4** (4.0 g, 12.8 mmol) was diluted with acetonitrile (50 mL) and the solution was dropped into the flask *via* a dropping funnel over one hour. The reaction mixture was warmed to room temperature and stirred overnight. Acetonitrile was removed through rotary evaporator. The crude product was purified by recrystallization with hot acetone. The crystal was further washed with cold acetone (2x 20 mL) to give product **6** (3.71 g) as white powder with 63% yield. $^1$H NMR (400 MHz, Acetonitrile-*d3*) δ 9.57 (s, 4H), 7.91 (s, 8H), 6.68 (s, 8H).

**Synthesis of diacetonitrile-calix[4]-imidazoyl-iron(II) trifluoromethanesulfonate 7**

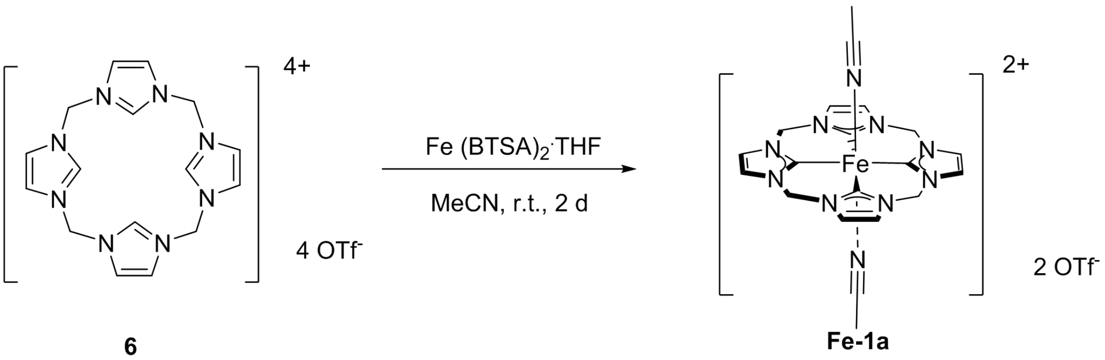

Synthesis of **Fe-1a** was conducted completely in the glovebox.

Calix-tetra-imidazolium trifluoromethanesulfonate **6** (920 mg, 1 mmol) was dissolved in acetonitrile (30 ml) in a 100 ml flask and cooled to -35 °C. Fe(BTSA)$_2$(THF) (1.0 g, 2.2 mmol) was dissolved in acetonitrile (20 mL) and cooled to -35 °C. The latter solution was added into the solution of **6** through a dropper within 5 mins, and the mixture was stirred at room temperature for 2 days. The solvent was removed under vacuum resulting in an orange residue. The residue was redissolved with acetonitrile (20 mL) and filtered over dried silica gel column with MeCN as eluent. The orange band fraction was collected and dried *via* vacuum, giving crude product as yellow solid. The crude product was purified through precipitation with MeCN/ Et$_2$O solvent system. The orange precipitation was collected through filtration and dried, giving product **Fe-1a** (558 mg) as an orange powder with 72 % yield. $^1$H NMR (400 MHz, Acetonitrile-*d*3) δ 7.50 (s, 8H), 6.26 (s, 8H). 13C NMR (101 MHz, Acetonitrile-*d*3) δ 204.2, 121.9, 62.5.

**Synthesis of diDBIDP-calix[4]-imidazoyl] Fe(II) trifluoromethanesulfonate Fe-1**

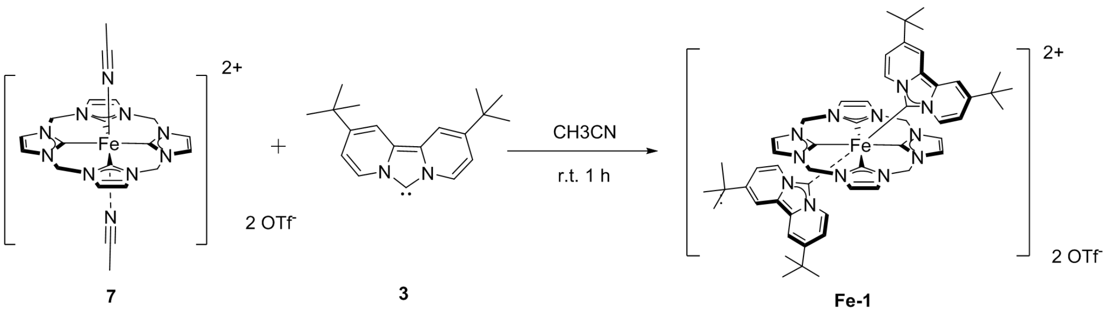

Synthesis of **Fe-1** was conducted completely in the glovebox.

Diacetonitrile-calix[4]-imidazoyl-iron(II) trifluoromethanesulfonate **Fe-1a** (74.8 mg, 0.1 mmol) was dissolved in MeCN (20 ml ) in a 50 ml flask. DBIDP **3** (112 mg, 0.4 mmol) was added into the solution of **7**. The color of the clear solution changed from orange to dark red within minutes. The mixture was stirred for 1 h under room temperature. The dark red solution was concentrated to 5 ml through vacuum. Diethyl ether was dropped in until the clear solution becomes cloudy. The suspension was stirred for 1 h and filtrated to collect the solid as fraction 1. The filtrate was added diethyl ether (40 ml) and stirred for 1 h. The suspension was filtrated and the solid was collected as fraction 2. Fraction 2 was confirmed as the product through NMR. The **Fe-1** (88 mg) was obtained as orange solid with 71 % yield. $^1$H NMR (400 MHz, Acetonitrile-*d*3) δ 7.71-7.70 (m, 4H), 7.30 (s, 8H), 7.10-7.08 (d, *J* = 8.0 Hz, 4H), 6.63-6.61 (dd, *J* = 2.0, 2.0 Hz, 4H) 6.27-6.24 (d, *J* = 12.4 Hz,4H), 4.12-4.09 (d, *J* = 12.4 Hz,4H), 1.27 (s, 18H). 13C NMR (101 MHz, Acetonitrile-*d*3) δ 213.4, 168.6, 140.9, 124.4, 123.1, 120.9, 119.6, 115.4, 112.0, 34.0, 29.3. Elementary analysis, calculated $C_{60}H_{64}F_6FeN_{12}O_6S_2{}^{2-}$: C, 54.46; H, 5.22; N, 13.61; S, 5.19; found: C, 53.21; H, 5.15; N, 12.94; S, 4.86;

**Synthesis of bis(1H-benzimidazol-1-yl)methane 9**

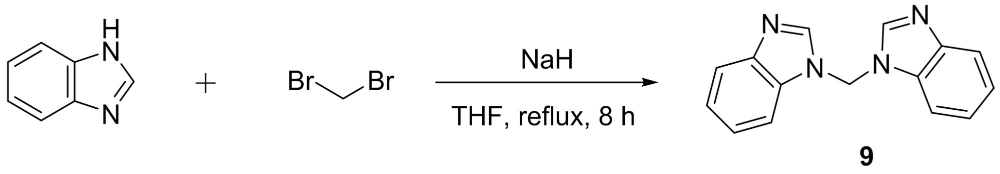

Benzimidazol (23.4 g, 200 mmol) and NaH (4.8 g, 200 mmol) were added in a 250 ml flask. Dibromomethane (7 ml, 100 mmol) and THF (100 ml) was added subsequently. The mixture was stirred under 80 $^{o}$C to reflux fo 8 h. The solvent was removed *via* rotary evaporator and white solid precipitated. The solid was washed with saturated NaCl and extracted with DCM (3 x 100 ml). The organic phase was collected and dried, and further purification through recrystallization to give product **9** (3.86 g) as white solid with 78 % yield. $^1$H NMR (400 MHz, DMSO-*d*6) δ 8.79 (s, 2H), 7.91-7.89 (d, J = 8 Hz, 2H), 7.67-7.65 (d,J = 8 Hz, 2H), 7.32-7.20 (m, 4H), 6.90 (s, 2H)

**Synthesis of calix[4]-benzimidazoyl trifluoromethanesulfonate 10**

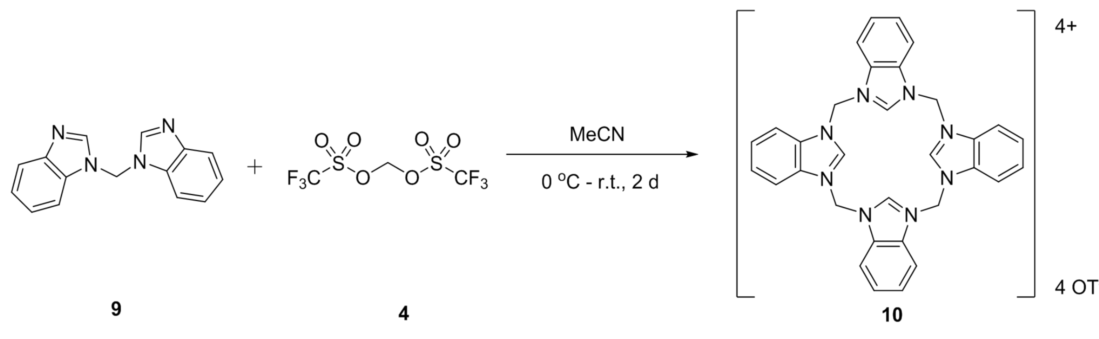

Methylene bis-benzimidazole **9** (2.48 g, 10 mmol) and acetonitrile (400 mL) were added into a 1000 ml round flask. The solution was cooled down to 0 °C *via* ice bath. Bis(trifluoromethanesulfonate) **4** (3.13 g, 10 mmol) was diluted with acetonitrile (50 mL) and the solution was dropped slowly into the flask *via* a dropping funnel over one hour. The reaction mixture was warmed to room temperature and stirred overnight. The solvent was removed through rotary evaporator and the crude product obtained was purified by recrystallization with hot acetone. The crystal was further washed with cold acetone (3 x 20 mL) to give product **10** (3.96 g) as white solid with 71 % yield. $^1$H NMR (400 MHz, DMSO-*d6*) δ 10.73 (s, 4H), 8.66-8.62 (m, 8H), 7.93-7.85 (m, 16H).

## Synthesis of diacetonitrile-calix[4]-benzimidazoyl-iron(II) trifluoromethanesulfonate Fe-2a

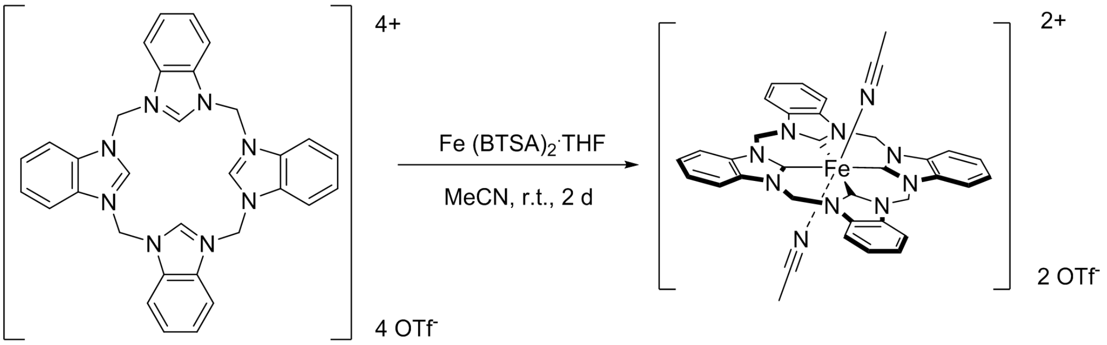

**10** **Fe-2a**

The synthesis of **Fe-2a** was conducted in the glovebox.

Calix[4]-benzimidazoyl trifluoromethanesulfonate **10** (1.12 g, 1 mmol) was dissolved in acetonitrile (30 ml) in a 100 ml flask and cooled to -35 °C. Fe(BTSA)$_2$(THF) (1.0 g, 2.1 mmol) was dissolved in acetonitrile (20 mL) and cooled to -35 °C. The latter clear green solution was dropped slowly into the solution of **10** within 5 mins under room temperature, and the mixture was stirred at room temperature for 2 days. The solvent was removed under vacuum resulting in an orange residue. The residue was redissolved with acetonitrile (20 mL) and filtered over dried silica gel column with MeCN as eluent. The yellow band fraction was collected and dried under vacuum, giving crude product as yellow solid. The crude product was purified through precipitation with MeCN/Et$_2$O solvent system. The precipitation was collected through filtration and dried, giving product **Fe-2a** (431 mg) as bright yellow powder with 45 % yield. $^1$H NMR (400 MHz, Acetonitrile-*d*3) δ 8.14-8.10 (m, 8H), 7.76-7.61 (m, 8H), 6.96 (s, 1H). 13C NMR (101 MHz, Acetonitrile-*d*3) δ 215.1, 135.0, 123.5, 110.1, 58.0.

### Synthesis of diDBIDP-calix[4]-benzimidazoyl-iron(II) trifluoromethanesulfonate Fe-2

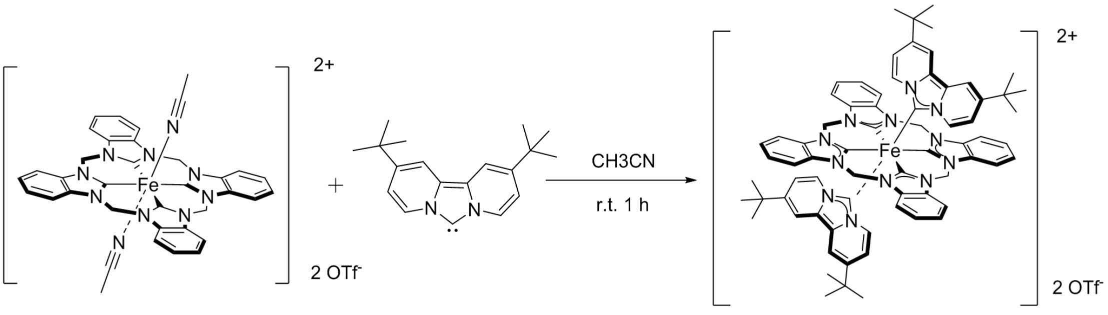

Fe-2a DBIDP 3 Fe-2

Diacetonitrile-calix[4]-benzimidazoyl-iron(II) trifluoromethanesulfonate **Fe-2a** (96 mg, 0.1 mmol) was dissolved in MeCN (20 ml ) in a 50 ml flask. DBIDP **3** (112 mg, 0.4 mmol) was added into the solution of **Fe-2a**. The color of the clear solution changed from yellow to dark red within minutes. The mixture was stirred for 1 h under room temperature. The dark red solution was concentrated to 5 ml through vacuum. Diethyl ether was dropped in until the clear solution became cloudy. The suspension was stirred for 1 h and filtrated to collect the solid as fraction 1. The filtrate was added diethyl ether (40 ml) and stirred for 1 h. The suspension was filtrated and the precipitation was collected as fraction 2. Fraction 2 was confirmed as the product through NMR. The **Fe-2** (92 mg) was obtained as yellow solid with 63 % yield. $^1$H NMR (400 MHz, Acetonitrile-*d*3) δ 7.77-7.69 (m, 8H), 7.68 (s, 8H), 7.43-7.41 (m, 8H), 7.13-7.10 (m, 8H), 6.27-6.24 (dd, *J* = 2.4, 2.0 Hz,4H), 4.47-4.44 (d, *J* = 12.8 Hz,2H), 1.05 (s, 18H). Elementary analysis, calculated $C_{76}H_{72}F_6FeN_{12}O_6S_2^{2-}$: C, 60.25; H, 5.06; N, 11.71; S, 4.47; found: C, 58.71; H, 4.85; N, 11.39; S, 4.34;

### Oxidation of Fe-1a to Fe(III)-1a

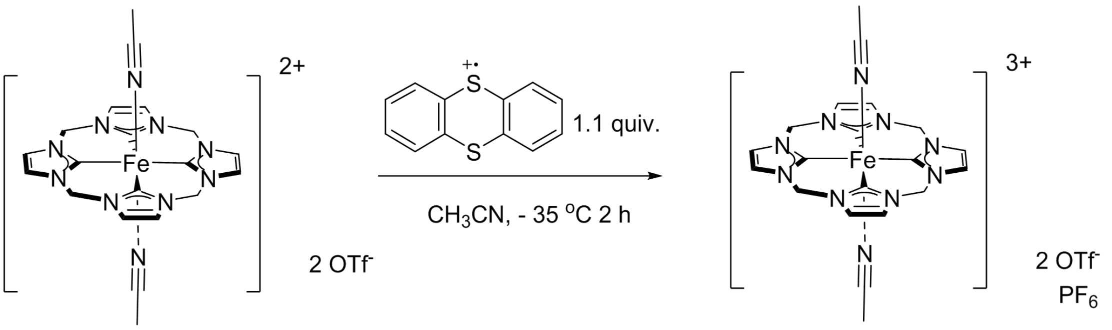

**Fe(III)-1a**

Diacetonitrile-calix[4]-imidazoyl-iron(II) trifluoromethanesulfonate **Fe-1a** (74.8 mg, 0.1 mmol) was dissolved in MeCN (20 ml ) in a 50 ml flask and cooled to - 35 °C. Thianthrene cationic radical (24 mg, 0.11 mmol) was dissolved in MeCN (5 ml) and cooled to - 35 °C. The latter clear blue solution was dropped in the solution of **Fe-1a** and stirred for 2 h. The purpule solution was concentrated to 5 ml and precipitate with Diethyl ether. The purple precipitation was collected and dried, confirmed by NMR as **Fe(III)-1a** (32 mg) with 35% yield. $^1$H NMR (400 MHz, Acetonitrile-*d*3) δ 44.39 (s, 8 H).

**Ligand replacement of Fe(III)-1a**

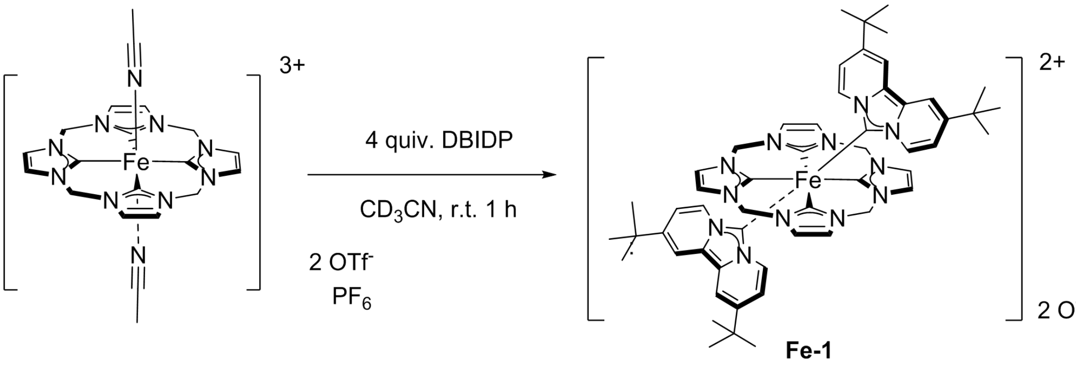

**Fe-1**

**Fe(III)-1a** (46 mg, 0.05 mmol) was dissolved in to 2 ml CD$_3$CN in a J.YOUNG NMR tube. 4 equivalence of DBIDP was added into the NMR tube and shook for 0.5 h. The NMR for the crude product turns clear. The solution was transferred into a 50 mL flask and precipitated with diethyl ether. The orange precipitation was collected and dried, verified *via* NMR to be **Fe-1** (43 mg) with 69 % yield. $^1$H NMR (400 MHz, Acetonitrile-*d*3) δ 7.71-7.70 (t, 4H), 7.30 (s, 8H), 7.12-7.09( dd, 4H), 6.65-6.62(dd, 4H) 6.27-6.24(d, 4H), 4.12-4.09 (d, 4H), 1.27 (s, 18H). 13C NMR (101 MHz, Acetonitrile-*d*3) δ 213.4, 168.6, 140.9, 124.4, 123.1, 120.9, 119.6, 115.4, 112.0, 34.0, 29.3. Elementary analysis, calculated: C, 54.46; H, 5.22; N, 13.61; S, 5.19; found,: C, 53.21; H, 5.15; N, 12.94; S, 4.86;

### Oxidation of Fe-1 to Fe(III)-1

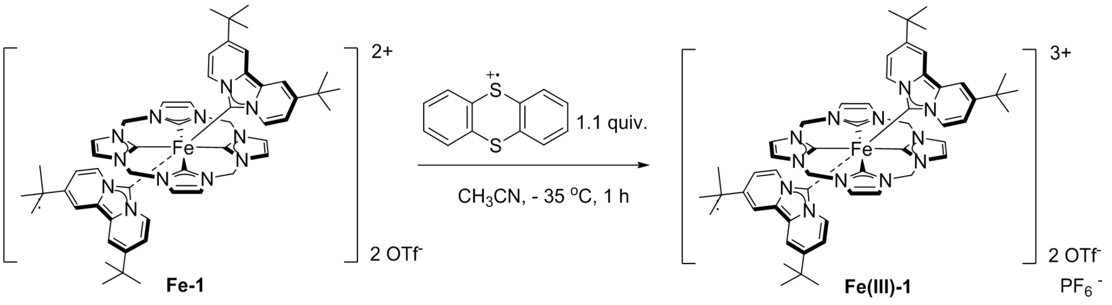

**Fe-1** (50 mg, 0.04 mmol) was dissolved in MeCN (10 ml ) in a 50 ml flask and cooled to - 35 $^{o}$C. Thianthrene cationic radical (11 mg, 0.05 mmol) was dissolved in MeCN (5 ml) and cooled to - 35 $^{o}$C. The latter clear blue solution was dropped in the solution of **Fe-1a** and stirred for 1 h. The purpule solution was concentrated to 2 ml and precipitate with Diethyl ether. The purple precipitation was collected and dried, confirmed by NMR as **Fe(III)-1a** (31 mg) with 49 % yield. Verified through UV-Vis Absorption.

## 2.8.3 NMR spectrum and Crystal data

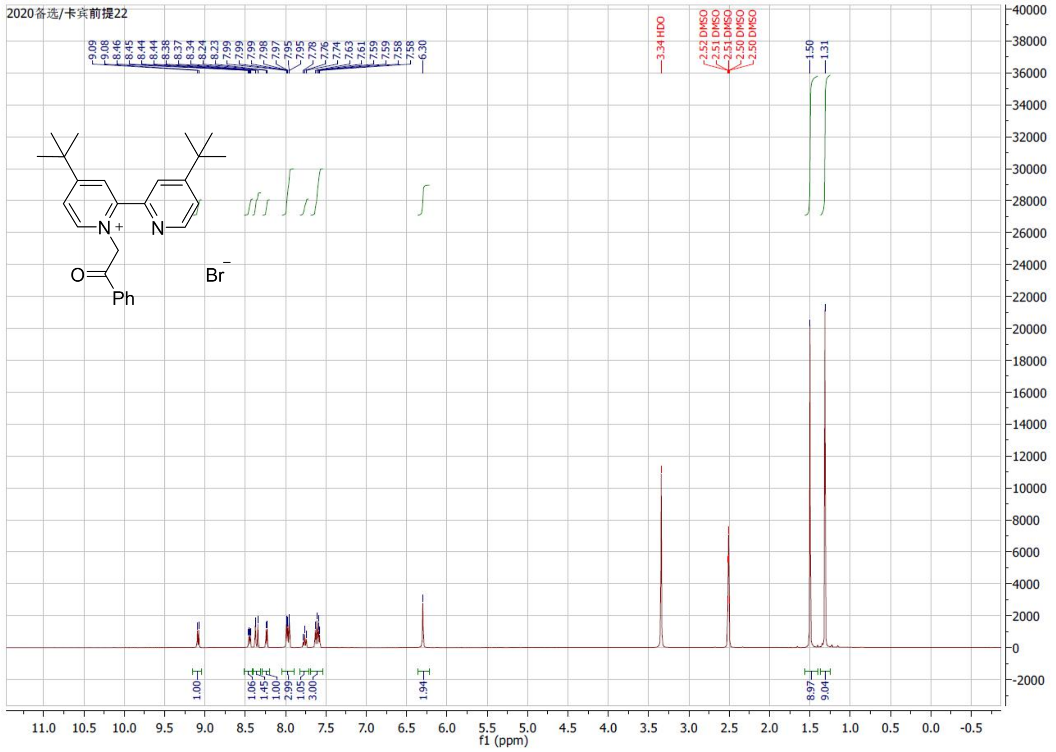

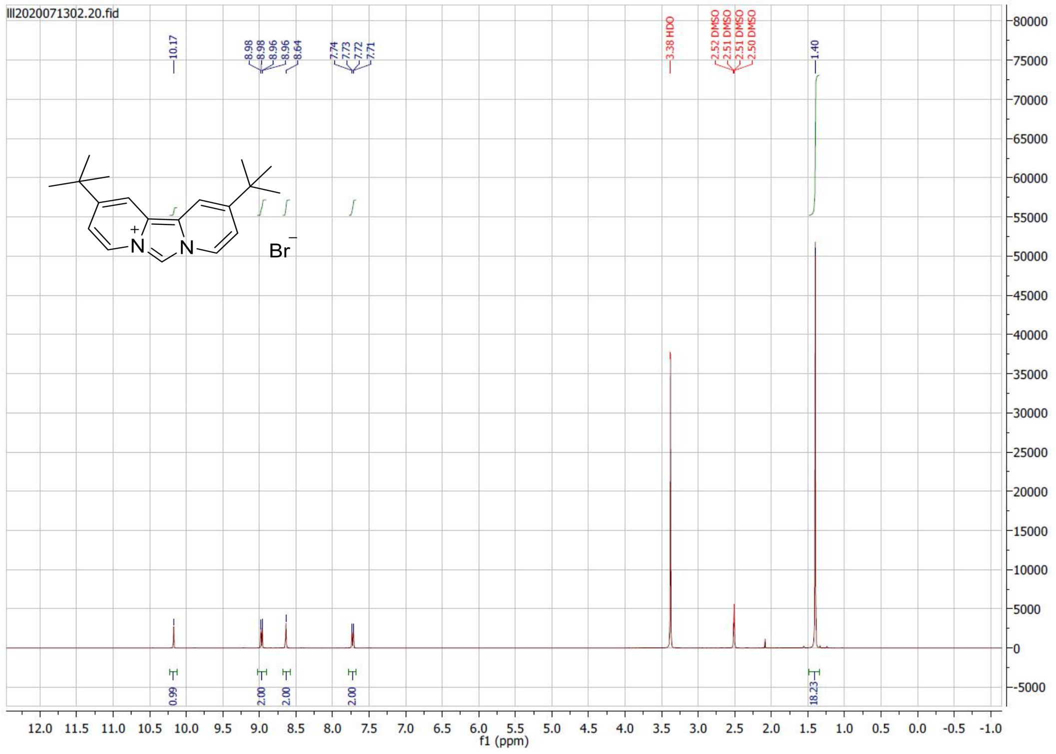

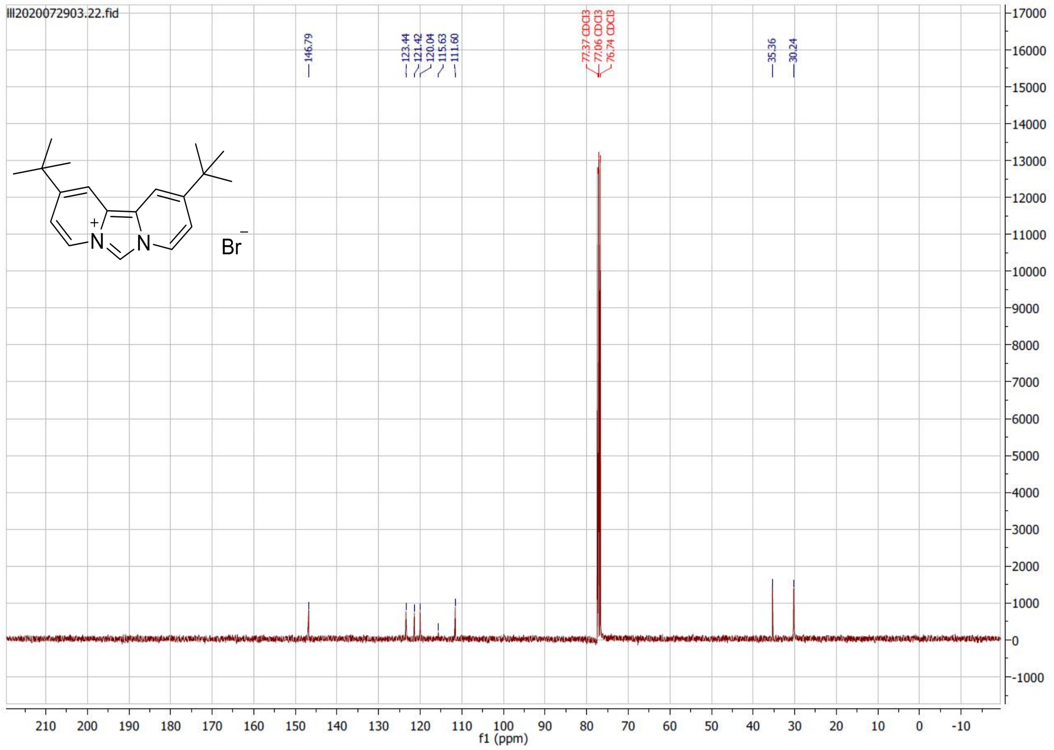
lll2020072903.22.fid
146.79
123.44
121.42
120.04
115.63
111.60
77.37 CDCl3
77.06 CDCl3
76.74 CDCl3
35.36
30.24
Br
+
N
N
17000
16000
15000
14000
13000
12000
11000
10000
9000
8000
7000
6000
5000
4000
3000
2000
1000
0
-1000
210 200 190 180 170 160 150 140 130 120 110 100 90 80 70 60 50 40 30 20 10 0 -10
f1 (ppm)

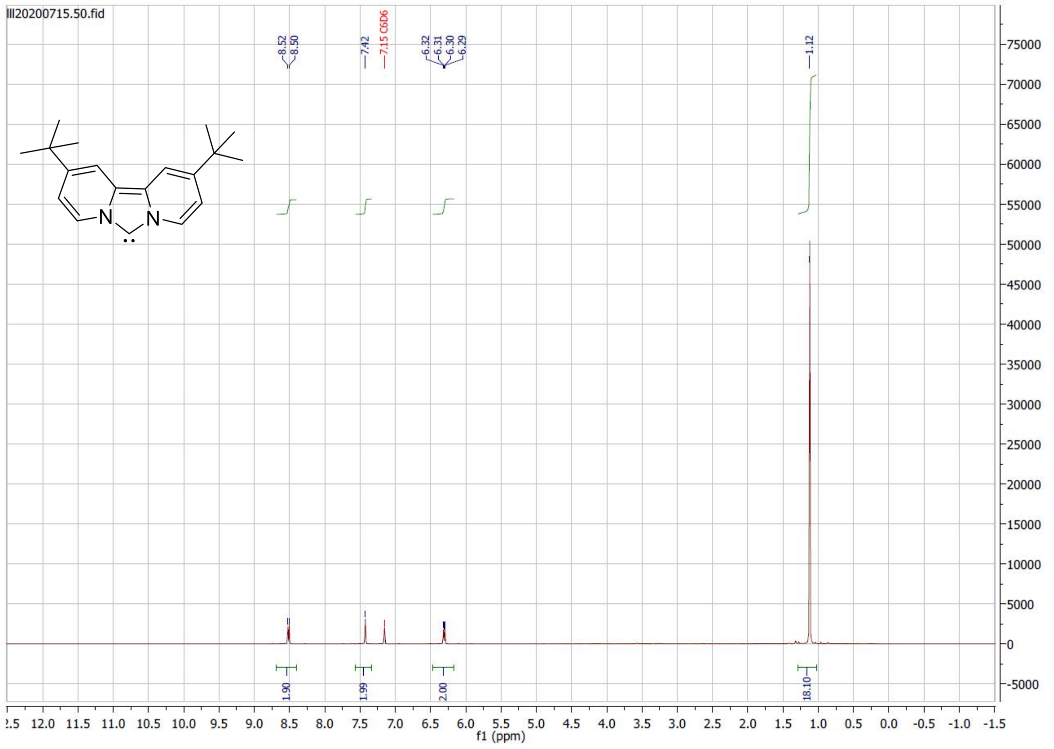
lll20200715.50.fid
8.52
8.50
7.42
7.15 C6D6
6.32
6.31
6.30
6.29
1.12
N
N
75000
70000
65000
60000
55000
50000
45000
40000
35000
30000
25000
20000
15000
10000
5000
0
-5000
1.90
1.99
2.00
18.10
2.5 12.0 11.5 11.0 10.5 10.0 9.5 9.0 8.5 8.0 7.5 7.0 6.5 6.0 5.5 5.0 4.5 4.0 3.5 3.0 2.5 2.0 1.5 1.0 0.5 0.0 -0.5 -1.0 -1.5
f1 (ppm)

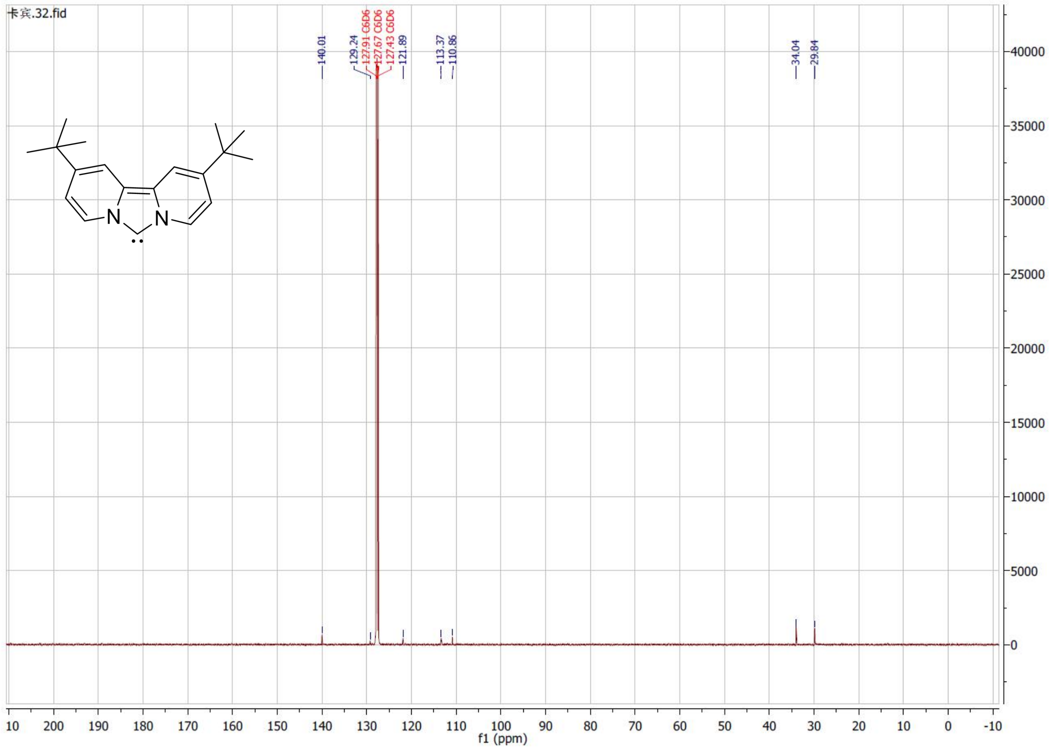
卡宾.32.fid
140.01
129.24
127.91 C6D6
127.67 C6D6
127.43 C6D6
121.89
113.37
110.86
34.04
29.84
N
N
40000
35000
30000
25000
20000
15000
10000
5000
0
10
200
190
180
170
160
150
140
130
120
110
100
90
80
70
60
50
40
30
20
10
0
-10
f1 (ppm)

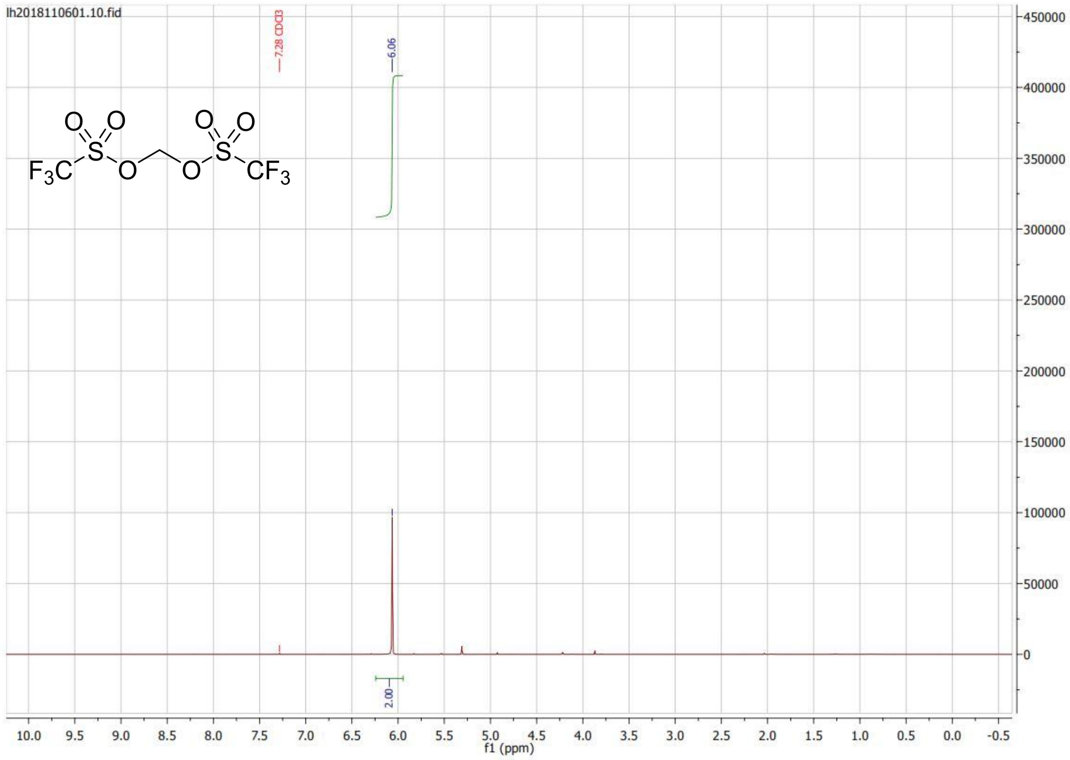
lh2018110601.10.fid
7.28 CDCl3
6.06
O
O
O
O
$F_3C$
S
O
O
S
$CF_3$
2.00
450000
400000
350000
300000
250000
200000
150000
100000
50000
0
10.0
9.5
9.0
8.5
8.0
7.5
7.0
6.5
6.0
5.5
5.0
4.5
4.0
3.5
3.0
2.5
2.0
1.5
1.0
0.5
0.0
-0.5
f1 (ppm)

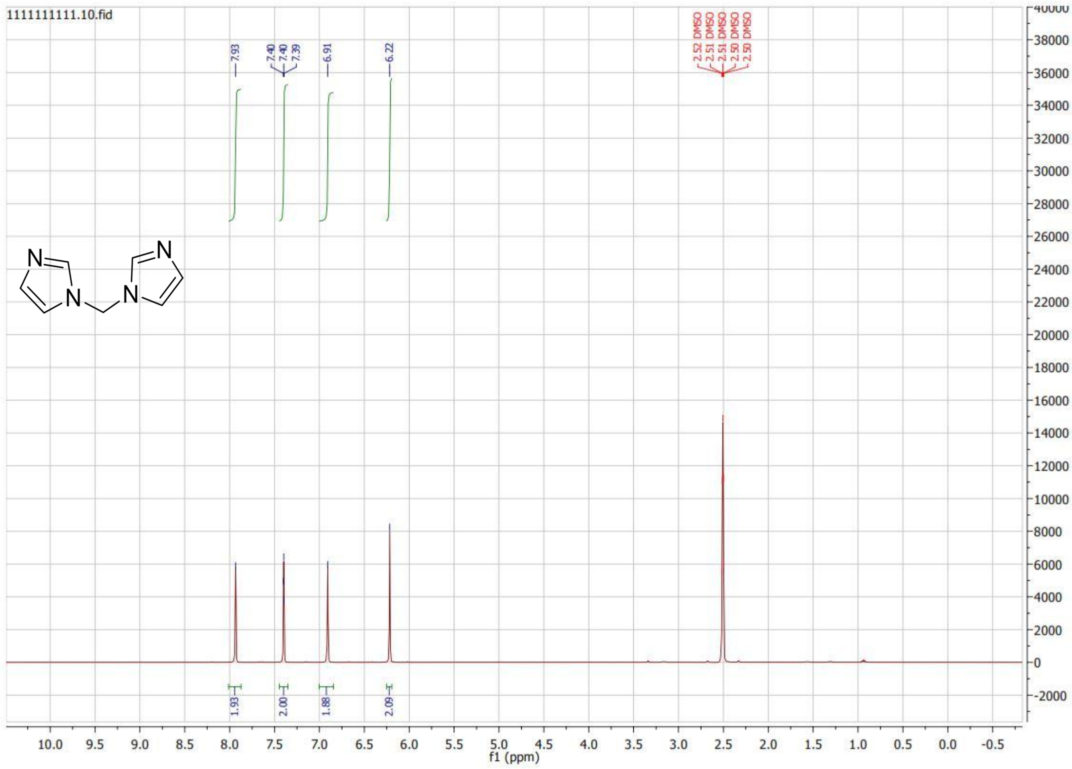
1111111111.10.fid
7.93
7.40
7.40
7.39
6.91
6.22
2.52 DMSO
2.51 DMSO
2.51 DMSO
2.50 DMSO
2.50 DMSO
N
N
N
N
1.93
2.00
1.88
2.09
10.0 9.5 9.0 8.5 8.0 7.5 7.0 6.5 6.0 5.5 5.0 4.5 4.0 3.5 3.0 2.5 2.0 1.5 1.0 0.5 0.0 -0.5
f1 (ppm)
40000 38000 36000 34000 32000 30000 28000 26000 24000 22000 20000 18000 16000 14000 12000 10000 8000 6000 4000 2000 0 -2000

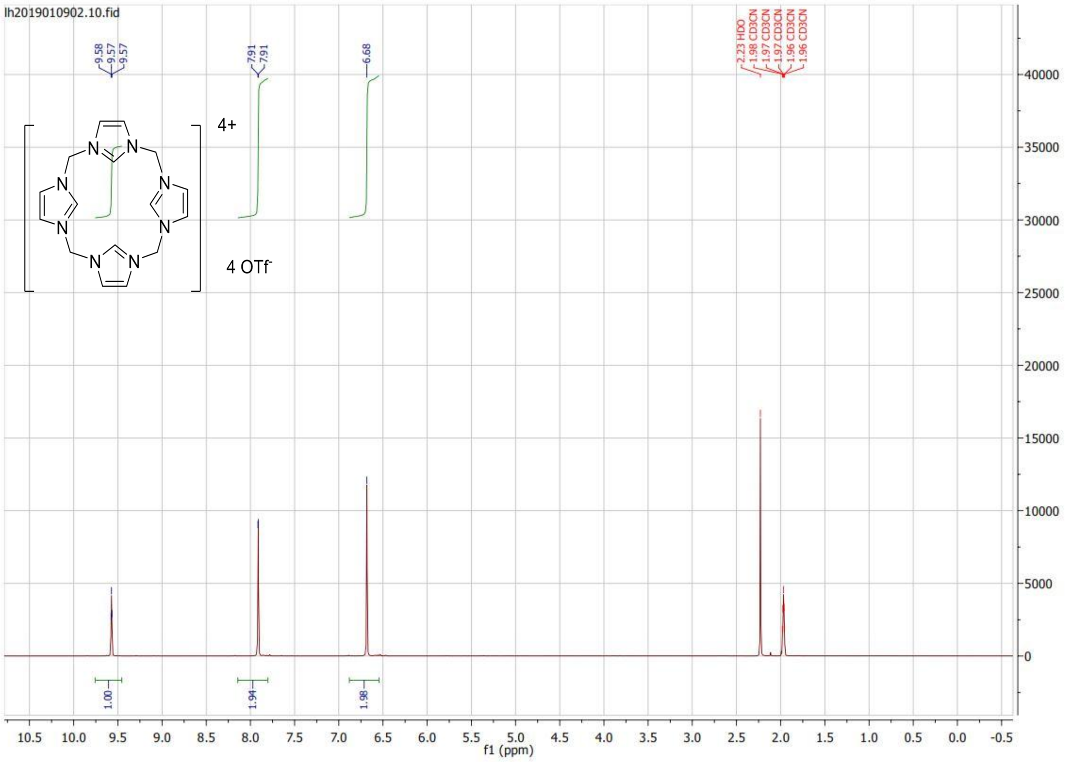
lh2019010902.10.fid
9.58
9.57
9.57
7.91
7.91
6.68
2.23 HDO
1.98 CD3CN
1.97 CD3CN
1.97 CD3CN
1.96 CD3CN
1.96 CD3CN
4+
4 OTf-
N
1.00
1.94
1.98
10.5 10.0 9.5 9.0 8.5 8.0 7.5 7.0 6.5 6.0 5.5 5.0 4.5 4.0 3.5 3.0 2.5 2.0 1.5 1.0 0.5 0.0 -0.5
f1 (ppm)
40000 35000 30000 25000 20000 15000 10000 5000 0

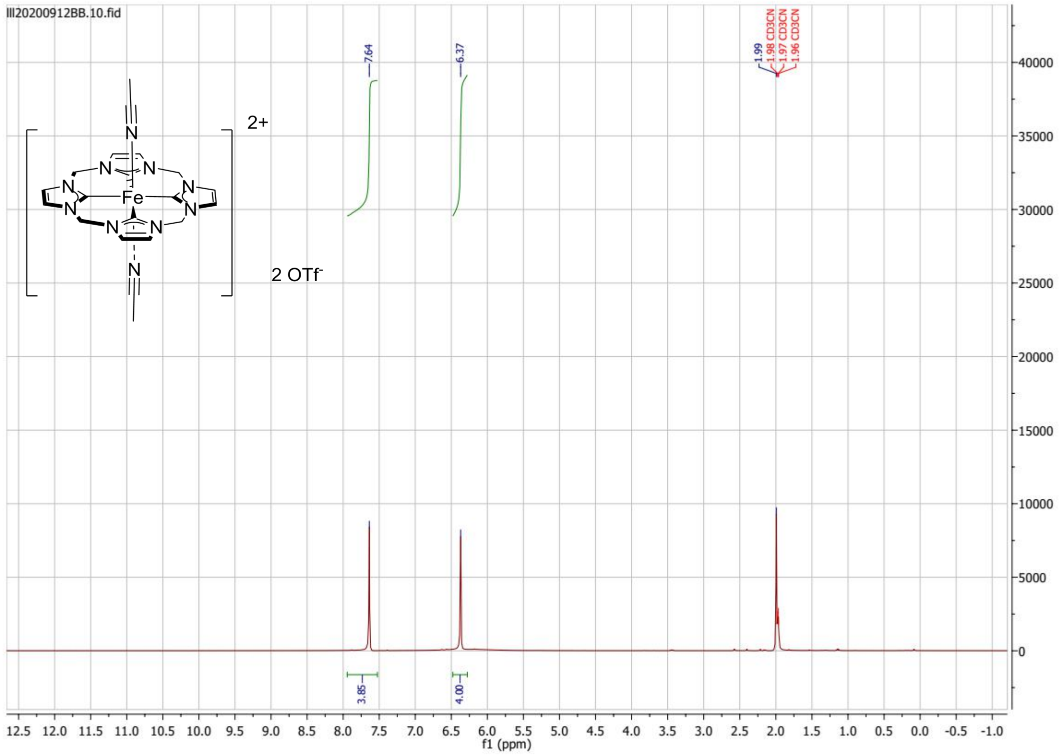
III20200912BB.10.fid
7.64
6.37
1.99
1.98 CD3CN
1.97 CD3CN
1.96 CD3CN
2+
Fe
N
2 OTf-
3.85
4.00
12.5 12.0 11.5 11.0 10.5 10.0 9.5 9.0 8.5 8.0 7.5 7.0 6.5 6.0 5.5 5.0 4.5 4.0 3.5 3.0 2.5 2.0 1.5 1.0 0.5 0.0 -0.5 -1.0
f1 (ppm)
40000
35000
30000
25000
20000
15000
10000
5000
0

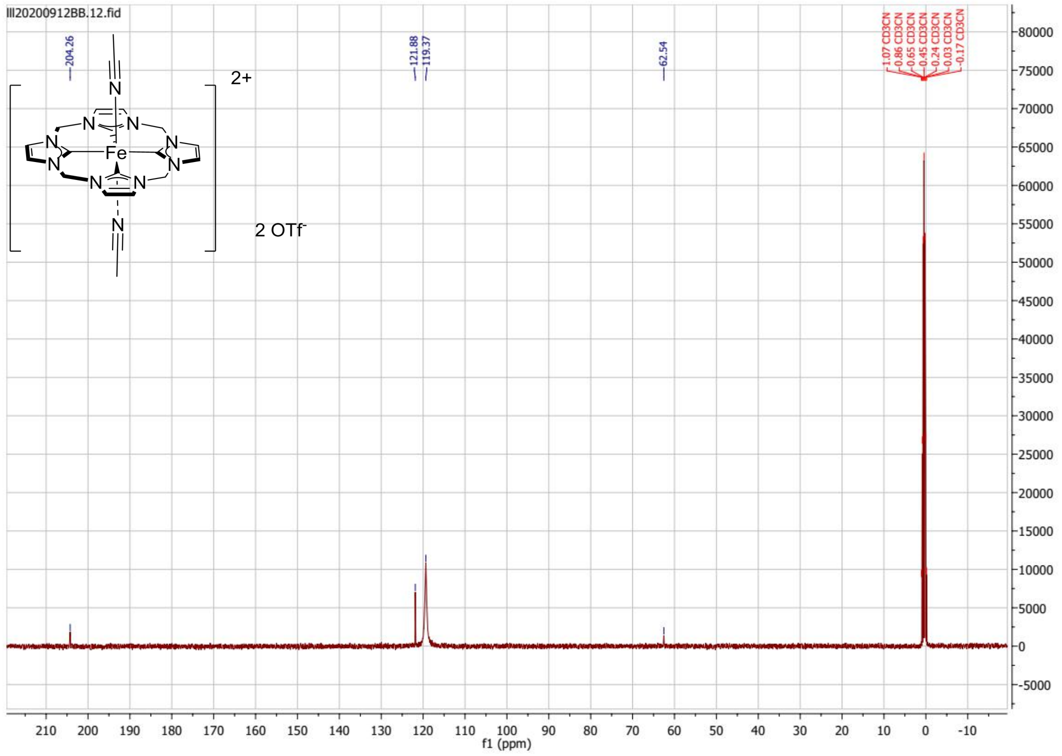
III20200912BB.12.fid
204.26
121.88
119.37
62.54
1.07 CD3CN
0.86 CD3CN
0.65 CD3CN
0.45 CD3CN
0.24 CD3CN
0.03 CD3CN
-0.17 CD3CN
2+
Fe
N
2 OTf-
210 200 190 180 170 160 150 140 130 120 110 100 90 80 70 60 50 40 30 20 10 0 -10
f1 (ppm)
80000
75000
70000
65000
60000
55000
50000
45000
40000
35000
30000
25000
20000
15000
10000
5000
0
-5000

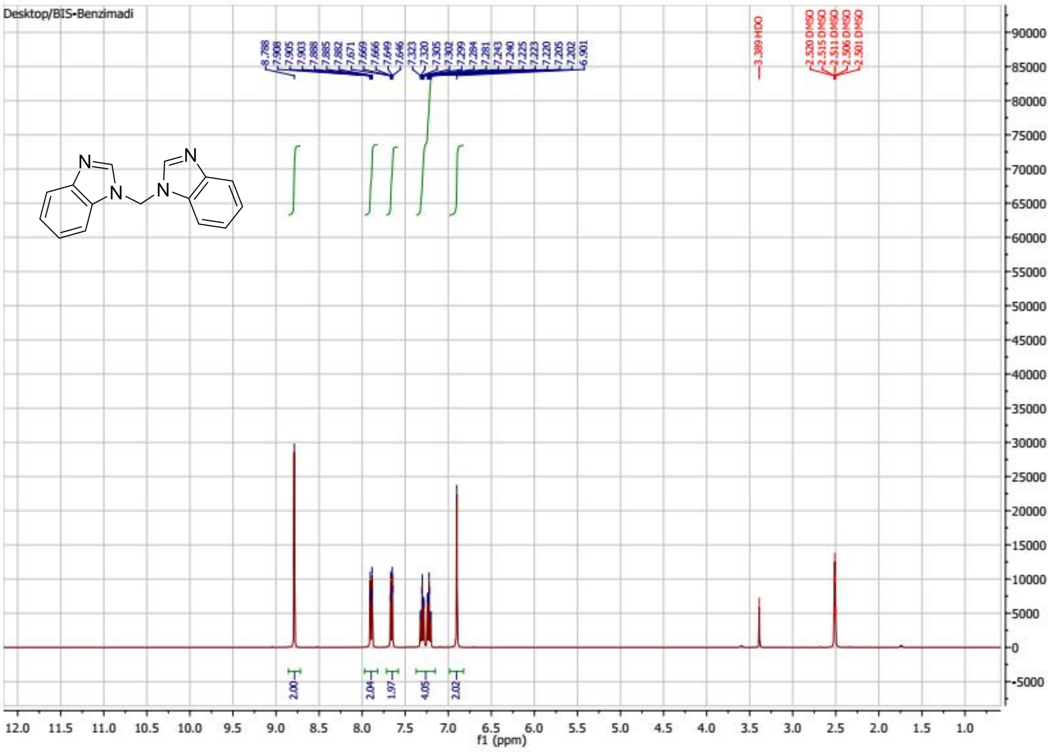
Desktop/BIS-Benzimadi
8.788
7.908
7.905
7.903
7.888
7.885
7.882
7.671
7.669
7.666
7.649
7.646
7.323
7.320
7.305
7.302
7.299
7.284
7.281
7.243
7.240
7.225
7.223
7.220
7.205
7.202
6.901
3.389 HDO
2.520 DMSO
2.515 DMSO
2.511 DMSO
2.506 DMSO
2.501 DMSO
N
N
N
N
2.00
2.04
1.97
4.05
2.02
90000
85000
80000
75000
70000
65000
60000
55000
50000
45000
40000
35000
30000
25000
20000
15000
10000
5000
0
-5000
12.0 11.5 11.0 10.5 10.0 9.5 9.0 8.5 8.0 7.5 7.0 6.5 6.0 5.5 5.0 4.5 4.0 3.5 3.0 2.5 2.0 1.5 1.0
f1 (ppm)

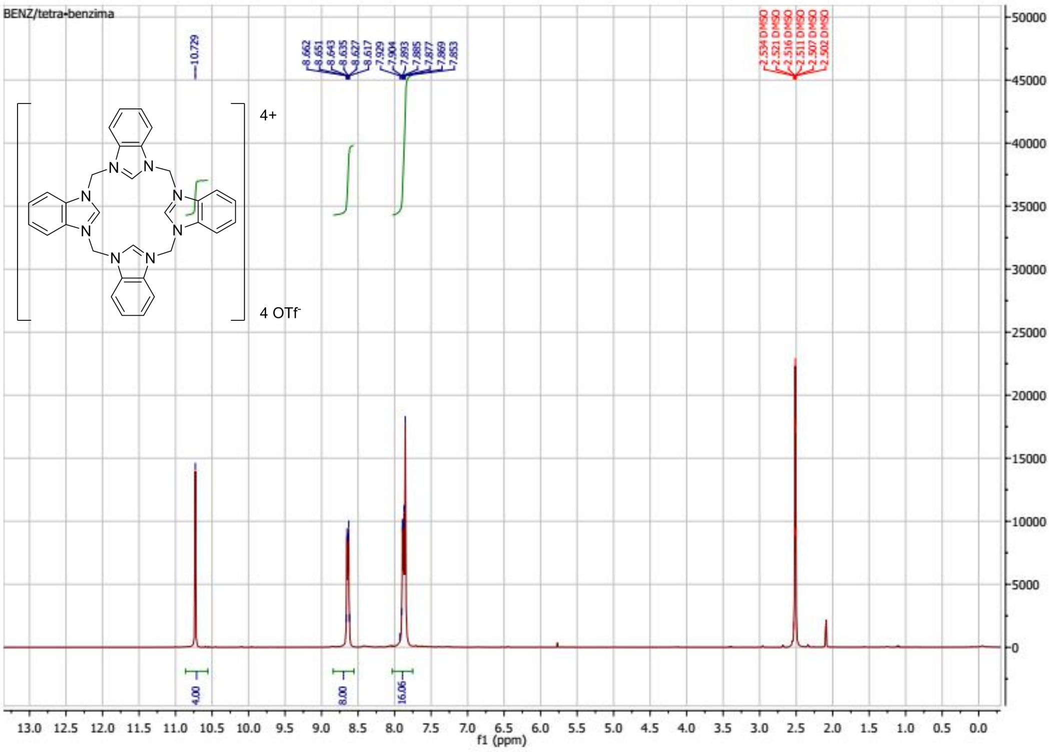
BENZ/tetra-benzima
10.729
8.662
8.651
8.643
8.635
8.627
8.617
7.929
7.904
7.893
7.885
7.877
7.869
7.853
2.534 DMSO
2.521 DMSO
2.516 DMSO
2.511 DMSO
2.507 DMSO
2.502 DMSO
4+
4 OTf⁻
N
N
N
N
N
N
N
N
4.00
8.00
16.06
50000
45000
40000
35000
30000
25000
20000
15000
10000
5000
0
13.0 12.5 12.0 11.5 11.0 10.5 10.0 9.5 9.0 8.5 8.0 7.5 7.0 6.5 6.0 5.5 5.0 4.5 4.0 3.5 3.0 2.5 2.0 1.5 1.0 0.5 0.0
f1 (ppm)

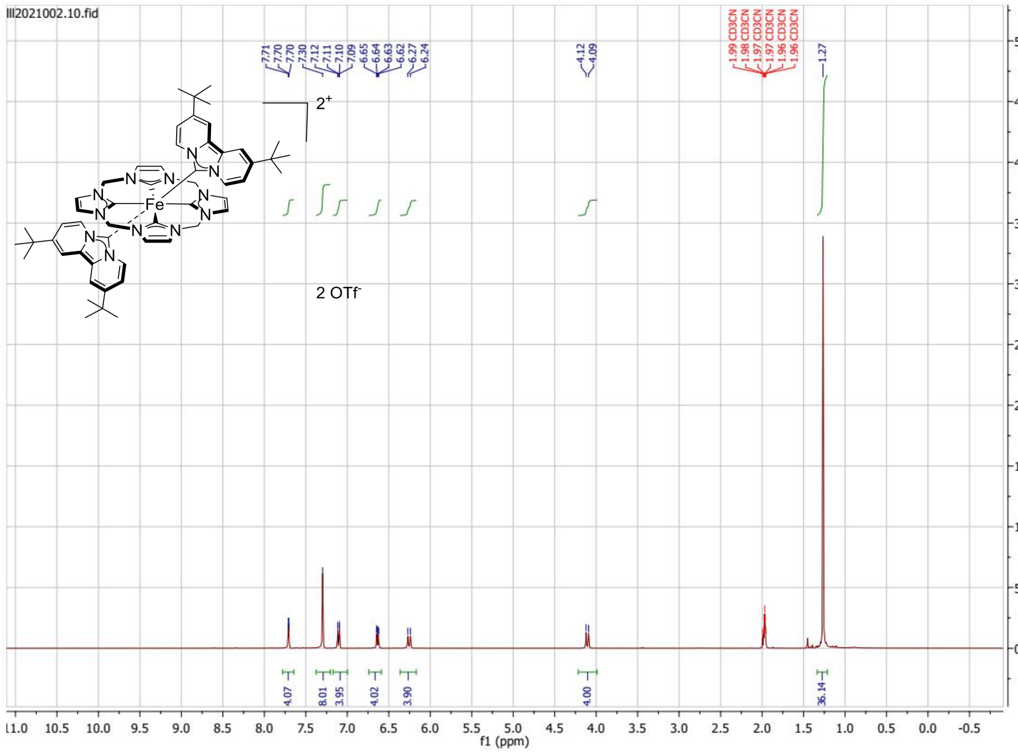
III2021002.10.fid
7.71
7.70
7.70
7.30
7.12
7.11
7.10
7.09
6.65
6.64
6.63
6.62
6.27
6.24
4.12
4.09
1.99 CD3CN
1.98 CD3CN
1.97 CD3CN
1.97 CD3CN
1.96 CD3CN
1.96 CD3CN
1.27
2+
Fe
N
2 OTf-
4.07
8.01
3.95
4.02
3.90
4.00
36.14
11.0 10.5 10.0 9.5 9.0 8.5 8.0 7.5 7.0 6.5 6.0 5.5 5.0 4.5 4.0 3.5 3.0 2.5 2.0 1.5 1.0 0.5 0.0 -0.5
f1 (ppm)
50000 45000 40000 35000 30000 25000 20000 15000 10000 5000 0

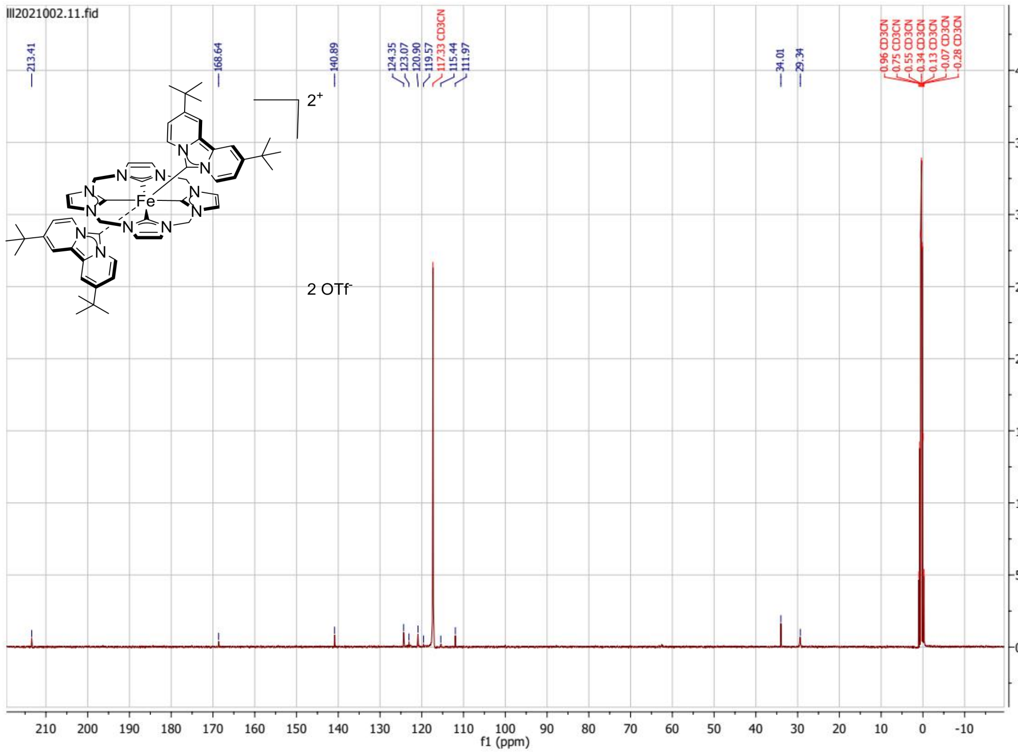
III2021002.11.fid
213.41
168.64
140.89
124.35
123.07
120.90
119.57
117.33 CD3CN
115.44
111.97
34.01
29.34
0.96 CD3CN
0.75 CD3CN
0.55 CD3CN
0.34 CD3CN
0.13 CD3CN
-0.07 CD3CN
-0.28 CD3CN
2+
Fe
N
2 OTf-
210 200 190 180 170 160 150 140 130 120 110 100 90 80 70 60 50 40 30 20 10 0 -10
f1 (ppm)
400000 350000 300000 250000 200000 150000 100000 50000 0

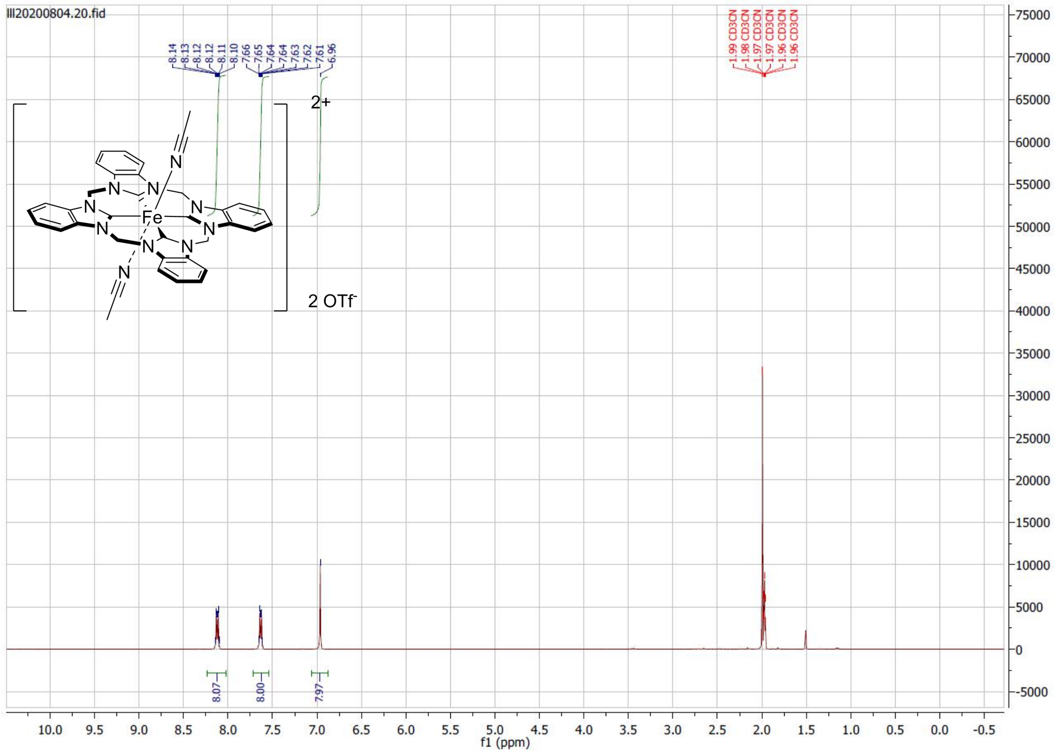
lll20200804.20.fid
8.14
8.13
8.12
8.12
8.11
8.10
7.66
7.65
7.64
7.64
7.63
7.62
7.61
6.96
1.99 CD3CN
1.98 CD3CN
1.97 CD3CN
1.97 CD3CN
1.96 CD3CN
1.96 CD3CN
2+
2 OTf⁻
N
Fe
8.07
8.00
7.97
f1 (ppm)
10.0
9.5
9.0
8.5
8.0
7.5
7.0
6.5
6.0
5.5
5.0
4.5
4.0
3.5
3.0
2.5
2.0
1.5
1.0
0.5
0.0
-0.5
75000
70000
65000
60000
55000
50000
45000
40000
35000
30000
25000
20000
15000
10000
5000
0
-5000

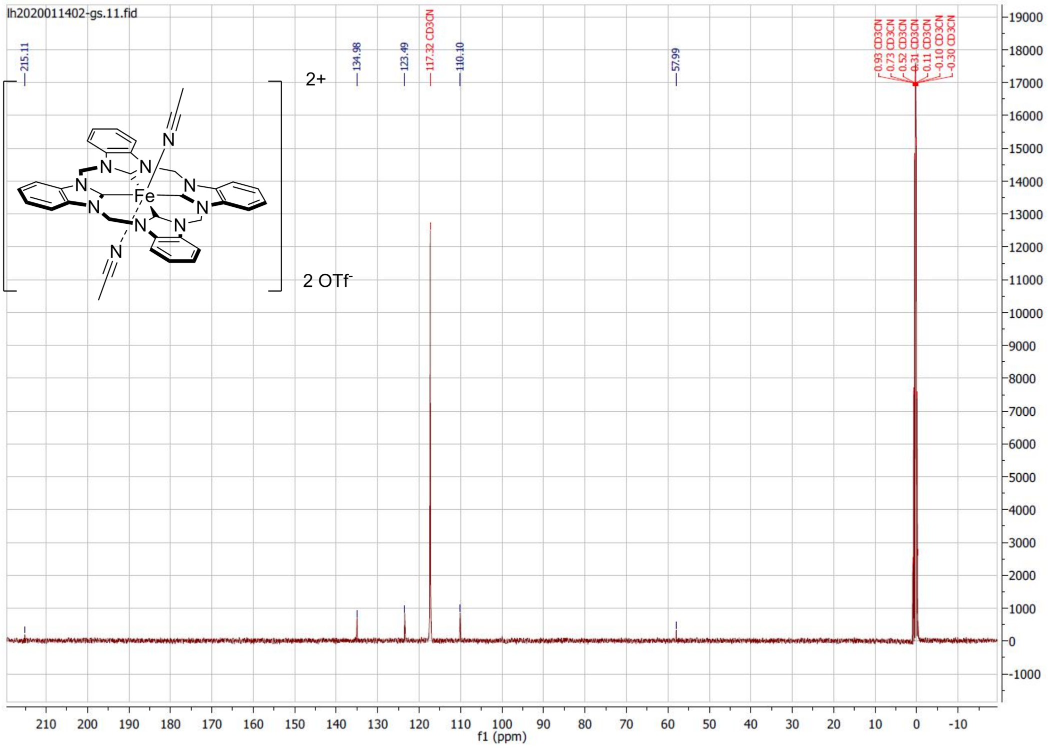
lh2020011402-gs.11.fid
215.11
134.98
123.49
117.32 CD3CN
110.10
57.99
0.93 CD3CN
0.73 CD3CN
0.52 CD3CN
0.31 CD3CN
0.11 CD3CN
-0.10 CD3CN
-0.30 CD3CN
2+
2 OTf⁻
N
Fe
f1 (ppm)
210
200
190
180
170
160
150
140
130
120
110
100
90
80
70
60
50
40
30
20
10
0
-10
19000
18000
17000
16000
15000
14000
13000
12000
11000
10000
9000
8000
7000
6000
5000
4000
3000
2000
1000
0
-1000

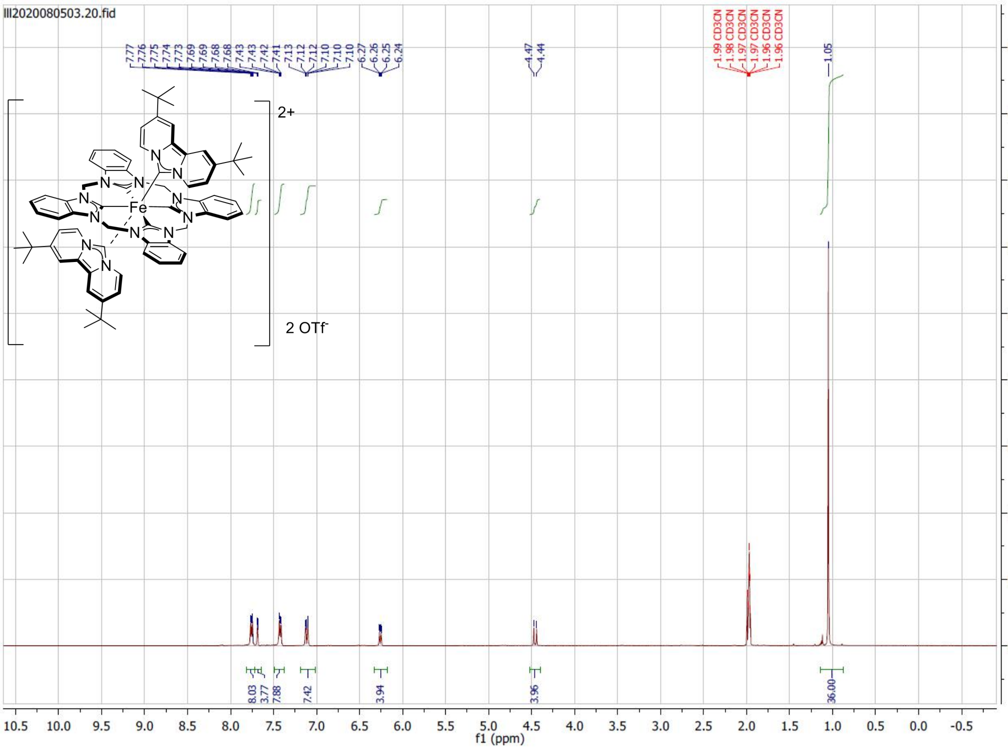
III2020080503.20.fid
7.77
7.76
7.75
7.74
7.73
7.69
7.69
7.68
7.68
7.43
7.43
7.42
7.41
7.13
7.12
7.12
7.10
7.10
7.10
6.27
6.26
6.25
6.24
4.47
4.44
1.99 CD3CN
1.98 CD3CN
1.97 CD3CN
1.97 CD3CN
1.96 CD3CN
1.96 CD3CN
1.05
2+
Fe
N
2 OTf⁻
8.03
3.77
7.88
7.42
3.94
3.96
36.00
45000
40000
35000
30000
25000
20000
15000
10000
5000
0
10.5 10.0 9.5 9.0 8.5 8.0 7.5 7.0 6.5 6.0 5.5 5.0 4.5 4.0 3.5 3.0 2.5 2.0 1.5 1.0 0.5 0.0 -0.5
f1 (ppm)

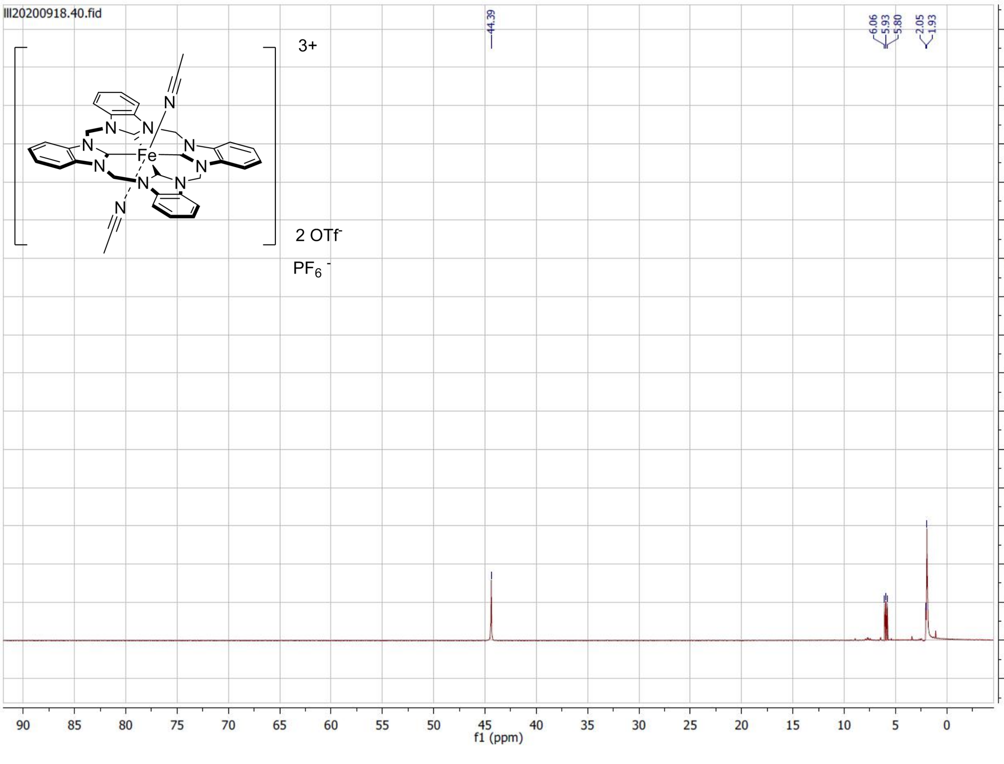
III20200918.40.fid
44.39
6.06
5.93
5.80
2.05
1.93
3+
Fe
N
2 OTf⁻
PF₆⁻
32000
30000
28000
26000
24000
22000
20000
18000
16000
14000
12000
10000
8000
6000
4000
2000
0
-2000
90 85 80 75 70 65 60 55 50 45 40 35 30 25 20 15 10 5 0
f1 (ppm)

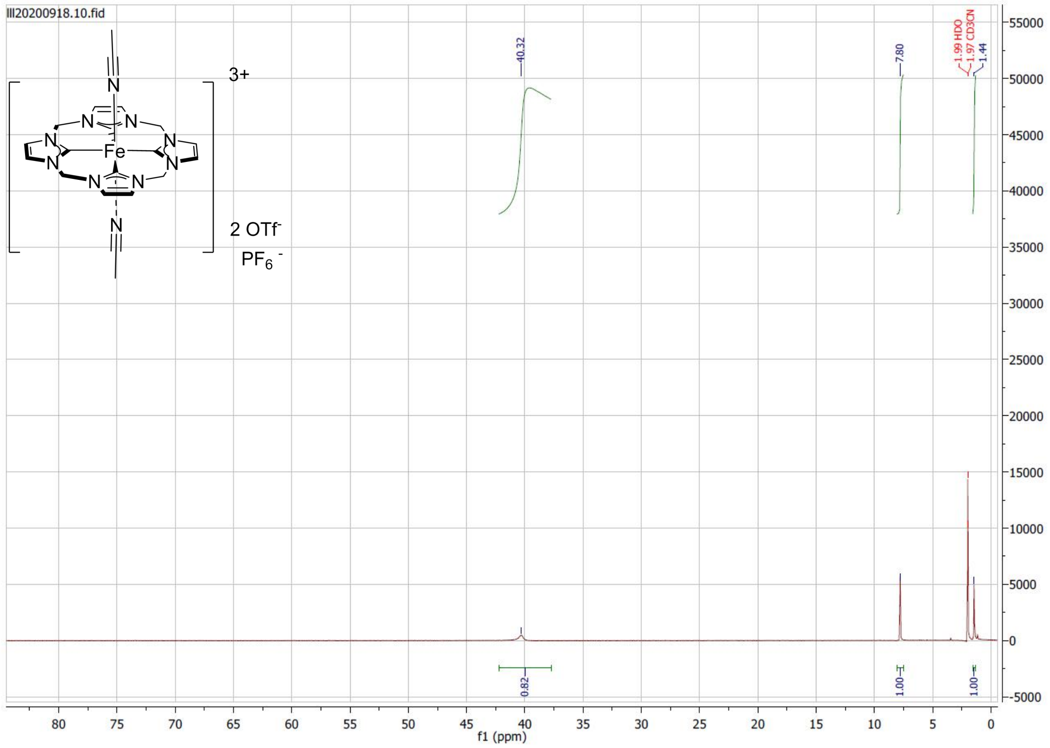

## Crystal data for Fe-2

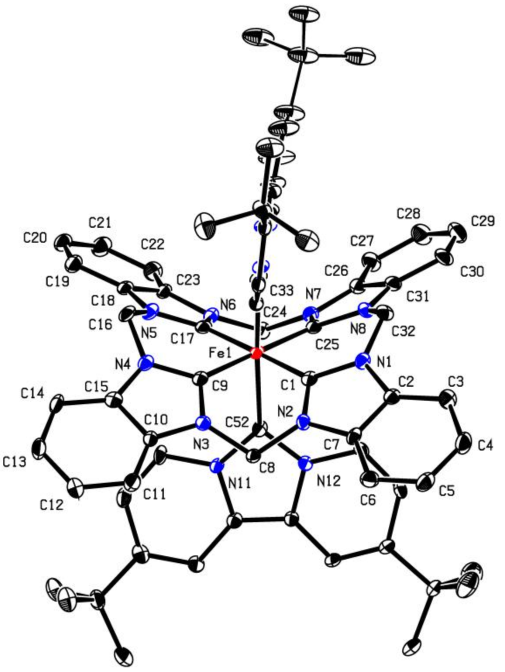

A clear yellow fragment-like specimen of C74H73F6FeN13O6S2, approximate dimensions 0.094 mm x 0.101 mm x 0.173 mm, was used for the X-ray crystallographic analysis. The X-ray intensity data were measured on a Bruker D8 Venture Duo IMS system equipped with a Helios opticmonochromator and a Mo IMS microsource (λ = 0.71073 Å).

**Table 1. Sample and crystal data for Fe-2.**

| | |
|---|---|
| **Chemical formula** | C74H73F6FeN13O6S2 |
| **Formula weight** | 1474.42 |
| **Temperature** | 100(2) K |
| **Wavelength** | 0.71073 Å |
| **Crystal size** | 0.094 x 0.101 x 0.173 mm |
| **Crystal habit** | clear yellow fragment |
| **Crystal system** | triclinic |
| **Space group** | P -1 |
| **Unit cell dimensions** | a = 14.0444(11) Å α = 68.210(3)° |
| | b = 17.7573(16) Å β = 84.515(3)° |
| | c = 17.9985(16) Å γ = 70.374(3)° |
| **Volume** | 3923.6(6) Å3 |
| **Z** | 2 |
| **Density (calculated)** | 1.248 g/cm3 |
| **Absorption coefficient** | 0.317 mm-1 |
| **F(000)** | 1536 |

**Table 2. Data collection and structure refinement for Fe-2.**

| | |
|---|---|
| **Diffractometer** | Bruker D8 Venture Duo IMS |
| **Radiation source** | IMS microsource, Mo |
| **Theta range for data collection** | 2.00 to 25.35° |
| **Index ranges** | -16<=h<=16, -21<=k<=21, -21<=l<=21 |
| **Reflections collected** | 183405 |
| **Independent reflections** | 14374 [R(int) = 0.1057] |
| **Coverage of independent reflections** | 100.0% |
| **Absorption correction** | Multi-Scan |
| **Max. and min. transmission** | 0.9710 and 0.9470 |
| **Refinement method** | Full-matrix least-squares on $F^2$ |
| **Refinement program** | SHELXL-2018/3 (Sheldrick, 2018) |
| **Function minimized** | $\Sigma w(F_o^2 - F_c^2)^2$ |
| **Data / restraints / parameters** | 14374 / 932 / 1127 |
| **Goodness-of-fit on $F^2$** | 1.114 |
| **Δ/σmax** | 0.009 |

| | |
|---|---|
| **Final R indices** | 12010 data; $I>2\sigma(I)$ R1 = 0.0679, wR2 = 0.1620 |
| | all data R1 = 0.0812, wR2 = 0.1691 |
| **Weighting scheme** | $w=1/[\sigma^2(Fo^2)+(0.0769P)^2+7.5544P]$<br>where $P=(F_o^2+2F_c^2)/3$ |
| **Largest diff. peak and hole** | 0.786 and -0.903 $e\AA^{-3}$ |
| **R.M.S. deviation from mean** | 0.086 $e\AA^{-3}$ |

## Table 3. Bond lengths (Å) for Fe-2

| | | | |
|---|---|---|---|
| Fe1-C1 | 1.869(3) | Fe1-C9 | 1.870(3) |
| Fe1-C17 | 1.878(3) | Fe1-C25 | 1.881(3) |
| Fe1-C33 | 2.028(3) | Fe1-C52 | 2.028(3) |
| N1-C1 | 1.364(4) | N1-C2 | 1.406(4) |
| N1-C32 | 1.462(4) | C1-N2 | 1.352(4) |
| N2-C7 | 1.403(4) | N2-C8 | 1.461(4) |
| C2-C3 | 1.388(5) | C2-C7 | 1.397(5) |
| N3-C9 | 1.366(4) | N3-C10 | 1.401(4) |
| N3-C8 | 1.463(4) | C3-C4 | 1.390(5) |
| C3-H3 | 0.95 | N4-C9 | 1.367(4) |
| N4-C15 | 1.395(4) | N4-C16 | 1.459(4) |
| C4-C5 | 1.393(5) | C4-H4 | 0.95 |
| N5-C17 | 1.365(4) | N5-C18 | 1.393(4) |
| N5-C16 | 1.465(4) | C5-C6 | 1.389(5) |
| C5-H5 | 0.95 | N6-C17 | 1.375(4) |
| N6-C23 | 1.400(4) | N6-C24 | 1.462(4) |
| C6-C7 | 1.382(5) | C6-H6 | 0.95 |
| N7-C25 | 1.351(4) | N7-C26 | 1.403(4) |
| N7-C24 | 1.463(4) | C8-H8A | 0.99 |
| C8-H8AB | 0.99 | N8-C25 | 1.372(4) |
| N8-C31 | 1.391(4) | N8-C32 | 1.467(4) |
| N9-C34 | 1.385(5) | N9-C33 | 1.387(4) |
| N9-C38 | 1.408(4) | N10-C33 | 1.386(4) |
| N10-C43 | 1.389(4) | N10-C39 | 1.413(4) |
| C10-C11 | 1.371(5) | C10-C15 | 1.404(5) |
| C11-C12 | 1.391(5) | C11-H11 | 0.95 |
| N11-C52 | 1.386(4) | N11-C53 | 1.392(4) |
| N11-C57 | 1.405(4) | C12-C13 | 1.399(5) |
| C12-H12 | 0.95 | N12-C62 | 1.391(4) |
| N12-C52 | 1.391(4) | N12-C58 | 1.399(4) |
| N13-C73 | 1.129(6) | C13-C14 | 1.382(5) |
| C13-H13 | 0.95 | C29-C30 | 1.374(6) |

| | | | |
|---|---|---|---|
| C29-C28 | 1.404(5) | C29-H29 | 0.95 |
| C28-C27 | 1.384(5) | C28-H28 | 0.95 |
| C27-C26 | 1.385(5) | C27-H27 | 0.95 |
| C26-C31 | 1.401(5) | C24-H24A | 0.99 |
| C24-H24B | 0.99 | C23-C22 | 1.383(5) |
| C23-C18 | 1.397(5) | C22-C21 | 1.388(5) |
| C22-H22 | 0.95 | C21-C20 | 1.396(6) |
| C21-H21 | 0.95 | C16-H16A | 0.99 |
| C16-H16B | 0.99 | C15-C14 | 1.394(5) |
| C14-H14 | 0.95 | C18-C19 | 1.391(5) |
| C19-C20 | 1.390(5) | C19-H19 | 0.95 |
| C20-H20 | 0.95 | C32-H32A | 0.99 |
| C32-H32B | 0.99 | C31-C30 | 1.389(5) |
| C30-H30 | 0.95 | C34-C35 | 1.352(6) |
| C34-H34 | 0.95 | C35-C36 | 1.453(7) |
| C35-C36A | 1.502(18) | C37-C36A | 1.237(15) |
| C37-C36 | 1.404(7) | C37-C38 | 1.422(5) |
| C38-C39 | 1.377(5) | C39-C40 | 1.405(5) |
| C40-C41 | 1.353(5) | C40-H40 | 0.95 |
| C41-C42 | 1.439(5) | C41-C48 | 1.524(5) |
| C42-C43 | 1.343(5) | C42-H42 | 0.95 |
| C43-H43 | 0.95 | C48-C50 | 1.526(5) |
| C48-C51 | 1.539(5) | C48-C49 | 1.545(5) |
| C49-H49A | 0.98 | C49-H49B | 0.98 |
| C49-H49C | 0.98 | C50-H50A | 0.98 |
| C50-H50B | 0.98 | C50-H50C | 0.98 |
| C51-H51A | 0.98 | C51-H51B | 0.98 |
| C51-H51C | 0.98 | C68-C67 | 1.527(7) |
| C68-H68A | 0.98 | C68-H68B | 0.98 |
| C68-H68C | 0.98 | C67-C70 | 1.518(7) |
| C67-C60 | 1.527(5) | C67-C69 | 1.531(6) |
| C66-C63 | 1.540(5) | C66-H66A | 0.98 |
| C66-H66B | 0.98 | C66-H66C | 0.98 |
| C65-C63 | 1.532(5) | C65-H65A | 0.98 |
| C65-H65B | 0.98 | C65-H65C | 0.98 |
| C64-C63 | 1.537(5) | C64-H64A | 0.98 |
| C64-H64B | 0.98 | C64-H64C | 0.98 |
| C63-C55 | 1.529(5) | C62-C61 | 1.344(5) |
| C62-H62 | 0.95 | C61-C60 | 1.426(5) |
| C61-H61 | 0.95 | C60-C59 | 1.353(5) |
| C59-C58 | 1.415(4) | C59-H59 | 0.95 |
| C58-C57 | 1.376(5) | C57-C56 | 1.414(5) |
| C56-C55 | 1.364(5) | C56-H56 | 0.95 |

| | | | |
|---|---|---|---|
| C55-C54 | 1.428(5) | C54-C53 | 1.355(5) |
| C54-H54 | 0.95 | C53-H53 | 0.95 |
| C70-H70A | 0.98 | C70-H70B | 0.98 |
| C70-H70C | 0.98 | C69-H69A | 0.98 |
| C69-H69B | 0.98 | C69-H69C | 0.98 |
| C73-C74 | 1.445(7) | C74-H74A | 0.98 |
| C74-H74B | 0.98 | C74-H74C | 0.98 |
| C71-F1 | 1.330(6) | C71-F2 | 1.335(6) |
| C71-F3 | 1.339(5) | C71-S1 | 1.818(5) |
| S1-O2 | 1.440(4) | S1-O1 | 1.440(4) |
| S1-O3 | 1.444(4) | C71A-F1A | 1.330(6) |
| C71A-F2A | 1.336(6) | C71A-F3A | 1.340(5) |
| C71A-S1A | 1.818(5) | S1A-O2A | 1.439(4) |
| S1A-O1A | 1.442(4) | S1A-O3A | 1.444(4) |
| C72-F4 | 1.322(5) | C72-F5 | 1.339(5) |
| C72-F6 | 1.342(5) | C72-S2 | 1.834(5) |
| S2-O4 | 1.435(3) | S2-O5 | 1.440(3) |
| S2-O6 | 1.442(3) | C72A-F4A | 1.321(6) |
| C72A-F5A | 1.340(6) | C72A-F6A | 1.343(6) |
| C72A-S2A | 1.834(6) | S2A-O4A | 1.437(5) |
| S2A-O5A | 1.439(5) | S2A-O6A | 1.442(5) |
| C36-C44 | 1.529(6) | C44-C46 | 1.517(6) |
| C44-C47 | 1.521(9) | C44-C45 | 1.536(7) |
| C45-H45A | 0.98 | C45-H45B | 0.98 |
| C45-H45C | 0.98 | C46-H46A | 0.98 |
| C46-H46B | 0.98 | C46-H46C | 0.98 |
| C47-H47A | 0.98 | C47-H47B | 0.98 |
| C47-H47C | 0.98 | C36A-C44A | 1.529(6) |
| C44A-C46A | 1.517(6) | C44A-C47A | 1.521(9) |
| C44A-C45A | 1.536(7) | C45A-H45D | 0.98 |
| C45A-H45E | 0.98 | C45A-H45F | 0.98 |
| C46A-H46D | 0.98 | C46A-H46E | 0.98 |
| C46A-H46F | 0.98 | C47A-H47D | 0.98 |
| C47A-H47E | 0.98 | C47A-H47F | 0.98 |

**Table 4. Bond angles (°) for Fe-2**

| | | | |
|---|---|---|---|
| C1-Fe1-C9 | 89.88(15) | C1-Fe1-C17 | 179.04(15) |
| C9-Fe1-C17 | 89.42(15) | C1-Fe1-C25 | 90.29(15) |
| C9-Fe1-C25 | 179.13(14) | C17-Fe1-C25 | 90.40(15) |
| C1-Fe1-C33 | 89.07(13) | C9-Fe1-C33 | 92.22(14) |
| C17-Fe1-C33 | 91.61(13) | C25-Fe1-C33 | 88.64(14) |
| C1-Fe1-C52 | 86.23(13) | C9-Fe1-C52 | 87.62(14) |

|  |  |  |  |
|---|---|---|---|
| C17-Fe1-C52 | 93.09(13) | C25-Fe1-C52 | 91.53(14) |
| C33-Fe1-C52 | 175.29(13) | C1-N1-C2 | 110.4(3) |
| C1-N1-C32 | 123.1(3) | C2-N1-C32 | 126.5(3) |
| N2-C1-N1 | 106.3(3) | N2-C1-Fe1 | 126.6(2) |
| N1-C1-Fe1 | 126.9(3) | C1-N2-C7 | 111.0(3) |
| C1-N2-C8 | 123.5(3) | C7-N2-C8 | 124.6(3) |
| C3-C2-C7 | 121.9(3) | C3-C2-N1 | 131.9(3) |
| C7-C2-N1 | 106.1(3) | C9-N3-C10 | 111.2(3) |
| C9-N3-C8 | 123.1(3) | C10-N3-C8 | 124.6(3) |
| C2-C3-C4 | 116.4(3) | C2-C3-H3 | 121.8 |
| C4-C3-H3 | 121.8 | C9-N4-C15 | 111.4(3) |
| C9-N4-C16 | 121.2(3) | C15-N4-C16 | 127.4(3) |
| C3-C4-C5 | 121.6(3) | C3-C4-H4 | 119.2 |
| C5-C4-H4 | 119.2 | C17-N5-C18 | 111.6(3) |
| C17-N5-C16 | 121.6(3) | C18-N5-C16 | 126.3(3) |
| C6-C5-C4 | 121.8(3) | C6-C5-H5 | 119.1 |
| C4-C5-H5 | 119.1 | C17-N6-C23 | 111.3(3) |
| C17-N6-C24 | 121.2(3) | C23-N6-C24 | 127.4(3) |
| C7-C6-C5 | 116.7(3) | C7-C6-H6 | 121.7 |
| C5-C6-H6 | 121.7 | C6-C7-C2 | 121.6(3) |
| C6-C7-N2 | 132.4(3) | C2-C7-N2 | 106.0(3) |
| C25-N7-C26 | 111.7(3) | C25-N7-C24 | 121.2(3) |
| C26-N7-C24 | 127.0(3) | N2-C8-N3 | 112.3(3) |
| N2-C8-H8A | 109.1 | N3-C8-H8A | 109.1 |
| N2-C8-H8AB | 109.1 | N3-C8-H8AB | 109.1 |
| H8A-C8-H8AB | 107.9 | C25-N8-C31 | 110.9(3) |
| C25-N8-C32 | 123.0(3) | C31-N8-C32 | 125.5(3) |
| C34-N9-C33 | 128.3(3) | C34-N9-C38 | 117.9(3) |
| C33-N9-C38 | 113.8(3) | N3-C9-N4 | 105.3(3) |
| N3-C9-Fe1 | 126.2(2) | N4-C9-Fe1 | 127.9(2) |
| C33-N10-C43 | 128.7(3) | C33-N10-C39 | 113.7(3) |
| C43-N10-C39 | 117.6(3) | C11-C10-N3 | 132.5(3) |
| C11-C10-C15 | 121.6(3) | N3-C10-C15 | 105.9(3) |
| C10-C11-C12 | 117.6(3) | C10-C11-H11 | 121.2 |
| C12-C11-H11 | 121.2 | C52-N11-C53 | 128.3(3) |
| C52-N11-C57 | 113.8(3) | C53-N11-C57 | 117.9(3) |
| C11-C12-C13 | 120.4(4) | C11-C12-H12 | 119.8 |
| C13-C12-H12 | 119.8 | C62-N12-C52 | 128.6(3) |
| C62-N12-C58 | 117.9(3) | C52-N12-C58 | 113.5(3) |
| C14-C13-C12 | 122.7(3) | C14-C13-H13 | 118.7 |
| C12-C13-H13 | 118.7 | C30-C29-C28 | 121.9(3) |
| C30-C29-H29 | 119 | C28-C29-H29 | 119 |
| C27-C28-C29 | 121.7(4) | C27-C28-H28 | 119.1 |

| | | | |
|---|---|---|---|
| C29-C28-H28 | 119.1 | C28-C27-C26 | 116.2(3) |
| C28-C27-H27 | 121.9 | C26-C27-H27 | 121.9 |
| C27-C26-C31 | 122.1(3) | C27-C26-N7 | 132.6(3) |
| C31-C26-N7 | 105.2(3) | N7-C25-N8 | 105.4(3) |
| N7-C25-Fe1 | 127.8(2) | N8-C25-Fe1 | 126.4(2) |
| N6-C24-N7 | 110.8(3) | N6-C24-H24A | 109.5 |
| N7-C24-H24A | 109.5 | N6-C24-H24B | 109.5 |
| N7-C24-H24B | 109.5 | H24A-C24-H24B | 108.1 |
| C22-C23-C18 | 122.1(3) | C22-C23-N6 | 132.1(3) |
| C18-C23-N6 | 105.8(3) | C23-C22-C21 | 116.1(3) |
| C23-C22-H22 | 121.9 | C21-C22-H22 | 121.9 |
| C22-C21-C20 | 122.0(3) | C22-C21-H21 | 119 |
| C20-C21-H21 | 119 | N4-C16-N5 | 111.5(3) |
| N4-C16-H16A | 109.3 | N5-C16-H16A | 109.3 |
| N4-C16-H16B | 109.3 | N5-C16-H16B | 109.3 |
| H16A-C16-H16B | 108 | C14-C15-N4 | 132.4(3) |
| C14-C15-C10 | 121.5(3) | N4-C15-C10 | 106.0(3) |
| C13-C14-C15 | 116.1(3) | C13-C14-H14 | 121.9 |
| C15-C14-H14 | 121.9 | N5-C17-N6 | 104.8(3) |
| N5-C17-Fe1 | 127.9(3) | N6-C17-Fe1 | 127.2(2) |
| C19-C18-N5 | 131.8(3) | C19-C18-C23 | 121.8(3) |
| N5-C18-C23 | 106.4(3) | C20-C19-C18 | 116.1(3) |
| C20-C19-H19 | 122 | C18-C19-H19 | 122 |
| C19-C20-C21 | 121.8(3) | C19-C20-H20 | 119.1 |
| C21-C20-H20 | 119.1 | N10-C33-N9 | 101.0(3) |
| N10-C33-Fe1 | 129.3(2) | N9-C33-Fe1 | 129.1(2) |
| N1-C32-N8 | 111.7(3) | N1-C32-H32A | 109.3 |
| N8-C32-H32A | 109.3 | N1-C32-H32B | 109.3 |
| N8-C32-H32B | 109.3 | H32A-C32-H32B | 107.9 |
| C30-C31-N8 | 132.2(3) | C30-C31-C26 | 121.2(3) |
| N8-C31-C26 | 106.5(3) | C29-C30-C31 | 116.7(3) |
| C29-C30-H30 | 121.6 | C31-C30-H30 | 121.6 |
| C35-C34-N9 | 121.1(3) | C35-C34-H34 | 119.5 |
| N9-C34-H34 | 119.5 | C34-C35-C36 | 124.0(4) |
| C34-C35-C36A | 114.1(5) | C36A-C37-C38 | 115.7(7) |
| C36-C37-C38 | 121.3(4) | C39-C38-N9 | 105.8(3) |
| C39-C38-C37 | 133.1(3) | N9-C38-C37 | 121.1(3) |
| C38-C39-C40 | 133.3(3) | C38-C39-N10 | 105.6(3) |
| C40-C39-N10 | 121.0(3) | C41-C40-C39 | 120.8(3) |
| C41-C40-H40 | 119.6 | C39-C40-H40 | 119.6 |
| C40-C41-C42 | 117.2(3) | C40-C41-C48 | 124.4(3) |
| C42-C41-C48 | 118.4(3) | C43-C42-C41 | 122.6(3) |
| C43-C42-H42 | 118.7 | C41-C42-H42 | 118.7 |

| | | | |
|---|---|---|---|
| C42-C43-N10 | 120.7(3) | C42-C43-H43 | 119.6 |
| N10-C43-H43 | 119.6 | C41-C48-C50 | 112.2(3) |
| C41-C48-C51 | 109.5(3) | C50-C48-C51 | 109.3(3) |
| C41-C48-C49 | 108.3(3) | C50-C48-C49 | 108.7(3) |
| C51-C48-C49 | 108.8(3) | C48-C49-H49A | 109.5 |
| C48-C49-H49B | 109.5 | H49A-C49-H49B | 109.5 |
| C48-C49-H49C | 109.5 | H49A-C49-H49C | 109.5 |
| H49B-C49-H49C | 109.5 | C48-C50-H50A | 109.5 |
| C48-C50-H50B | 109.5 | H50A-C50-H50B | 109.5 |
| C48-C50-H50C | 109.5 | H50A-C50-H50C | 109.5 |
| H50B-C50-H50C | 109.5 | C48-C51-H51A | 109.5 |
| C48-C51-H51B | 109.5 | H51A-C51-H51B | 109.5 |
| C48-C51-H51C | 109.5 | H51A-C51-H51C | 109.5 |
| H51B-C51-H51C | 109.5 | C67-C68-H68A | 109.5 |
| C67-C68-H68B | 109.5 | H68A-C68-H68B | 109.5 |
| C67-C68-H68C | 109.5 | H68A-C68-H68C | 109.5 |
| H68B-C68-H68C | 109.5 | C70-C67-C68 | 109.6(4) |
| C70-C67-C60 | 109.0(4) | C68-C67-C60 | 109.7(3) |
| C70-C67-C69 | 108.9(4) | C68-C67-C69 | 108.9(4) |
| C60-C67-C69 | 110.7(3) | C63-C66-H66A | 109.5 |
| C63-C66-H66B | 109.5 | H66A-C66-H66B | 109.5 |
| C63-C66-H66C | 109.5 | H66A-C66-H66C | 109.5 |
| H66B-C66-H66C | 109.5 | C63-C65-H65A | 109.5 |
| C63-C65-H65B | 109.5 | H65A-C65-H65B | 109.5 |
| C63-C65-H65C | 109.5 | H65A-C65-H65C | 109.5 |
| H65B-C65-H65C | 109.5 | C63-C64-H64A | 109.5 |
| C63-C64-H64B | 109.5 | H64A-C64-H64B | 109.5 |
| C63-C64-H64C | 109.5 | H64A-C64-H64C | 109.5 |
| H64B-C64-H64C | 109.5 | C55-C63-C65 | 111.8(3) |
| C55-C63-C64 | 110.4(3) | C65-C63-C64 | 108.8(3) |
| C55-C63-C66 | 108.3(3) | C65-C63-C66 | 108.4(3) |
| C64-C63-C66 | 109.2(3) | C61-C62-N12 | 120.9(3) |
| C61-C62-H62 | 119.6 | N12-C62-H62 | 119.6 |
| C62-C61-C60 | 122.1(3) | C62-C61-H61 | 119 |
| C60-C61-H61 | 119 | C59-C60-C61 | 118.0(3) |
| C59-C60-C67 | 124.0(3) | C61-C60-C67 | 118.0(3) |
| C60-C59-C58 | 120.3(3) | C60-C59-H59 | 119.9 |
| C58-C59-H59 | 119.9 | C57-C58-N12 | 106.2(3) |
| C57-C58-C59 | 132.9(3) | N12-C58-C59 | 120.9(3) |
| C58-C57-N11 | 105.5(3) | C58-C57-C56 | 133.2(3) |
| N11-C57-C56 | 121.2(3) | C55-C56-C57 | 120.3(3) |
| C55-C56-H56 | 119.8 | C57-C56-H56 | 119.8 |
| C56-C55-C54 | 117.3(3) | C56-C55-C63 | 122.7(3) |

|  |  |  |  |
|---|---|---|---|
| C54-C55-C63 | 120.0(3) | C53-C54-C55 | 122.9(3) |
| C53-C54-H54 | 118.6 | C55-C54-H54 | 118.6 |
| C54-C53-N11 | 120.1(3) | C54-C53-H53 | 119.9 |
| N11-C53-H53 | 119.9 | N11-C52-N12 | 100.9(3) |
| N11-C52-Fe1 | 129.1(2) | N12-C52-Fe1 | 127.8(2) |
| C67-C70-H70A | 109.5 | C67-C70-H70B | 109.5 |
| H70A-C70-H70B | 109.5 | C67-C70-H70C | 109.5 |
| H70A-C70-H70C | 109.5 | H70B-C70-H70C | 109.5 |
| C67-C69-H69A | 109.5 | C67-C69-H69B | 109.5 |
| H69A-C69-H69B | 109.5 | C67-C69-H69C | 109.5 |
| H69A-C69-H69C | 109.5 | H69B-C69-H69C | 109.5 |
| N13-C73-C74 | 179.4(5) | C73-C74-H74A | 109.5 |
| C73-C74-H74B | 109.5 | H74A-C74-H74B | 109.5 |
| C73-C74-H74C | 109.5 | H74A-C74-H74C | 109.5 |
| H74B-C74-H74C | 109.5 | F1-C71-F2 | 107.5(5) |
| F1-C71-F3 | 106.9(5) | F2-C71-F3 | 107.3(5) |
| F1-C71-S1 | 111.7(4) | F2-C71-S1 | 111.6(4) |
| F3-C71-S1 | 111.6(4) | O2-S1-O1 | 115.4(4) |
| O2-S1-O3 | 114.4(4) | O1-S1-O3 | 115.4(4) |
| O2-S1-C71 | 102.6(3) | O1-S1-C71 | 102.8(3) |
| O3-S1-C71 | 103.6(3) | F1A-C71A-F2A | 107.5(5) |
| F1A-C71A-F3A | 107.1(5) | F2A-C71A-F3A | 107.2(5) |
| F1A-C71A-S1A | 112.0(5) | F2A-C71A-S1A | 111.3(5) |
| F3A-C71A-S1A | 111.4(5) | O2A-S1A-O1A | 115.1(5) |
| O2A-S1A-O3A | 114.5(4) | O1A-S1A-O3A | 115.4(5) |
| O2A-S1A-C71A | 102.8(4) | O1A-S1A-C71A | 102.7(4) |
| O3A-S1A-C71A | 103.9(4) | F4-C72-F5 | 108.2(4) |
| F4-C72-F6 | 107.9(4) | F5-C72-F6 | 107.3(4) |
| F4-C72-S2 | 111.9(4) | F5-C72-S2 | 111.1(4) |
| F6-C72-S2 | 110.3(4) | O4-S2-O5 | 114.6(3) |
| O4-S2-O6 | 115.3(3) | O5-S2-O6 | 114.3(3) |
| O4-S2-C72 | 103.6(3) | O5-S2-C72 | 102.9(3) |
| O6-S2-C72 | 103.9(3) | F4A-C72A-F5A | 107.9(7) |
| F4A-C72A-F6A | 107.8(7) | F5A-C72A-F6A | 107.5(7) |
| F4A-C72A-S2A | 112.4(6) | F5A-C72A-S2A | 111.0(6) |
| F6A-C72A-S2A | 110.0(6) | O4A-S2A-O5A | 114.2(6) |
| O4A-S2A-O6A | 115.2(6) | O5A-S2A-O6A | 114.5(6) |
| O4A-S2A-C72A | 103.4(5) | O5A-S2A-C72A | 103.0(5) |
| O6A-S2A-C72A | 104.4(5) | C37-C36-C35 | 114.1(4) |
| C37-C36-C44 | 125.5(4) | C35-C36-C44 | 120.2(4) |
| C46-C44-C47 | 109.4(5) | C46-C44-C36 | 110.6(4) |
| C47-C44-C36 | 109.3(4) | C46-C44-C45 | 108.2(4) |
| C47-C44-C45 | 110.7(4) | C36-C44-C45 | 108.8(4) |

| | | | |
|---|---|---|---|
| C44-C45-H45A | 109.5 | C44-C45-H45B | 109.5 |
| H45A-C45-H45B | 109.5 | C44-C45-H45C | 109.5 |
| H45A-C45-H45C | 109.5 | H45B-C45-H45C | 109.5 |
| C44-C46-H46A | 109.5 | C44-C46-H46B | 109.5 |
| H46A-C46-H46B | 109.5 | C44-C46-H46C | 109.5 |
| H46A-C46-H46C | 109.5 | H46B-C46-H46C | 109.5 |
| C44-C47-H47A | 109.5 | C44-C47-H47B | 109.5 |
| H47A-C47-H47B | 109.5 | C44-C47-H47C | 109.5 |
| H47A-C47-H47C | 109.5 | H47B-C47-H47C | 109.5 |
| C37-C36A-C35 | 121.9(8) | C37-C36A-C44A | 119.7(11) |
| C35-C36A-C44A | 114.0(8) | C46A-C44A-C47A | 109.4(5) |
| C46A-C44A-C36A | 110.6(4) | C47A-C44A-C36A | 109.2(5) |
| C46A-C44A-C45A | 108.2(4) | C47A-C44A-C45A | 110.6(4) |
| C36A-C44A-C45A | 108.8(5) | C44A-C45A-H45D | 109.5 |
| C44A-C45A-H45E | 109.5 | H45D-C45A-H45E | 109.5 |
| C44A-C45A-H45F | 109.5 | H45D-C45A-H45F | 109.5 |
| H45E-C45A-H45F | 109.5 | C44A-C46A-H46D | 109.5 |
| C44A-C46A-H46E | 109.5 | H46D-C46A-H46E | 109.5 |
| C44A-C46A-H46F | 109.5 | H46D-C46A-H46F | 109.5 |
| H46E-C46A-H46F | 109.5 | C44A-C47A-H47D | 109.5 |
| C44A-C47A-H47E | 109.5 | H47D-C47A-H47E | 109.5 |
| C44A-C47A-H47F | 109.5 | H47D-C47A-H47F | 109.5 |
| H47E-C47A-H47F | 109.5 | | |

## Table 5. Torsion angles (°) for Fe-2

| | | | |
|---|---|---|---|
| C2-N1-C1-N2 | 4.5(3) | C32-N1-C1-N2 | -176.8(3) |
| C2-N1-C1-Fe1 | -170.0(2) | C32-N1-C1-Fe1 | 8.6(4) |
| C9-Fe1-C1-N2 | 28.6(3) | C25-Fe1-C1-N2 | -150.6(3) |
| C33-Fe1-C1-N2 | 120.8(3) | C52-Fe1-C1-N2 | -59.0(3) |
| C9-Fe1-C1-N1 | -158.0(3) | C25-Fe1-C1-N1 | 22.9(3) |
| C33-Fe1-C1-N1 | -65.8(3) | C52-Fe1-C1-N1 | 114.4(3) |
| N1-C1-N2-C7 | -5.1(3) | Fe1-C1-N2-C7 | 169.5(2) |
| N1-C1-N2-C8 | -174.4(3) | Fe1-C1-N2-C8 | 0.1(4) |
| C1-N1-C2-C3 | 173.1(3) | C32-N1-C2-C3 | -5.5(6) |
| C1-N1-C2-C7 | -2.2(4) | C32-N1-C2-C7 | 179.2(3) |
| C7-C2-C3-C4 | -0.3(5) | N1-C2-C3-C4 | -175.0(3) |
| C2-C3-C4-C5 | -0.8(5) | C3-C4-C5-C6 | 0.7(6) |
| C4-C5-C6-C7 | 0.5(5) | C5-C6-C7-C2 | -1.6(5) |
| C5-C6-C7-N2 | 176.2(3) | C3-C2-C7-C6 | 1.6(5) |
| N1-C2-C7-C6 | 177.5(3) | C3-C2-C7-N2 | -176.8(3) |
| N1-C2-C7-N2 | -0.9(3) | C1-N2-C7-C6 | -174.4(4) |
| C8-N2-C7-C6 | -5.1(6) | C1-N2-C7-C2 | 3.7(4) |

| | | | |
|---|---|---|---|
| C8-N2-C7-C2 | 172.9(3) | C1-N2-C8-N3 | -36.5(4) |
| C7-N2-C8-N3 | 155.6(3) | C9-N3-C8-N2 | 35.1(4) |
| C10-N3-C8-N2 | -157.3(3) | C10-N3-C9-N4 | 4.9(3) |
| C8-N3-C9-N4 | 174.0(3) | C10-N3-C9-Fe1 | -166.7(2) |
| C8-N3-C9-Fe1 | 2.4(4) | C15-N4-C9-N3 | -4.7(3) |
| C16-N4-C9-N3 | 175.7(3) | C15-N4-C9-Fe1 | 166.8(2) |
| C16-N4-C9-Fe1 | -12.8(4) | C1-Fe1-C9-N3 | -29.7(3) |
| C17-Fe1-C9-N3 | 149.7(3) | C33-Fe1-C9-N3 | -118.7(3) |
| C52-Fe1-C9-N3 | 56.6(3) | C1-Fe1-C9-N4 | 160.5(3) |
| C17-Fe1-C9-N4 | -20.1(3) | C33-Fe1-C9-N4 | 71.5(3) |
| C52-Fe1-C9-N4 | -113.2(3) | C9-N3-C10-C11 | 174.2(4) |
| C8-N3-C10-C11 | 5.3(6) | C9-N3-C10-C15 | -3.3(4) |
| C8-N3-C10-C15 | -172.3(3) | N3-C10-C11-C12 | -175.4(3) |
| C15-C10-C11-C12 | 1.8(5) | C10-C11-C12-C13 | -1.5(5) |
| C11-C12-C13-C14 | 0.0(6) | C30-C29-C28-C27 | -1.2(6) |
| C29-C28-C27-C26 | 1.5(6) | C28-C27-C26-C31 | -0.4(5) |
| C28-C27-C26-N7 | 176.6(4) | C25-N7-C26-C27 | -174.4(4) |
| C24-N7-C26-C27 | 6.0(6) | C25-N7-C26-C31 | 2.9(4) |
| C24-N7-C26-C31 | -176.7(3) | C26-N7-C25-N8 | -4.7(4) |
| C24-N7-C25-N8 | 174.9(3) | C26-N7-C25-Fe1 | 167.8(2) |
| C24-N7-C25-Fe1 | -12.6(4) | C31-N8-C25-N7 | 4.7(4) |
| C32-N8-C25-N7 | 175.9(3) | C31-N8-C25-Fe1 | -167.9(2) |
| C32-N8-C25-Fe1 | 3.3(4) | C1-Fe1-C25-N7 | 160.5(3) |
| C17-Fe1-C25-N7 | -18.9(3) | C33-Fe1-C25-N7 | -110.5(3) |
| C52-Fe1-C25-N7 | 74.2(3) | C1-Fe1-C25-N8 | -28.6(3) |
| C17-Fe1-C25-N8 | 152.1(3) | C33-Fe1-C25-N8 | 60.5(3) |
| C52-Fe1-C25-N8 | -114.8(3) | C17-N6-C24-N7 | -45.8(4) |
| C23-N6-C24-N7 | 135.9(3) | C25-N7-C24-N6 | 47.8(4) |
| C26-N7-C24-N6 | -132.6(3) | C17-N6-C23-C22 | 177.6(4) |
| C24-N6-C23-C22 | -4.0(6) | C17-N6-C23-C18 | -1.3(4) |
| C24-N6-C23-C18 | 177.2(3) | C18-C23-C22-C21 | 1.5(5) |
| N6-C23-C22-C21 | -177.2(3) | C23-C22-C21-C20 | -0.5(5) |
| C9-N4-C16-N5 | 46.3(4) | C15-N4-C16-N5 | -133.3(3) |
| C17-N5-C16-N4 | -39.4(4) | C18-N5-C16-N4 | 149.3(3) |
| C9-N4-C15-C14 | -173.9(3) | C16-N4-C15-C14 | 5.7(6) |
| C9-N4-C15-C10 | 2.7(3) | C16-N4-C15-C10 | -177.7(3) |
| C11-C10-C15-C14 | -0.4(5) | N3-C10-C15-C14 | 177.4(3) |
| C11-C10-C15-N4 | -177.5(3) | N3-C10-C15-N4 | 0.4(3) |
| C12-C13-C14-C15 | 1.3(5) | N4-C15-C14-C13 | 175.1(3) |
| C10-C15-C14-C13 | -1.1(5) | C18-N5-C17-N6 | -3.7(4) |
| C16-N5-C17-N6 | -176.2(3) | C18-N5-C17-Fe1 | 171.8(2) |
| C16-N5-C17-Fe1 | -0.7(5) | C23-N6-C17-N5 | 3.0(3) |
| C24-N6-C17-N5 | -175.5(3) | C23-N6-C17-Fe1 | -172.5(2) |

|  |  |  |  |
|---|---|---|---|
| C24-N6-C17-Fe1 | 8.9(4) | C9-Fe1-C17-N5 | 26.9(3) |
| C25-Fe1-C17-N5 | -154.0(3) | C33-Fe1-C17-N5 | -65.3(3) |
| C52-Fe1-C17-N5 | 114.4(3) | C9-Fe1-C17-N6 | -158.6(3) |
| C25-Fe1-C17-N6 | 20.5(3) | C33-Fe1-C17-N6 | 109.2(3) |
| C52-Fe1-C17-N6 | -71.0(3) | C17-N5-C18-C19 | -175.9(3) |
| C16-N5-C18-C19 | -3.9(6) | C17-N5-C18-C23 | 3.0(4) |
| C16-N5-C18-C23 | 175.0(3) | C22-C23-C18-C19 | -0.9(5) |
| N6-C23-C18-C19 | 178.1(3) | C22-C23-C18-N5 | -180.0(3) |
| N6-C23-C18-N5 | -1.0(3) | N5-C18-C19-C20 | 178.0(3) |
| C23-C18-C19-C20 | -0.8(5) | C18-C19-C20-C21 | 1.8(5) |
| C22-C21-C20-C19 | -1.2(6) | C43-N10-C33-N9 | -179.8(3) |
| C39-N10-C33-N9 | -0.5(4) | C43-N10-C33-Fe1 | -8.0(5) |
| C39-N10-C33-Fe1 | 171.3(3) | C34-N9-C33-N10 | -178.5(4) |
| C38-N9-C33-N10 | 1.1(4) | C34-N9-C33-Fe1 | 9.6(6) |
| C38-N9-C33-Fe1 | -170.7(3) | C1-N1-C32-N8 | -41.8(4) |
| C2-N1-C32-N8 | 136.7(3) | C25-N8-C32-N1 | 35.4(4) |
| C31-N8-C32-N1 | -154.7(3) | C25-N8-C31-C30 | 175.7(4) |
| C32-N8-C31-C30 | 4.8(6) | C25-N8-C31-C26 | -3.0(4) |
| C32-N8-C31-C26 | -173.9(3) | C27-C26-C31-C30 | -1.2(5) |
| N7-C26-C31-C30 | -178.8(3) | C27-C26-C31-N8 | 177.8(3) |
| N7-C26-C31-N8 | 0.1(4) | C28-C29-C30-C31 | -0.3(6) |
| N8-C31-C30-C29 | -177.1(4) | C26-C31-C30-C29 | 1.4(5) |
| C33-N9-C34-C35 | -176.0(4) | C38-N9-C34-C35 | 4.3(6) |
| N9-C34-C35-C36 | 0.9(8) | N9-C34-C35-C36A | -16.4(9) |
| C34-N9-C38-C39 | 178.3(3) | C33-N9-C38-C39 | -1.4(4) |
| C34-N9-C38-C37 | -3.5(6) | C33-N9-C38-C37 | 176.7(4) |
| C36A-C37-C38-C39 | -164.3(9) | C36-C37-C38-C39 | 175.0(5) |
| C36A-C37-C38-N9 | 18.2(10) | C36-C37-C38-N9 | -2.5(7) |
| N9-C38-C39-C40 | -177.1(4) | C37-C38-C39-C40 | 5.1(8) |
| N9-C38-C39-N10 | 0.9(4) | C37-C38-C39-N10 | -176.9(4) |
| C33-N10-C39-C38 | -0.3(4) | C43-N10-C39-C38 | 179.1(3) |
| C33-N10-C39-C40 | 178.0(3) | C43-N10-C39-C40 | -2.5(5) |
| C38-C39-C40-C41 | 178.4(4) | N10-C39-C40-C41 | 0.6(5) |
| C39-C40-C41-C42 | 1.9(5) | C39-C40-C41-C48 | -175.6(3) |
| C40-C41-C42-C43 | -2.7(5) | C48-C41-C42-C43 | 175.0(3) |
| C41-C42-C43-N10 | 0.8(5) | C33-N10-C43-C42 | -178.9(3) |
| C39-N10-C43-C42 | 1.8(5) | C40-C41-C48-C50 | -2.8(5) |
| C42-C41-C48-C50 | 179.7(3) | C40-C41-C48-C51 | -124.3(4) |
| C42-C41-C48-C51 | 58.2(4) | C40-C41-C48-C49 | 117.2(4) |
| C42-C41-C48-C49 | -60.3(4) | C52-N12-C62-C61 | 174.4(3) |
| C58-N12-C62-C61 | -2.9(5) | N12-C62-C61-C60 | 1.4(5) |
| C62-C61-C60-C59 | 1.5(5) | C62-C61-C60-C67 | 178.8(3) |
| C70-C67-C60-C59 | -124.6(4) | C68-C67-C60-C59 | 115.4(4) |

|  |  |  |  |
|---|---|---|---|
| C69-C67-C60-C59 | -4.8(6) | C70-C67-C60-C61 | 58.3(5) |
| C68-C67-C60-C61 | -61.7(5) | C69-C67-C60-C61 | 178.1(4) |
| C61-C60-C59-C58 | -2.7(5) | C67-C60-C59-C58 | -179.9(4) |
| C62-N12-C58-C57 | 180.0(3) | C52-N12-C58-C57 | 2.2(4) |
| C62-N12-C58-C59 | 1.7(4) | C52-N12-C58-C59 | -176.0(3) |
| C60-C59-C58-C57 | -176.5(4) | C60-C59-C58-N12 | 1.2(5) |
| N12-C58-C57-N11 | 0.2(3) | C59-C58-C57-N11 | 178.2(3) |
| N12-C58-C57-C56 | -176.4(3) | C59-C58-C57-C56 | 1.6(7) |
| C52-N11-C57-C58 | -2.6(4) | C53-N11-C57-C58 | 179.1(3) |
| C52-N11-C57-C56 | 174.5(3) | C53-N11-C57-C56 | -3.8(5) |
| C58-C57-C56-C55 | 175.1(4) | N11-C57-C56-C55 | -1.0(5) |
| C57-C56-C55-C54 | 3.8(5) | C57-C56-C55-C63 | -174.3(3) |
| C65-C63-C55-C56 | -4.6(5) | C64-C63-C55-C56 | -125.8(4) |
| C66-C63-C55-C56 | 114.7(4) | C65-C63-C55-C54 | 177.4(3) |
| C64-C63-C55-C54 | 56.1(4) | C66-C63-C55-C54 | -63.3(4) |
| C56-C55-C54-C53 | -2.0(5) | C63-C55-C54-C53 | 176.2(3) |
| C55-C54-C53-N11 | -2.9(5) | C52-N11-C53-C54 | -172.4(3) |
| C57-N11-C53-C54 | 5.6(5) | C53-N11-C52-N12 | -178.2(3) |
| C57-N11-C52-N12 | 3.7(3) | C53-N11-C52-Fe1 | 17.7(5) |
| C57-N11-C52-Fe1 | -160.4(2) | C62-N12-C52-N11 | 179.0(3) |
| C58-N12-C52-N11 | -3.5(3) | C62-N12-C52-Fe1 | -16.6(5) |
| C58-N12-C52-Fe1 | 160.9(2) | F1-C71-S1-O2 | 59.7(6) |
| F2-C71-S1-O2 | -60.7(6) | F3-C71-S1-O2 | 179.2(7) |
| F1-C71-S1-O1 | 179.8(6) | F2-C71-S1-O1 | 59.5(6) |
| F3-C71-S1-O1 | -60.7(7) | F1-C71-S1-O3 | -59.7(6) |
| F2-C71-S1-O3 | 180.0(6) | F3-C71-S1-O3 | 59.9(7) |
| F1A-C71A-S1A-O2A | 60.3(8) | F2A-C71A-S1A-O2A | -60.1(7) |
| F3A-C71A-S1A-O2A | -179.7(8) | F1A-C71A-S1A-O1A | -179.8(7) |
| F2A-C71A-S1A-O1A | 59.7(7) | F3A-C71A-S1A-O1A | -59.9(8) |
| F1A-C71A-S1A-O3A | -59.3(7) | F2A-C71A-S1A-O3A | -179.8(7) |
| F3A-C71A-S1A-O3A | 60.6(8) | F4-C72-S2-O4 | -178.5(5) |
| F5-C72-S2-O4 | 60.5(5) | F6-C72-S2-O4 | -58.4(5) |
| F4-C72-S2-O5 | -58.9(5) | F5-C72-S2-O5 | -179.9(5) |
| F6-C72-S2-O5 | 61.3(5) | F4-C72-S2-O6 | 60.6(5) |
| F5-C72-S2-O6 | -60.4(5) | F6-C72-S2-O6 | -179.3(4) |
| F4A-C72A-S2A-O4A | 175.6(9) | F5A-C72A-S2A-O4A | 54.7(9) |
| F6A-C72A-S2A-O4A | -64.2(9) | F4A-C72A-S2A-O5A | -65.2(9) |
| F5A-C72A-S2A-O5A | 173.9(9) | F6A-C72A-S2A-O5A | 55.0(9) |
| F4A-C72A-S2A-O6A | 54.8(9) | F5A-C72A-S2A-O6A | -66.2(9) |
| F6A-C72A-S2A-O6A | 174.9(9) | C38-C37-C36-C35 | 7.1(8) |
| C38-C37-C36-C44 | -177.3(5) | C34-C35-C36-C37 | -6.5(8) |
| C34-C35-C36-C44 | 177.6(5) | C37-C36-C44-C46 | -6.0(8) |
| C35-C36-C44-C46 | 169.4(5) | C37-C36-C44-C47 | 114.5(6) |

|  |  |  |  |
|---|---|---|---|
| C35-C36-C44-C47 | -70.2(7) | C37-C36-C44-C45 | -124.6(6) |
| C35-C36-C44-C45 | 50.7(7) | C38-C37-C36A-C35 | -32.7(15) |
| C38-C37-C36A-C44A | 172.1(7) | C34-C35-C36A-C37 | 32.9(15) |
| C34-C35-C36A-C44A | -170.6(6) | C37-C36A-C44A-C46A | 0.1(13) |
| C35-C36A-C44A-C46A | -157.0(10) | C37-C36A-C44A-C47A | 120.5(12) |
| C35-C36A-C44A-C47A | -36.5(10) | C37-C36A-C44A-C45A | -118.6(12) |
| C35-C36A-C44A-C45A | 84.3(10) |  |  |

# References:

[1] A. Hagfeldt, G. Boschloo, L. Sun, L. Kloo, H. Pettersson, *Chem. Rev.*, **2010**, *110*, 6595-6663.

[2] B. E. Hardin, E. T. Hoke, P. B. Armstrong, J.-H. Yum, P. Comte, T. Torres, J. M. J. Fréchet, M. K. Nazeeruddin, M. Grätzel, M. D. McGehee, *Nature Photonics*, **2009**, *3*, 406-411.

[3] H. S. Jung, J.-K. Lee, *J. Phys. Chem. Lett.*, **2013**, *4*, 1682-1693.

[4] M. Beley, P. C. Gros, *Organometallics*, **2014**, *33*, 4590-4606.

[5] J. E. Monat, J. K. McCusker, *J. Am. Chem. Soc.*, **2000**, *122*, 4092-4097.

[6] C. Consani, M. Prémont-Schwarz, A. ElNahhas, C. Bressler, F. van Mourik, A. Cannizzo, M. Chergui, *Angew. Chem. Int. Ed.*, **2009**, *48*, 7184-7187.

[7] E. Jakubikova, D. N. Bowman, *Acc. Chem. Res.*, **2015**, *48*, 1441-1449.

[8] J. K. McCusker, K. N. Walda, R. C. Dunn, J. D. Simon, D. Magde, D. N. Hendrickson, *J. Am. Chem. Soc.*, **1993**, *115*, 298-307.

[9] Y. Liu, P. Persson, V. Sundström, K. Wärnmark, *Acc. Chem. Res.*, **2016**, *49*, 1477-1485.

[10] P. Chábera, K. S. Kjaer, O. Prakash, A. Honarfar, Y. Liu, L. A. Fredin, T. C. B. Harlang, S. Lidin, J. Uhlig, V. Sundström, R. Lomoth, P. Persson, K. Wärnmark, *J. Phys. Chem. Lett.*, **2018**, *9*, 459-463.

[11] Y. Liu, K. S. Kjaer, L. A. Fredin, P. Chábera, T. Harlang, S. E. Canton, S. Lidin, J. Zhang, R. Lomoth, K.-E. Bergquist, P. Persson, K. Wärnmark, V. Sundström, *Chem. Eur. J.*, **2015**, *21*, 3628-3639.

[12] P. Zimmer, L. Burkhardt, A. Friedrich, J. Steube, A. Neuba, R. Schepper, P. Müller, U. Flörke, M. Huber, S. Lochbrunner, M. Bauer, *Inorg. Chem.*, **2017**, *57*, 360-373.

[13] T. Duchanois, L. Liu, M. Pastore, A. Monari, C. Cebrián, Y. Trolez, M. Darari, K. Magra, A. Francés-Monerris, E. Domenichini, M. Beley, X. Assfeld, S. Haacke, P. Gros, *Inorganics*, **2018**, *6*, 63.

[14] M. R. Anneser, S. Haslinger, A. Pöthig, M. Cokoja, J.-M. Basset, F. E. Kühn, *Inorg. Chem.*, **2015**, *54*, 3797-3804.

[15] M. A. Bernd, F. Dyckhoff, B. J. Hofmann, A. D. Böth, J. F. Schlagintweit, J. Oberkofler, R. M. Reich, F. E. Kühn, *J. Catal.*, **2020**, *391*, 548-561.

[16] P. S. Braterman, J. I. Song, R. D. Peacock, *Inorg. Chem.*, **1992**, *31*, 555-559.

[17] R. Field, L. C. Liu, W. Gawelda, C. Lu, R. J. D. Miller, *Chem. Eur. J.*, **2016**, *22*, 5118-5122.

[18] W. Gawelda, A. Cannizzo, V.-T. Pham, F. van Mourik, C. Bressler, M. Chergui, *J. Am. Chem. Soc.*, **2007**, *129*, 8199-8206.

# 3. The Mechanism Study of new visible light catalyzed construction of seven- and eight-membered ring compounds[1]

This Chapter is based on:

Dawen Xu, Han Li, Guangxing Pan, Pan Huang, Oberkofler Jens, Robert M. Reich, Hao Guo,* Fritz E. Kühn.* “Visible light-induced dehydrohalogenative coupling for intramolecular α-alkenylation: A way to build seven- and eight-membered rings” *Org. Lett.*, **2020**, *22*, 4372-4377.

## 3.1 Introduction

Medium sized ring (seven-membered ring to eleven-membered ring) and macrocyclic (12-membered ring and above) compounds are widely found in nature. Early research on medium and macrocyclic compounds mostly originated from the extraction and separation of biological tissues such as terrestrial plants[2], marine organisms, pathogenic fungi and bacteria[3] in nature[4]. Limited by sources and research, the application of such compounds in actual production has been greatly restricted. With the development of chemical science and technology, chemists have been able to purposefully synthesize required medium and macrocyclic compounds under laboratory conditions. This progress has also given such compounds a very wide range of applications in the fields of anticancer drugs[5], antibiotics[6], and pesticides[7], etc.

At present, exploring methods for efficiently constructing such cyclic skeletons remains to be one of the research hotspots in the field of macrocyclic compounds. Commonly used classical methods can be simply classified as: acid catalysis[8], base catalysis[9], free radical cyclization[10], transition metal catalysis[11], and cycloaddition expansion[12], etc[13]. With the widespread application of visible light catalysis in the field of organic synthesis in recent years, scientists have also tried to simulate the natural "photosynthesis" reactions, using photocyclization reactions to synthesize various cyclic compounds under laboratory conditions. Among all of these reactions developed, one of the most classic ones is the

[2+2]-photocycloaddition reaction[14].

Chemists have synthesized a variety of cyclic compounds covering small ring, medium sized ring, and macrocyclic skeletons with [2+2]-photocycloaddition, which have played an important role in bio-medicine and other fields[15]. However, while providing a new method for the construction of cyclic compounds, this method also has certain limitations. From a theoretical point of view, the classical [2+2]-halocyclization reaction can only obtain a cyclic skeleton of four-parallel X-membered ring. Such compounds are not as widely used as other cyclic compounds due to the steric distortion of the 4-membered ring. Moreover, the single-ring skeleton compounds are also the most existed cyclic compound. Therefore, in total synthetic chemistry, what is needed is the method that can efficiently construct independent medium and macrocycles.

Life in nature should be based on various basic chemical reactions to gradually synthesize a variety of complex central and macrocyclic natural products. Perhaps, the [2+2]-photocyclization reaction that chemists are currently familiar with is the basis for the further synthesis of more complex ring system natural products.

Since the four-membered ring is relatively easy to open, if the stable ring opening of the four-parallel X-membered ring under mild conditions can be achieved, the [2+2]-photocyclization reaction can be used to effectively synthesize a series of single Cyclic compound. However, due to the conditions required for the cycloaddition and ring-opening reaction are different, how to find a suitable condition to achieve tandem [2+2]-photocycloaddition and retro-[2+2]-photocycloaddition is very challenging.

## 3.2 Scope of Substrate

In our previous work, a photocatalytic intramolecular [2+2]-photocycloaddition has been discovered, following subsequent open-ring reaction, yielding a series of medium sized ring compounds (seven-membered ring and eight-membered ring) with good to excellent yields (**Scheme 1**).

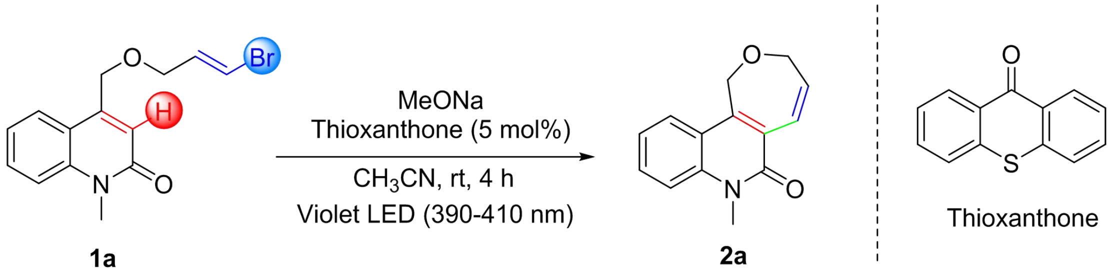

**Scheme 1**: Photocatalytic intramolecular [2+2]-photocycloaddition

In this work, the reaction conditions were optimized and the optimal reaction conditions were obtained as: 1.2 equivalent of sodium methoxide as additive, acetonitrile as the solvent, 5 mol% thioxanthone as photocatalyst, under violet LED (390-410 nm) and room temperature.

With this optimized reaction conditions at hand, the research on the scope of the substrates was conducted. A series of substrates with different functional groups at different positions were studied. The results of the experiment show that this reaction has a very good universality.

1. Quinolinone skeleton substrates showed excellent tolerance to various functional group substituents, including phenyl, perfluorophenyl, trifluoromethyl, methoxy carbonyl, cyano, nitro, and carbonyl. The reaction can obtain the corresponding 7-membered ring compound **2a-2h** with excellent yield (**Scheme 2**).

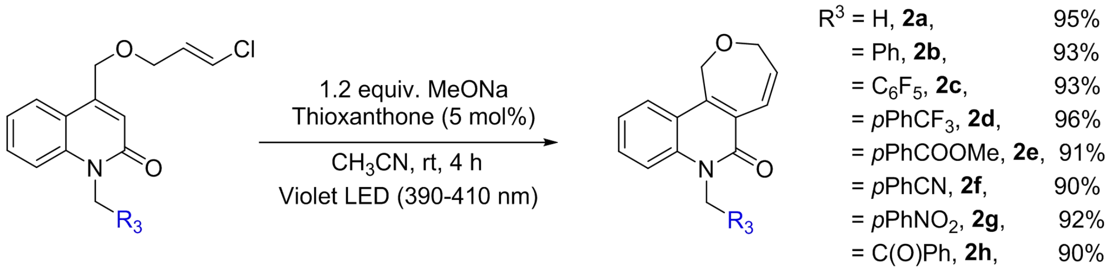

**Scheme 2**: Scope of substrate with quinolinone skeleton

2. Whether there are heteroatoms on the side chain connected by quinolinone skeleton has no obvious influence on the reaction. The reaction can still obtain the corresponding medium sized ring compound(**2i-2l**) with good yields (**Scheme 3**).

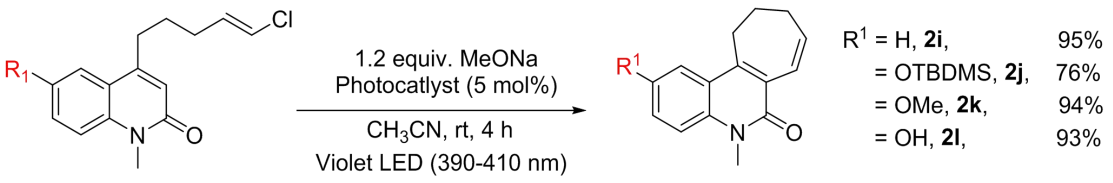

**Scheme 3**: Scope of substrate with substitution on side of quinolinone

3. This reaction also has good general applicability to coconut skeleton substrates. Although the reaction proceeds with relatively low efficiency, the product (**2m-2o**) can still be obtained in good yield (**Scheme 4**).

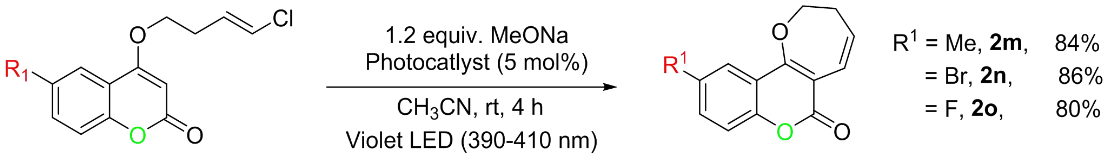

**Scheme 4:** Scope of Substrate with coconut skeleton

At the beginning, the following possible reaction mechanism was proposed (**Scheme 5**).

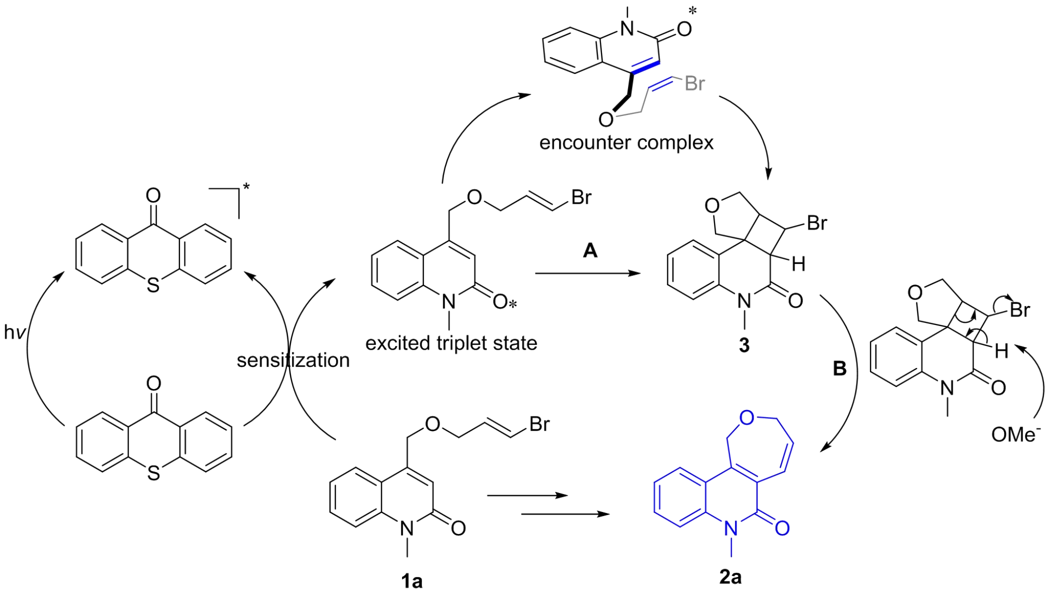

**Scheme 5**: Early proposed possible Mechanism

In order to better understand this reaction, a more in-depth study and exploration of this reaction mechanism have been carried out.

## 3.3 Exploration of mechanism

### 3.3.1 Control experiments of 1a

The reaction substrate **1a** was taken as the research object under standard conditions (**Scheme 6**). Starting from our design concept for this reaction, the sequence of the reaction should be to first carry out intramolecular cycloaddition to form a 4-5-membered ring compound, and then further open the ring to form the corresponding seven-membered ring compound **2a**. So the presence of reaction intermediate **3a** should be able to observed in the reaction. As expected, the intermediate **3a** has been successfully observed and isolated. Furthermore, the role of the factors of standard conditions in the production of intermediate **3a** has been explored. The results show that both light and catalyst are necessary conditions for this step, indicating that this is a standard photocatalytic [2+2] cyclization reaction. The intermediate **3a** can be isolated in the presence of base, but when there is no base, **3a** is obtained as main product of the control reaction. This result shows that the presence of base is not a necessary condition for the first half of the reaction. Therefore, a conclusion can be achieved that compound **3a** (all in the form of **rac-3a**) is indeed the intermediate of the reaction.

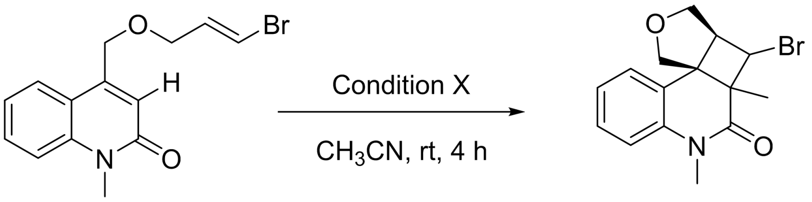

**1a** *rac*-**3a**

| ConditionX | hν | Thioxanthone | Base | Product **3a** |
|---|---|---|---|---|
| **A** $_1$ | ✓ | ✓ | ✓ | ✓ |
| **B** $_2$ | ✓ | ✓ | × | ✓ |
| **C** $_3$ | ✓ | × | ✓ | × |
| **D** $_4$ | × | ✓ | ✓ | × |

**Scheme 6**: Control experiment with *rac*-**3a** as target product

### 3.3.2 [2+2] Photocyclization reaction

The [2+2] photocyclization part of the reaction has been studied, which is also the formation method of **rac-3a**. According to the "rule of five"[16], the intramolecular [2+2]-photocycloaddition proceeds through a chair transition configuration. With this transition state reaction, we can not only obtain seven-membered compounds, but also smoothly produce the eight-membered ring product with 1*Z*, 3*Z*-configuration is obtained at a high rate. It is worth pointing out that， for ((3-bromoallyl)oxy)methyl substituted substrate, *cis*- intermediate product **3** will be obtained as the only configuration due to the structure of this transition state ， resulting in *cis*- 7 member ring product **2**. While for ((4-bromobut-3-en-1-yl)oxy)methyl substituted reactants, a mixture of *trans*- and *cis*- mid product **3** will be produced, which will further epimerize to the *cis*-product **3** completely under base, further corresponding *cis* 8 member ring product **2** (**Scheme 7**).

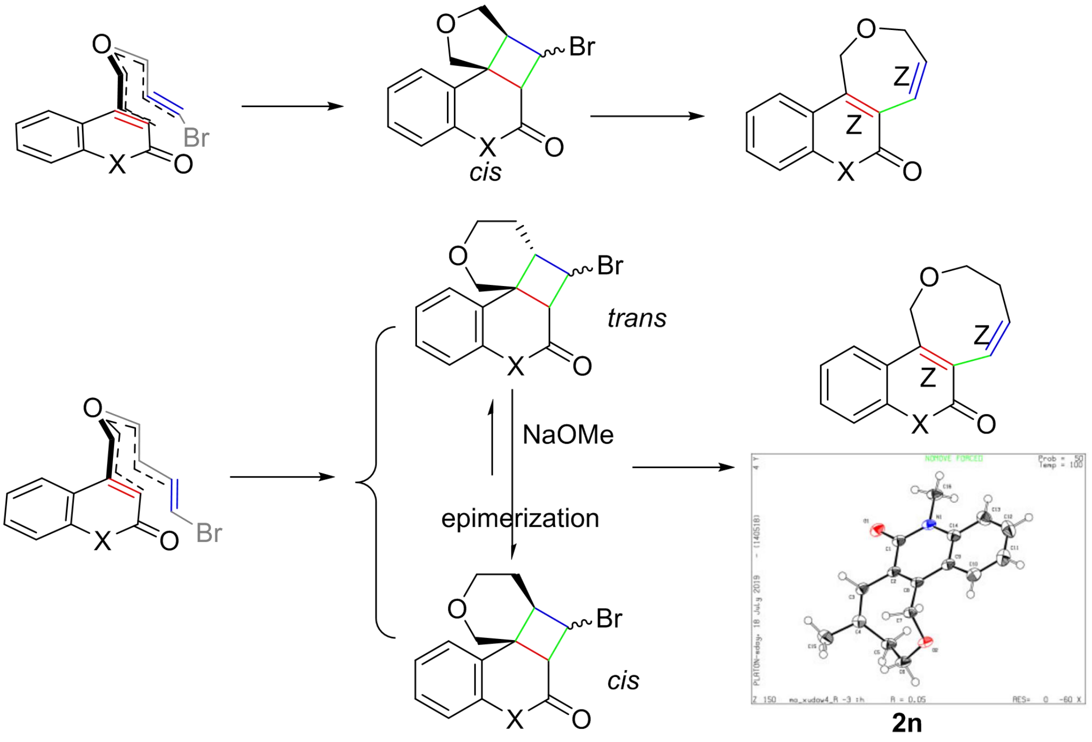

**Scheme 7**: [2+2] Photocyclization following "rule of five[17]"

According to this theory, compounds with 9-membered rings and above cannot be synthesized through this reaction, because the two double bond reaction sites cannot match. In fact, **1s** and **1t** have been synthesized to verify this conjecture. As expected, the corresponding nine-membered ring and ten-membered compound can not be obtained. The reaction did not get any intermediates, only the starting materials were recovered, because the reaction was terminated in the first step - [2+2] photocyclization addition (**Scheme 8**).

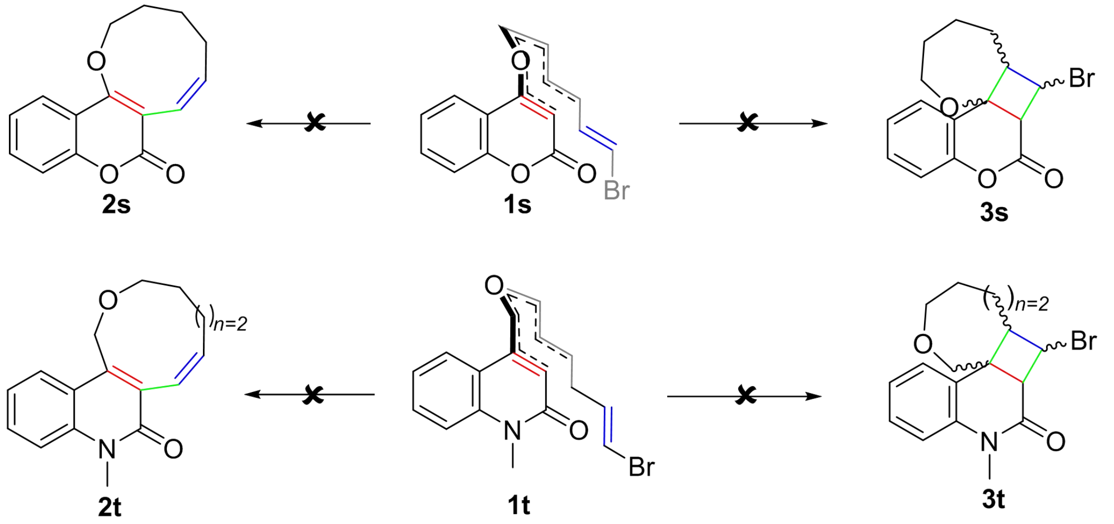

**Scheme 8**: Illustration for the failure of synthesis of 9- and 10- membered ring compound

### 3.3.3 Control experiments of intermediate *rac*-3a

After studying the first half of the reaction, ***rac*-3a** was taken as the substrate to conduct a controlled experiment to further study the reaction (**Scheme 9**). The results show that ***rac*-3a** can successfully obtain our target compound **2a** with excellent yield under standard conditions. However, product **2a** cannot be obtained in the absence of any of the three conditions among light, photocatalyst thioxanthone and MeONa. This not only verifies that the base plays an indispensable role in the conversion of ***rac*-3a** to the final product **2a**. On the other hand, the ring-opening reaction of ***rac*-3a** is a photoreaction.

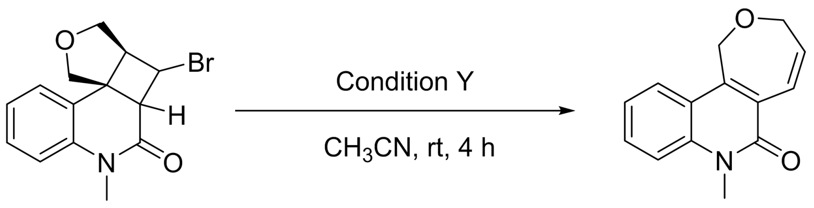

*rac*-**3a**

**2a**

| ConditionY | hν | Thioxanthone | Base | Product **2a** |
|---|---|---|---|---|
| $\mathbf{A}_2$ | ✓ | ✓ | ✓ | ✓ |
| $\mathbf{B}_2$ | ✓ | ✓ | × | × |
| $\mathbf{C}_2$ | ✓ | × | ✓ | × |
| $\mathbf{D}_2$ | × | ✓ | ✓ | × |

**Scheme 9**: Control experiment of *rac*-**3a**

By now, the conclusion can be drawn that the entire process from reactant **1a** to substrate **2a** requires the participation of light and optical catalyst, indicating that the entire reaction is a photochemical reaction. ***rac*-3a** is an intermediate in this reaction. The presence of alkali has no obvious effect on the first half of the reaction, but it is a necessary reaction condition for ring opening in the second half.

This discovery makes us have to re-examine the possible mechanism process we proposed at the beginning. Because in our initial understanding of the reaction, the ring-opening reaction of ***rac*-3a** should be a pure base-induced ring-opening reaction, not a photoreaction process. In addition, when studying the effect of the leaving group of the reaction substrate on the reaction, different halogens show a very obviously different effect on the efficiency of the reaction. When the substituent is bromine or iodine(**1a,1q**), the reaction can obtain the corresponding seven-membered ring compound with excellent yield. However, when the substituent is chlorine(**1p**), the yield of the reaction drops sharply to only 25%. This result indicates that the leaving effect of the leaving group has an extremely important influence on the reaction process. However, the proposed mechanism previously proposed could not perfectly explain this huge influence (**Scheme 10**).

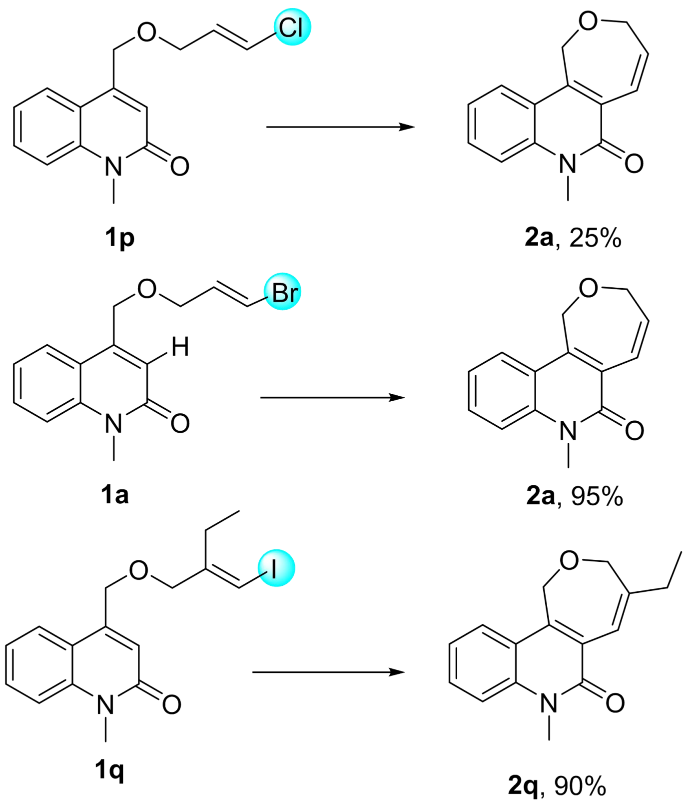

**Scheme 10**: Effect of different halogens on the reaction

Various signs indicate that the ring-opening reaction process of ***rac*-3a** is a light-induced, base-involved photoreaction, which is different from our assumption. Thus a more in-depth exploration of the mechanism of the reaction was performed. Taking the reaction intermediate ***rac*-3a** as the research object, the two diastereomers of ***rac*-3a, *rac*-3a-1** and ***rac*-3a-2** were successfully separated and characterized. In the following research, the two isomers were utilized as reaction substrates to conduct a more detailed control reaction study.

### 3.3.4 Control experiments of intermediate *rac*-4a

To our delight, another key intermediate ***rac*-4a** of the reaction was successfully isolated with 99% isolation yield when there is only base existed. This fully shows that the reaction process from ***rac*-3a** ring opening to the final product **2a** is not a one-step reaction as envisaged, but a step-by-step reaction. That is, the intramolecular elimination reaction is firstly carried out by ***rac*-3a** under the induction of base to produce intermediate ***rac*-4a**, and then a photocatalytic retro- [2+2] cyclization reaction is carried out by ***rac*-4a** to produce the final 7-membered ring product **2a** (**Scheme 11**). The existence of this elimination reaction can also explain the huge influence of different halogens on the reaction process. In addition, the existence of ***rac*-4a** also provides an explanation for the subsequent light reaction. Because the generated double bond and the carbonyl group on the quinoline are conjugated, in this case, the carbonyl group can effectively transfer energy to the double bond after being excited by the photocatalyst.

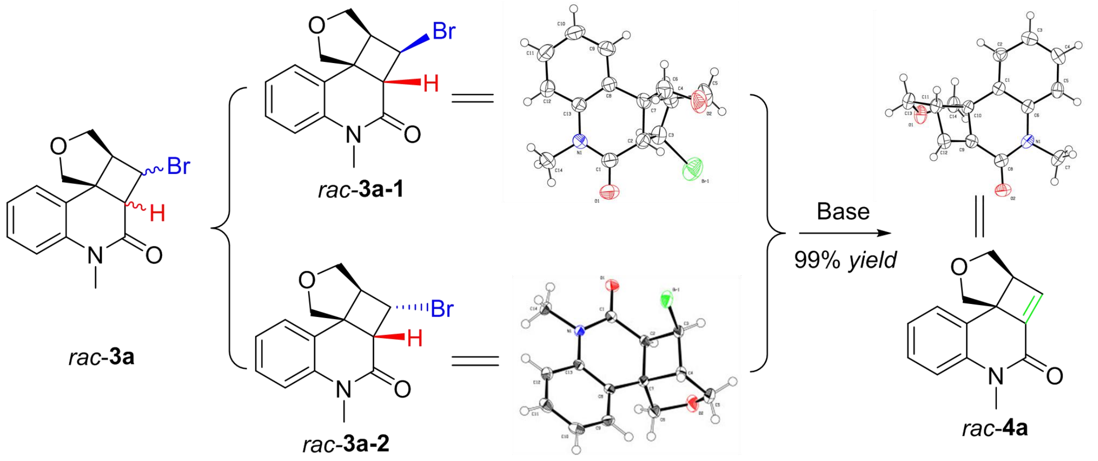

**Scheme 11**: Formation of intermediate *rac*-**4a**

Therefore, ***rac*-4a** was once again used as the reaction substrate to conduct controlled experiments, trying to figure out the reaction conditions required for the final product **2a** from the ***rac*-4a** reaction (**Scheme 12**). The results show that ***rac*-4a** can successfully produce the final product **2a** with a 95% yield under standard conditions, which demonstrates that ***rac*-4a** is indeed an intermediate in the reaction. In addition, the presence or absence of base does not affect the direction and efficiency of the reaction. Both light and photocatalyst are indispensable in the reaction. Apparently, this step is a visible light-induced retro [2+2]-photocycloaddition, and every factor at this step appears to be clear. As a cyclic olefin compound, the space twisting tension of ***rac*-4a** will further increase, which also constitutes one of its driving forces for further ring opening. After being sensitized by the photocatalyst, the carbonyl group of ***rac*-4a** can transfer energy to the double bond conjugated to it. This energy is also the main driving force and energy source for the ring-opening reaction of ***rac*-4a**.

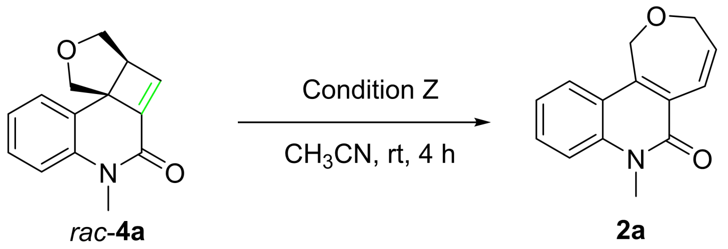

| ConditionZ | hν | Thioxanthone | Base | Product **2a** |
|---|---|---|---|---|
| **A** $_3$ | ✓ | ✓ | ✓ | 95% |
| **B** $_3$ | ✓ | ✓ | × | 95% |
| **C** $_3$ | ✓ | × | ✓ | × |
| **D** $_3$ | × | ✓ | ✓ | × |

**Scheme 12**: Control experiments of *rac*-**4a**

In addition, all seven-membered ring products are (1*Z*,3*Z*)-1,3-diene compounds. In terms of mechanism, photochemically allowed disrotation would give (1*Z*,3*Z*)-1,3-dienes, while the thermochemical conrotation process would afford (1*Z*,3*E*)-1,3-dienes[18]. Moreover, these two configurations cannot be easily converted to each other at room temperature (**Scheme 13**). This only option of the open-ring products **2** is another proof for the conclusion that this step is a visible light-induced retro [2+2] photocycloaddition reaction.

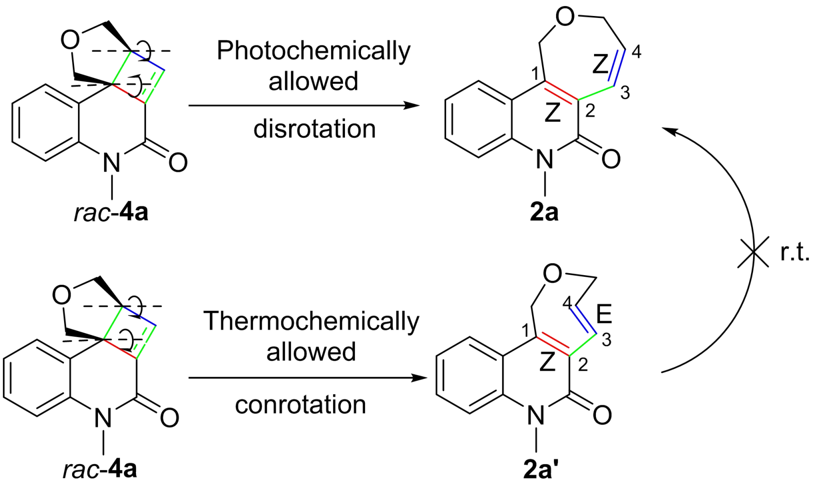

Disrotatory and conrotatory ring-opening of *rac*-**4a**

**Scheme 13**: Disrotatory and conrotatory ring-opening of *rac*-**4a**

To further verify the existence of the elimination step in the reaction, **1u** without bromine atom in the alkene chain and **1v** with bromine atom at the inner position of alkene moiety were synthesized and reacted under standard condition. In theory, the presence of bromine atom and the position does not affect the progress of the photocatalyzed [2+2] cycloaddition reaction, but it will stop at the elimination step due to the absence of the leaving group. The final result is as expected, the [2+2]-photocycloaddition product ***rac*-3u** or ***rac*-3v** was obtained respectively under standard condition, but further intermediate elimination product **4** and final seven-membered ring product **2** was not detected (**Scheme 14**).

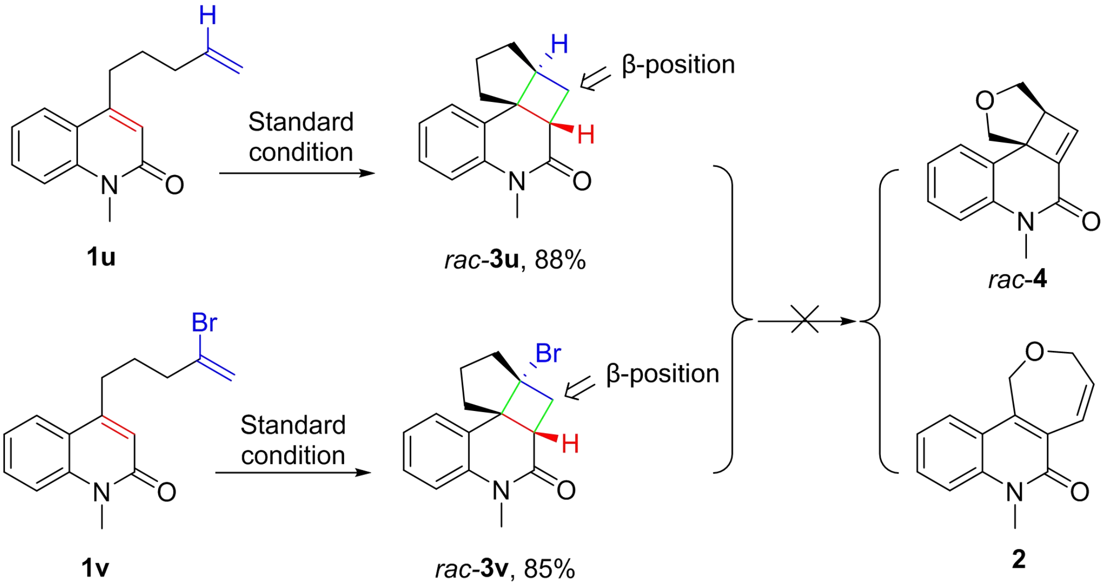

**Scheme 14**: Reaction of **1u** and **1v** under standard condition

## 3.4 Proposed Mechanism

Hence, all the key intermediates have been figured out, and every step of this reaction appears to be clear. The possible mechanism of the reaction was proposed as follows (**Scheme 15**):

### 1. [2+2]-Photocycloaddition of 1a

Upon irradiated under visible light, the photosensitizer thioxanthone is excited and sensitizes **1a** to excited triplet state **1a*** subsequently[19]. **1a*** undergos [2+2]-photocycloaddition and yields the brominated cyclobutane intermediates *rac*-**3a**.

### 2. Elimination of rac-3a

With the acidic α-H of the carbonyl moiety and leaving group at β-position, *rac*-**3a** is able to conduct the elimination of HBr with the function of NaOMe, resulting in cyclobutene intermediate *rac*-**4a**.

### 3. Retro [2+2]-photocycloaddition

*rac*-**4a** is further sensitized into the excited triplet state *rac*-**4a*** by irradiated thioxanthone. Driven by the space distortion strain of the cyclobutene structure, *rac*-**4a*** undergoes a photochemically retro [2+2]-photocycloaddition with exclusive (1*Z*, 3*Z*)-1,3-diene selectivity, yielding the final dehydrohalogenative coupling product **2a**.

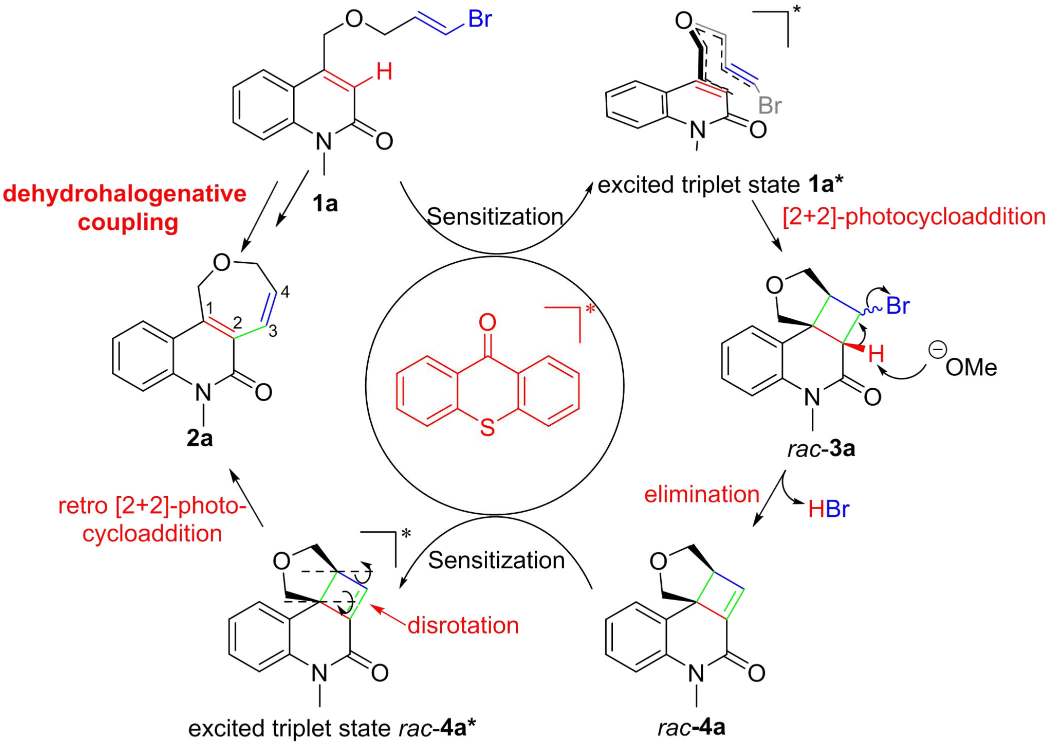

**Scheme 15**: Proposed possible Mechanism

## 3.5 Conclusion

A visible light-induced reaction to synthesize a series of mid-ring compounds has been discovered and studied. All products are obtained with good to excellent yields under mild condition by cascading [2+2]-photocycloaddition and retro- [2+2]-photocycloaddition. The mechanism has been studied in detail and in depth, and two key intermediates in the reaction have been discovered and isolated. A deep understanding of every factor in the reaction has been formed through step-by-step control experiments with starting materials and intermediates. A series of compounds and experiments have been specially designed for mutual verification, and finally a possible mechanism of the reaction was proposed. It is worth pointing out that this reaction provides a new strategy and method for the synthesis of mid-ring compounds. We also expect that this method can be expanded and more widely used.

# 3.6 Experimental Section

## 3.5.1 General experimental methods

$^1$H (400 MHz) and $^{13}$C (100 MHz) NMR spectrum were acquired on a Bruker Avance Ultrashield 400 MHz and Bruker DPX 400 MHz spectrometer. Anhydrous solvents were obtained from a M. Braun SPS purification system.

## 3.5.2 Synthesis

**Synthesis of *E*-4-(((3-bromoallyl)oxy)methyl)quinolin-2(1*H*)-one**

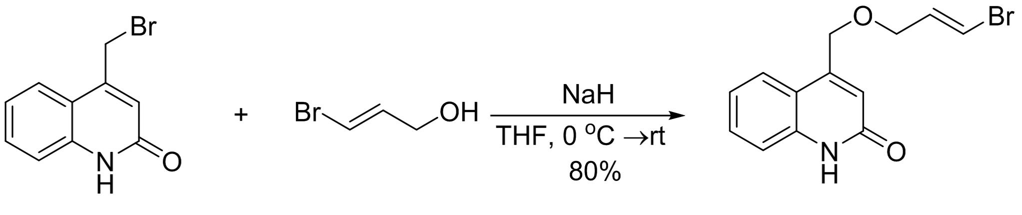

*E*-3-bromoprop-2-en-1-ol (164 mg, 1.2 mmol) and anhydrous THF (10 mL) were added into a 50 ml schlenk flask. NaH (48 mg, 2 mmol) was added after the mixture was stirred under 0 °C for 10 min. After stirring under 0 °C for 2 h, 4-(bromomethyl)quinolin-2(1*H*)-one (238 mg, 1 mmol) was added under Argon and further stirred overnight. Cool the mixture to 0 °C and add

1 N HCl (10 mL). The solvent was removed under vacuum and the residue was filtered. The crude product was washed with water (10 mL × 3), and dried under vacuum, affording *E*-4-(((3-bromoallyl)oxy)methyl)quinolin-2(1*H*)-one as a solid (234 mg, 80%). Mp: 217.3-218.1 °C (*n*-hexane/ethyl acetate). $^1$H NMR (400 MHz, DMSO-$d_6$) δ 11.71 (s, 1H, N-H), 7.66 (d, *J* = 7.7 Hz, 1H, Ar-H), 7.50 (t, *J* = 8.2 Hz, 1H, Ar-H), 7.32 (d, *J* = 8.1 Hz, 1H, Ar-H), 7.18 (t, *J* = 7.6 Hz, 1H, Ar-H), 6.67 (d, *J* = 13.6 Hz, 1H, Alkene-H), 6.54-6.36 (m, 2H, Alkene-H), 4.75 (s, 2H, Alkane-H), 4.09 (dd, *J* = 6.1, 1.3 Hz, 2H, Alkane-H). $^{13}$C NMR (101 MHz, DMSO-$d_6$) δ 162.0, 147.6, 139.3, 134.8, 130.8, 124.6, 122.2, 119.5, 117.8, 116.0, 109.7, 70.1, 68.4. IR (neat) 3062, 1646, 1613, 1556, 1513, 1439 cm$^{-1}$. HRMS (ESI): calcd for $C_{13}H_{13}BrNO_2^+$ [M+H]$^+$: 294.0124, found: 294.0124

**E-4-(((3-bromoallyl)oxy)methyl)-1-(4-(trifluoromethyl)benzyl)quinolin-2(1*H*)-one (1d)**

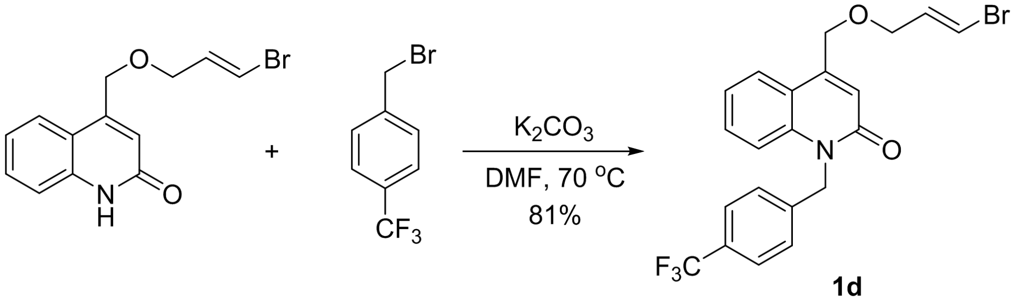

The reaction of *E*-4-(((3-bromoallyl)oxy)methyl)quinolin-2(1*H*)-one (441 mg, 1.5 mmol), 1-(bromomethyl)-4-(trifluoromethyl)benzene (718 mg, 3 mmol), $K_2CO_3$ (621 mg, 4.5 mmol), and DMF (15 mL) under standard conditions affords **1d** as a solid (547 mg, 81%). Mp: 91.1-92.2 °C (*n*-hexane/ethyl acetate). $^1$H NMR (400 MHz, Chloroform-*d*) δ 7.71 (d, *J* = 7.8 Hz, 1H), 7.56 (d, *J* = 8.1 Hz, 2H), 7.45 (t, *J* = 7.8 Hz, 1H), 7.32 (d, *J* = 8.0 Hz, 2H), 7.25-7.16 (m, 2H), 6.91 (s, 1H), 6.46 (d, *J* = 13.6 Hz, 1H), 6.36 (dt, *J* = 13.6, 6.0 Hz, 1H), 5.61 (s, 2H), 4.78 (s, 2H), 4.12 (d, *J* = 5.7 Hz, 2H). $^{13}$C NMR (101 MHz, Chloroform-*d*) δ 162.0, 146.0, 140.5, 139.2, 133.3, 130.8, 129.5, 126.9, 125.9, 125.87, 125.83, 125.80, 124.8, 122.5, 119.7, 119.4, 115.2, 109.3, 70.5, 68.8, 45.5. IR (neat) 1729, 1649, 1593, 1454, 1419 cm$^{-1}$. HRMS (ESI): calcd for $C_{21}H_{18}BrF_3NO_2^+$ [M+H]$^+$: 452.0468, found: 452.0467.

**E-4-(((3-bromoallyl)oxy)methyl)-1-(4-methoxycarbonylbenzyl)quinolin-2(1*H*)-one (1e)**

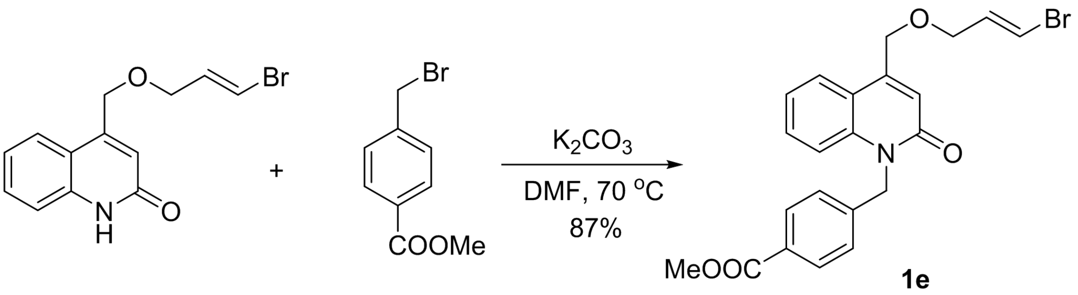

The reaction of *E*-4-(((3-bromoallyl)oxy)methyl)quinolin-2(1*H*)-one (450 mg, 1.5 mmol), methyl 4-(bromomethyl)benzoate (687 mg, 3 mmol), $K_2CO_3$ (621 mg, 4.5 mmol), and DMF (15 mL) under standard conditions affords **1e** as a solid (576 mg, 87%). Mp: 137.5-138.9 °C (*n*-hexane/ethyl acetate). $^1$H NMR (400 MHz, Chloroform-*d*) δ 7.97 (d, $J$ = 8.2 Hz, 2H), 7.70 (d, $J$ = 8.0 Hz, 1H), 7.42 (t, $J$ = 7.8 Hz, 1H), 7.28-7.16 (m, 2H), 7.24-7.15 (m, 2H), 6.92 (s, 1H), 6.46 (d, $J$ = 13.6 Hz, 1H), 6.36 (dt, $J$ = 13.6, 5.6 Hz, 1H), 5.61 (s, 2H), 4.77 (s, 2H), 4.12 (d, $J$ = 5.8 Hz, 2H), 3.88 (s, 3H). $^{13}$C NMR (101 MHz, Chloroform-*d*) δ 166.7, 162.1, 145.9, 141.6, 139.2, 133.4, 130.8, 130.2, 129.3, 126.5, 124.7, 122.4, 119.7, 119.4, 115.3, 109.3, 70.5, 68.8, 52.1, 45.7. IR (neat) 1707, 1651, 1593, 1457, 1434, 1425 cm$^{-1}$. HRMS (ESI): calcd for $C_{22}H_{21}BrNO_4^+$ [M+H]$^+$: 442.0648, found: 442.0648

**_E_-4-(((3-bromoallyl)oxy)methyl)-1-(4-cyanobenzyl)quinolin-2(1_H_)-one (1f)**

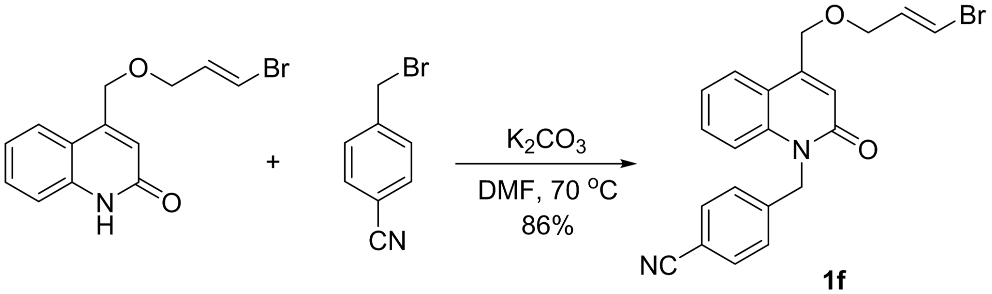

The reaction of *E*-4-(((3-bromoallyl)oxy)methyl)quinolin-2(1*H*)-one (445 mg, 1.5 mmol), 4-(bromomethyl)benzonitrile (580 mg, 3 mmol), $K_2CO_3$ (621 mg, 4.5 mmol), and DMF (15 mL) under standard conditions gives **1f** as a solid (526 mg, 86%). Mp: 130.9-132.0 °C (*n*-hexane/ethyl acetate). $^1$H NMR (400 MHz, Chloroform-*d*) δ 7.71 (d, $J$ = 8.0 Hz, 1H), 7.59 (d, $J$ = 8.2 Hz, 2H), 7.45 (t, $J$ = 7.8 Hz, 1H), 7.31 (d, $J$ = 8.1 Hz, 2H), 7.26-7.21 (m, 1H), 7.13 (d, $J$ = 8.6 Hz, 1H), 6.91 (s, 1H), 6.45 (d, $J$ = 13.6 Hz, 1H), 6.36 (dt, $J$ = 13.6, 6.0 Hz, 1H), 5.60 (s, 2H), 4.77 (s, 2H), 4.12 (d, *J* = 5.7 Hz, 2H). $^{13}$C NMR (101 MHz, Chloroform-*d*) δ 161.9, 146.1, 141.9, 139.0, 133.3, 132.6, 130.9, 127.3, 124.9, 122.6, 119.5, 119.4, 118.5, 114.9, 111.4, 109.3, 70.5, 68.7, 45.5. IR (neat) 2226, 1651, 1591, 1458, 1432, 1413 cm$^{-1}$. HRMS (ESI): calcd for $C_{21}H_{18}BrN_2O_2^+$ [M+H]$^+$: 409.0546, found: 409.0546.

### *E*-4-(((3-bromoallyl)oxy)methyl)-1-(4-nitrobenzyl)quinolin-2(1*H*)-one (1g)

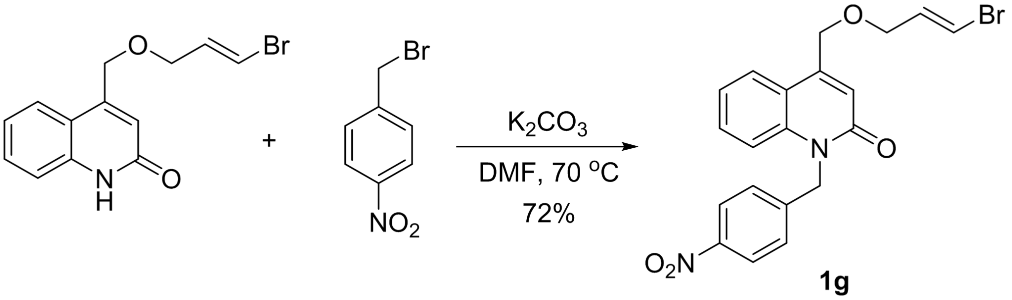

The reaction of *E*-4-(((3-bromoallyl)oxy)methyl)quinolin-2(1*H*)-one (294 mg, 1 mmol), 1-(bromomethyl)-4-nitrobenzene (259 mg, 1.2 mmol), $K_2CO_3$ (621 mg, 4.5 mmol), and DMF (15 mL) under standard conditions affords **1g** as a solid (309 mg, 72%). Mp: 165.9-166.7 °C (*n*-hexane/ethyl acetate). $^1$H NMR (400 MHz, Chloroform-*d*) δ 8.16 (d, *J* = 8.6 Hz, 2H), 7.72 (d, *J* = 8.0 Hz, 1H), 7.45 (t, *J* = 7.8 Hz, 1H), 7.37 (d, *J* = 8.6 Hz, 2H), 7.26-7.21 (m, 1H), 7.14 (d, *J* = 8.5 Hz, 1H), 6.92 (s, 1H), 6.46 (d, *J* = 13.6 Hz, 1H), 6.36 (dt, *J* = 13.6, 6.0 Hz, 1H), 5.65 (s, 2H), 4.78 (s, 2H), 4.13 (d, *J* = 5.7 Hz, 2H). $^{13}$C NMR (101 MHz, Chloroform-*d*) δ 161.9, 147.3, 146.2, 143.9, 139.0, 133.3, 130.9, 127.4, 124.9, 124.1, 122.6, 119.5, 119.4, 114.9, 109.3, 70.5, 68.7, 45.4. IR (neat) 1648, 1590, 1515, 1458, 1440, 1417 cm$^{-1}$. HRMS (ESI): calcd for $C_{20}H_{18}BrN_2O_4^+$ [M+H]$^+$: 429.0444, found: 429.0444.

### *E*-4-(((3-bromoallyl)oxy)methyl)-1-(2-oxo-2-phenylethyl)quinolin-2(1*H*)-one (1h)

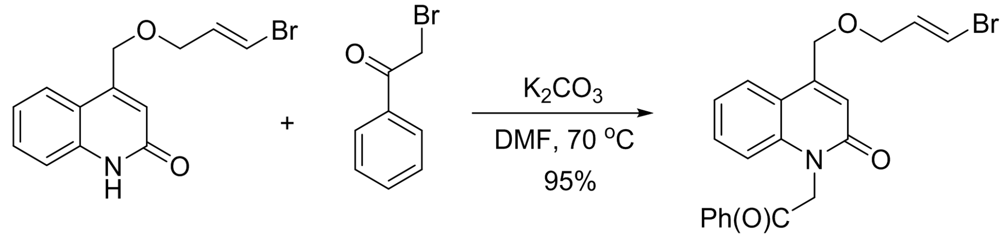

**1h**

The reaction of *E*-4-(((3-bromoallyl)oxy)methyl)quinolin-2(1*H*)-one (294 mg, 1 mmol), 2-bromo-1-phenylethan-1-one (256 mg, 1.2 mmol), $K_2CO_3$ (276 mg, 2 mmol), and DMF (10 mL) under standard conditions affords **1h** as a solid (390 mg, 95%). Mp: 173.5-174.6 °C (*n*-hexane/ethyl acetate). $^1$H NMR (400 MHz, Chloroform-*d*) δ 8.09 (d, *J* = 7.1 Hz, 2H), 7.71 (dd, *J* = 8.1, 1.5 Hz, 1H), 7.66 (t, *J* = 7.4 Hz, 1H), 7.54 (t, *J* = 7.7 Hz, 2H), 7.46 (t, *J* = 7.1 Hz, 1H), 7.23 (t, *J* = 7.1 Hz, 1H), 7.00 (d, *J* = 8.0 Hz, 1H), 6.87 (s, 1H), 6.44 (dt, *J* = 13.6, 1.2 Hz, 1H), 6.34 (dt, *J* = 13.6, 5.6 Hz, 1H), 5.82 (s, 2H), 4.77 (s, 2H), 4.10 (dd, *J* = 5.7, 1.3 Hz, 2H). $^{13}$C NMR (101 MHz, Chloroform-*d*) δ 192.3, 146.0, 139.4, 134.8, 134.0, 133.4, 130.7, 128.9, 128.1, 124.6, 122.3, 119.1, 114.5, 109.1, 70.3, 68.7, 48.6. IR (neat) 1690, 1653, 1595, 1449, 1424 cm$^{-1}$. HRMS (ESI): calcd for $C_{21}H_{19}BrNO_3^+$ [M+H]$^+$: 412.0543, found: 412.0543.

### *E*-4-((6-bromohex-5-en-1-yl)oxy)-2*H*-chromen-2-one (1s)

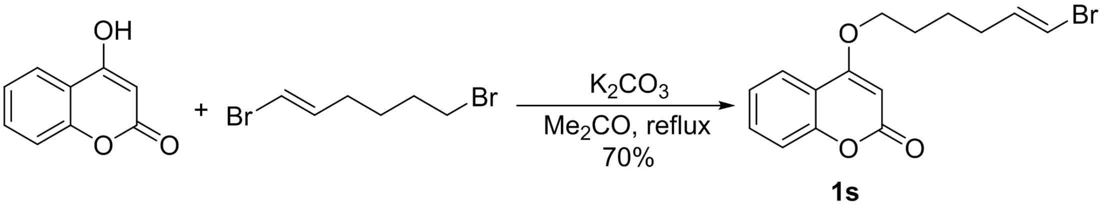

4-hydroxy-2*H*-chromen-2-one (160 mg, 1 mmol), *E*-1,6-dibromohex-1-ene (290 mg, 1.2 mmol), $K_2CO_3$ (417 mg, 3 mmol), and anhydrous acetone (10 mL) are reacted under standard conditions to give **1s** as a solid (226 mg, 70%). $^1$H NMR (500 MHz, Chloroform-*d*) δ 7.81 (dd, *J* = 7.9, 1.6 Hz, 1H), 7.55 (ddd, *J* = 8.7, 7.3, 1.6 Hz, 1H), 7.32 (d, *J* = 8.4 Hz, 1H), 7.30-7.26 (m, 1H), 6.20 (dt, *J* = 10.8, 5.6 Hz, 1H), 6.10 (dt, *J* = 10.8 Hz, 1.2 Hz, 1H), 5.66 (s, 1H), 4.13 (t, *J* = 6.2 Hz, 2H), 2.17 (qd, *J* = 7.3, 1.3 Hz, 2H), 1.99-1.89 (m, 2H), 1.71-1.60 (m, 2H). $^{13}$C NMR (126 MHz, Chloroform-*d*) δ 164.5, 161.9, 152.3, 136.1, 131.3, 122.8, 121.9, 115.7, 114.7, 104.1, 89.4, 67.9, 31.4, 26.8, 24.0. IR (neat) 1708, 1620, 1607, 1565, 1495, 1475, 1454, 1417 cm$^{-1}$. HRMS (ESI): calcd for $C_{15}H_{16}BrO_3^+$ [M+H]$^+$: 323.0277, found: 323.0275.

### *E*-4-(((6-bromohex-5-en-1-yl)oxy)methyl)-1-methylquinolin-2(1*H*)-one (1t)

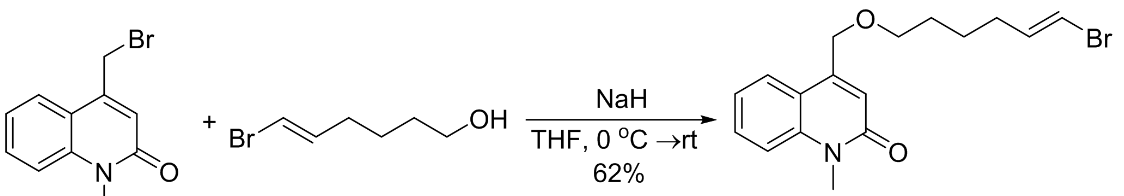

**1t**

The reaction of 4-(bromomethyl)-1-methylquinolin-2(1*H*)-one (252 mg, 1 mmol), *E*-6-bromohex-5-en-1-ol[15] (214 mg, 1.2 mmol), NaH (48 mg, 2 mmol), and THF (10 mL) under standard conditions affords **1t** as a solid (217 mg, 62%). Mp: 56.1-57.1 °C (*n*-hexane/ethyl acetate). $^1$H NMR (500 MHz, Chloroform-*d*) δ 7.72 (dd, *J* = 8.0, 1.5 Hz, 1H), 7.62-7.54 (m, 1H), 7.39 (dd, *J* = 8.5, 1.0 Hz, 1H), 7.28-7.22 (m, 1H), 6.81 (s, 1H), 6.14 (dt, *J* = 11.4, 6.0 Hz, 1H), 6.01 (dt, *J* = 11.4, 1.2 Hz, 1H), 4.71 (d, *J* = 1.2 Hz, 2H), 3.73 (s, 3H), 3.55 (t, *J* = 6.3 Hz, 2H), 2.11-2.01 (m, 2H), 1.68-1.62 (m, 2H), 1.54-1.45 (m, 2H). $^{13}$C NMR (126 MHz, Chloroform-*d*) δ 161.0, 144.6, 138.9, 136.6, 129.5, 123.5, 120.9, 118.7, 118.2, 113.5, 103.4, 69.6, 68.5, 31.6, 28.3, 27.9, 24.1. IR (neat) 1655, 1617, 1592, 1564, 1456 cm$^{-1}$. HRMS (ESI): calcd for $C_{17}H_{21}BrNO_2^+$ [M+H]$^+$: 350.0750, found: 350.0748.

### 7-(4-(Trifluoromethyl)benzyl)-3,7-dihydrooxepino[4,3-c]quinolin-6(1*H*)-one (2d)

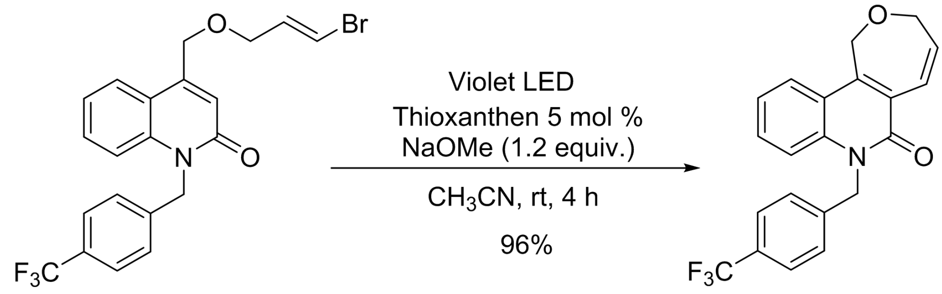

**1d** **2d**

**1d** (45 mg, 0.1 mmol), thioxanthone (1.1 mg, 0.005 mmol), NaOMe (6.5 mg, 0.12 mmol), and CH3CN (10 mL) are reacted under standard conditions to give **2d** as a solid (36 mg, 96%). Mp: 89.1-90.1 °C (*n*-hexane/ethyl acetate). $^1$H NMR (400 MHz, Chloroform-*d*) δ 7.85 (d, *J* = 8.2 Hz, 1H), 7.55 (d, *J* = 8.1 Hz, 2H), 7.41 (t, *J* = 7.8 Hz, 1H), 7.32 (d, *J* = 8.0 Hz, 2H), 7.26-7.20 (m, 1H), 7.19-7.14 (m, 2H), 6.25 (dt, *J* = 12.5, 3.0 Hz, 1H), 5.65 (s, 2H), 4.99 (s, 2H), 4.64 (t, *J* = 2.4 Hz, 2H). $^{13}$C NMR (101 MHz, Chloroform-*d*) δ 161.5, 145.3, 140.4, 138.1, 136.5, 130.4, 129.8, 129.5, 127.2, 126.9, 125.9, 125.82, 125.78, 125.7, 125.4, 124.4, 123.9, 122.73, 122.66, 119.5, 115.1, 73.6, 65.8, 46.3. IR (neat) 1635, 1598, 1458 cm$^{-1}$. HRMS (ESI): calcd for $C_{21}H_{17}F_3NO_2^+$ [M+H]$^+$: 372.1206, found: 372.1206.

### 7-(4-Methoxycarbonylbenzyl)-3,7-dihydrooxepino[4,3-c]quinolin-6(1*H*)-one (2e)

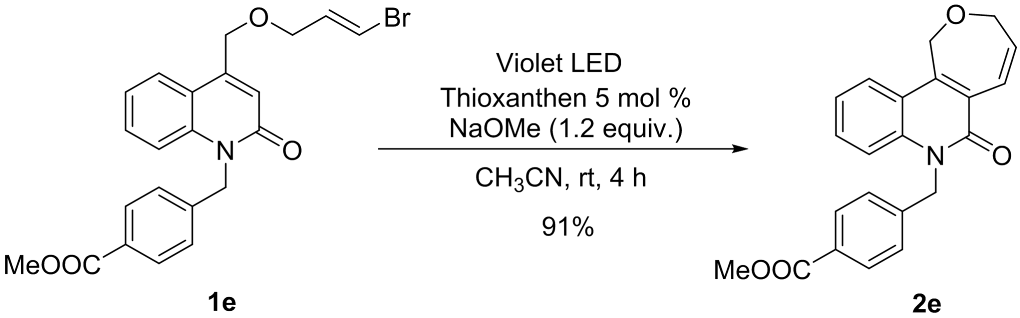

The reaction of **1e** (44 mg, 0.1 mmol), thioxanthone (1.1 mg, 0.005 mmol), NaOMe (6.5 mg, 0.12 mmol), and $CH_3CN$ (10 mL) under standard conditions affords **2e** as an oil (33 mg, 91%). $^1$H NMR (400 MHz, Chloroform-*d*) δ 7.96 (d, *J* = 8.3 Hz, 2H), 7.83 (d, *J* = 8.0 Hz, 1H), 7.38 (t, *J* = 7.5 Hz, 1H), 7.28-7.12 (m, 5H), 6.24 (dt, *J* = 12.5, 3.0 Hz, 1H), 5.65 (s, 2H), 4.98 (s, 2H), 4.64 (t, *J* = 2.5 Hz, 2H), 3.88 (s, 3H). $^{13}$C NMR (101 MHz, Chloroform-*d*) δ 166.7, 161.5, 145.3, 141.6, 138.1, 136.4, 130.3, 130.1, 129.2, 127.2, 126.5, 124.4, 124.0, 122.6, 119.5, 115.2, 73.6, 65.7, 52.1, 46.5. IR (neat) 1719, 1641, 1457, 1436, 1416 cm$^{-1}$. HRMS (ESI): calcd for $C_{22}H_{20}NO_4^+$ [M+H]$^+$: 362.1387, found: 362.1386.

### 7-(4-Cyanobenzyl)-3,7-dihydrooxepino[4,3-c]quinolin-6(1*H*)-one (2f)

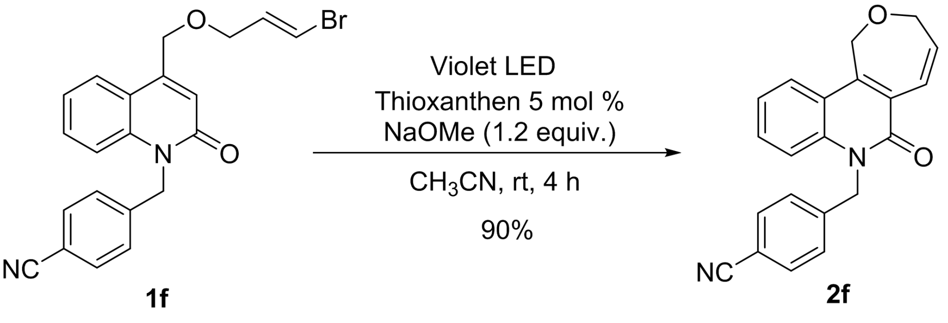

The reaction of **1f** (41 mg, 0.1 mmol), thioxanthone (1.1 mg, 0.005 mmol), NaOMe (6.5 mg, 0.12 mmol), and $CH_3CN$ (10 mL) under standard conditions affords **2f** as a solid (30 mg, 90%). Mp: 110.1-110.7 °C (*n*-hexane/ethyl acetate). $^1$H NMR (400 MHz, Chloroform-*d*) δ 7.86 (d, *J* = 8.0 Hz, 1H), 7.59 (d, *J* = 8.0 Hz, 2H), 7.41 (t, *J* = 8.0 Hz, 1H), 7.31 (d, *J* = 8.0 Hz, 2H), 7.26-7.21 (m, 1H), 7.13 (t, *J* = 11.0 Hz, 2H), 6.25 (dt, *J* = 12.4, 2.9 Hz, 1H), 5.65 (s, 2H), 4.99 (s, 2H), 4.65 (s, 2H). $^{13}$C NMR (101 MHz, Chloroform-*d*) δ 161.4, 145.4, 141.9, 137.9, 136.6, 132.7, 130.4, 127.3, 127.2, 124.6, 123.8, 122.9, 119.5, 118.6, 114.9, 111.3, 73.6, 65.7, 46.4. IR (neat) 2250, 1718, 1642, 1456, 1436 cm$^{-1}$. Anal. Calc. for $C_{21}H_{16}N_2O_2$ (328.12), C, 76.81; H, 4.91; N, 8.53. found: C, 77.01; H, 5.20; N, 8.61.

**7-(4-Nitrobenzyl)-3,7-dihydrooxepino[4,3-c]quinolin-6(1*H*)-one (2g)**

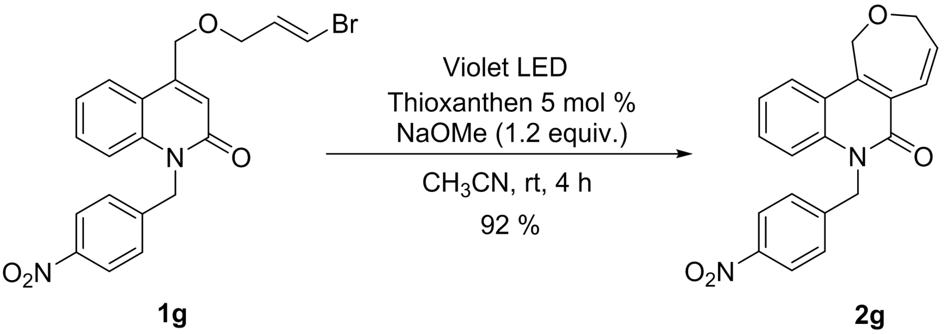

The reaction of **1g** (43 mg, 0.1 mmol), thioxanthone (1.1 mg, 0.005 mmol), NaOMe (6.5 mg, 0.12 mmol), and $CH_3CN$ (10 mL) under standard conditions affords **2g** as a solid (32 mg, 92%). Mp: 120.5-121.7 °C (*n*-hexane/ethyl acetate). $^{1}$H NMR (400 MHz, Chloroform-*d*) δ 8.17 (d, *J* = 8.3 Hz, 2H), 7.87 (d, *J* = 8.3 Hz, 1H), 7.48-7.34 (m, 3H), 7.25-7.22 (m, 1H), 7.20-7.08 (m, 2H), 6.26 (dt, *J* = 13.2, 3.1 Hz, 1H), 5.69 (s, 2H), 5.00 (s, 2H), 4.66 (s, 2H). $^{13}$C NMR (101 MHz, Chloroform-*d*) δ 161.4, 145.5, 143.9, 137.9, 136.7, 130.4, 127.4, 127.2, 124.6, 124.1, 123.8, 122.9, 119.6, 114.9, 73.6, 65.8, 46.2. IR (neat) 1624, 1586, 1512, 1455, 1435 cm$^{-1}$. HRMS (ESI): calcd for $C_{20}H_{17}N_2O_4^+$ $[M+H]^+$: 349.1183, found: 349.1182.

**7-(2-Oxo-2-phenylethyl)-3,7-dihydrooxepino[4,3-c]quinolin-6(1*H*)-one (2h)**

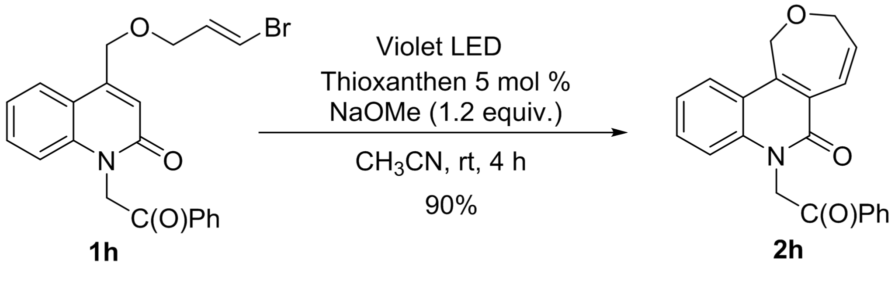

The reaction of **1h** (41 mg, 0.1 mmol), thioxanthone (1.1 mg, 0.005 mmol), NaOMe (6.5 mg, 0.12 mmol), and $CH_3CN$ (10 mL) under standard conditions affords **2h** as an oil (30 mg, 90%). $^1$H NMR (400 MHz, Chloroform-*d*) δ 8.10 (d, *J* = 7.8 Hz, 2H), 7.84 (d, *J* = 8.2 Hz, 1H), 7.66 (t, *J* = 7.4 Hz, 1H), 7.54 (t, *J* = 7.5 Hz, 2H), 7.42 (t, *J* = 7.8 Hz, 1H), 7.22 (d, *J* = 7.6 Hz, 1H), 7.12 (d, *J* = 12.7 Hz, 1H), 6.98 (d, *J* = 8.5 Hz, 1H), 6.21 (dt, *J* = 12.7, 3.3 Hz, 1H), 5.86 (s, 2H), 4.98 (s, 2H), 4.62 (s, 2H). $^{13}$C NMR (101 MHz, Chloroform-*d*) δ 192.4, 161.3, 145.4, 138.5, 136.1, 133.9, 130.3, 129.0, 128.2, 127.1, 124.5, 124.1, 122.6, 119.5, 114.5, 73.3, 65.9, 49.4. IR (neat) 1690, 1653, 1595, 1469, 1450, 1424 cm$^{-1}$. HRMS (ESI): calcd for $C_{21}H_{18}NO_3^+$ $[M+H]^+$: 332.1281, found: 332.1281.

### 6-Methyl-1,2,3,3a,4,4a-hexahydrocyclopenta[2,3]cyclobuta[1,2-c]quinolin-5(6*H*)-one (*rac*-3u)

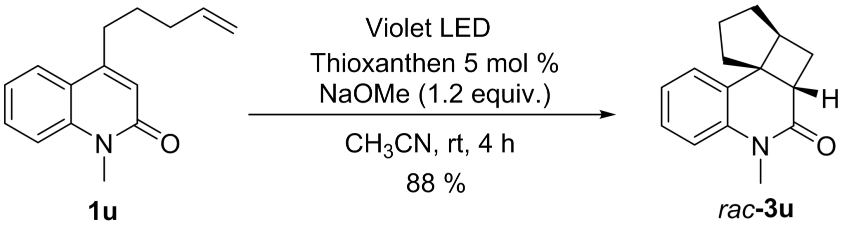

The reaction of **1u**[16] (23 mg, 0.1 mmol), thioxanthone (1.1 mg, 0.005 mmol), NaOMe (6.5 mg, 0.12 mmol), and $CH_3CN$ (10 mL) under standard conditions affords *rac*-**3u** as a solid (20 mg, 88%). $^1$H NMR (400 MHz, Chloroform-*d*) δ 7.22 (t, *J* = 7.7 Hz, 1H), 7.15 (d, *J* = 7.7 Hz, 1H), 7.05 (t, *J* = 7.4 Hz, 1H), 6.97 (d, *J* = 8.3 Hz, 1H), 3.37 (s, 3H), 3.11-2.99 (m, 1H), 2.68-2.43 (m, 2H), 2.17-2.02 (m, 3H), 1.99-1.83 (m, 3H), 1.71-1.64 (m, 1H).

### 3a-Bromo-6-methyl-1,2,3,3a,4,4a-hexahydrocyclopenta[2,3]cyclobuta[1,2-c]quinolin-5(6*H*)-one (*rac*-3v)

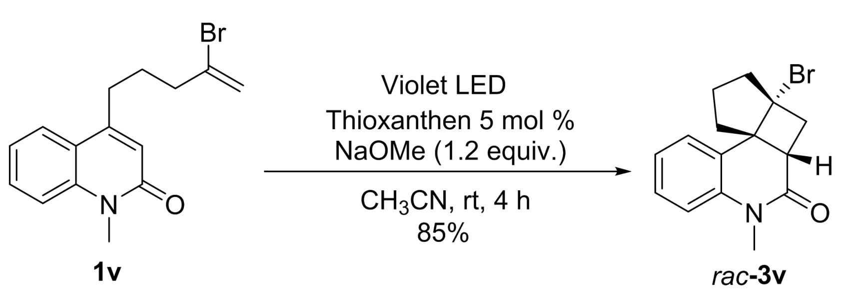

The reaction of **1v** (31 mg, 0.1 mmol), thioxanthone (1.1 mg, 0.005 mmol), NaOMe (6.5 mg, 0.12 mmol), and $CH_3CN$ (10 mL) under standard conditions affords *rac*-**3v** as an oil (26 mg, 85%). $^1H$ NMR (400 MHz, Methylene Chloride-$d_2$) δ 7.32 (t, $J$ = 7.7 Hz, 1H), 7.24-7.09 (m, 2H), 7.04 (d, $J$ = 8.3 Hz, 1H), 3.35 (s, 3H), 3.12-2.91 (m, 2H), 2.89-2.78 (m, 1H), 2.50-2.31 (m, 2H), 2.25-1.96 (m, 4H). $^{13}C$ NMR (101 MHz, Methylene Chloride-$d_2$) δ 168.6, 140.3, 129.1, 128.8, 125.3, 122.8, 115.0, 71.3, 56.5, 46.1, 43.9, 41.5, 39.0, 29.3, 25.0. IR (neat) 1625, 1592, 1570, 1453 cm$^{-1}$. HRMS (ESI): calcd for $C_{15}H_{17}BrNO^+$ [M+H]$^+$: 306.0488, found: 306.0489

### Synthesis of 4-bromo-6-methyl-3,3a,4,4a-tetrahydro-1*H*-furo[3',4':2,3]cyclobuta[1,2-c]quinolin-5(6*H*)-one (*rac*-3a-1 and *rac*-3a-2)

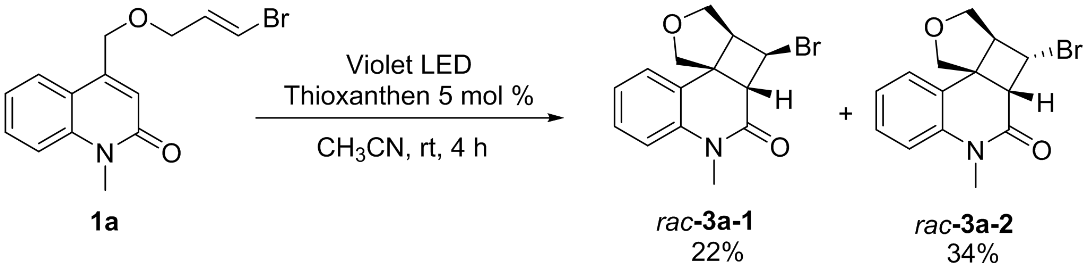

**1a** (31 mg, 0.1 mmol), thioxanthone (1.1 mg, 0.005 mmol), and $CH_3CN$ (10 mL) are added into an Schlenk tube under argon atmosphere. The reaction is stirred under violet LED at room temperature for 4 h, with monitoring with TLC (eluent: *n*-hexane/EA = 3:1). The solvent of the reaction is removed, and the orange residue is purified through silica gel chromatography with *n*-hexane/EA = 5:1 as eluent. *rac*-**3a-1** and *rac*-**3a-2** are obtained as solids. *rac*-**3a-1** (7 mg, 22%). $^1H$ NMR (400 MHz, Chloroform-*d*) δ 7.32 (t, $J$ = 7.0 Hz, 1H), 7.25 (d, $J$ = 8.0 Hz, 1H), 7.11 (t, $J$ = 7.5 Hz, 1H), 7.04 (d, $J$ = 8.2 Hz, 1H), 4.77 (t, $J$ = 8.3 Hz, 1H), 4.57 (d, $J$ = 10.4 Hz, 1H), 4.16-4.07 (m, 1H), 4.03 (d, $J$ = 9.4 Hz, 1H), 3.68 (d, $J$ = 9.4 Hz, 1H), 3.59 (d, $J$ = 8.6 Hz, 1H), 3.39 (s, 3H), 3.17 (t, $J$ = 7.4 Hz, 1H). $^{13}C$ NMR (101 MHz, Chloroform-*d*) δ 165.8, 139.4, 128.9, 127.1, 123.5, 121.7, 115.4, 78.6, 71.8, 57.0, 50.4, 49.2, 44.3, 29.1. IR (neat) 1664, 1600, 1468, 1419, 1366 cm$^{-1}$. HRMS (ESI): calcd for $C_{14}H_{15}BrNO^+$ [M+H]$^+$: 308.0281, found: 308.0281. Supplementary crystallographic data for *rac*-**3a-1** have been deposited at the Cambridge Crystallographic Data Center. CCDC: 1986917.

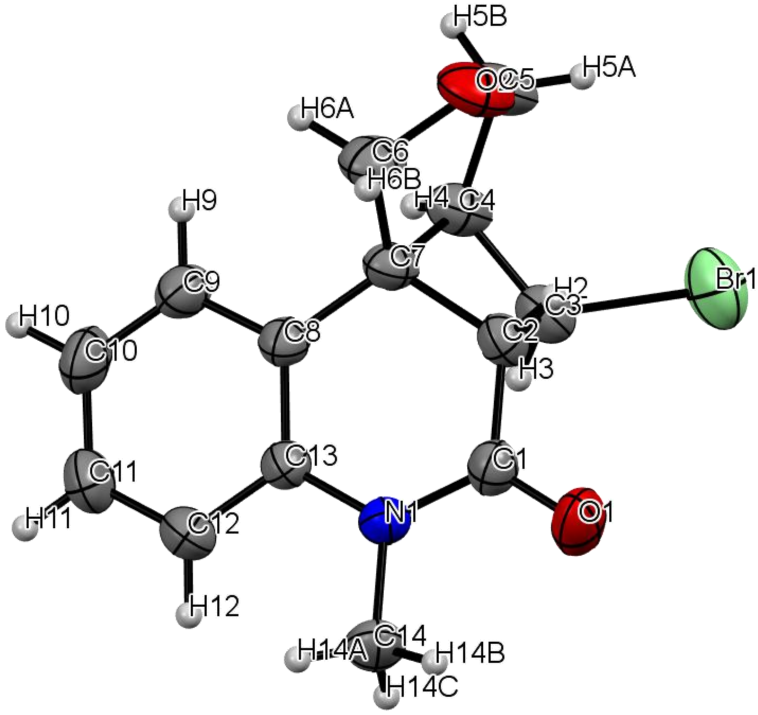

| | |
|---|---|
| Compound | *rac*-**3a-1** |
| formula | $C_{14}H_{14}BrNO_2$ |
| CCDC number | 1986917 |
| fw | 308.17 |
| color/habit | clear colourless fragment |
| Cryst. Dimens. [$mm^3$] | 0.05 x 0.05 x 0.05 |
| Cryst. Syst. | monoclinic |
| space group | $P2_1/n$ |
| a [Å] | 9.1885(6) |
| b [Å] | 14.2679(9) |
| c [Å] | 10.1298(6) |

| | |
|---|---|
| α [deg] | 90 |
| β [deg] | 107.630(2) |
| γ [deg] | 90 |
| V [Å$^3$] | 1265.65(14) |
| Z | 4 |
| T [K] | 298(2) |
| D$_{calcd}$ [g/cm$^{-3}$] | 1.617 |
| μ [mm$^{-1}$] | 2.890 |
| ϑ range [deg] | 5.2 to 59.3 |
| index range (h, k, l) | -11<=h<=11, -18<=k<=18, -12<=l<=12 |
| Reflections collected | 18648 |
| No. of indep reflns/R$_{int}$ | 2725 / 0.042 |
| No. of data/ restraints/params | 2465 / 0 / 164 |
| R1/wR2 ($I$>2σ(I)) | 0.0531/0.1576 |
| R1/wR2 (*all data*) | 0.0565/0.1621 |
| GOF (on F$^2$) | 1.068 |
| Largest diff peak and hole [e Å$^{-3}$] | 1.432/-1.100 |

*rac*-**3a-2** (11 mg, 34%). $^1$H NMR (400 MHz, Methylene Chloride-*d*$_2$) δ 7.32 (td, *J* = 8.4, 2.0 Hz, 1H), 7.23 (dd, *J* = 7.7, 1.6 Hz, 1H), 7.11 (td, *J* = 7.5, 1.1 Hz, 1H), 7.06 (d, *J* = 8.4 Hz, 1H), 4.44 (dd, *J* = 8.6, 2.3 Hz, 1H), 4.15 (d, *J* = 10.4 Hz, 1H), 4.02 (d, *J* = 9.6 Hz, 1H), 3.92 (dd, *J* = 10.4, 6.4 Hz, 1H), 3.76 (dd, *J* = 8.5, 1.7 Hz, 1H), 3.65 (d, *J* = 9.6 Hz, 1H), 3.39 (s, 3H), 3.20 (d, *J* = 7.0 Hz, 1H). $^{13}$C NMR (101 MHz, Methylene Chloride-*d*$_2$) δ 165.1, 140.2, 128.9, 126.7, 123.7, 123.5, 115.6, 79.0, 74.1, 62.2, 49.4, 47.5, 46.8, 29.3. IR (neat) 1662, 1599, 1467, 1367 cm$^{-1}$. HRMS (ESI): calcd for $C_{14}H_{15}BrNO^+$ $[M+H]^+$: 308.0281, found: 308.0281. Supplementary crystallographic data for *rac*-**3a-2** have been deposited at the Cambridge Crystallographic Data Center. CCDC: 1990199.

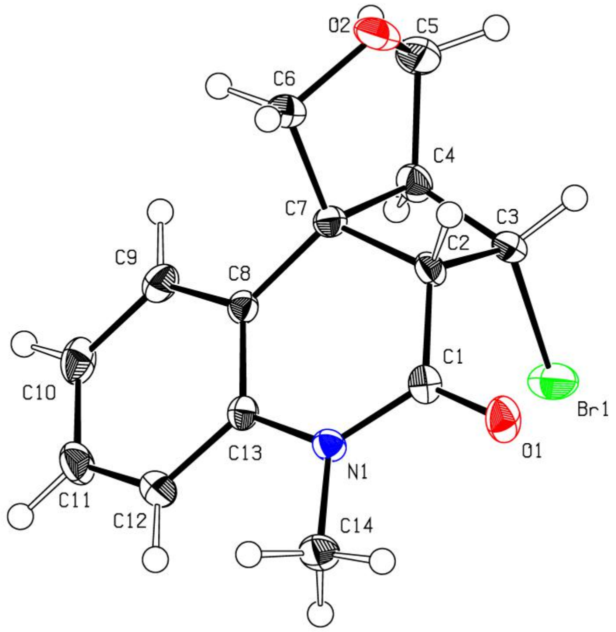

Ortep drawing with 50% ellipsoids for *rac*-**3a-2**

| Compound | *rac*-**3a-2** |
|---|---|
| formula | $C_{14}H_{14}BrNO_2$ |
| CCDC number | 1990199 |
| fw | 308.17 |
| color/habit | clear colourless fragment |
| Cryst. Dimens. [mm$^3$] | 0.084 x 0.211 x 0.243 |
| Cryst. Syst. | monoclinic |

| | |
|---|---|
| space group | $P$ 1 $2_1$/n 1 |
| a [Å] | 7.5317(15) |
| b [Å] | 10.0907(19) |
| c [Å] | 16.552(3) |
| α [deg] | 90 |
| β [deg] | 96.368(8) |
| γ [deg] | 90 |
| V [$Å^3$] | 1250.2(4) |
| Z | 4 |
| T [K] | 100(2) |
| $D_{calcd}$ [$g/cm^{-3}$] | 1.637 |
| μ [$mm^{-1}$] | 3.281 |
| ϑ range [deg] | 2.37 to 25.35 |
| index range (h, k, l) | $-9 \leq h \leq 9$<br>$-12 \leq k \leq 12$<br>$-19 \leq I \leq 19$ |
| Reflections collected | 16733 |
| no. of indep reflns/$R_{int}$ | 2283/0.0651 |
| no. of data/ restraints/params | 2283/0/164 |
| R1/wR2 ($I$>2σ(I)) | 0.0296/0.0753 |
| R1/wR2 (*all data*) | 0.0314/0.0766 |

| | |
|---|---|
| GOF (on F$^2$) | 1.061 |
| Largest diff peak and hole [e Å$^{-3}$] | 0.470/-0.555 |

### **Synthesis of 6-methyl-3,3a-dihydro-1*H*-furo[3',4':2,3]cyclobuta[1,2-c]quinolin-5(6*H*)-one (*rac*-4a)**

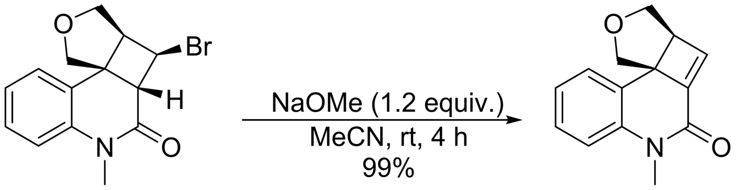

*rac*-**3a-1** *rac*-**4a**

*rac*-**3a-1** (31 mg, 0.1 mmol), NaOMe (6.5 mg, 0.12 mmol), and anhydrous MeCN (10 mL) are added into a 25 mL Schlenk flask under Ar. The mixture is further degassed and stirred for 4 h at room temperature under Ar. The solvent is removed through rotary evaporator, and the residue is purified through silica gel chromatography with PE/EA = 3:1 as eluent. *rac*-**4a** is obtained as a solid (22 mg, 99%). Mp 83.1-84.1 °C (petroleum ether/ethyl acetate). $^1$H NMR (400 MHz, Chloroform-*d*) δ 7.35-7.27 (m, 2H), 7.10 (t, $J$ = 6.8 Hz, 1H), 7.02 (d, $J$ = 7.9 Hz, 1H), 6.66 (s, 1H), 4.00 (d, $J$ = 9.8 Hz, 2H), 3.64-3.54 (m, 1H), 3.49-3.41 (m, 1H), 3.36 (s, 3H), 3.26 (d, $J$ = 9.8 Hz, 1H). $^{13}$C NMR (101 MHz, $CDCl_3$) $\delta$ 159.8, 142.3, 140.6, 140.2, 128.6, 127.0, 126.5, 123.4, 116.0, 71.8, 67.9, 55.8, 54.6, 29.3; IR (neat) 1676, 1627, 1598, 1456 cm$^{-1}$. HRMS (EI) calcd for $C_{14}H_{14}NO_2^+$ [M+H]$^+$: 228.1019, found: 228.1018. Supplementary crystallographic data for *rac*-**4a** have been deposited at the Cambridge Crystallographic Data Center. CCDC: 1986918.

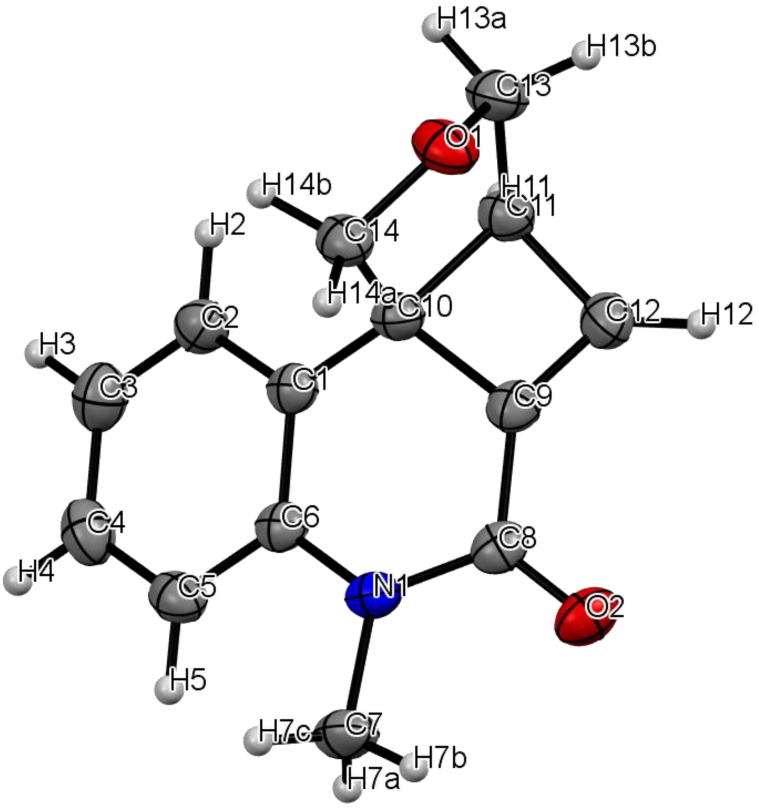

Ortep drawing with 50% ellipsoids for *rac*-**4a**

| Compound | *rac*-**4a** |
|---|---|
| formula | $C_{14}H_{13}NO_2$ |
| CCDC number | 1986918 |
| fw | 227.27 |
| color/habit | clear colourless fragment |
| Cryst. Dimens. [mm$^3$] | 0.09 x 0.08 x 0.07 |
| Cryst. Syst. | monoclinic |
| space group | $P\ 2_1/c$ |
| a [Å] | 9.0750(2) |

| | |
|---|---|
| b [Å] | 9.0233(2) |
| c [Å] | 13.9880(3) |
| α [deg] | 90 |
| β [deg] | 107.620(1) |
| γ [deg] | 90 |
| V [Å$^3$] | 1091.69(4) |
| Z | 4 |
| T [K] | 180(2) |
| $D_{calcd}$ [g/cm$^{-3}$] | 1.383 |
| μ [mm$^{-1}$] | 0.750 |
| ϑ range [deg] | 3.560 to 26.37 |
| index range (h, k, l) | -10<=h<=10, -10<=k<=10, -16<=l<=16 |
| Reflections collected | 1936 |
| no. of indep reflns/$R_{int}$ | 1936/ 0.039 |
| no. of data/ restraints/params | 13949 / 0 / 155 |
| R1/wR2 ($I$>2σ(I)) | 0.0387/0.0990 |
| R1/wR2 (*all data*) | 0.0344/0.0924 |
| GOF (on F$^2$) | 1.072 |
| Largest diff peak and hole [e Å$^{-3}$] | 0.36/-0.16 |

## Procedure for the transformation of rac-3a-2 into rac-4a

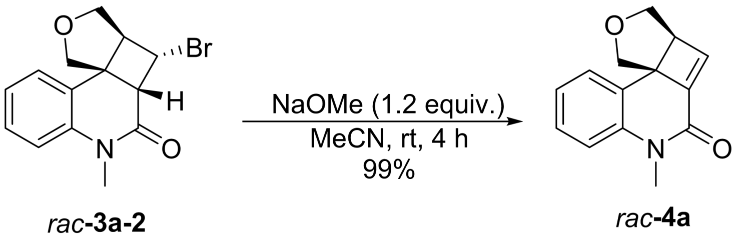

*rac*-**3a-2** (31 mg, 0.1 mmol), NaOMe (6.5 mg, 0.12 mmol), and anhydrous MeCN (10 mL) are added into a 25 mL Schlenk flask under Ar. The mixture is further degassed with Ar and stirred for 4 h at room temperature under Ar. The solvent is removed through rotary evaporator, and the residue is purified through silica gel chromatography with PE/EA = 3:1 as eluent. *rac*-**4a** is obtained as a solid (22 mg, 99%).

**Procedure for the transformation of rac-3a-1 into 2a**

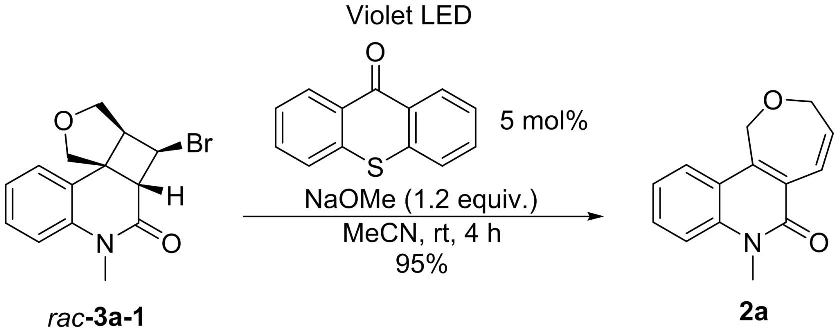

*rac*-**3a-1** (16 mg, 0.05 mmol), NaOMe (3.3 mg, 0.06 mmol), thioxanthone (0.6 mg, 0.0028 mmol), and anhydrous MeCN (10 mL) are added into a 25 mL Schlenk flask under Ar. The mixture is stirred and irradiated under Ar at room temperature. The reaction is stopped after 4 h with TLC monitoring. The solvent is removed through rotary evaporator, and the residue is purified through silica gel chromatography with PE/EA = 3:1 as eluent. **2a** is obtained as oil (10.5 mg, 95%).

**Procedure for the transformation of rac-3a-2 into 2a**

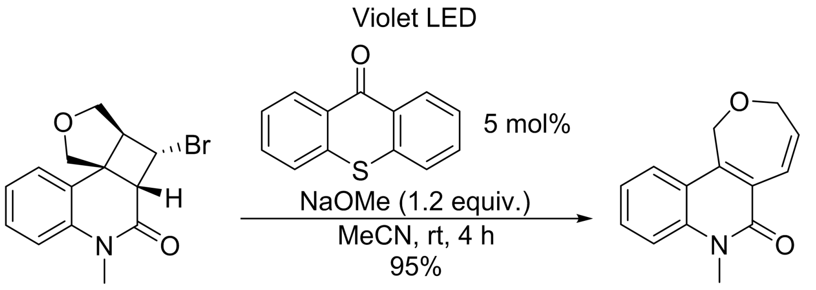

*rac*-**3a-2** **2a**

*rac*-**3a-2** (31 mg, 0.1 mmol), NaOMe (6.5 mg, 0.12 mmol), thioxanthone (1.1 mg, 0.005 mmol), and anhydrous MeCN (10 mL) are added into a 25 mL Schlenk flask under Ar. The mixture is stirred and irradiated under Ar at room temperature. The reaction is stopped after 4 h with TLC monitoring. The solvent is removed through rotary evaporator, and the residue is purified through silica gel chromatography with PE/EA = 3:1 as eluent. **2a** is obtained as oil (22 mg, 95%).

**Procedure for the transformation of rac-4a into 2a**

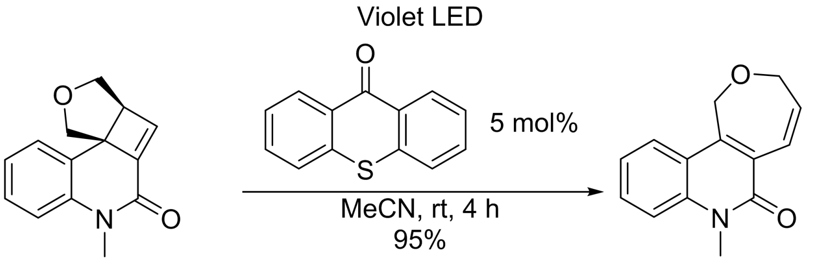

*rac*-**4a** **2a**

*rac*-**4a** (23 mg, 0.1 mmol), thioxanthone (1.1 mg, 0.005 mmol), and anhydrous MeCN (10 mL) are added into a 25 mL Schlenk flask under Ar. The mixture is stirred and irradiated under Ar at room temperature. The reaction is stopped after 4 h with TLC monitoring. The solvent is removed through rotary evaporator, and the residue is purified through silica gel chromatography with PE/EA = 3:1 as eluent. **2a** is obtained as oil (21 mg, 95%).

**Procedure for gram scale experiment of 1a to 2a**

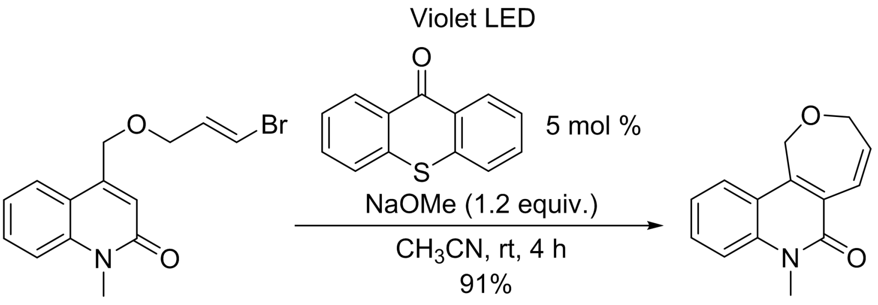

**1a**
1.002 g

**2a**
0.672 g

(500 mL) are added **1a** (1002 mg, 3.25 mmol), thioxanthone (34.5 mg, 0.1625 mmol), NaOMe (210.9 mg, 3.9 mmol), and anhydrous $CH_3CN$ (325 mL) are added into a dried three-necked flask under Ar.The mixture is stirred and irradiated under Ar at room temperature. The reaction is stopped after 4 h with TLC monitoring. The solvent is removed through rotary evaporator, and the residue is purified through silica gel chromatography with PE/EA = 3:1 as eluent. **2a** is obtained as oil (672 mg, 91%).

### 3.7 Reproduction acknowledgement

Reproduced from Ref. *Org. Lett.*, **2020**, *22*, 4372-4377. Acknowledgement goes to Royal Sociedy of Chemistry.

# 3.5.3 NMR Spectrum

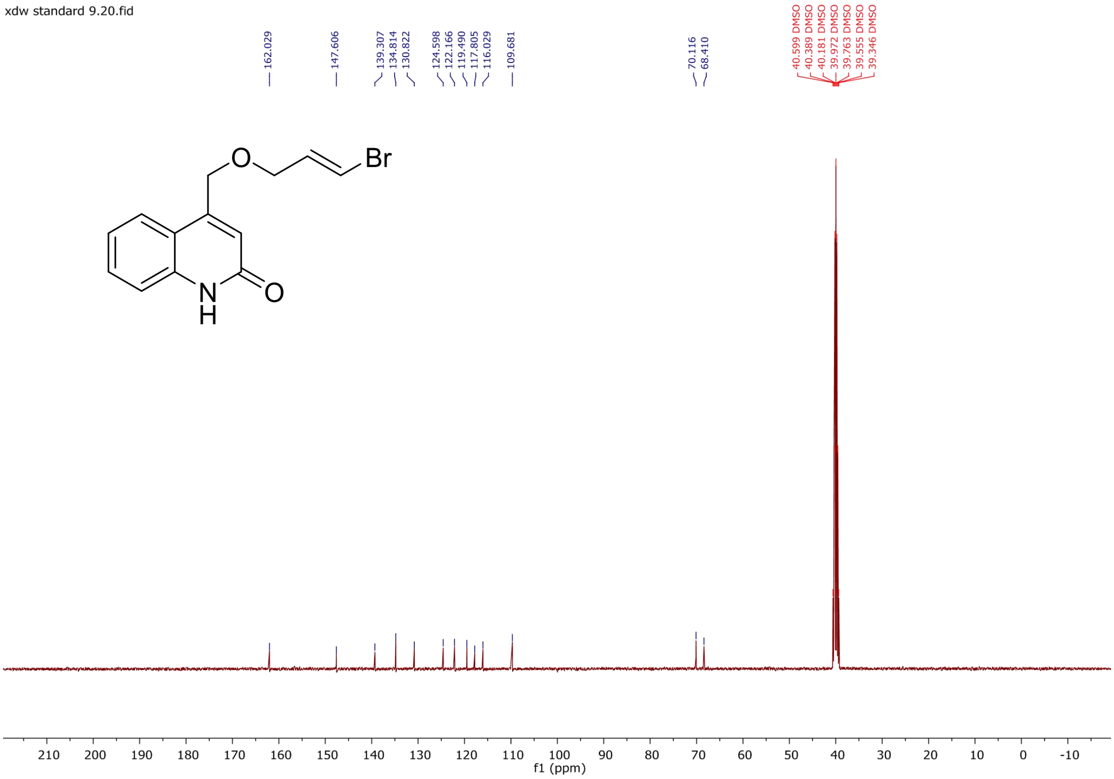

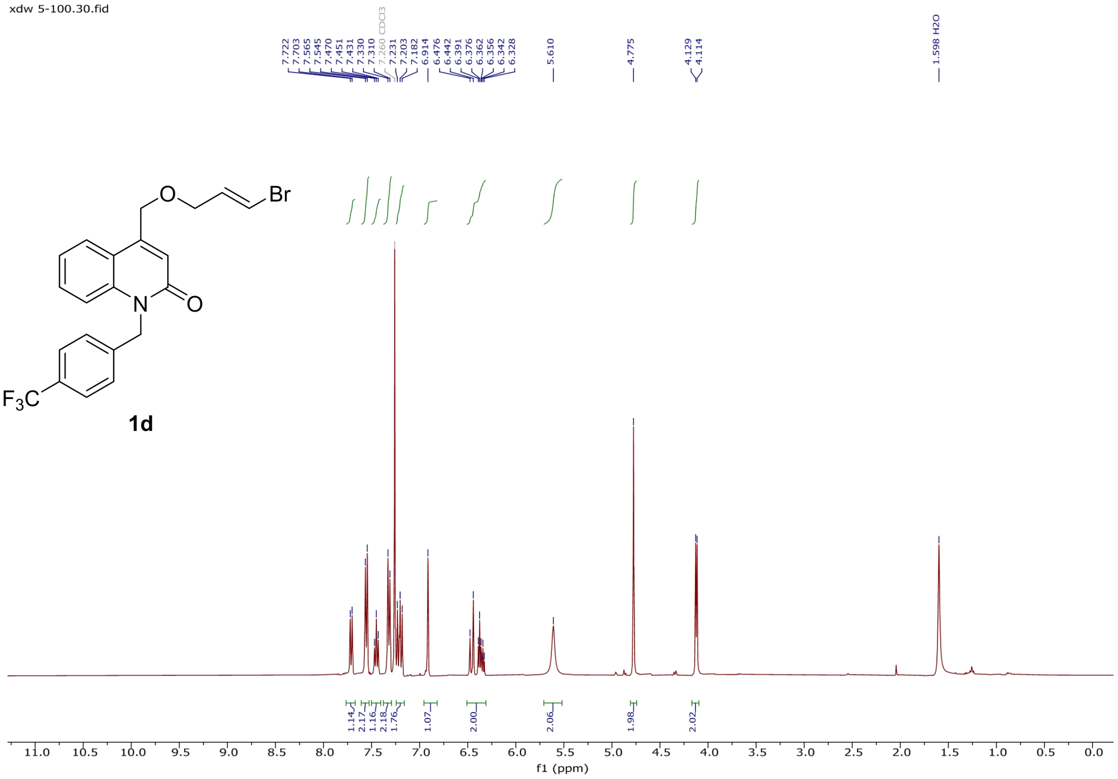

**1d**

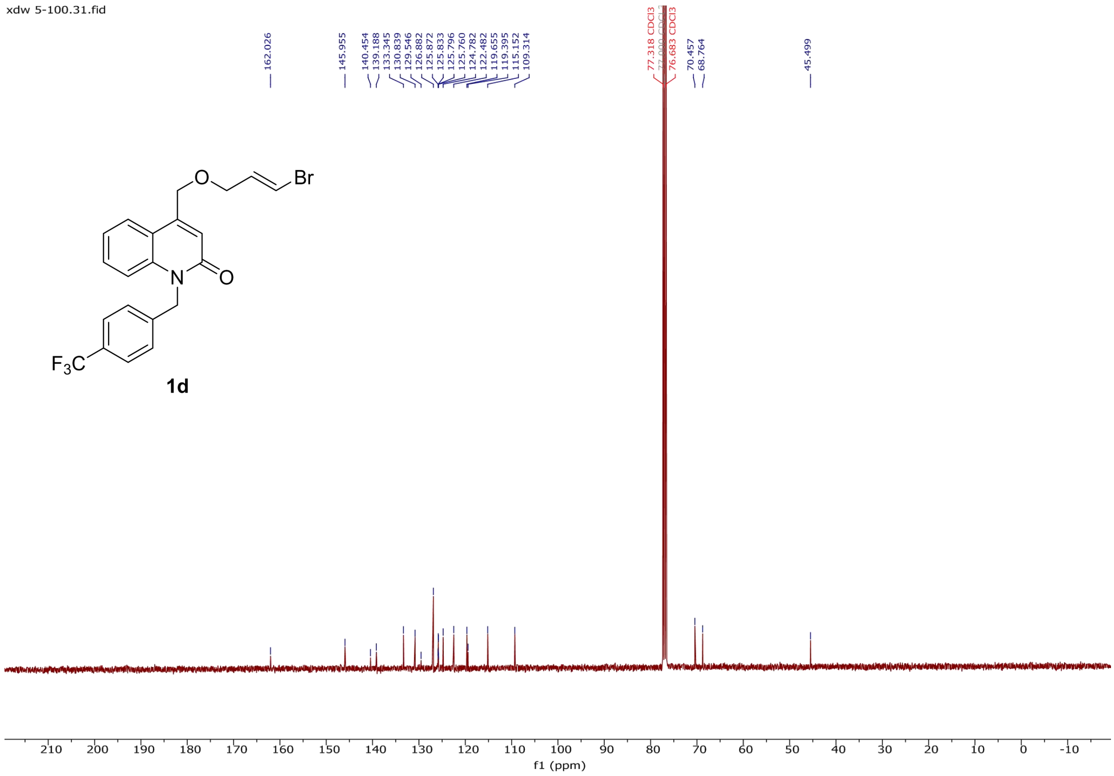
xdw 5-100.31.fid
162.026
145.955
140.454
139.188
133.345
130.839
129.546
126.882
125.872
125.833
125.796
125.760
124.782
122.482
119.655
119.395
115.152
109.314
77.318 CDCl3
77.000 CDCl3
76.683 CDCl3
70.457
68.764
45.499
O
Br
N
O
F3C
1d
210
200
190
180
170
160
150
140
130
120
110
100
90
80
70
60
50
40
30
20
10
0
-10
f1 (ppm)

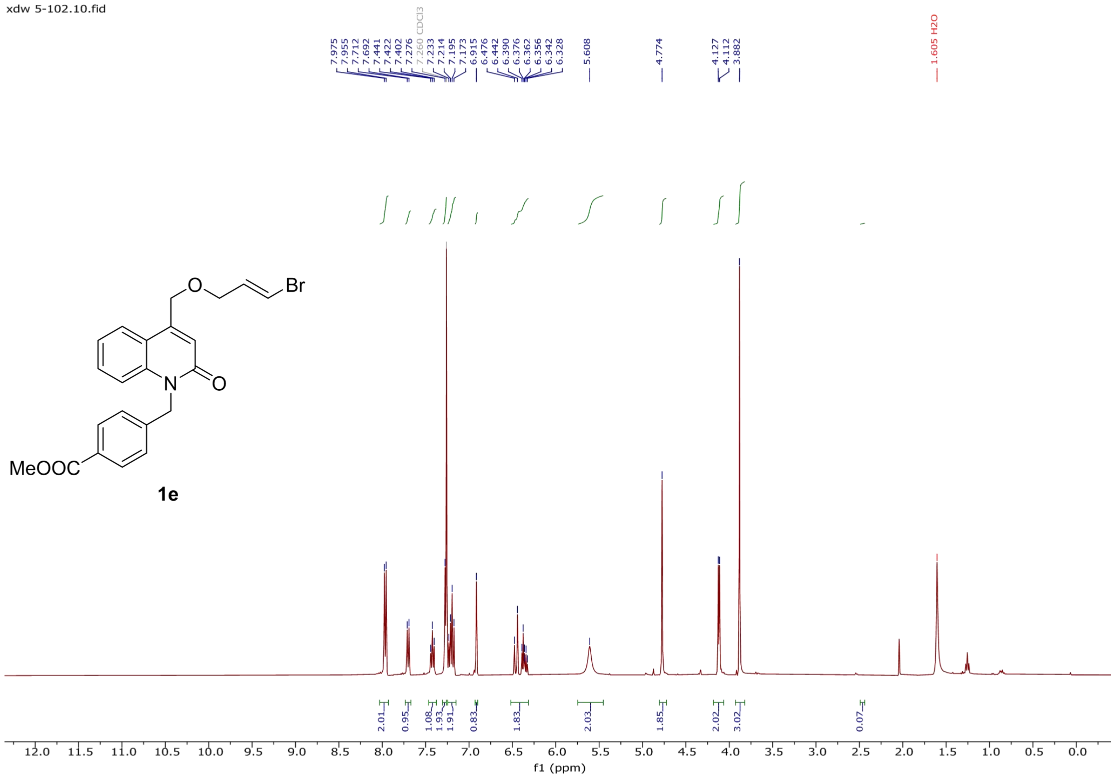
xdw 5-102.10.fid
7.975
7.955
7.712
7.692
7.441
7.422
7.402
7.276
7.260 CDCl3
7.233
7.214
7.195
7.173
6.915
6.476
6.442
6.390
6.376
6.362
6.356
6.342
6.328
5.608
4.774
4.127
4.112
3.882
1.605 H2O
O
Br
N
O
MeOOC
1e
2.01
0.95
1.08
1.93
1.91
0.83
1.83
2.03
1.85
2.02
3.02
0.07
12.0
11.5
11.0
10.5
10.0
9.5
9.0
8.5
8.0
7.5
7.0
6.5
6.0
5.5
5.0
4.5
4.0
3.5
3.0
2.5
2.0
1.5
1.0
0.5
0.0
f1 (ppm)

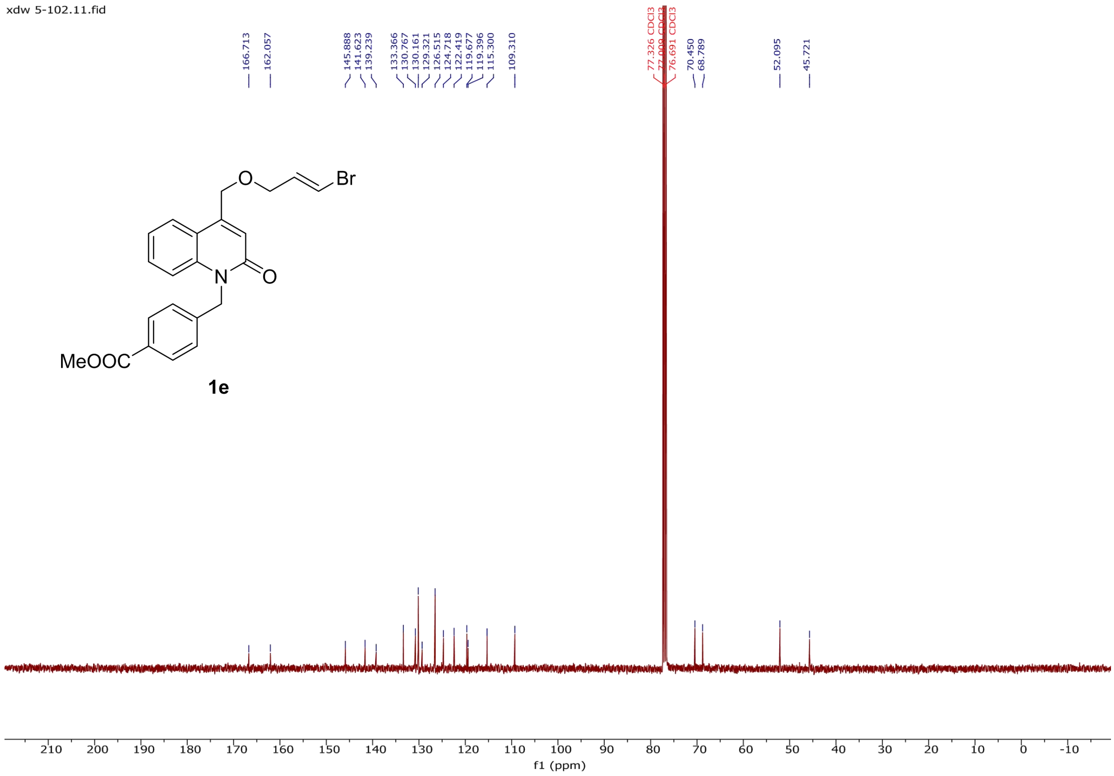
xdw 5-102.11.fid
166.713
162.057
145.888
141.623
139.239
133.366
130.767
130.161
129.321
126.515
124.718
122.419
119.677
119.396
115.300
109.310
77.326 CDCl3
77.009 CDCl3
76.691 CDCl3
70.450
68.789
52.095
45.721
O
Br
N
O
MeOOC
210
200
190
180
170
160
150
140
130
120
110
100
90
80
70
60
50
40
30
20
10
0
-10
f1 (ppm)

**1e**

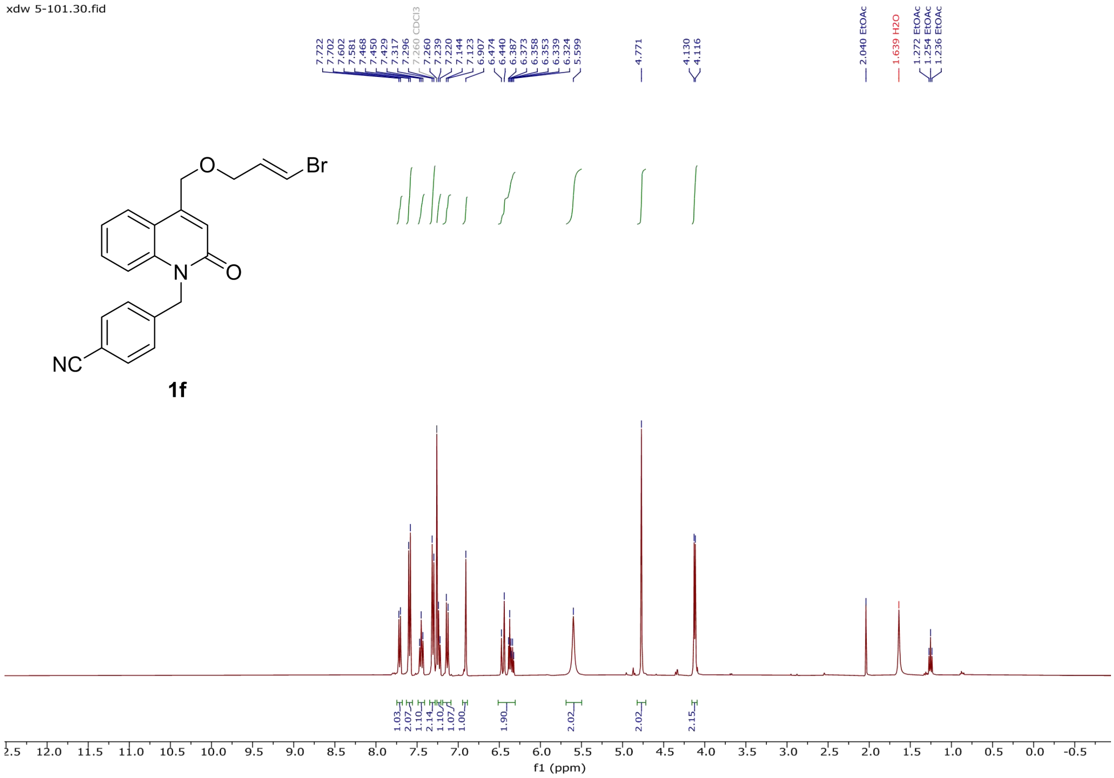
xdw 5-101.30.fid
7.722
7.702
7.602
7.581
7.468
7.450
7.429
7.317
7.296
7.260 CDCl3
7.260
7.239
7.220
7.144
7.123
6.907
6.474
6.440
6.387
6.373
6.358
6.353
6.339
6.324
5.599
4.771
4.130
4.116
2.040 EtOAc
1.639 H2O
1.272 EtOAc
1.254 EtOAc
1.236 EtOAc
O
Br
N
O
NC
1.03
2.07
1.10
2.14
1.10
1.07
1.00
1.90
2.02
2.02
2.15
2.5
12.0
11.5
11.0
10.5
10.0
9.5
9.0
8.5
8.0
7.5
7.0
6.5
6.0
5.5
5.0
4.5
4.0
3.5
3.0
2.5
2.0
1.5
1.0
0.5
0.0
-0.5
f1 (ppm)

**1f**

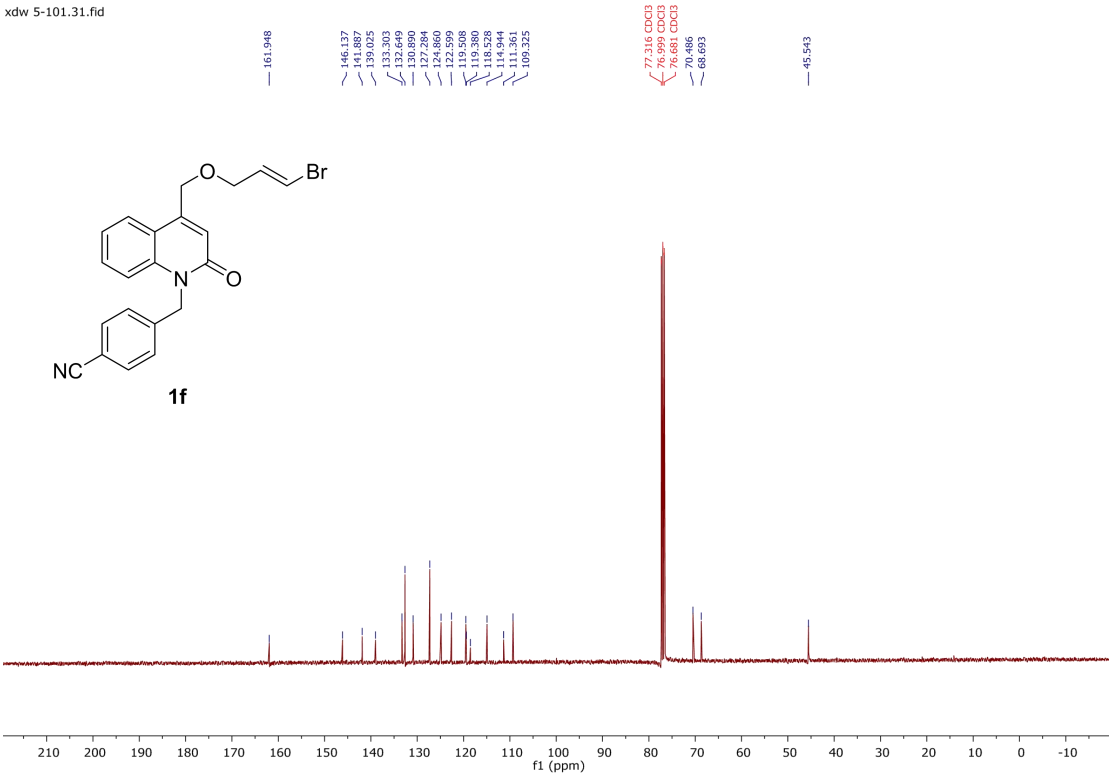
xdw 5-101.31.fid
161.948
146.137
141.887
139.025
133.303
132.649
130.890
127.284
124.860
122.599
119.508
119.380
118.528
114.944
111.361
109.325
77.316 CDCl3
76.999 CDCl3
76.681 CDCl3
70.486
68.693
45.543
O
Br
N
O
NC
1f
210 200 190 180 170 160 150 140 130 120 110 100 90 80 70 60 50 40 30 20 10 0 -10
f1 (ppm)

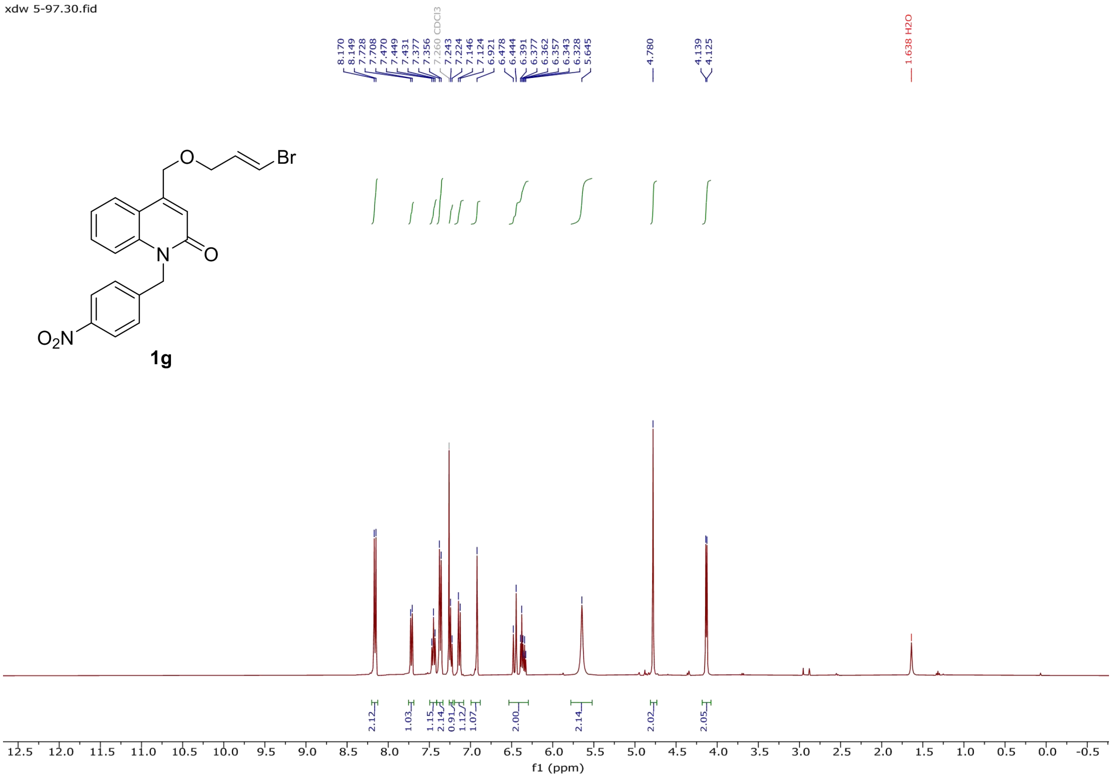
xdw 5-97.30.fid
8.170
8.149
7.728
7.708
7.470
7.449
7.431
7.377
7.356
7.260 CDCl3
7.243
7.224
7.146
7.124
6.921
6.478
6.444
6.391
6.377
6.362
6.357
6.343
6.328
5.645
4.780
4.139
4.125
1.638 H2O
O
Br
N
O
$O_2N$
1g
2.12
1.03
1.15
2.14
0.91
1.12
1.07
2.00
2.14
2.02
2.05
12.5 12.0 11.5 11.0 10.5 10.0 9.5 9.0 8.5 8.0 7.5 7.0 6.5 6.0 5.5 5.0 4.5 4.0 3.5 3.0 2.5 2.0 1.5 1.0 0.5 0.0 -0.5
f1 (ppm)

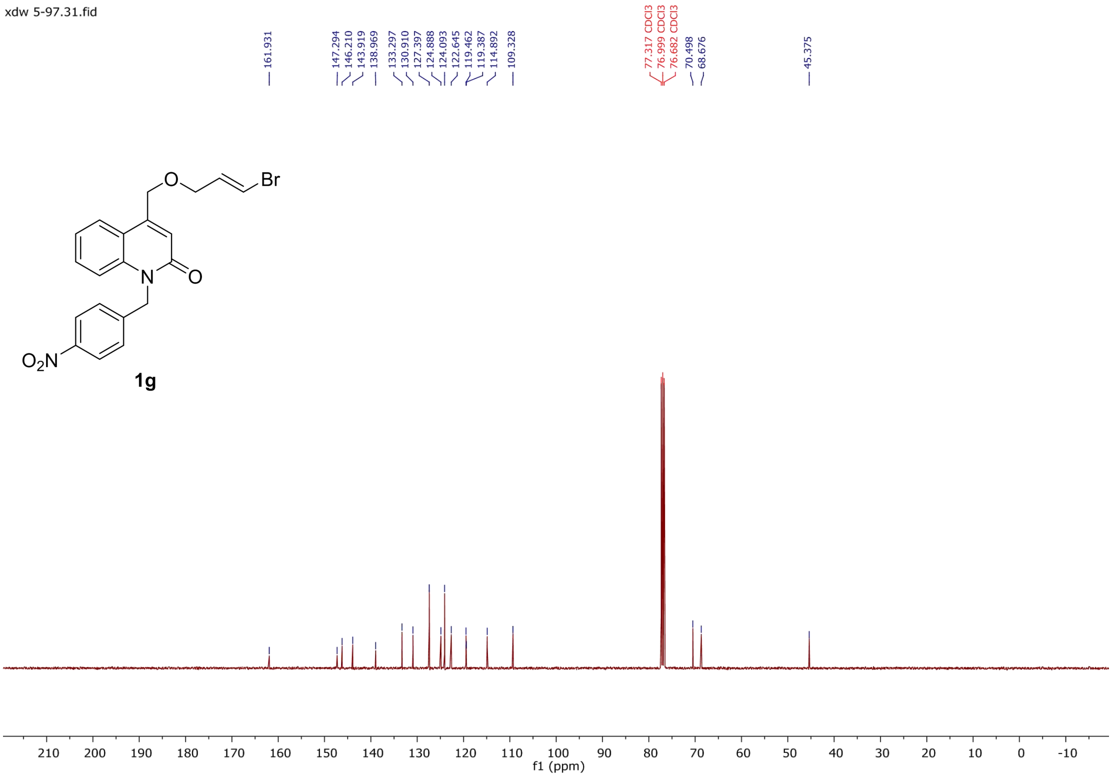
xdw 5-97.31.fid
161.931
147.294
146.210
143.919
138.969
133.297
130.910
127.397
124.888
124.093
122.645
119.462
119.387
114.892
109.328
77.317 CDCl3
76.999 CDCl3
76.682 CDCl3
70.498
68.676
45.375
Br
O
N
O
$O_2N$
210
200
190
180
170
160
150
140
130
120
110
100
90
80
70
60
50
40
30
20
10
0
-10
f1 (ppm)

**1g**

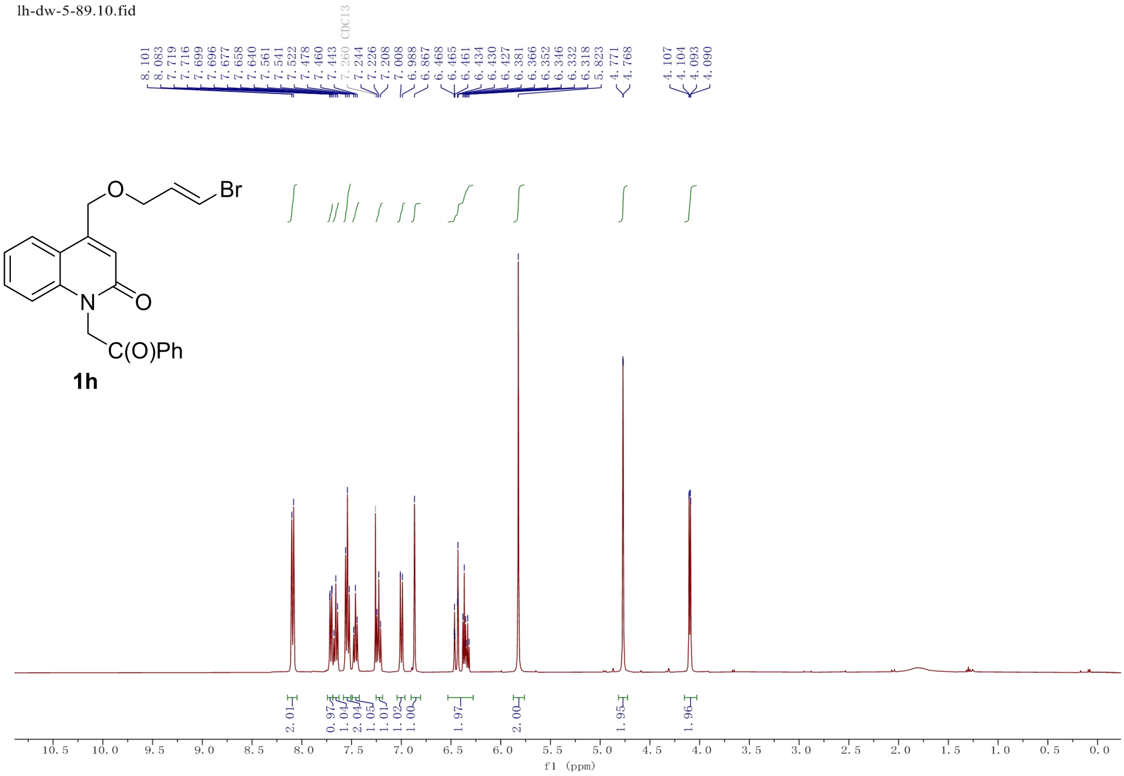
lh-dw-5-89.10.fid
8.101
8.083
7.719
7.716
7.699
7.696
7.677
7.658
7.640
7.561
7.541
7.522
7.478
7.460
7.443
7.260 CDCl3
7.244
7.226
7.208
7.008
6.988
6.867
6.468
6.465
6.461
6.434
6.430
6.427
6.381
6.366
6.352
6.346
6.332
6.318
5.823
4.771
4.768
4.107
4.104
4.093
4.090
O
Br
N
O
C(O)Ph
2.01
0.97
1.04
2.04
1.05
1.01
1.02
1.00
1.97
2.00
1.95
1.96
10.5
10.0
9.5
9.0
8.5
8.0
7.5
7.0
6.5
6.0
5.5
5.0
4.5
4.0
3.5
3.0
2.5
2.0
1.5
1.0
0.5
0.0
f1 (ppm)

**1h**

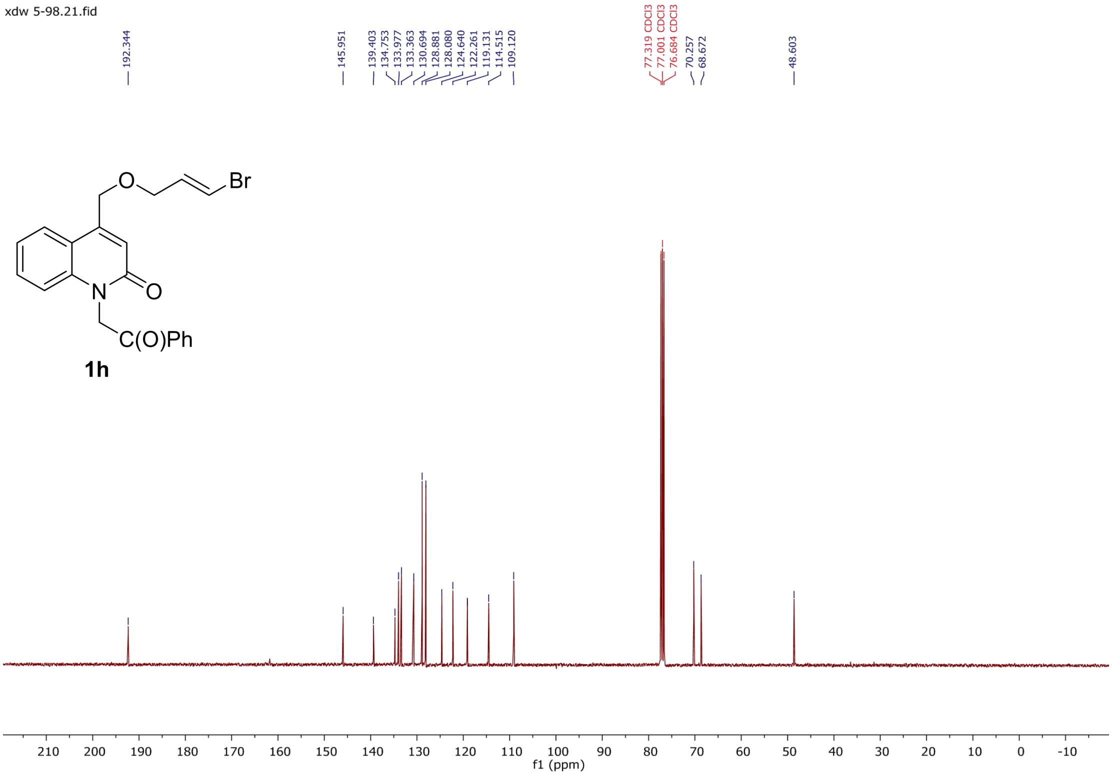
xdw 5-98.21.fid
192.344
145.951
139.403
134.753
133.977
133.363
130.694
128.881
128.080
124.640
122.261
119.131
114.515
109.120
77.319 CDCl3
77.001 CDCl3
76.684 CDCl3
70.257
68.672
48.603
Br
O
N
O
C(O)Ph
210
200
190
180
170
160
150
140
130
120
110
100
90
80
70
60
50
40
30
20
10
0
-10
f1 (ppm)

**1h**

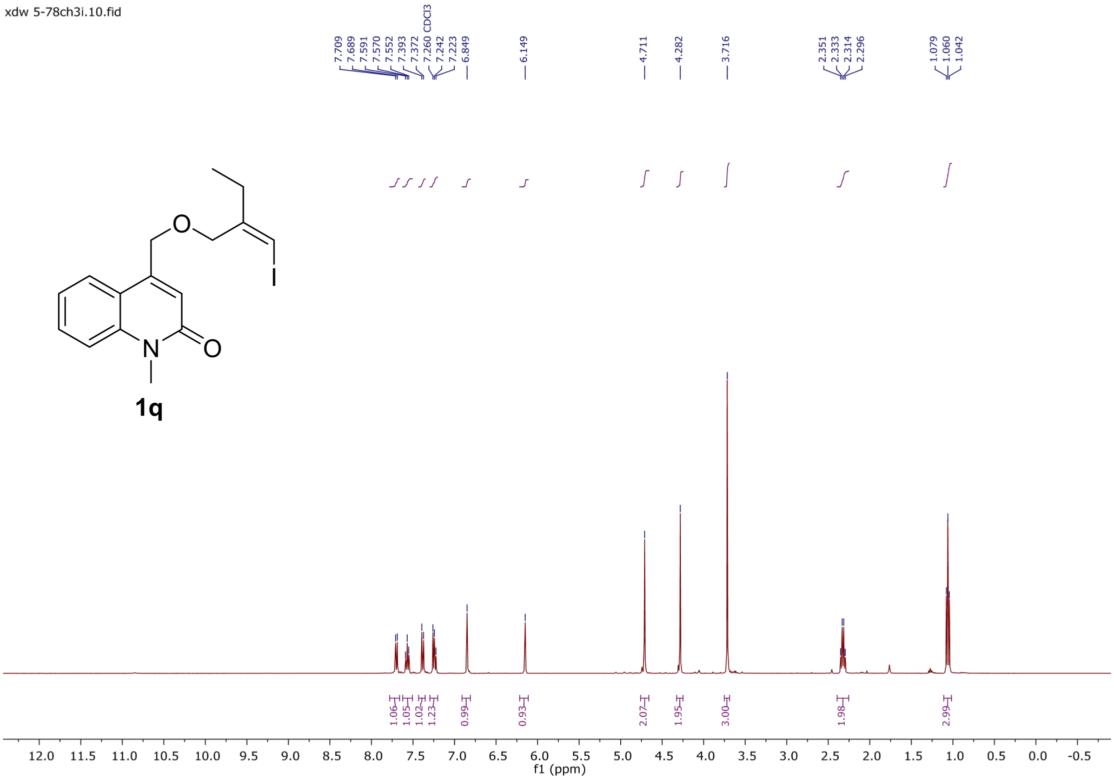
xdw 5-78ch3i.10.fid
7.709
7.689
7.591
7.570
7.552
7.393
7.372
7.260 CDCl3
7.242
7.223
6.849
6.149
4.711
4.282
3.716
2.351
2.333
2.314
2.296
1.079
1.060
1.042
O
I
N
O
1.06
1.05
1.02
1.23
0.99
0.93
2.07
1.95
3.00
1.98
2.99
12.0
11.5
11.0
10.5
10.0
9.5
9.0
8.5
8.0
7.5
7.0
6.5
6.0
5.5
5.0
4.5
4.0
3.5
3.0
2.5
2.0
1.5
1.0
0.5
0.0
-0.5
f1 (ppm)

**1q**

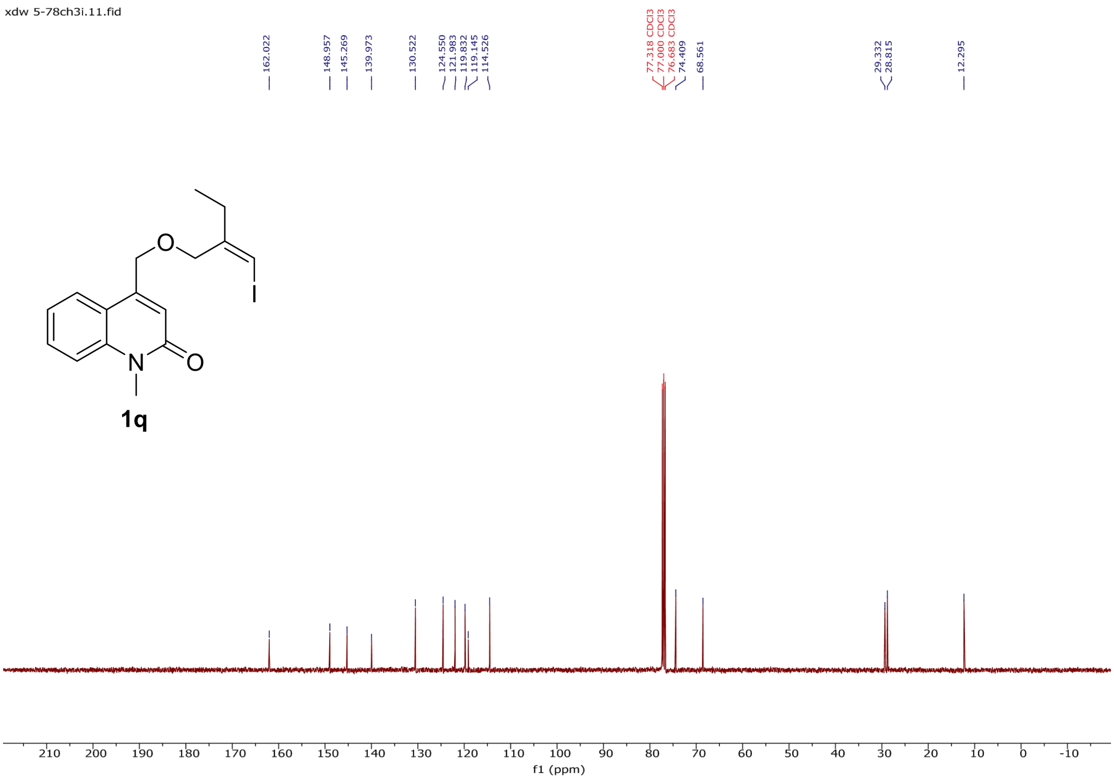
xdw 5-78ch3i.11.fid
162.022
148.957
145.269
139.973
130.522
124.550
121.983
119.832
119.145
114.526
77.318 CDCl3
77.000 CDCl3
76.683 CDCl3
74.409
68.561
29.332
28.815
12.295
O
I
N
O
210 200 190 180 170 160 150 140 130 120 110 100 90 80 70 60 50 40 30 20 10 0 -10
f1 (ppm)

**1q**

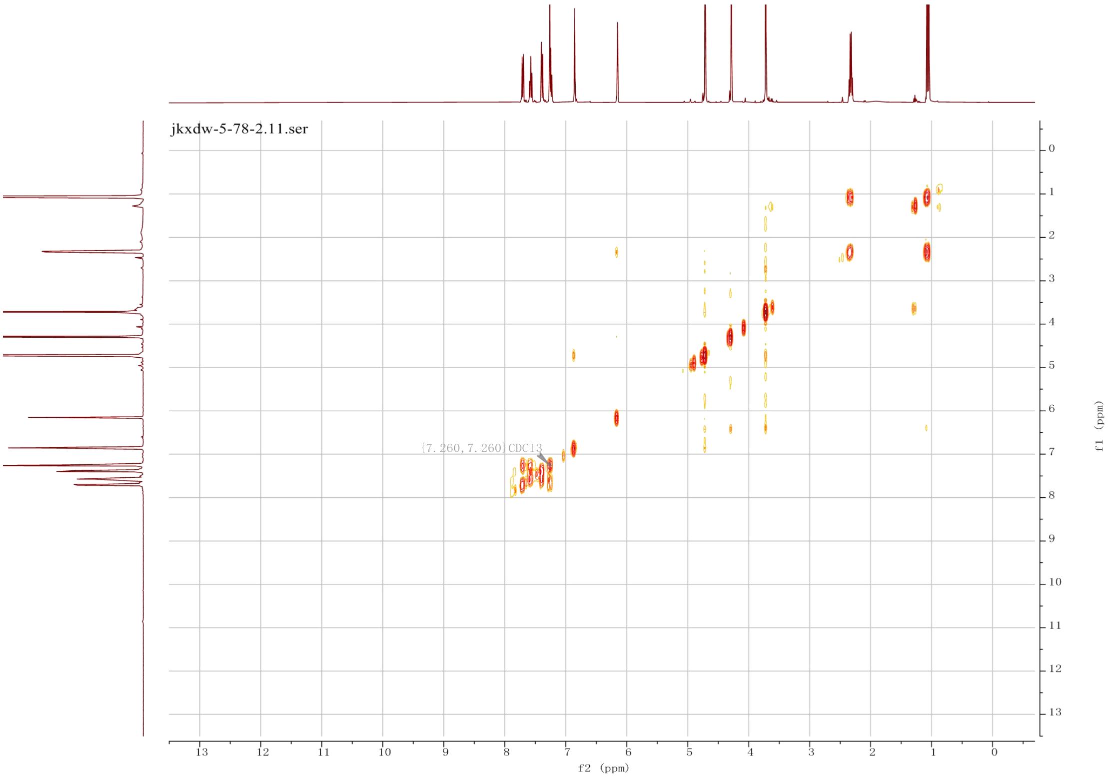
jkxdw-5-78-2.11.ser
[7.260, 7.260] CDCl3
13 12 11 10 9 8 7 6 5 4 3 2 1 0
f2 (ppm)
0 1 2 3 4 5 6 7 8 9 10 11 12 13
f1 (ppm)

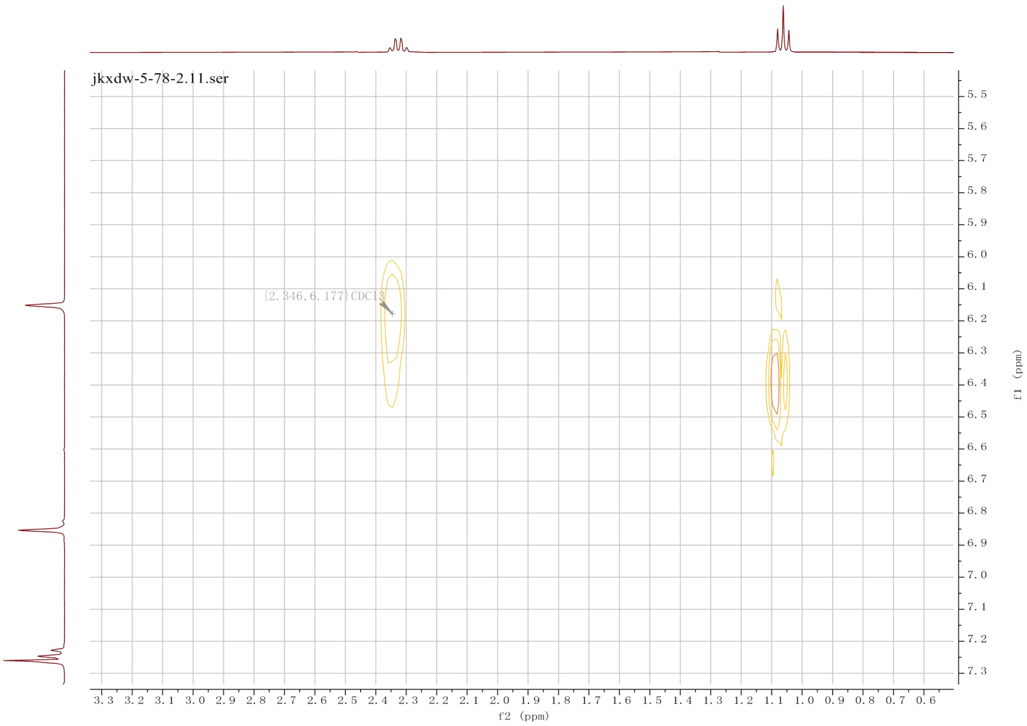
jkxdw-5-78-2.11.ser
(2.346, 6.177) CDCl3
f2 (ppm)
f1 (ppm)
3.3 3.2 3.1 3.0 2.9 2.8 2.7 2.6 2.5 2.4 2.3 2.2 2.1 2.0 1.9 1.8 1.7 1.6 1.5 1.4 1.3 1.2 1.1 1.0 0.9 0.8 0.7 0.6
5.5 5.6 5.7 5.8 5.9 6.0 6.1 6.2 6.3 6.4 6.5 6.6 6.7 6.8 6.9 7.0 7.1 7.2 7.3

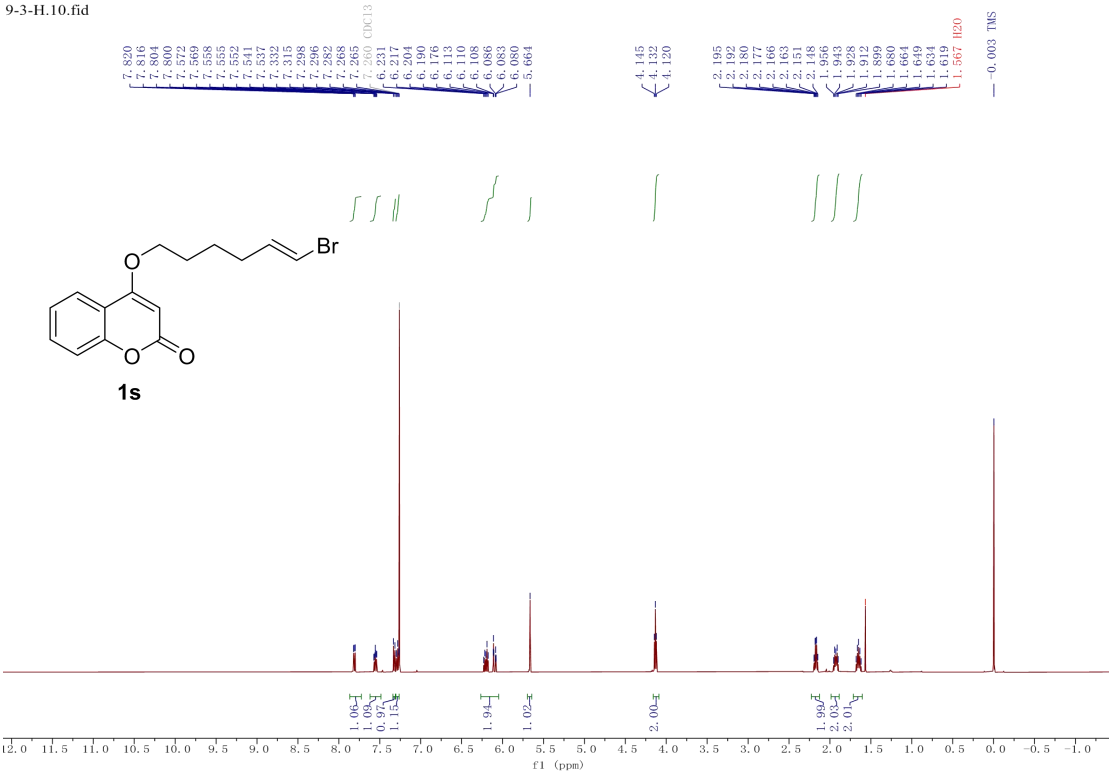
9-3-H.10.fid
7.820 7.816 7.804 7.800 7.572 7.569 7.558 7.555 7.552 7.541 7.537 7.332 7.315 7.298 7.296 7.282 7.268 7.265 7.260 CDCl3 6.231 6.217 6.204 6.190 6.176 6.113 6.110 6.108 6.086 6.083 6.080 5.664
4.145 4.132 4.120
2.195 2.192 2.180 2.177 2.166 2.163 2.151 2.148 1.956 1.943 1.928 1.912 1.899 1.680 1.664 1.649 1.634 1.619 1.567 H2O
-0.003 TMS
O
O
O
Br
1.06 1.09 0.97 1.15 1.94 1.02 2.00 1.99 2.03 2.01
12.0 11.5 11.0 10.5 10.0 9.5 9.0 8.5 8.0 7.5 7.0 6.5 6.0 5.5 5.0 4.5 4.0 3.5 3.0 2.5 2.0 1.5 1.0 0.5 0.0 -0.5 -1.0
f1 (ppm)

**1s**

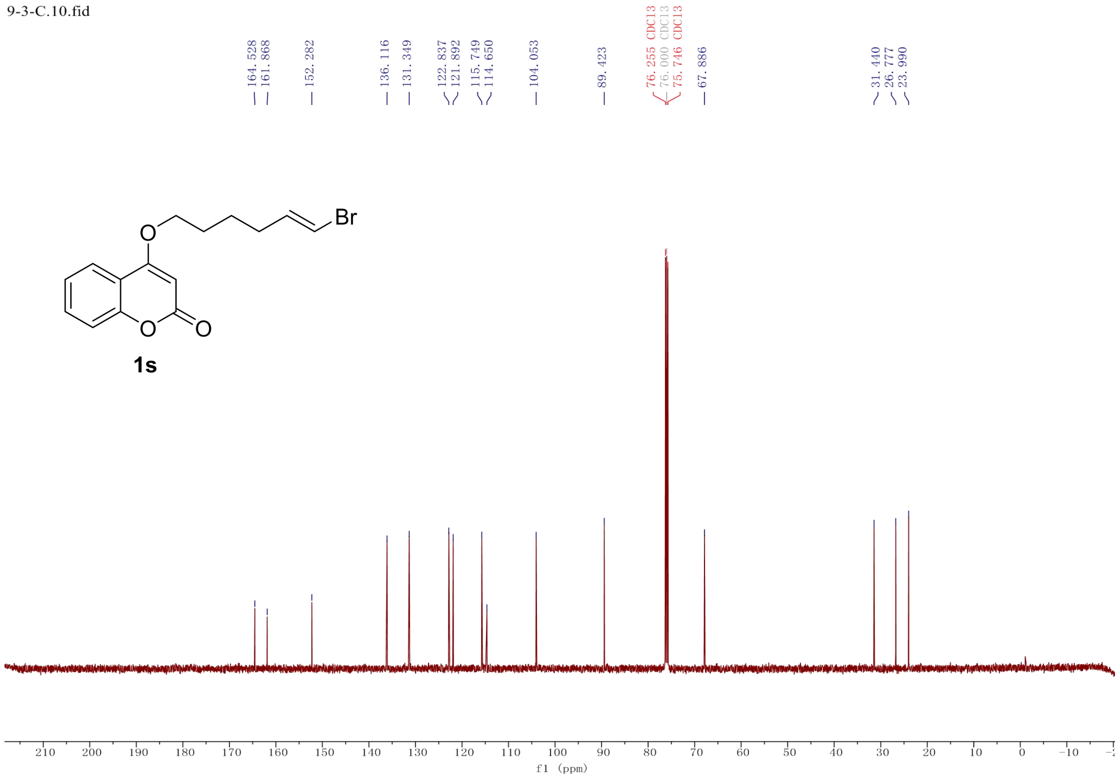
9-3-C.10.fid
164.528
161.868
152.282
136.116
131.349
122.837
121.892
115.749
114.650
104.053
89.423
76.255 CDCl3
76.000 CDCl3
75.746 CDCl3
67.886
31.440
26.777
23.990
O
Br
O
O
1s
210
200
190
180
170
160
150
140
130
120
110
100
90
80
70
60
50
40
30
20
10
0
−10
f1 (ppm)

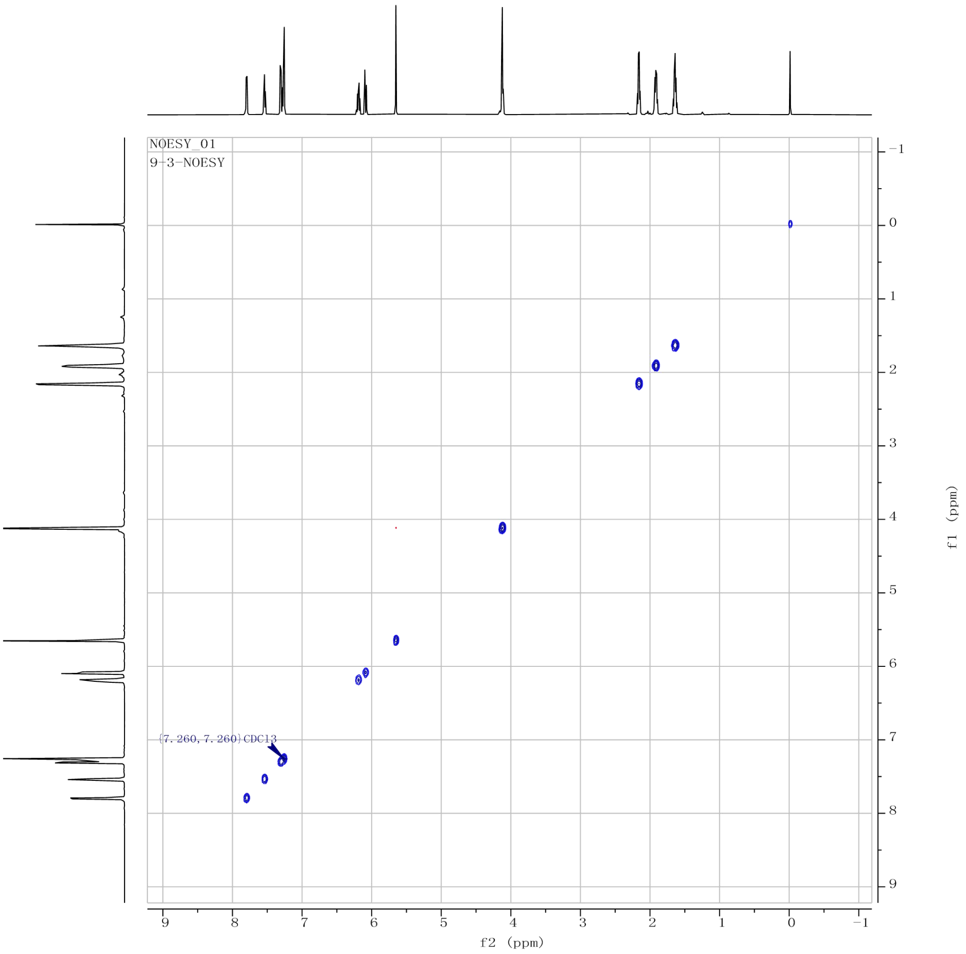
NOESY_01
9-3-NOESY
[7.260, 7.260] CDCl3
−1
0
1
2
3
4
5
6
7
8
9
f1 (ppm)
9
8
7
6
5
4
3
2
1
0
−1
f2 (ppm)

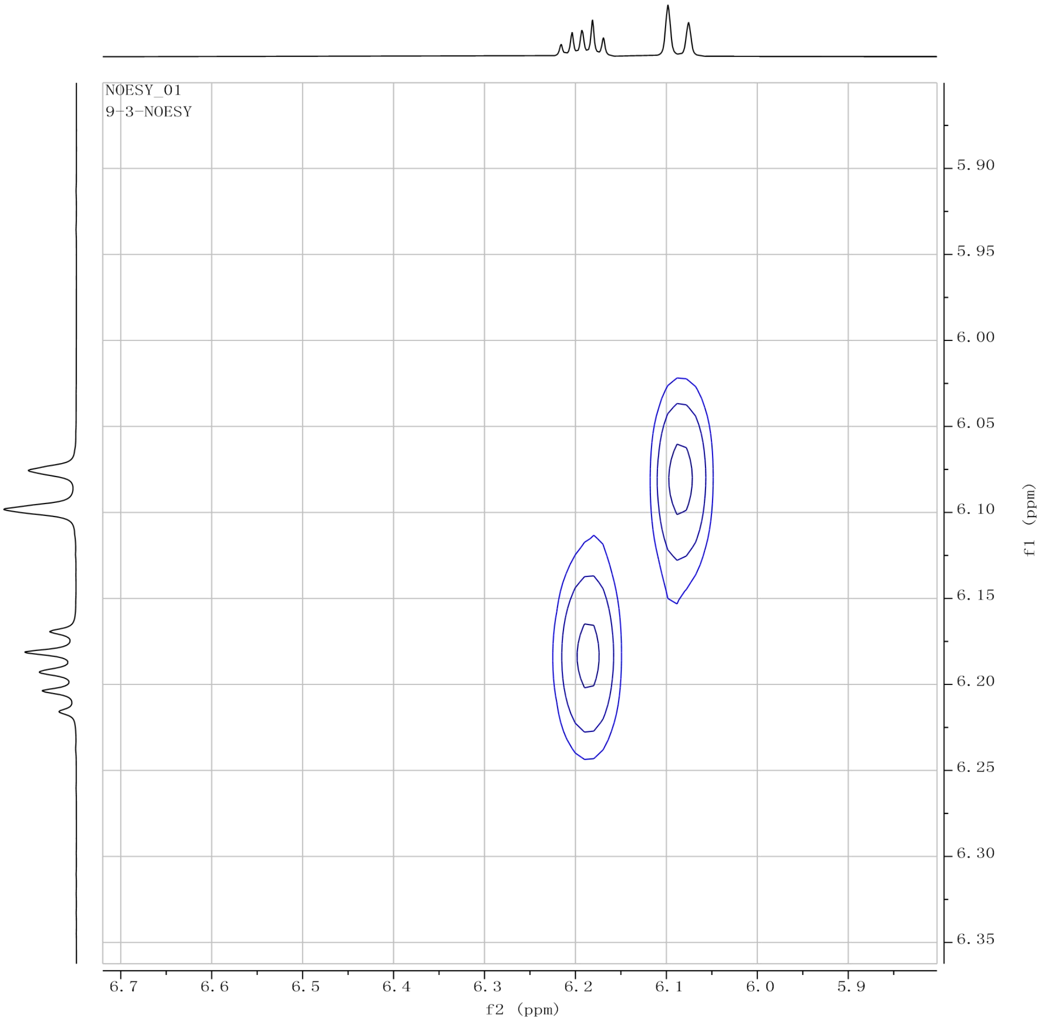
NOESY_01
9-3-NOESY
6.7
6.6
6.5
6.4
6.3
6.2
6.1
6.0
5.9
f2 (ppm)
5.90
5.95
6.00
6.05
6.10
6.15
6.20
6.25
6.30
6.35
f1 (ppm)

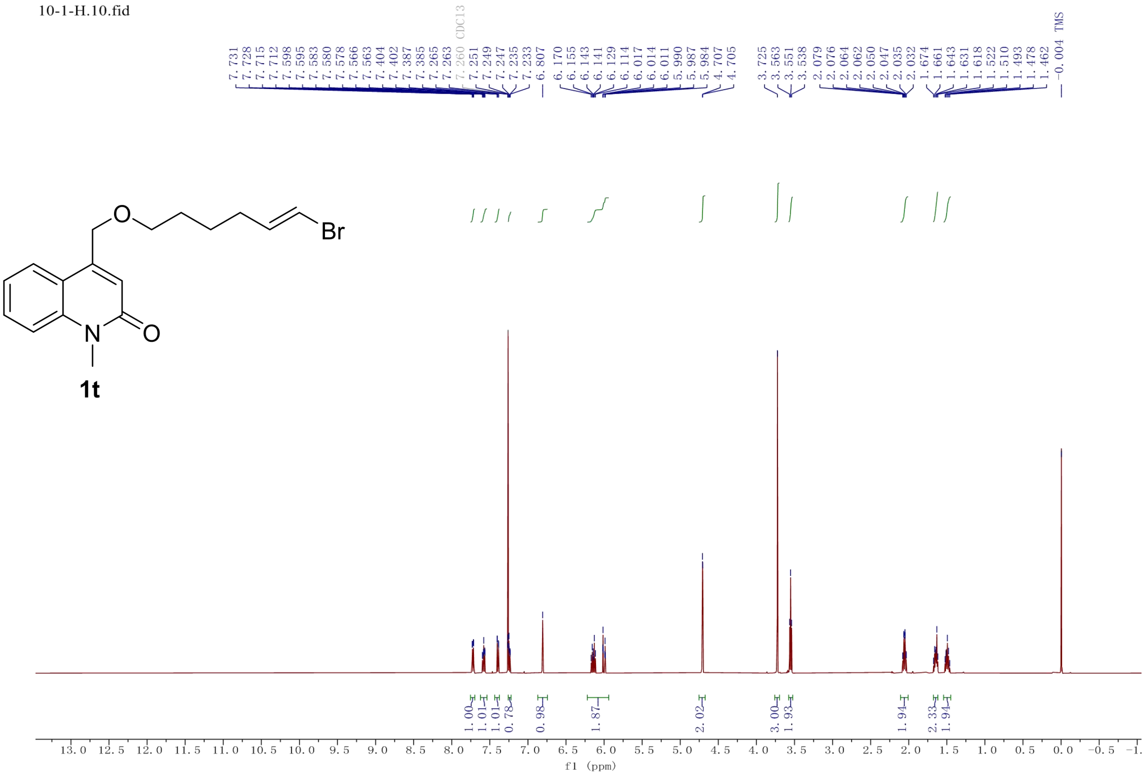
10-1-H.10.fid
7.731
7.728
7.715
7.712
7.598
7.595
7.583
7.580
7.578
7.566
7.563
7.404
7.402
7.387
7.385
7.265
7.263
7.260 CDCl3
7.251
7.249
7.247
7.235
7.233
6.807
6.170
6.155
6.143
6.141
6.129
6.114
6.017
6.014
6.011
5.990
5.987
5.984
4.707
4.705
3.725
3.563
3.551
3.538
2.079
2.076
2.064
2.062
2.050
2.047
2.035
2.032
1.674
1.661
1.643
1.631
1.618
1.522
1.510
1.493
1.478
1.462
-0.004 TMS
O
Br
N
O
1t
1.00
1.01
1.01
0.78
0.98
1.87
2.02
3.00
1.93
1.94
2.33
1.94
13.0
12.5
12.0
11.5
11.0
10.5
10.0
9.5
9.0
8.5
8.0
7.5
7.0
6.5
6.0
5.5
5.0
4.5
4.0
3.5
3.0
2.5
2.0
1.5
1.0
0.5
0.0
-0.5
-1.
f1 (ppm)

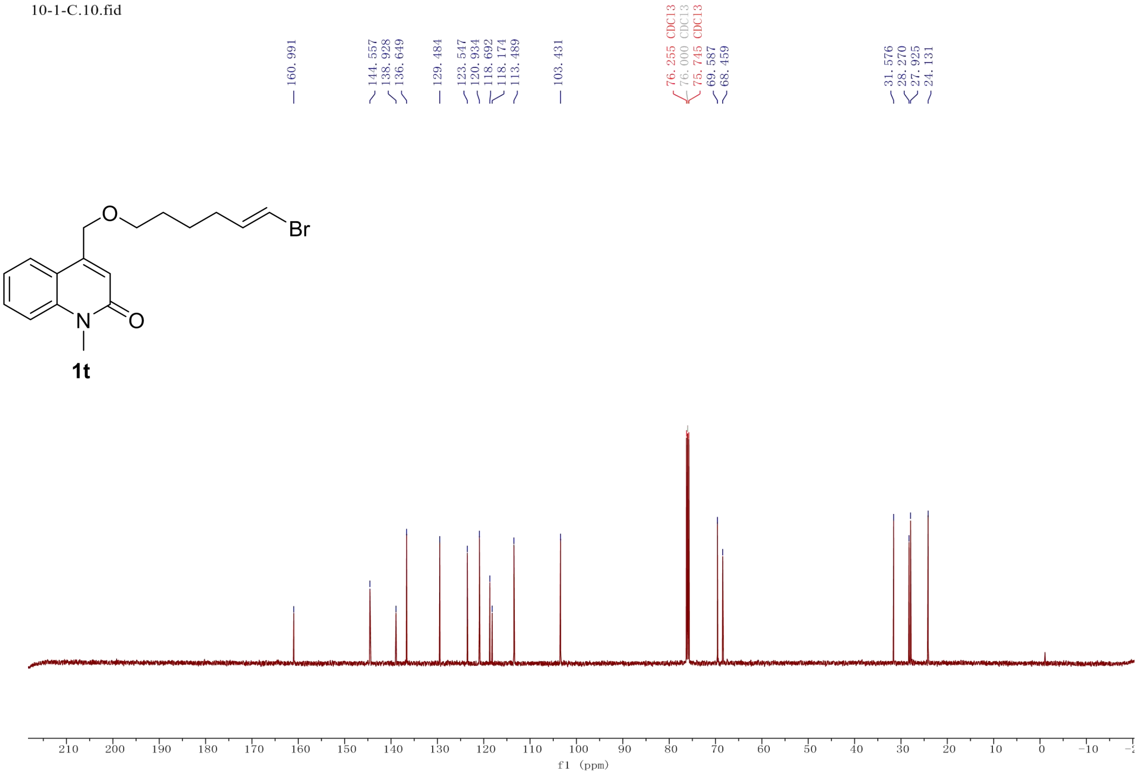
10-1-C.10.fid
160.991
144.557
138.928
136.649
129.484
123.547
120.934
118.692
118.174
113.489
103.431
76.255 CDCl3
76.000 CDCl3
75.745 CDCl3
69.587
68.459
31.576
28.270
27.925
24.131
O
Br
N
O
1t
210
200
190
180
170
160
150
140
130
120
110
100
90
80
70
60
50
40
30
20
10
0
-10
f1 (ppm)

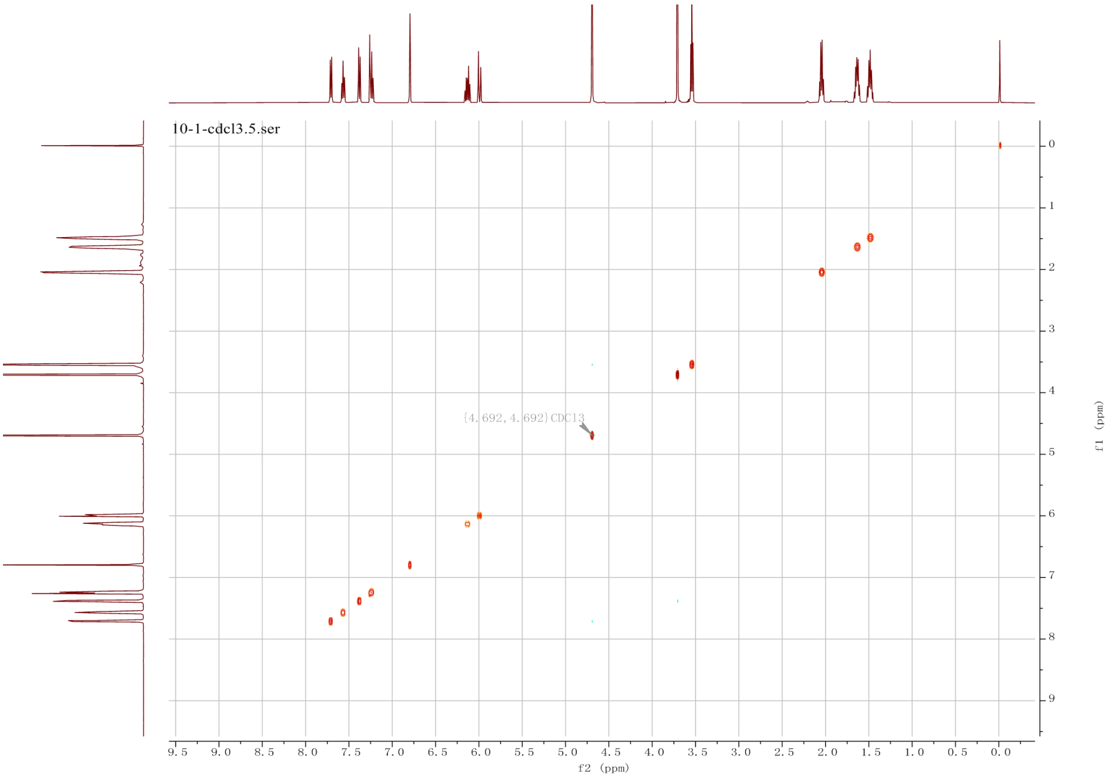
10-1-cdcl3.5.ser
{4.692,4.692}CDCl3
f2 (ppm)
f1 (ppm)
9.5
9.0
8.5
8.0
7.5
7.0
6.5
6.0
5.5
5.0
4.5
4.0
3.5
3.0
2.5
2.0
1.5
1.0
0.5
0.0
0
1
2
3
4
5
6
7
8
9

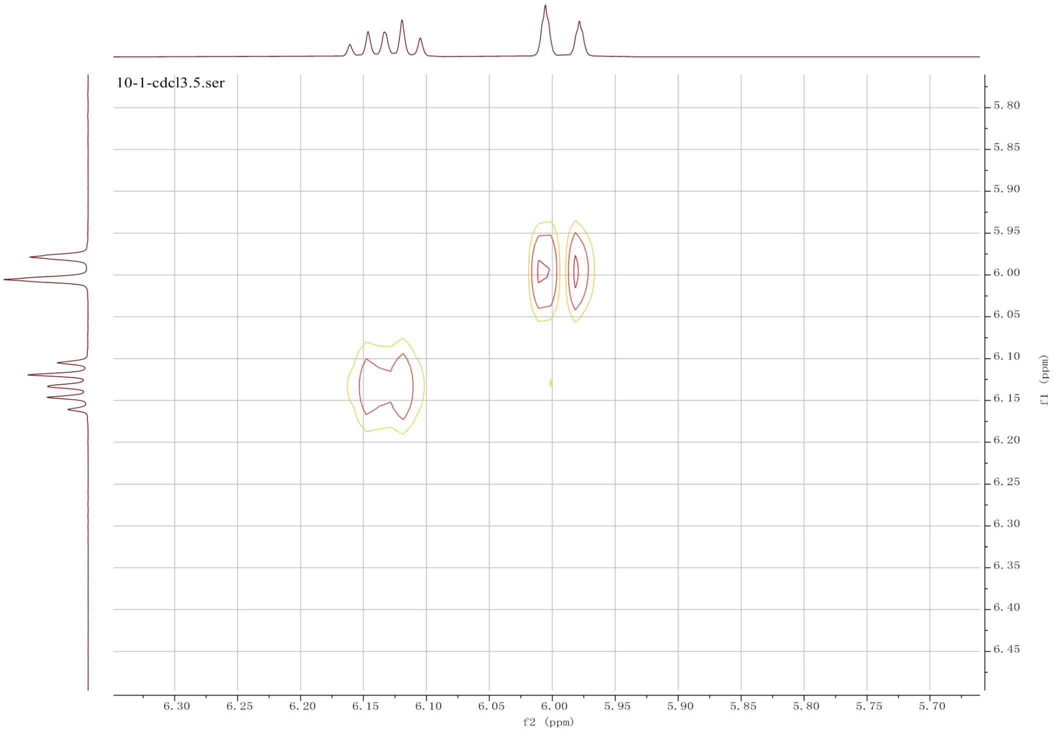
10-1-cdcl3.5.ser
f2 (ppm)
f1 (ppm)
6.30
6.25
6.20
6.15
6.10
6.05
6.00
5.95
5.90
5.85
5.80
5.75
5.70
5.80
5.85
5.90
5.95
6.00
6.05
6.10
6.15
6.20
6.25
6.30
6.35
6.40
6.45

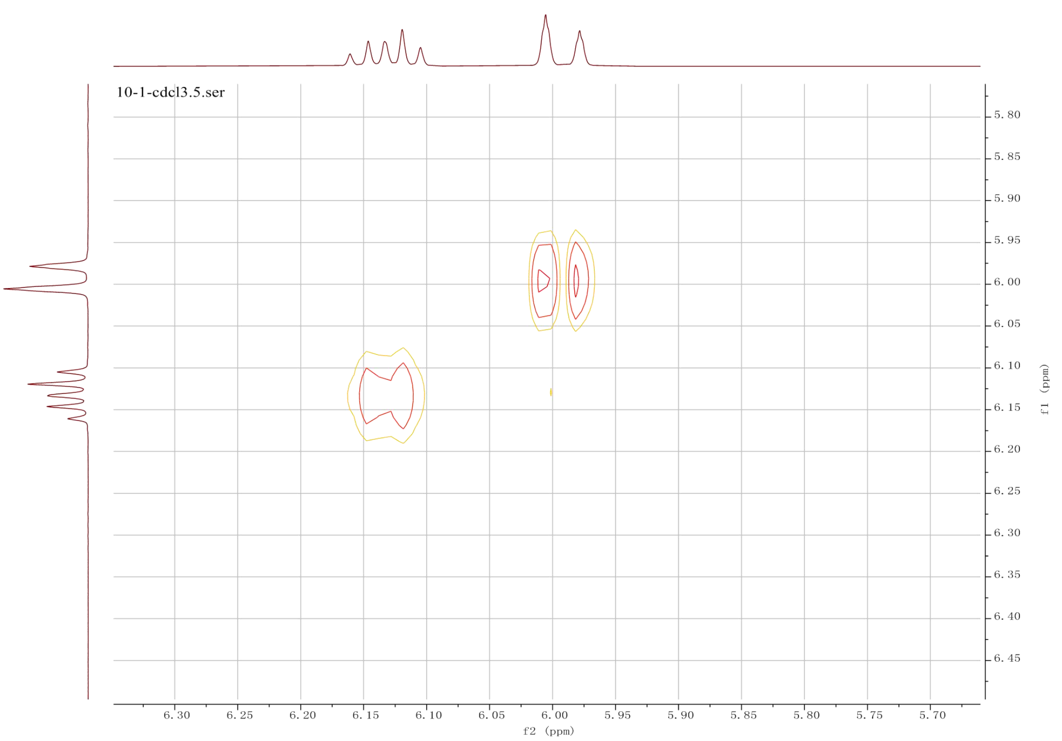
10-1-cdcl3.5.ser
f2 (ppm)
f1 (ppm)
6.30 6.25 6.20 6.15 6.10 6.05 6.00 5.95 5.90 5.85 5.80 5.75 5.70
5.80 5.85 5.90 5.95 6.00 6.05 6.10 6.15 6.20 6.25 6.30 6.35 6.40 6.45

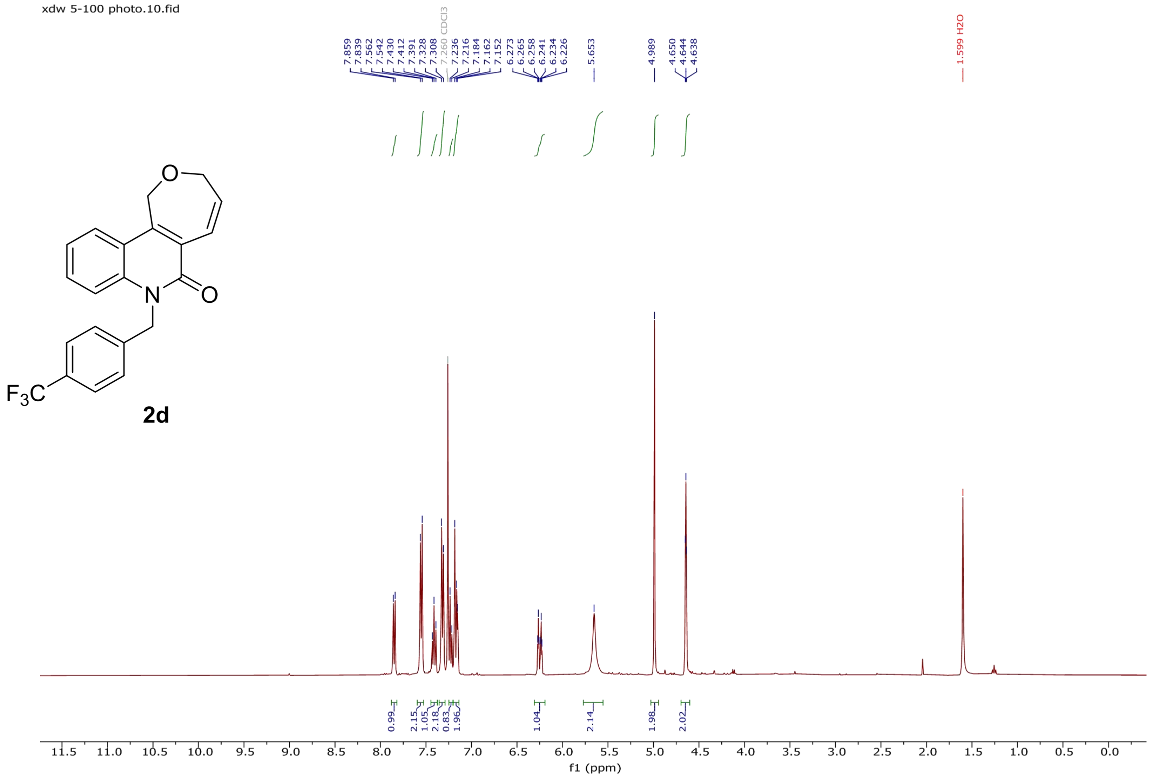
xdw 5-100 photo.10.fid
7.859
7.839
7.562
7.542
7.430
7.412
7.391
7.328
7.308
7.260 CDCl3
7.236
7.216
7.184
7.162
7.152
6.273
6.265
6.258
6.241
6.234
6.226
5.653
4.989
4.650
4.644
4.638
1.599 H2O
0.99
2.15
1.05
2.18
0.83
1.96
1.04
2.14
1.98
2.02
O
N
O
F3C
2d
11.5 11.0 10.5 10.0 9.5 9.0 8.5 8.0 7.5 7.0 6.5 6.0 5.5 5.0 4.5 4.0 3.5 3.0 2.5 2.0 1.5 1.0 0.5 0.0
f1 (ppm)

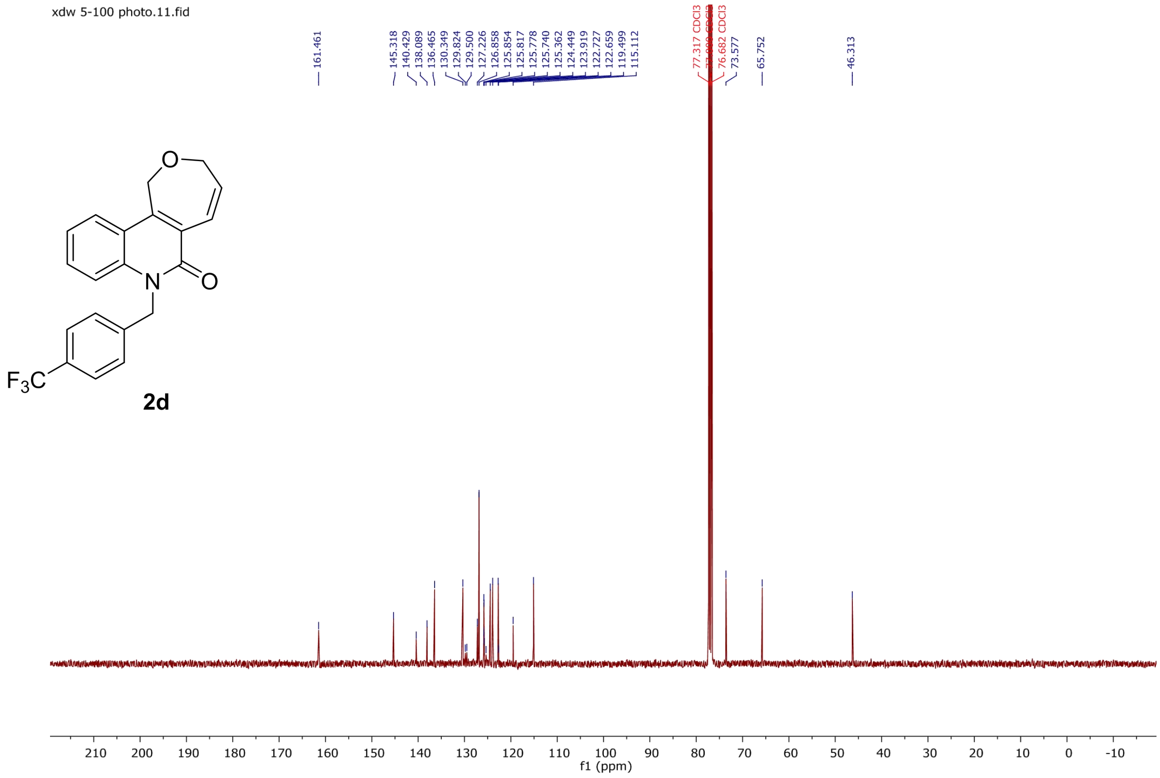
xdw 5-100 photo.11.fid
161.461
145.318
140.429
138.089
136.465
130.349
129.824
129.500
127.226
126.858
125.854
125.817
125.778
125.740
125.362
124.449
123.919
122.727
122.659
119.499
115.112
77.317 CDCl3
77.000 CDCl3
76.682 CDCl3
73.577
65.752
46.313
O
N
O
F3C
210
200
190
180
170
160
150
140
130
120
110
100
90
80
70
60
50
40
30
20
10
0
-10
f1 (ppm)

**2d**

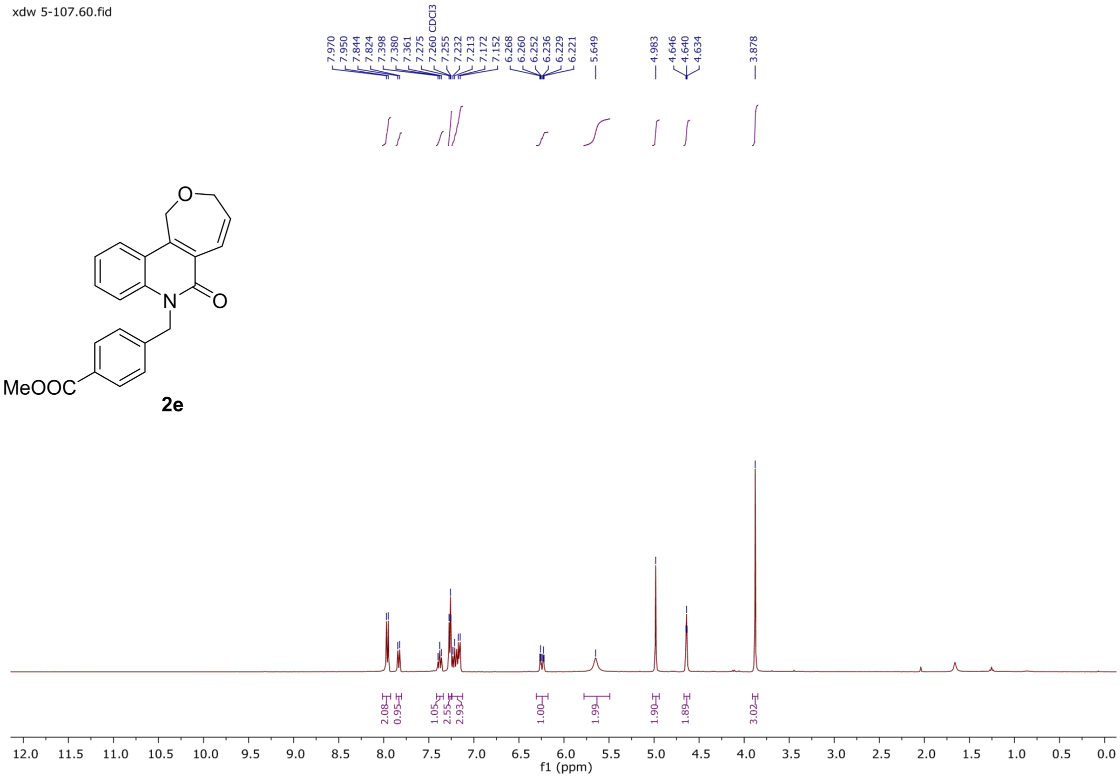
xdw 5-107.60.fid
7.970
7.950
7.844
7.824
7.398
7.380
7.361
7.275
7.260 CDCl3
7.255
7.232
7.213
7.172
7.152
6.268
6.260
6.252
6.236
6.229
6.221
5.649
4.983
4.646
4.640
4.634
3.878
MeOOC
O
N
O
2e
2.08
0.95
1.05
2.55
2.93
1.00
1.99
1.90
1.89
3.02
12.0
11.5
11.0
10.5
10.0
9.5
9.0
8.5
8.0
7.5
7.0
6.5
6.0
5.5
5.0
4.5
4.0
3.5
3.0
2.5
2.0
1.5
1.0
0.5
0.0
f1 (ppm)

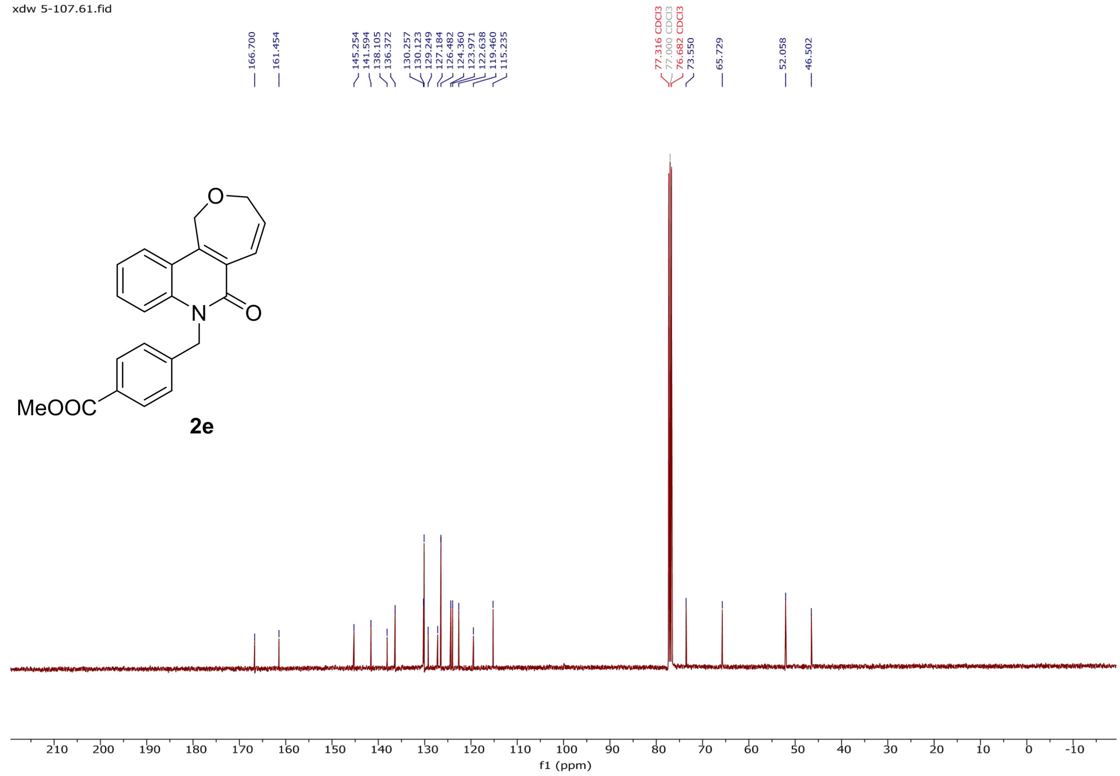
xdw 5-107.61.fid
166.700
161.454
145.254
141.594
138.105
136.372
130.257
130.123
129.249
127.184
126.482
124.360
123.971
122.638
119.460
115.235
77.316 CDCl3
77.000 CDCl3
76.682 CDCl3
73.550
65.729
52.058
46.502
MeOOC
O
N
O
2e
210
200
190
180
170
160
150
140
130
120
110
100
90
80
70
60
50
40
30
20
10
0
-10
f1 (ppm)

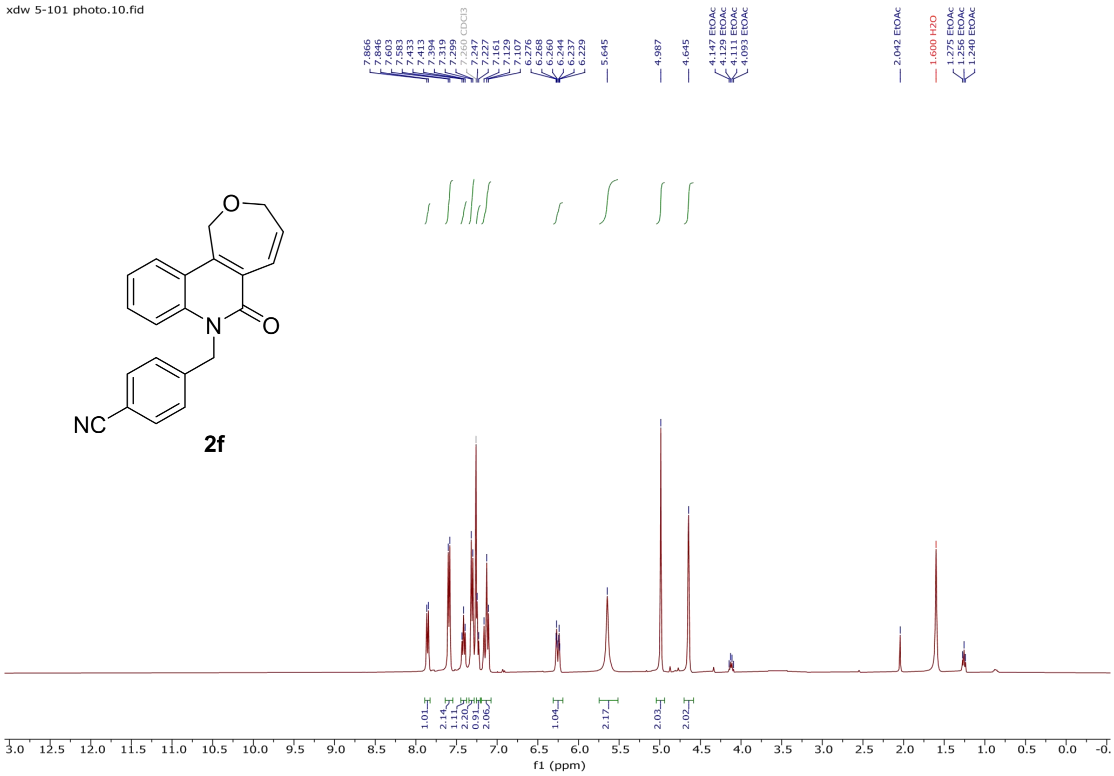
xdw 5-101 photo.10.fid
7.866
7.846
7.603
7.583
7.433
7.413
7.394
7.319
7.299
7.260 CDCl3
7.247
7.227
7.161
7.129
7.107
6.276
6.268
6.260
6.244
6.237
6.229
5.645
4.987
4.645
4.147 EtOAc
4.129 EtOAc
4.111 EtOAc
4.093 EtOAc
2.042 EtOAc
1.600 H2O
1.275 EtOAc
1.256 EtOAc
1.240 EtOAc
O
N
O
NC
2f
1.01
2.14
1.11
2.20
0.91
2.06
1.04
2.17
2.03
2.02
3.0
12.5
12.0
11.5
11.0
10.5
10.0
9.5
9.0
8.5
8.0
7.5
7.0
6.5
6.0
5.5
5.0
4.5
4.0
3.5
3.0
2.5
2.0
1.5
1.0
0.5
0.0
-0.
f1 (ppm)

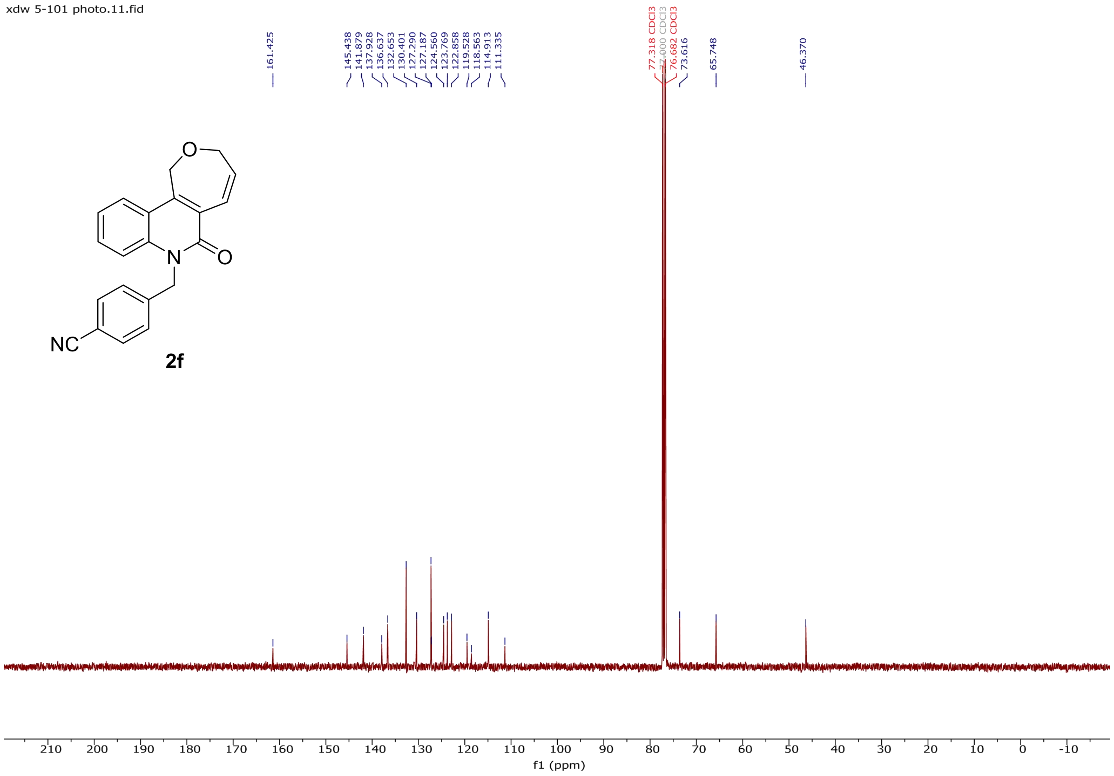
xdw 5-101 photo.11.fid
161.425
145.438
141.879
137.928
136.637
132.653
130.401
127.290
127.187
124.560
123.769
122.858
119.528
118.563
114.913
111.335
77.318 CDCl3
77.000 CDCl3
76.682 CDCl3
73.616
65.748
46.370
O
N
O
NC
2f
210
200
190
180
170
160
150
140
130
120
110
100
90
80
70
60
50
40
30
20
10
0
-10
f1 (ppm)

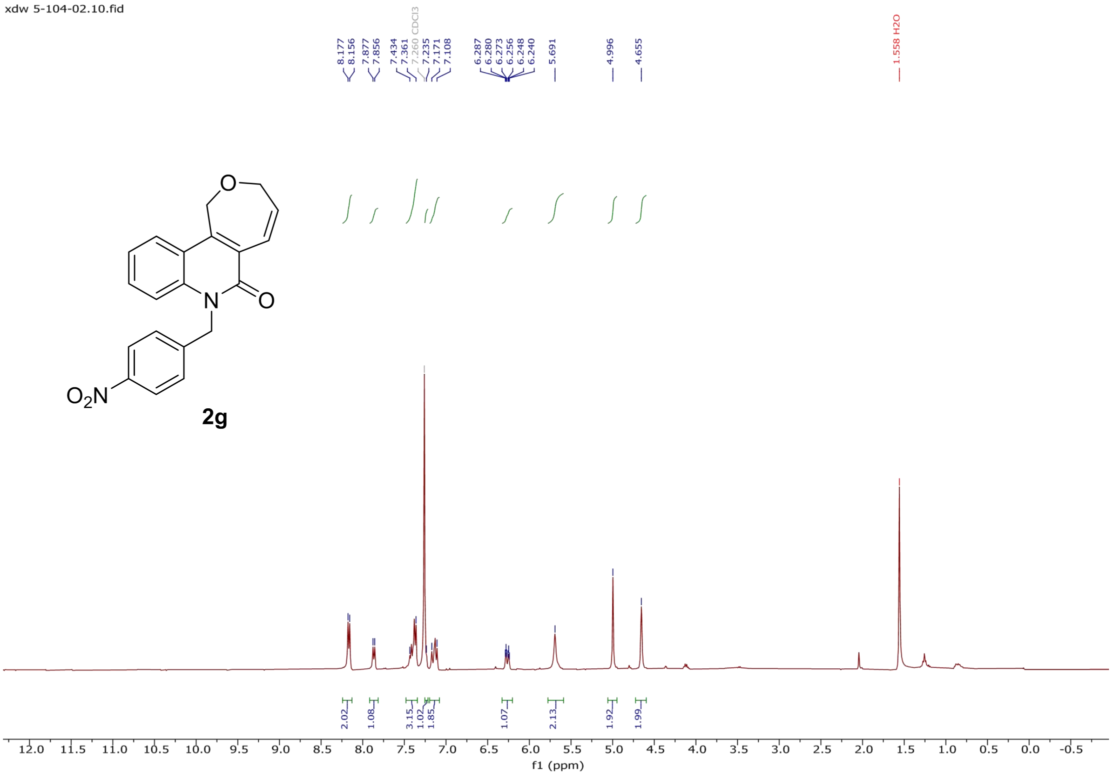
xdw 5-104-02.10.fid
8.177
8.156
7.877
7.856
7.434
7.361
7.260 CDCl3
7.235
7.171
7.108
6.287
6.280
6.273
6.256
6.248
6.240
5.691
4.996
4.655
1.558 H2O
O
N
O
$O_2N$
2g
2.02
1.08
3.15
1.02
1.85
1.07
2.13
1.92
1.99
12.0
11.5
11.0
10.5
10.0
9.5
9.0
8.5
8.0
7.5
7.0
6.5
6.0
5.5
5.0
4.5
4.0
3.5
3.0
2.5
2.0
1.5
1.0
0.5
0.0
-0.5
f1 (ppm)

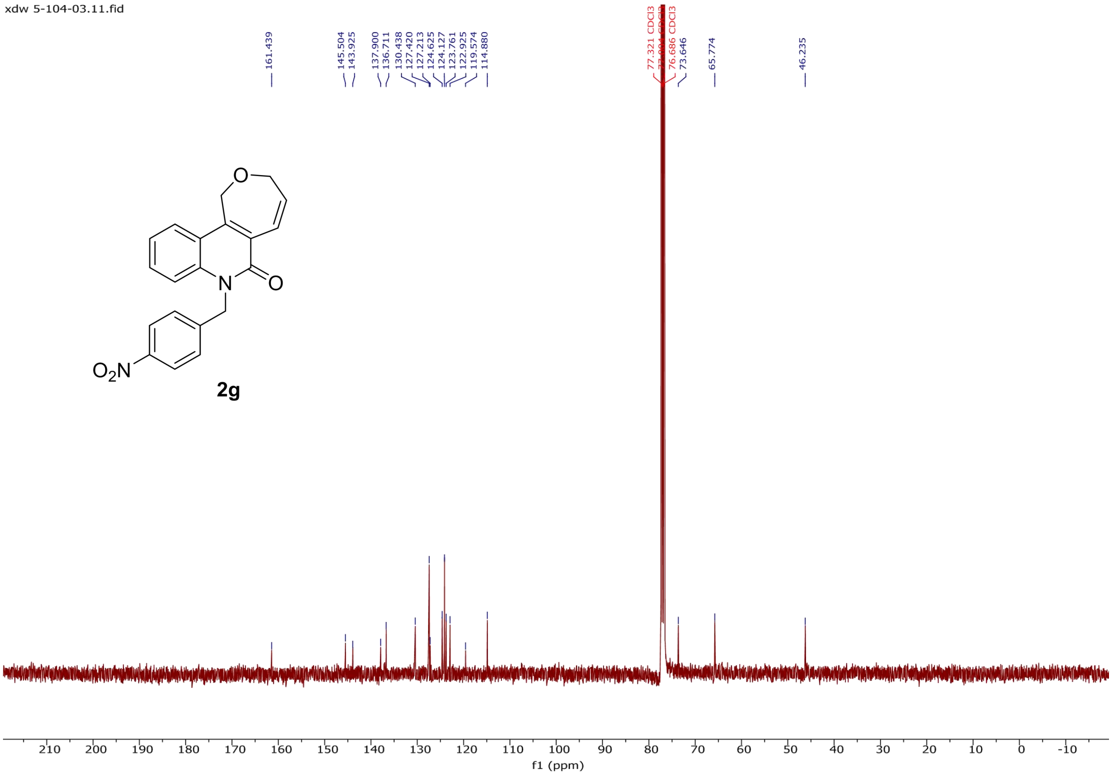
xdw 5-104-03.11.fid
161.439
145.504
143.925
137.900
136.711
130.438
127.420
127.213
124.625
124.127
123.761
122.925
119.574
114.880
77.321 CDCl3
77.004 CDCl3
76.686 CDCl3
73.646
65.774
46.235
O
N
O
$O_2N$
2g
210
200
190
180
170
160
150
140
130
120
110
100
90
80
70
60
50
40
30
20
10
0
-10
f1 (ppm)

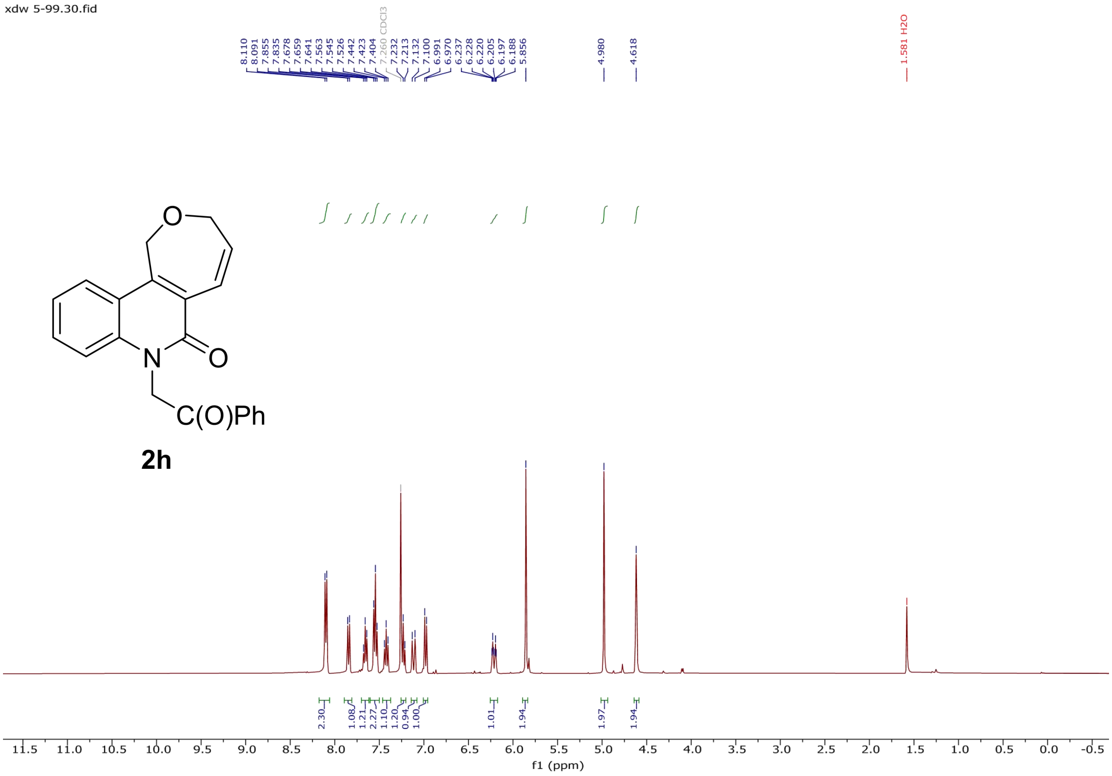
xdw 5-99.30.fid
8.110
8.091
7.855
7.835
7.678
7.659
7.641
7.563
7.545
7.526
7.442
7.423
7.404
7.260 CDCl3
7.232
7.213
7.132
7.100
6.991
6.970
6.237
6.228
6.220
6.205
6.197
6.188
5.856
4.980
4.618
1.581 H2O
O
N
O
C(O)Ph
2h
2.30
1.08
1.21
2.27
1.10
1.20
0.94
1.00
1.01
1.94
1.97
1.94
11.5
11.0
10.5
10.0
9.5
9.0
8.5
8.0
7.5
7.0
6.5
6.0
5.5
5.0
4.5
4.0
3.5
3.0
2.5
2.0
1.5
1.0
0.5
0.0
-0.5
f1 (ppm)

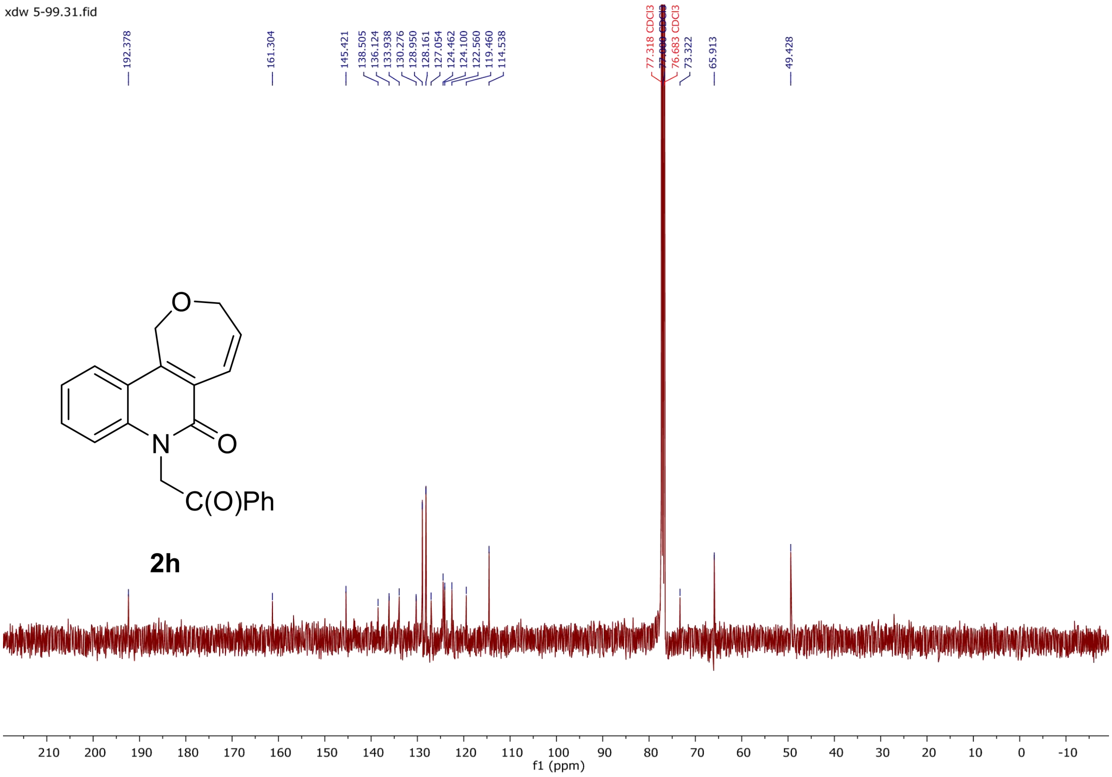
xdw 5-99.31.fid
192.378
161.304
145.421
138.505
136.124
133.938
130.276
128.950
128.161
127.054
124.462
124.100
122.560
119.460
114.538
77.318 CDCl3
77.000 CDCl3
76.683 CDCl3
73.322
65.913
49.428
O
N
O
C(O)Ph
2h
210
200
190
180
170
160
150
140
130
120
110
100
90
80
70
60
50
40
30
20
10
0
-10
f1 (ppm)

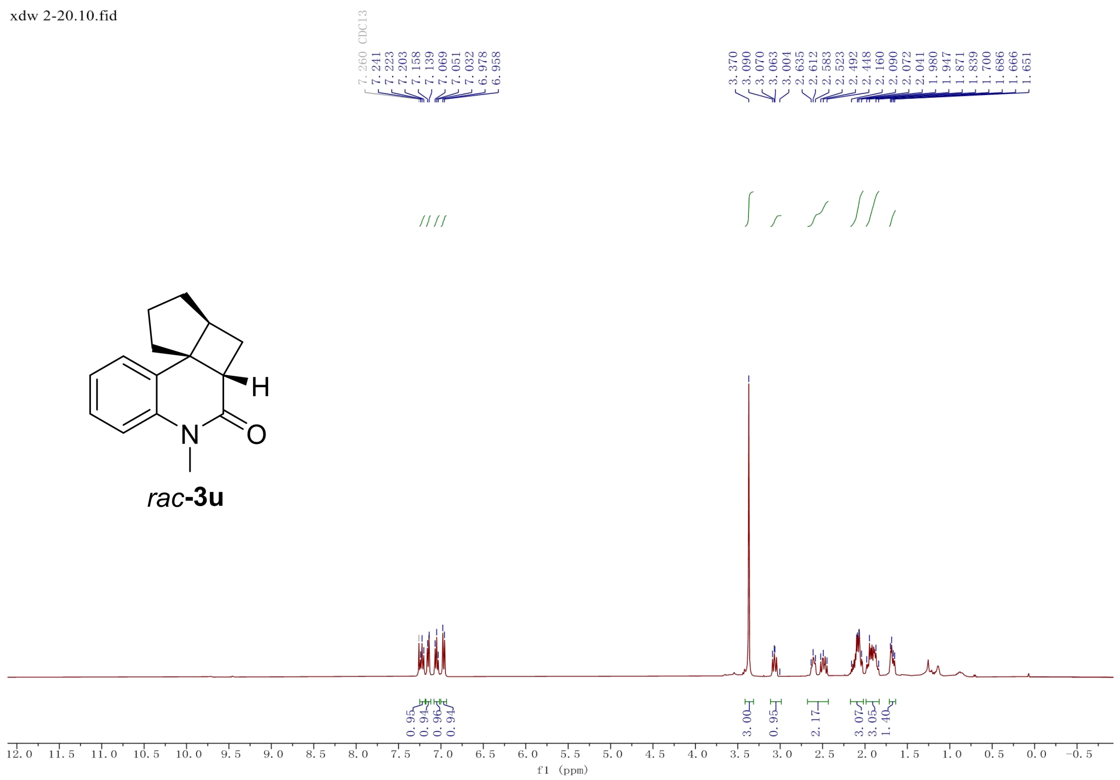
xdw 2-20.10.fid
7.260 CDCl3
7.241
7.223
7.203
7.158
7.139
7.069
7.051
7.032
6.978
6.958
3.370
3.090
3.070
3.063
3.001
2.635
2.612
2.583
2.523
2.492
2.448
2.160
2.090
2.072
2.041
1.980
1.947
1.871
1.839
1.700
1.686
1.666
1.651
H
N
O
0.95
0.94
0.96
0.94
3.00
0.95
2.17
3.07
3.05
1.40
12.0
11.5
11.0
10.5
10.0
9.5
9.0
8.5
8.0
7.5
7.0
6.5
6.0
5.5
5.0
4.5
4.0
3.5
3.0
2.5
2.0
1.5
1.0
0.5
0.0
-0.5
f1 (ppm)

*rac*-**3u**

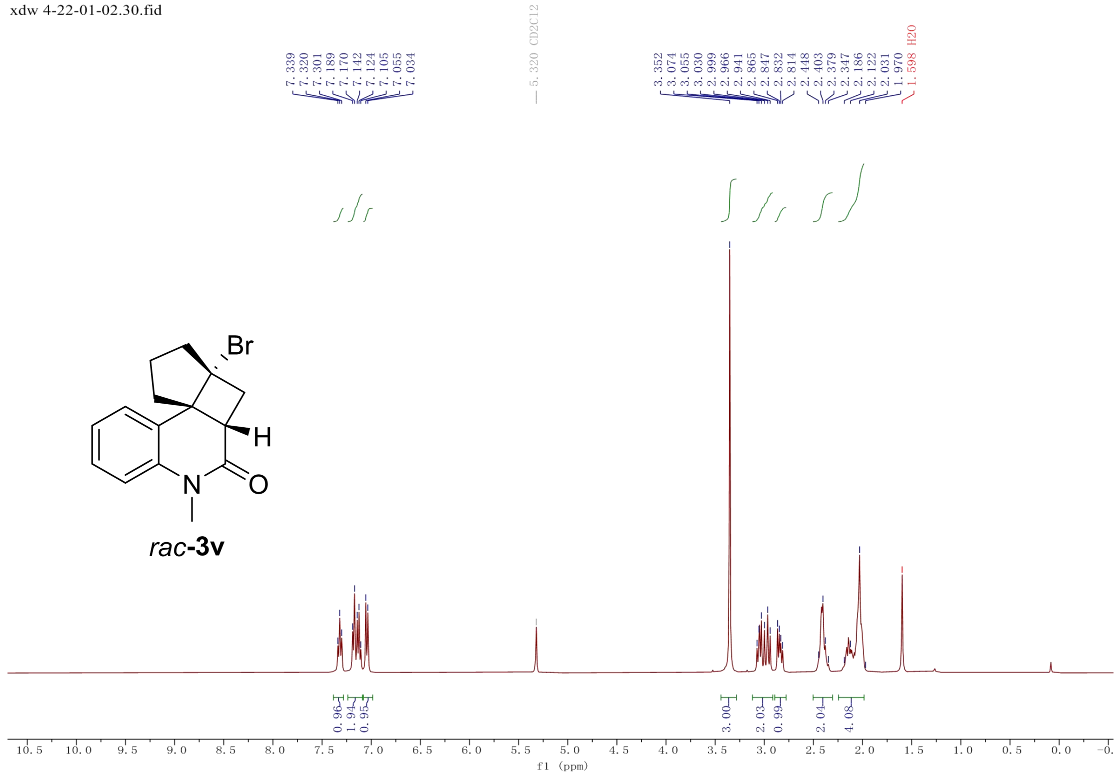
xdw 4-22-01-02.30.fid
7.339
7.320
7.301
7.189
7.170
7.142
7.124
7.105
7.055
7.034
5.320 CD2Cl2
3.352
3.074
3.055
3.030
2.999
2.966
2.941
2.865
2.847
2.832
2.814
2.448
2.403
2.379
2.347
2.186
2.122
2.031
1.970
1.598 H2O
Br
H
N
O
0.96
1.94
0.95
3.00
2.03
0.99
2.04
4.08
10.5
10.0
9.5
9.0
8.5
8.0
7.5
7.0
6.5
6.0
5.5
5.0
4.5
4.0
3.5
3.0
2.5
2.0
1.5
1.0
0.5
0.0
-0.
f1 (ppm)

*rac*-**3v**

xdw 4-22-01-022.30.fid

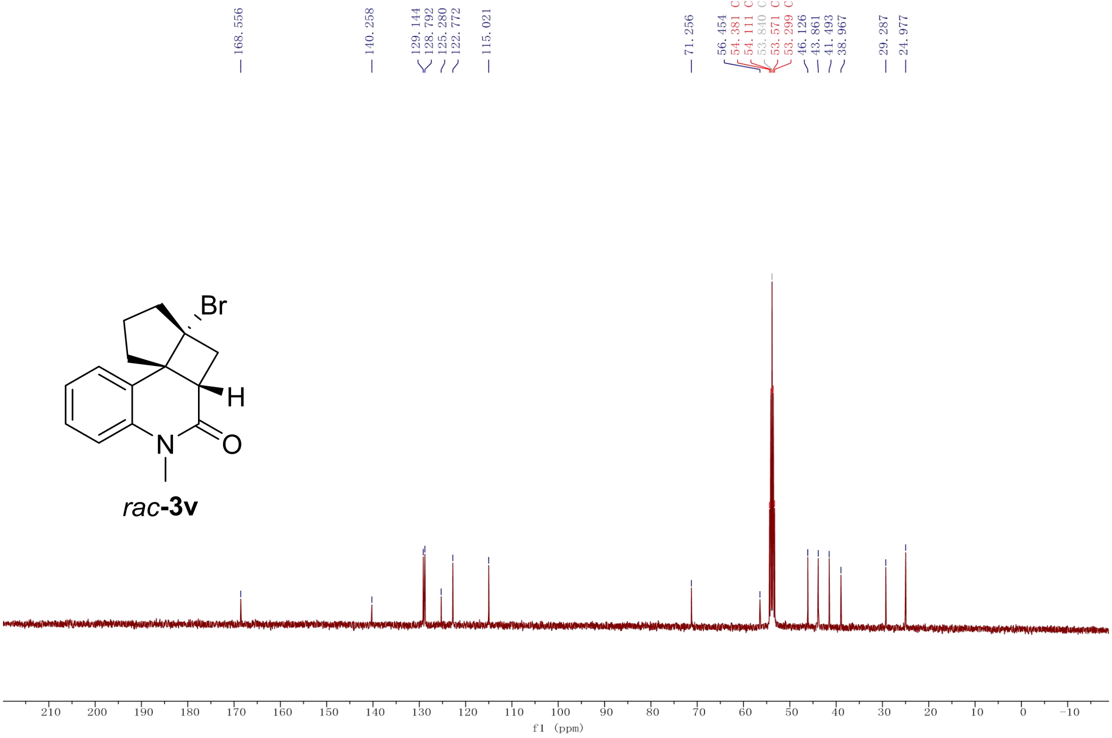

*rac*-**3v**

xdw-p1.30.fid

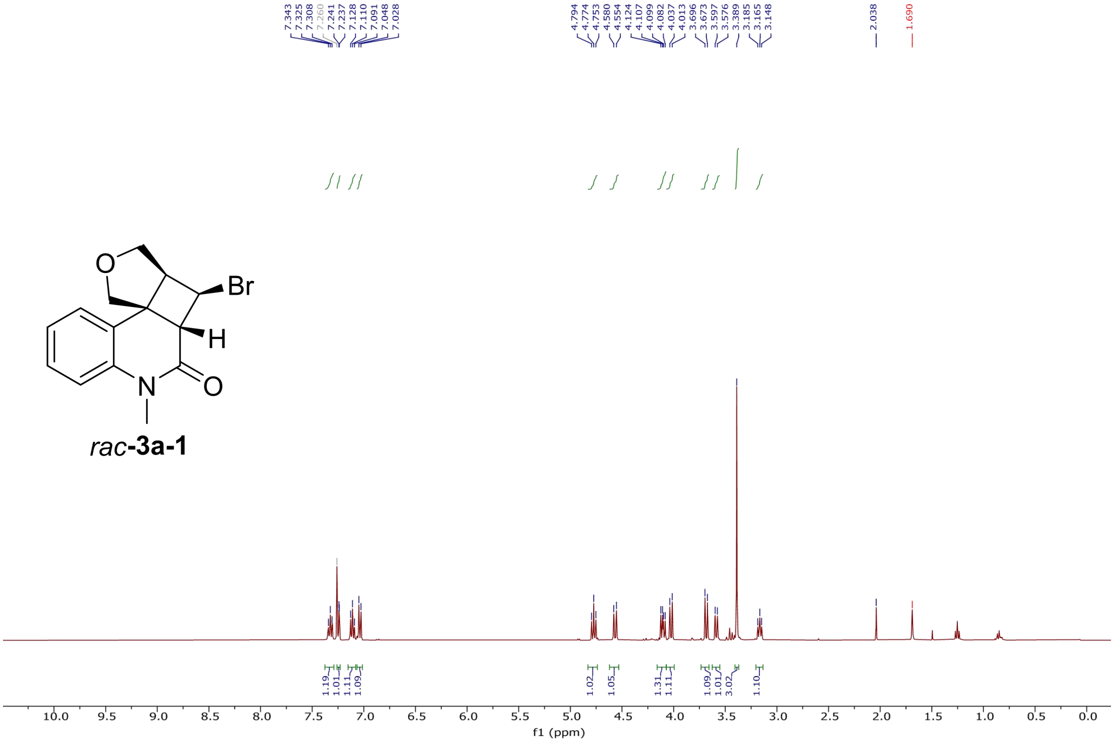

*rac*-**3a-1**

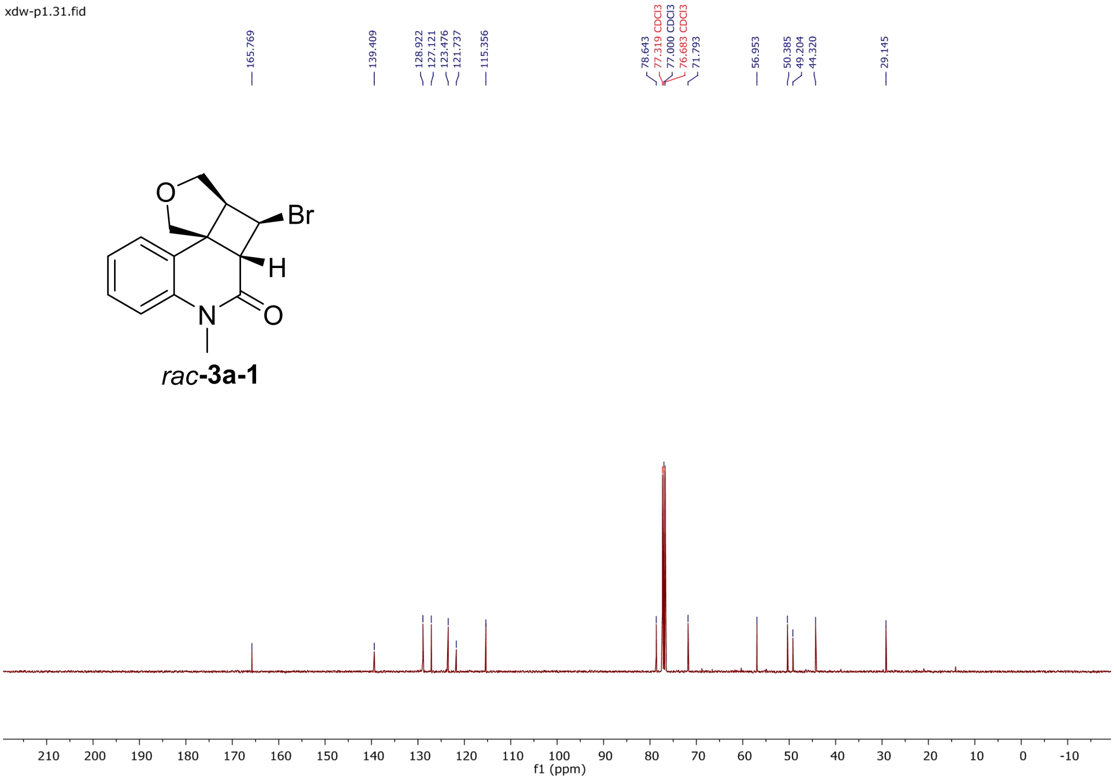

*rac*-**3a-1**

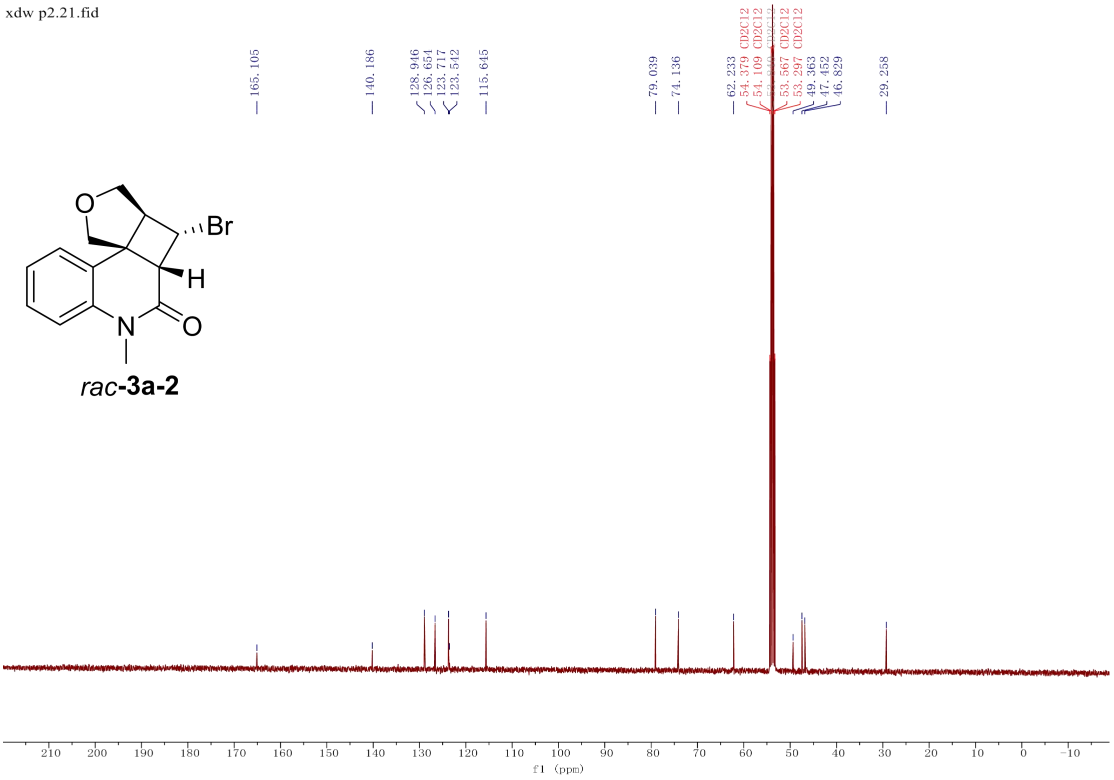

*rac*-**3a-2**

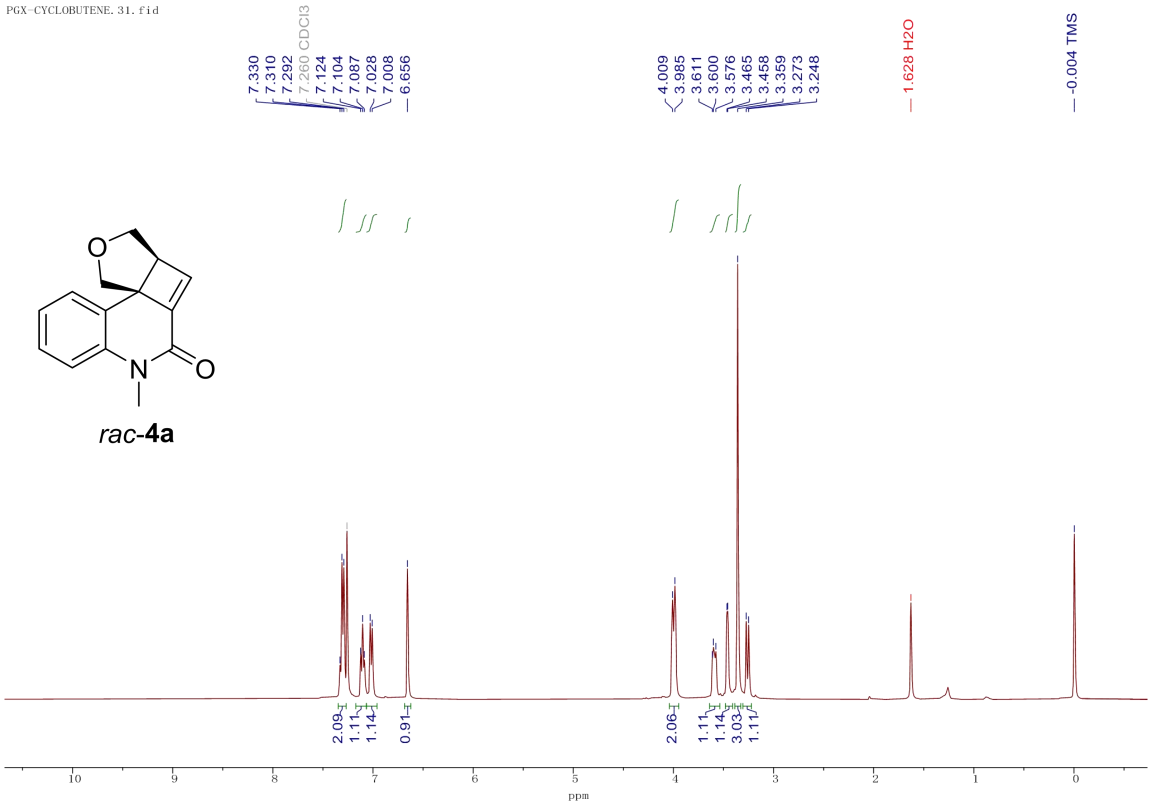
PGX-CYCLOBUTENE.31.fid
7.330
7.310
7.292
7.260 CDCl3
7.124
7.104
7.087
7.028
7.008
6.656
4.009
3.985
3.611
3.600
3.576
3.465
3.458
3.359
3.273
3.248
1.628 H2O
-0.004 TMS
2.09
1.11
1.14
0.91
2.06
1.11
1.14
3.03
1.11
rac-4a
10
9
8
7
6
5
4
3
2
1
0
ppm

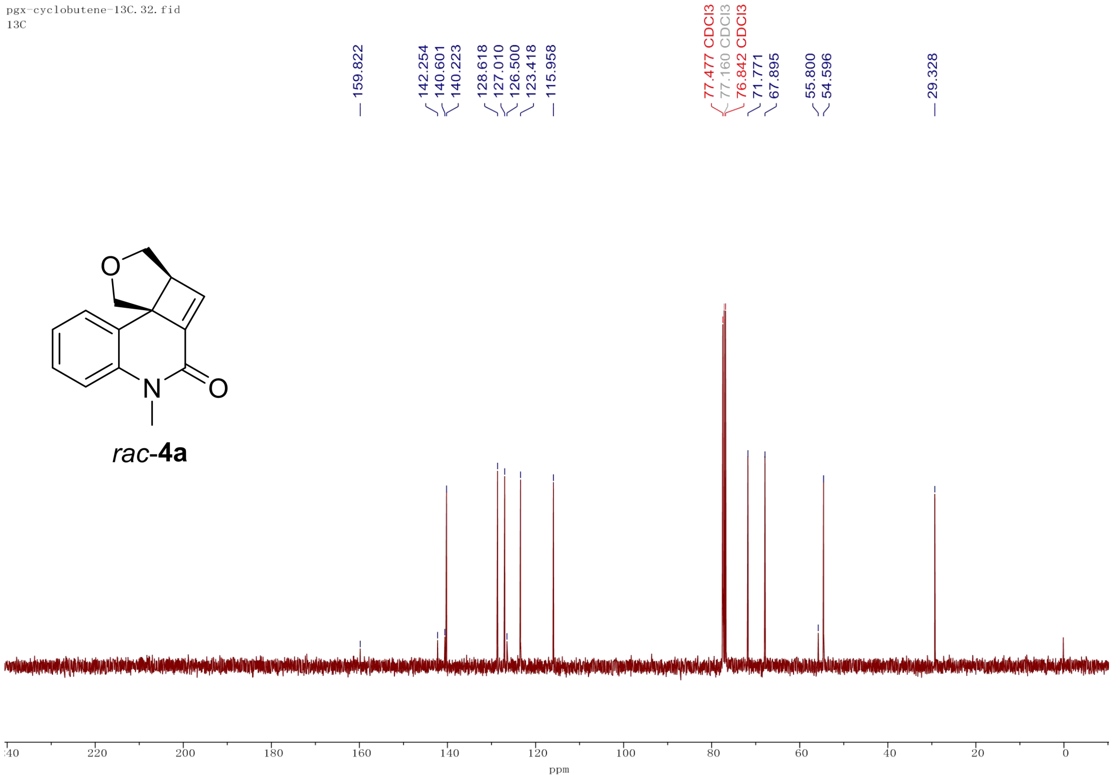
pgx-cyclobutene-13C.32.fid
13C
159.822
142.254
140.601
140.223
128.618
127.010
126.500
123.418
115.958
77.477 CDCl3
77.160 CDCl3
76.842 CDCl3
71.771
67.895
55.800
54.596
29.328
rac-4a
240
220
200
180
160
140
120
100
80
60
40
20
0
ppm

# References

[1] D. Xu, H. Li, G. Pan, P. Huang, J. Oberkofler, R. M. Reich, F. E. Kühn, H. Guo, *Org. Lett.*, **2020**, *22*, 4372-4377.

[2] A. J. B. Michael Entzeroth, Jon S. Mynderse, Richard E. Moore, *J. Org. Chem.*, **1984**, *50*, 1255-1259.

[3] H.-N. Chou, Y. Shimizu, G. Van Duyne, J. Clardy, *Tetrahedron Lett.*, **1985**, *26*, 2865-2868.

[4] F. J. Schmitz, S. P. Gunasekera, G. Yalamanchili, M. B. Hossain, D. Van der Helm, *J. Am. Chem. Soc.*, **1984**, *106*, 7251-7252.

[5] F. Gueritte-Voegelein, D. Guenard, F. Lavelle, M. T. Le Goff, L. Mangatal, P. Potier, *J. Med. Chem.*, **1991**, *34*, 992-998.

[6] I. Ojima, O. Duclos, S. D. Kuduk, C.-M. Sun, J. C. Slater, F. Lavelle, J. M. Veith, R. J. Bernacki, *Bioorg. Med. Chem. Lett.*, **1994**, *4*, 2631-2634.

[7] U. Nubbemeyer, **2001**, *216*, 125-196.

[8] Y. W. L. Zhang, Z.-J. Yao, S. Wang, Z.-X. Yu, *J. Am. Chem. Soc.*, **2015**, *137*, 13290-13300.

[9] M. Wang, Y. Yang, B. Song, L. Yin, S. Yan, Y. Li, *Org. Lett.*, **2019**, *22*, 155-159.

[10] K. Fukaya, Y. Tanaka, A. C. Sato, K. Kodama, H. Yamazaki, T. Ishimoto, Y. Nozaki, Y. M. Iwaki, Y. Yuki, K. Umei, T. Sugai, Y. Yamaguchi, A. Watanabe, T. Oishi, T. Sato, N. Chida, *Org. Lett.*, **2015**, *17*, 2570-2573.

[11] S. Kotha, R. R. Keesari, S. Ansari, *Synthesis*, **2019**, *51*, 3989-3997.

[12] H. Ni, X. Tang, W. Zheng, W. Yao, N. Ullah, Y. Lu, *Angew. Chem. Int. Ed.*, **2017**, *56*, 14222-14226.

[13] X.-Y. Liu, Y. Qin, *Acc. Chem. Res.*, **2019**, *52*, 1877-1891.

[14] H. Gan, M. G. Horner, B. J. Hrnjez, T. A. McCormack, J. L. King, Z. Gasyna, G. Chen, R. Gleiter, N.-c. C. Yang, *J. Am. Chem. Soc.*, **2000**, *122*, 12098-12111.

[15] T. B. R. Brimioulle, *Science*, **2013**, *342*, 840-843.

[16] D. J. Maradyn, A. C. Weedon, *J. Am. Chem. Soc.*, **1995**, *117*, 5359-5360.

[17] R. Srinivasan, K. H. Carlough, *J. Am. Chem. Soc.*, **1967**, *89*, 4932-4936.

[18] H. C. Longuet-Higgins, E. W. Abrahamson, *J. Am. Chem. Soc.*, **1965**, *87*, 2045-2046.

[19] J.-R. Chen, D.-M. Yan, Q. Wei, W.-J. Xiao, *ChemPhotoChem*, **2017**, *1*, 148-158.

# List of publications:

Dawen Xu, **Han Li**, Gguangxing Pan, Pan Huang, Jens Oberkofler, Robert. M. Reich, Fritz. E. Kühn*, Hao. Guo*, "Visible-Light-Induced Dehydrohalogenative Coupling for Intramolecular α-Alkenylation: A Way to Build Seven- and Eight-Membered Rings." *Org. Lett.*, **2020**, *22*, 4372-4377

Dawen Xu, Felix Kaiser, **Han Li**, Robert M. Reich, Hao Guo,* Fritz E. Kühn,*. "Highly selective $AlCl_3$ initiated intramolecular α-alkylation of α,β-unsaturated lactams and lactones." *Organic & Biomolecular Chemistry*, **2019**, 17, 49-52.

**Han Li**, Jonas Schlagintweit, Macro Bernd, Eva-Maria Esslinger, Christian Jandle, Dawen Xu, Robert. M. Reich, Hao Guo*, Fritz. E. Kühn* "Design and Synthesis of Heteroleptic Fe(II)-Hexa-N-Heterocyclic Carbene Complex with 130 ps Metal-to-Ligand Charge-Transfer state lifetime" Manuscript in preparation